Performance-Based Design Factors for Pile Foundations

WA-RD 827.1

Steven L. Kramer
Carlos Valdez
Benjamin Blanchette
Jack W. Baker

October 2014

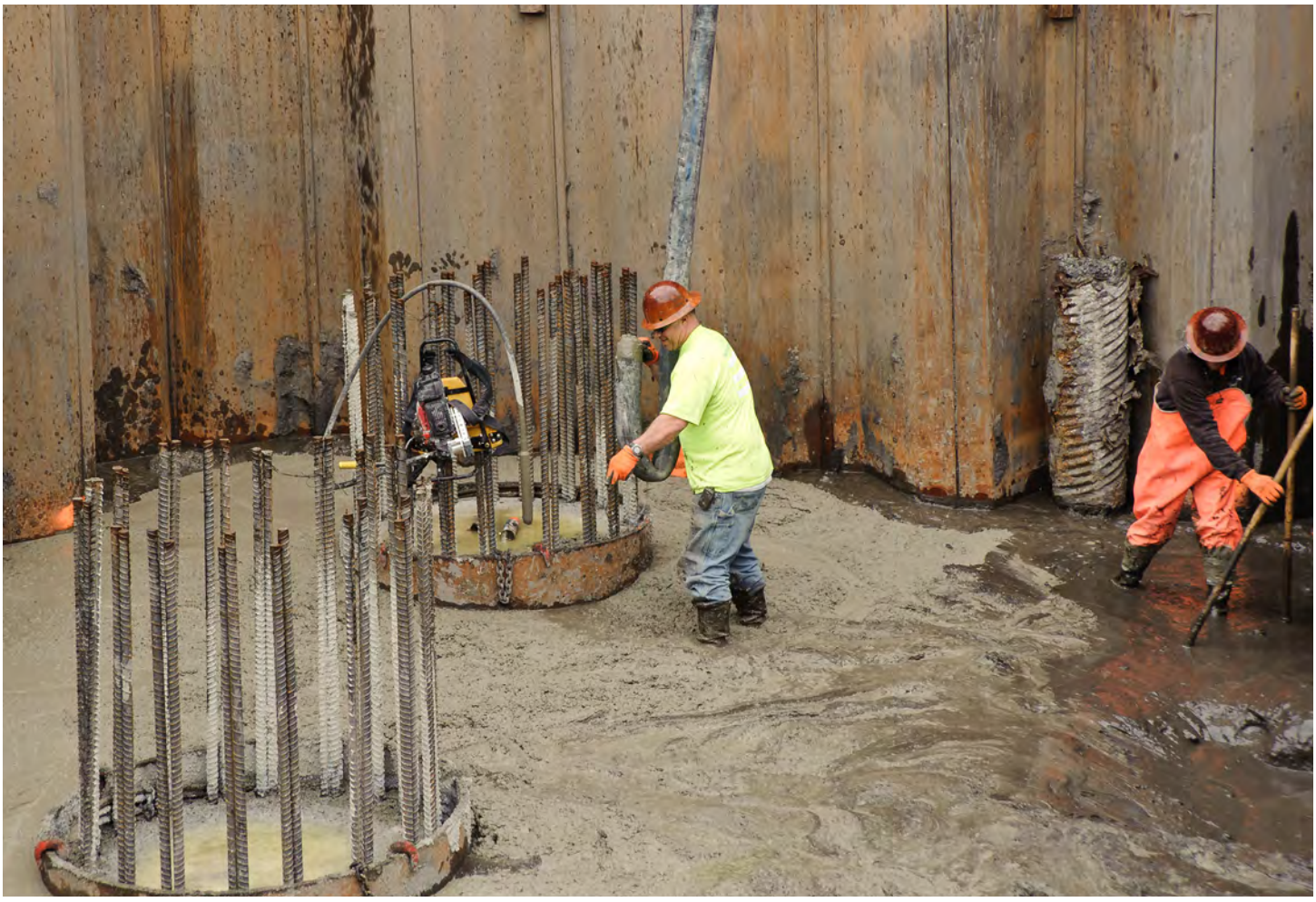

Washington State Department of Transportation
Office of Research & Library Services

WSDOT Research Report

Final Research Report
Agreement T4118-66
WA-RD 827.1

Performance-Based Design Factors for Pile Foundations

Steven L. Kramer
Department of Civil and Environmental Engineering
University of Washington

Carlos Valdez
Department of Civil and Environmental Engineering
University of Washington

Benjamin Blanchette
Department of Civil and Environmental Engineering
University of Washington

Jack W. Baker
Department of Civil and Environmental Engineering
Stanford University

PEER Report
Pacific Earthquake Engineering Research Center
College of Engineering
University of California, Berkeley

October 2014

Prepared for

The State of Washington
Department of Transportation
Lynn Peterson, Secretary

1. REPORT NO.	2. GOVERNMENT ACCESSION NO.	3. RECIPIENTS CATALOG NO
WA-RD 827.1		

4. TITLE AND SUBTITLE	5. REPORT DATE
Performance-Based Design Factors for Pile Foundations	October 2014
	6. PERFORMING ORGANIZATION CODE

7. AUTHOR(S)	8. PERFORMING ORGANIZATION REPORT NO.
Steven L. Kramer, Carlos Valdez, Benjamin Blanchette and Jack W. Baker	

9. PERFORMING ORGANIZATION NAME AND ADDRESS	10. WORK UNIT NO.
Pacific Earthquake Engineering Research Center College of Engineering University of California, Berkeley	11. CONTRACT OR GRANT NO. T4118-66

12. CO-SPONSORING AGENCY NAME AND ADDRESS	13. TYPE OF REPORT AND PERIOD COVERED
Washington State Department of Transportation 310 Maple Park Ave SE Olympia, WA 98504-7372 Research Manager: Kim Willoughby 360.705.7978	Final 14. SPONSORING AGENCY CODE

15. SUPPLEMENTARY NOTES

This study was conducted in cooperation with the U.S. Department of Transportation, Federal Highway Administration.

16. ABSTRACT

The seismic design of pile foundations is currently performed in a relatively simple, deterministic manner. This report describes the development of a performance-based framework to create seismic designs of pile group foundations that consider all potential levels of loading and their likelihoods of occurrence in a particular area.

Because of the multitude of factors that can exist at a site, development of a complete, integrated procedure that would extend from ground motions to limit state exceedance was not practical. To make the problem more useful to the research sponsors, a modular approach was developed. The framework allows for the development and use of a structural model with a simplified representation of the foundation system. The discrete soil model was developed using an equivalent linear format so that stiffness and damping characteristics were consistent with deformation levels. The foundation loads computed in these analyses were then applied to a three-dimensional soil-pile group model to compute the resulting displacements and rotations of the pile cap.

A computer program was developed to perform the calculations required to develop load and resistance factors and demand and capacity factors. The calculations allow a designer to select a return period for limit state exceedance and then select the corresponding factors that will produce a design that corresponds to the desired limit state exceedance rate.

17. KEY WORDS	18. DISTRIBUTION STATEMENT
LRFD, pile foundation, seismic design	

19. SECURITY CLASSIF. (of this report)	20. SECURITY CLASSIF. (of this page)	21. NO. OF PAGES	22. PRICE
None	None		

DISCLAIMER

The contents of this report reflect the views of the authors, who are responsible for the facts and the accuracy of the data presented herein. The contents do not necessarily reflect the official views or policies of the Washington State Department of Transportation or Federal Highway Administration. This report does not constitute a standard, specification, or regulation.

ABSTRACT

The seismic design of pile foundations is currently performed in a relatively simple, deterministic manner. This report describes the development of a performance-based framework to create seismic designs of pile group foundations that consider all potential levels of loading and their likelihoods of occurrence in a particular area.

Because of the multitude of factors that can exist at a site, development of a complete, integrated procedure that would extend from ground motions to limit state exceedance was not practical. To make the problem more useful to the research sponsors, a modular approach was developed. The framework allows for the development and use of a structural model with a simplified representation of the foundation system. The discrete soil model was developed using an equivalent linear format so that stiffness and damping characteristics were consistent with deformation levels. The foundation loads computed in these analyses were then applied to a three-dimensional soil-pile group model to compute the resulting displacements and rotations of the pile cap.

A computer program was developed to perform the calculations required to develop load and resistance factors and demand and capacity factors. The calculations allow a designer to select a return period for limit state exceedance and then select the corresponding factors that will produce a design that corresponds to the desired limit state exceedance rate.

CONTENTS

1 INTRODUCTION 1

1.1 PURPOSE OF RESEARCH 1
1.2 ORGANIZATION OF REPORT 2

2 PILE FOUNDATIONS 5

2.1 INTRODUCTION 5
2.2 SINGLE PILE BEHAVIOR 5
2.2.1 Axial (Downward) Load Response 5
2.2.1.1 Capacity Estimation from Pile and Soil Properties 5
2.2.1.2 Capacity Estimation from Driving Resistance 6
2.2.1.3 Capacity Estimation from Wave Equation Analysis 7
2.2.1.4 Capacity Estimation from Pile Driving Analysis 8
2.2.1.5 Capacity Estimation from Pile Load Test Results 8
2.2.1.6 Mobilization of Capacity 10
2.2.2 Axial (Uplift) Load Response 12
2.2.3 Lateral Load Response 12
2.2.3.1 Lateral Load Capacity 12
2.2.3.2 Pile-Soil Interaction 13
2.2.4 Pile Head Moment Response 21
2.3 PILE GROUP BEHAVIOR 21
2.3.1 Vertical Load Response 21
2.3.2 Lateral Load Response 22
2.3.2.1 Group Effect 23
2.3.3 Overturning Moment Response 25
2.4 PILE CAP RESISTANCE 25
2.5 DYNAMIC RESPONSE OF PILE FOUNDATIONS 27
2.6 SUMMARY 29

3 APPROACHES TO SEISMIC RESPONSE AND DESIGN 31

3.1 INTRODUCTION 31
3.2 SEISMIC PERFORMANCE 31
3.2.1 Ground Motion 32
3.2.2 System Response 32
3.2.3 Physical Damage 33
3.2.4 Losses 33
3.3 UNCERTAINTY IN GEOTECHNICAL DESIGN 34
3.3.1 Sources of Uncertainty in Demand (Loading) 34
3.3.2 Sources of Uncertainty in Capacity (Resistance) 35
3.3.3 Allowable Stress Design 36
3.3.3.1 Principles of Allowable Stress Design 36
3.3.3.2 Factors of Safety 36
3.3.4 Reliability Based Design 38
3.3.4.1 Probability in Design 38
3.3.4.2 Probability of failure 39
3.3.4.3 Reliability index 43
3.3.5 Load and Resistance Factor Design 44
3.3.5.1 LRFD Calibration 45

3.4 PERFORMANCE-BASED SEISMIC DESIGN 52
3.4.1 History of Performance-Based Seismic Design *52*
3.4.2 Discrete Hazard Level Approach *53*
3.4.3 Integral Hazard Level Approach *54*
3.4.3.1 Solution by Numerical Integration 54
3.4.3.2 Closed Form Solution for Response 55
3.5 A MODIFIED PERFORMANCE-BASED RESPONSE FRAMEWORK 56
3.5.1 Calculation of Response *57*
3.5.2 Closed Form Solution for Response *57*
3.6 SUMMARY 58

4 NUMERICAL MODEL OF PILE GROUP RESPONSE 61

4.1 INTRODUCTION 61
4.2 SOIL-FOUNDATION-BRIDGE MODELING CONCEPT 61
4.2.1 Bridge Modeling *62*
4.2.1.1 Structural Model 62
4.2.1.2 Foundation Model 63
4.2.1.3 Equivalent Linear Analysis Procedure 63
4.3 NUMERICAL MODELING USING OPENSEES 63
4.3.1 Dynamic BNWF Model *64*
4.3.2 Material Models *64*
4.4 MODEL VALIDATION 65
4.4.1 Static Loading *65*
4.4.1.1 Single Pile 66
4.4.1.2 Pile Group 67
4.4.2 Dynamic Loading *72*
4.4.2.1 Dynamic Response of a Pile Bent Structure 73
4.4.2.2 Dynamic Response of a Two-Span Bridge 74
4.5 SUMMARY 76

5 OPENSEES MODELING OF BRIDGE FOUNDATION RESPONSE 77

5.1 INTRODUCTION 77
5.2 SOIL-FOUNDATION-BRIDGE MODELING CONCEPT 77
5.2.1 Bridge Structure Modeling *78*
5.2.1.1 Structural Model 79
5.2.1.2 Foundation Compliance 79
5.2.1.3 Equivalent Linear Analysis Procedure 80
5.2.2 Foundation Modeling *80*
5.2.2.1 Piles 81
5.2.2.2 Pile Groups 81
5.2.2.3 Pile Caps 81
5.3 SOIL CONDITIONS 82
5.3.1 Sand Profile *82*
5.3.2 Clay Profile *82*
5.4 STATIC LOADING CONDITIONS 82
5.4.1 Static Load Response *83*
5.4.1.1 Reference Loads 83
5.4.1.2 Reference Displacements 84
5.4.1.3 Normalized Loads and Displacements 85
5.4.1.4 Computed Response 85
5.4.2 Static Load Combinations *88*
5.5 GROUND MOTIONS 88
5.6 RESPONSE OF REPRESENTATIVE PILE GROUP 92
5.6.1 Representative Pile Group *92*
5.6.2 Representative Loading Histories *92*
5.6.2.1 Response to Harmonic Loading 92

5.6.2.2 Response to Transient Loading 95
5.7 AGGREGATE RESPONSE 97
5.7.1 Normalization of Loading and Response 97
5.7.2 Effects of Structural Period 98
5.7.3 Effects of Pile Group Size 100
5.7.4 Effect of Yield Moment 103
5.7.5 Effect of Pile Cap Passive Resistance 106
5.7.6 Effect of Soil Shear Strength 107
5.7.7 Discussion 109
5.8 INTERPRETATION OF PILE GROUP RESPONSE 110
5.8.1 Normalization 110
5.8.2 Regression Analyses 110
5.8.3 Discussion 114

6 A PERFORMANCE-BASED DESIGN FRAMEWORK 115

6.1 INTRODUCTION 115
6.2 CAPACITY 116
6.2.1 Allowable Load as Capacity 116
6.2.2 Allowable Displacement as Capacity 117
6.3 LIMIT STATE CONCEPT 117
6.3.1 Calculation of Limit State Exceedance Rate 118
6.3.1.1 Force-Based Limit State 118
6.3.1.2 Displacement-Based Limit State 118
6.3.2 Closed-Form Solution for Limit State Exceedance Rates 119
6.3.2.1 Force-Based Limit States 119
6.3.2.2 Displacement-Based Capacity 120
6.4 LOAD AND RESISTANCE FACTOR FRAMEWORK 121
6.4.1 Calculation of Load and Resistance Factors 122
6.4.2 Closed-Form Solution 124
6.4.3 Randomness and Uncertainty 124
6.5 RESPONSE AND CAPACITY FACTOR DESIGN FRAMEWORK 126
6.5.1 Calculation of Demand and Capacity Factors 127
6.5.2 Closed-Form Solution 128
6.6 COMPUTATIONAL APPROACH 130
6.6.1 Read Input Data 131
6.6.2 Compute IM Hazard Curves 133
6.6.3 Compute LM Hazard Curves 133
6.6.4 Compute LM Limit State Hazard Curves 133
6.6.5 Perform Monte Carlo Simulation of LM-EDP Response 133
6.6.6 Perform Multiple Linear Regression Analyses on Coarse Grid EDP Data 134
6.6.7 Compute EDP Hazard Curves 135
6.6.8 Compute EDP Limit State Hazard Curves 136
6.6.9 Compute Load and Resistance Factors 137
6.6.9.1 Compute Demand and Capacity Factors 137
6.7 VALIDATION OF DCFD ANALYSES 137
6.7.1 Comparison with Closed-Form Solutions 137
6.7.1.1 Base Case System 138
6.7.1.2 Results of Closed-Form Comparative Analyses 138
6.7.1.3 Purely Deterministic Analysis 139
6.7.1.4 Variation of IM Hazard Curve 140
6.7.1.5 Variation of Load Model 141
6.7.1.6 Variation of Response Model 142
6.7.1.7 Inclusion of Load Model Uncertainty 142
6.7.1.8 Inclusion of Response Model Uncertainty 143
6.7.1.9 Inclusion of Load and Response Model Uncertainty 144
6.7.1.10 Inclusion of Load Model, Response Model, and Capacity Uncertainty 145

6.7.1.11 Discussion 148
6.7.2 Incremental Testing of Multiple Components *149*
6.8 DISCUSSION 157

7 DESIGN FACTORS 159

7.1 INTRODUCTION 159
7.2 DESIGN FACTORS 159
7.3 PARAMETRIC ANALYSES 160
7.3.1 Base Case Conditions *160*
7.3.1.1 Structure and Pile Group 160
7.3.1.2 Loading Conditions 160
7.3.1.3 Uncertainty Levels 161
7.3.2 Ground Motion Hazards *161*
7.3.3 Base Case Response and Design Factors *163*
7.3.4 Effects of Local Seismicity *167*
7.3.5 Effects of Pile Group Size *172*
7.3.6 Effects of Initial Static Loads *174*
7.3.7 Effects of Structural Behavior *176*
7.3.8 Effects of Load Measure Uncertainty *178*
7.3.9 Effects of Engineering Demand Parameter Uncertainty *179*
7.3.9.1 Effect of Soil Type 180
7.4 DISCUSSION 182

8 SUMMARY, CONCLUSIONS, AND RECOMMENDATIONS FOR FUTURE RESEARCH 183

8.1 INTRODUCTION 183
8.2 SUMMARY 183
8.3 CONCLUSIONS 186
8.4 RECOMMENDATIONS FOR FUTURE RESEARCH 190

9 REFERENCES 193

LIST OF FIGURES

2.1 Load vs. vertical pile head settlement from load tests on piles in (a) clay and (b) sand 9
2.2 Schematic illustration of Davisson procedure for evaluating vertical capacity from pile load test 10
2.3 Normalized *t-z* curve for clay and sand 11
2.4 Normalized *Q-z* curve for clay and sand 11
2.5 Static and dynamic BNWF Models: (a) BNWF Model (after Shin, 2007), and (b) Dynamic BNWF model 14
2.6 Back-calculated p-y curves for sand from field tests: (a) static, and (b) cyclic 16
2.7 Back-calculated p-y curves for stiff clay from field tests: (a) static, and (b) cyclic 16
2.8 Cyclic response of a rigid pile in soft clay: (a) test setup, and (b) cyclic p-y curves of clay 17
2.9 Shape of passive wedge controlling ultimate resistance at shallow depths 19
2.10 Coefficients as functions of friction angle 20
2.11 2014 Comparison of the ultimate soil resistance of soft clay (after Matlock, 1970), and sand 21
2.12 Soil zones of influence for a laterally loaded pile group 23
2.13 Schematic of pile alignment in a group 23
2.14 *p*-multipliers design curves 24
2.15 Schematic of rotational soil resistance due to pile cap rotation 25
2.16 2-D and 3-D lateral earth pressure wedges 26
2.17 Schematic illustration of equivalent springs and dashpots for modeling vertical/horizontal/ rotational impedance of pile group 27
2.18 Dynamic stiffness and damping behavior of pile groups subjected to (a) lateral load at pile cap, and (b) overturning moment applied to pile cap 28

3.1 Schematic illustration of the progression that leads to earthquake losses 32
3.2 Illustration of mean and nominal loads and resistances 39
3.3 An illustration of the probability of failure for normally distributed variables 40
3.4 An illustration of the effect of the dispersion of resistance on factor of safety 41
3.5 Illustration of the effect of the expected value and dispersion of resistance on factor of safety 41
3.6 An illustration of a probability density function $\boldsymbol{R-Q}$. 44
3.7 Schematic illustration of process by which response, damage, and loss are predicted 52
3.8 Combinations of earthquake hazard and performance levels proposed by Vision 2000 53
3.9 Schematic illustration of modified performance-based framework 56

4.1 Schematic illustration of forces and moments acting on pile cap. 62
4.2 Schematic of BNWF model with interface springs 64
4.3 Site layout and test set up 66
4.4 Lateral load vs. deflection for a single pile in sand 67
4.5 Bending moment vs. depth for a single pile in sand 67
4.6 Load vs. deflection for single pile and pile group by row 68
4.7 Typical *p-y* curves by row position for piles in group 68
4.8 Comparison of experimental and computed *p-y* curves for a single pile 69
4.9 Plot of pilehead load vs. deflection for the second trailing row of a 3x3 pile group – comparison of OpenSees response (OS BR) to measured response (BR) 69
4.10 Plot of pilehead load vs. deflection for the first trailing row of a 3x3 pile group – comparison of OpenSees response (OS MR) to measured response (MR) 70
4.11 Plot of pilehead load vs. deflection for the leading row of a 3x3 pile group – comparison of OpenSees response (OS LR) to measured response (LR) 70
4.12 Plot of bending moment vs. depth for the second trailing row of a 3x3 pile group – comparison of OpenSees response (OS BR) to measured response (BR) 71
4.13 Plot of bending moment vs. depth for the middle row of a 3x3 pile group – comparison of OpenSees response (OS MR) to measured response (MR) 71

4.14 Plot of bending moment vs. depth for the leading row of a 3x3 pile group – comparison of OpenSees response (OS LR) to measured response (LR) 72
4.15 Schematic drawing and test setup for single pile, two-pile bents, and two span bridge..... 72
4.16 Superstructure acceleration time histories for Bent-M2 obtained from centrifuge test and numerical simulations 73
4.17 Maximum pile bending moments for Bent-M2 obtained from centrifuge test and numerical simulations 74
4.18 Centrifuge and OpenSees bridge deck acceleration time histories at three bent locations for Northridge event, $a_{max} = 0.25g$ 75
4.19 Centrifuge and OpenSees pile bending moments for Northridge event, a_{max} = 0.25g 75

5.1 Schematic illustration of substructuring process used to separate response analysis into structural and geotechnical components 78
5.2 Schematic illustration of OpenSees pile group model showing only three loading components and one plane of *p-y* elements..... 81
5.3 Shear wave velocity profiles for sand and clay soil profiles 82
5.4 Normalized vertical load response for 3x3, 5x5, and 7x7 pile groups: (a) sand profile, (b) clay profile 86
5.5 Normalized horizontal load response for 3x3, 5x5, and 7x7 pile groups: (a) sand profile, (b) clay profile..... 87
5.6 Normalized overturning moment response for 3x3, 5x5, and 7x7 pile groups: (a) sand profile, (b) clay profile 87
5.7 Response spectra for fault normal components of ground motions 89
5.8 Response spectra for fault parallel components of ground motions..... 90
5.9 Response spectra for vertical components of ground motions. 90
5.10 Response of pile groups subjected to harmonic vertical loading 93
5.11 Response of pile groups subjected to harmonic lateral loading 94
5.12 Response of pile groups subjected to harmonic overturning moment 94
5.13 Settlement-rotation (*w*-□$_x$) response of pile groups subjected to harmonic overturning moments under different levels of static, vertical loading 95
5.14 Response of pile group to transient motions. Static Load Case 1: Q_{ns} = 0.2 and V_{ns} = 0.0 and Static Load Case 2: Q_{ns} = 0.2 and V_{ns} = 0.33 96
5.15 Response of pile group to transient motions. Static Load Case 1: Q_{sn} = 0.2 and V_{sn} = 0.0 and Static Load Case 2: Q_{sn} = 0.2 and V_{sn} = 0.33 97
5.16 Response of pile groups in sand profile with Q_{sn} = 0.40, V_{sn} = 0.33, and M_{sn} = 0.30 to earthquake loading: (a) peak vertical displacement vs. peak vertical load, and (b) normalized vertical displacement vs. normalized vertical load 98
5.17 Illustration of the effects of structural period on normalized response of 5x5 pile group in sand profile: (a) vertical displacement vs. vertical load, (b) horizontal displacement vs. horizontal load, and (c) rotation vs. overturning moment 99
5.18 Illustration of the effects of structural period on normalized response of 5x5 pile group in clay profile: (a) vertical displacement vs. vertical load, (b) horizontal displacement vs. horizontal load, and (c) rotation vs. overturning moment..... 100
5.19 Illustration of the effects of pile group size on normalized response of square pile groups in sand profile: (a) vertical displacement vs. vertical load, (b) horizontal displacement vs. horizontal load, and (c) rotation vs. overturning moment 101
5.20 Illustration of the effects of structural period on normalized response of square pile groups in clay profile: (a) vertical displacement vs. vertical load, (b) horizontal displacement vs. horizontal load, and (c) rotation vs. overturning moment 102
5.21 Normalized response of 3x3, 3x5, and 3x7 pile groups in sand profile: (a) vertical displacement vs. vertical load, (b) horizontal displacement vs. horizontal load in long direction, (c) horizontal displacement vs. horizontal load in short direction, (d) rotation vs. overturning moment about short axis, and (e) rotation vs. overturning moment about long axis. 103
5.22 Effects of yield moment on loads and moments applied to pile cap 104

5.23 Computed response of 5x5 pile group supporting T_o = 0.5 sec structure in sand profile for linear column and elasto-plastic column with three yield moments 105
5.24 Computed response of 5x5 pile group supporting T_o = 0.5 sec structure in clay profile for linear column and elasto-plastic column with three yield moments 106
5.25 Computed response of 5x5 pile group in sand profile for three levels of pile cap passive spring stiffness 107
5.26 Computed response of 5x5 pile group in sand profile for three friction angles 108
5.27 Computed response of 5x5 pile group in clay profile for three levels of undrained shear strength 109
5.28 Initial model for prediction of normalized horizontal displacement, u_n, as a function of normalized horizontal load, V_{xn} 111
5.29 Variation of residuals with secondary predictive variables for initial horizontal displacement, u_n, model: (a) vertical load, Q_n, (b) perpendicular horizontal load, V_{yn}, (c) moment about perpendicular axis, M_{yn}, and (d) moment about parallel axis, M_{xn}. 112
5.30 Variation of residuals with secondary predictive variables for final horizontal displacement, u_n, model: (a) vertical load, Q_n, (b) parallel horizontal load, V_{xn}, (c) perpendicular horizontal load, V_{yn}, (d) moment about perpendicular axis, M_{yn}, and (e) moment about parallel axis, M_{xn}. 113

6.1 Schematic illustration of load measure hazard curves for cases of no uncertainty, uncertainty in load given ground motion intensity, and uncertainties in load given ground motion intensity and capacity 123
6.2 Schematic illustration of main components of pgDF. 131
6.3 Comparison of closed-form and numerical solutions for deterministic base case vertical settlement problem and relatively coarse settlement increment 140
6.4 Comparison of closed-form and numerical solutions for deterministic base case problem with different *IM* hazard curves 141
6.5 Comparison of closed-form and numerical solutions for deterministic base case problem with different *IM-LM* relationships 141
6.6 Comparison of closed-form and numerical solutions for deterministic base case problem with different *LM-EDP* relationships 142
6.7 Comparison of closed-form and numerical load and response curves and load, resistance, demand, and capacity factors including the effects of load model uncertainty. 143
6.8 Comparison of closed-form and numerical load and response curves and load, resistance, demand, and capacity factors including the effects of response model uncertainty. 144
6.9 Comparison of closed-form and numerical load and response curves and load, resistance, demand, and capacity factors including the effects of both load and response model uncertainty 145
6.10 Comparison of closed-form and numerical load and response curves and load, resistance, demand, and capacity factors including the effects of force capacity uncertainty 146
6.11 Comparison of closed-form and numerical load and response curves and load, resistance, demand, and capacity factors including the effects of response capacity uncertainty. 147
6.12 Comparison of closed-form and numerical load and response curves and load, resistance, demand, and capacity factors including the effects of both force and response capacity uncertainty. 148
6.13 Results of single load component (i.e., $w = f(Q)$) analysis with no uncertainty. 150
6.14 Results of dual load component (i.e., $w = f(Q,V_x)$) analysis with no uncertainty. 151
6.15 Results of full load measure vector (i.e., $w = f(Q,V_x,V_y, M_x, M_y)$) analysis with no uncertainty. . 152
6.16 Results of analyses with inclusion of uncertainty in *IM-LM* relationship (β_I = 0.30). 153
6.17 Results of analyses with inclusion of uncertainty in *LM-EDP* relationship (β_R = 0.50). 154
6.18 Result of analyses with uncertainty in force capacity included along with uncertainties in force and response 155
6.19 Result of analyses with uncertainty in force capacity and response capacity included with uncertainty in force and response 156

6.20 Result of analyses with uncertainty in static and reference loads, force, response, force capacity, and response capacity 157

7.1 Spectral acceleration hazard curves for selected cities in California and Washington 163
7.2 Hazard curves for vertical load and settlement for base case system in sand profile located in San Francisco. 164
7.3 Load and resistance factor curves, and demand and capacity factor curves for base case system in sand profile located in San Francisco 165
7.4 *LM* hazard curves for base case analysis of San Francisco site 166
7.5 *EDP* hazard curves for base case analysis of San Francisco site. 166
7.6 Load and resistance factors from base case analysis of San Francisco site 167
7.7 Demand and capacity factors from base case analysis of San Francisco site 167
7.8 Hazard curves for horizontal load and lateral displacement for Eureka 168
7.9 Hazard curves for horizontal load and lateral displacement for Irvine 168
7.10 Load and resistance factors and demand and capacity factors for lateral loads and displacements at Eureka 169
7.11 Load and resistance factors and demand and capacity factors for lateral loads and displacements at Irvine 169
7.12 Hazard curves for horizontal load and lateral displacement for Aberdeen 170
7.13 Hazard curves for horizontal load and lateral displacement for Seattle 170
7.14 Load and resistance factors and demand and capacity factors for lateral loads and displacements at Aberdeen 170
7.15 Load and resistance factors and demand and capacity factors for lateral loads and displacements at Seattle 170
7.16 Illustration of reduction of demand factor with increasing ground motion hazard curve slope. 172
7.17 Effect of pile group size on vertical load hazard curves 172
7.18 Vertical load and resistance factors for pile groups of different sizes 172
7.19 Effect of pile group size on settlement hazard curves 173
7.20 Settlement displacement demand and capacity factors for pile groups of different sizes 173
7.21 Effect of pile group size on lateral load hazard curves 174
7.22 Lateral load and resistance factors for pile groups of different sizes 174
7.23 Effect of pile group size on lateral displacement hazard curves 174
7.24 Lateral displacement demand and capacity factors for pile groups of different sizes 174
7.25 Effects of static loads on lateral displacement hazard curves 175
7.26 Demand and capacity factors for base case system subjected to static load cases defined in Table 7.5 175
7.27 Variation of lateral load with spectral acceleration for different nonlinear structural models ... 176
7.28 Effects of structural response nonlinearity on lateral load hazard curves 177
7.29 Effects of structural response nonlinearity on load and resistance factors 177
7.30 Effects of structural response nonlinearity on lateral displacement hazard curves 177
7.31 Effects of structural response nonlinearity on demand and capacity factors 177
7.32 Lateral load hazard curves for different levels of uncertainty in lateral load given spectral acceleration 178
7.33 Load and resistance factors for different levels of uncertainty in lateral load given spectral acceleration 178
7.34 Lateral displacement hazard curves for different levels of uncertainty in lateral load given spectral acceleration 179
7.35 Demand and capacity factors for different levels of uncertainty in lateral load given spectral acceleration 179
7.36 Lateral load hazard curves for different levels of uncertainty in lateral displacement 179
7.37 Load and resistance factors for different levels of uncertainty in lateral displacement 179
7.38 Lateral displacement hazard curves for different levels of uncertainty in lateral displacement. 180
7.39 Demand and capacity factors for different levels of uncertainty in lateral displacement 180

7.40 Hazard curves for vertical load and settlement for base case system in clay profile located in San Francisco. 181
7.41 Load and resistance factor curves, and demand and capacity factor curves for base case system in clay profile located in San Francisco 181

LIST OF TABLES

2.1	Representative values of ϵ_{50} for normally consolidated clay	18
2.2	Representative values of ϵ_{50} for overconsolidated clays	18
3.1	Factor of safety on ultimate axial geotechnical capacity based on level of construction control	37
3.2	Relationship between Reliability Index and Probability of Failure	44
3.3	Coefficient of variation (C.O.V.) for typical geotechnical parameters	48
5.1	Characteristics of model bridge structure	79
5.2	Sand profile reference loads	84
5.3	Clay profile reference loads	84
5.4	Sand profile reference displacements	85
5.5	Clay profile reference displacements	85
5.6	Initial static load states used in analyses	88
5.7	Ground motions used in response analyses	91
5.8	Final predictive models for normalized displacements/rotations	114
6.1	Resistance factors for pile capacity by dynamic analysis and static load tests	117
7.1	Base case *IM-LM* relationships	161
7.2	Base case uncertainty levels	161
7.3	Spectral acceleration (T = 0.5 sec) values (g) for 16 cities in California and Washington (g).	162
7.4	Coefficients for idealized power law approximation of spectral acceleration hazard curve	171
7.5	Static load cases	174

1 Introduction

Pile foundations are commonly used to support heavy loads when near-surface soils are too weak or too compressible to support the loads without excessive settlement or lateral deflection. Bridges are often located at sites where weak and compressible soils exist, and are therefore frequently supported by pile foundations. The behavior of pile foundations can be quite complicated, and their design must consider a variety of potential loading conditions. Pile foundation design seeks to ensure that the foundation has adequate capacity to ensure stability under all potential loading conditions.

Pile foundations can be subjected to both vertical and lateral loads, and to overturning moments. These loads may exist under static conditions, depending on the site topography, bridge type, and bridge design. The same components may also be applied dynamically due to traffic loading, impact loading, and natural hazards. Among the most important of these natural hazards are earthquakes. Earthquakes have caused damage to bridges in many past earthquakes, and a great deal of attention has been paid to the seismic design of bridges. Pile foundations must also be designed to resist earthquake loads without exceeding the supporting capacity of the soil or undergoing excessive deflection or rotations.

1.1 PURPOSE OF RESEARCH

The purpose of this research was to develop a framework in which new concepts of performance-based earthquake engineering could be used to guide the development of load and resistance factors for force-based seismic design of pile foundations, and to develop procedures for computing analogous factors for displacement-based design. The performance-based approach is based on a framework developed by the Pacific Earthquake Engineering Research (PEER) Center over the past 10-12 years. This framework has been shown to produce seismic evaluations that are more complete and consistent when applied in areas of different seismicity. These characteristics have great potential benefit in the development of reliability-based design procedures since they account for all anticipated levels of ground shaking, rather than single levels that most existing design procedures are based upon. By considering the effects of weak ground motions that occur relatively frequently and strong ground motions that occur only very rarely, the performance-based framework allows differences in local seismicity to be considered and accounted for in the design process. The application of the performance-based approach has shown that consistent application of conventional procedures for design and evaluation can lead to inconsistent actual seismic demand and response levels in different seismic environments.

The PEER framework for performance-based earthquake engineering is inherently probabilistic. It explicitly recognizes and accounts for uncertainties in earthquake ground

motions, system response to those motions, physical damage resulting from the response, and losses due to the physical damage. All of these quantities and the relationships between them are uncertain. In the case of pile foundations, the relationships are complicated by the number of load and response quantities that must be considered, and by the interdependence of those quantities on each other. A pile foundation can be considered to be subjected to five significant components of loading – vertical loads, horizontal loads in two orthogonal directions, and overturning moments about two orthogonal horizontal axes. Torsion is not considered to be significant for individual pile foundations. These five components of loading produce five components of response – vertical displacement, lateral displacements in two orthogonal directions, and rocking rotations about two orthogonal axes. Each component of response, however, is influenced by all five components of loading. This situation required modification of the basic PEER framework to render the reliability-based design problem tractable, and to develop a numerical analysis capable of computing reliability-based design factors.

Seismic design can be accomplished in a number of different ways. Historically, design has been based on loads and resistances, and reliability-based design has commonly been implemented using a load and resistance factor approach. For essentially static loading conditions, time-invariant load and resistance factors can be developed for a given reliability index, or probability of failure. For seismic design, however, load and resistance factors must account for the variability in loading that can occur – high levels of loading can occur in strong earthquakes that occur relatively rarely, and lower levels of loading can occur in weaker earthquakes that occur more frequently. To develop a design that considers all potential levels of loading and their likelihoods of occurrence in a particular area, performance-based concepts can be used to combine the results of probabilistic seismic hazard analyses with probabilistic structural and foundation response analyses to predict a mean annual rate of failure, which is approximately equal to an annual probability of failure. Load and resistance factors consistent with an annual probability of failure can then be determined.

1.2 ORGANIZATION OF REPORT

The report is organized into eight chapters with additional data provided in appendices. Following this introductory chapter, Chapter 2 presents a brief review of the behavior of pile foundations and the manner in which their capacities and load-deformation behavior is usually determined. Chapter 3 describes different approaches to the evaluation of seismic response and to seismic design, and introduces the PEER performance-based earthquake engineering framework. The chapter also introduces a modification of the PEER framework that allows it to be applied to different bridge and foundation systems in a computationally feasible way. Chapter 4 describes the numerical model used to predict the response of pile foundations in this research project. The validation of a pile group model developed using the finite element program, OpenSees, against full-scale and model pile tests is described. Chapter 5 describes the typical behavior of the OpenSees model under various dynamic loading conditions. Numerous analyses of pile groups subjected to five components of dynamic loading were performed with different levels of initial (static) loading, different levels of dynamic loading, and different structural conditions. The results of these analyses, and their characterization through a statistical model, are described. The development of procedures for computing force-based load and resistance factors and displacement-based demand and capacity factors within a

performance-based earthquake engineering framework is described in Chapter 6. Chapter 6 also describes a computer program developed to implement the performance-based framework, and shows how it matches theoretical behavior for conditions where theoretical solutions exist. Chapter 7 applies the computer program to a number of different foundation design situations in different seismic environments to illustrate the effects of different factors on load, resistance, demand, and capacity factors. Finally, Chapter 8 provides a summary of the work, conclusions, and recommendations for future developments.

2 Pile Foundations

2.1 INTRODUCTION

Pile foundations are commonly used to support loads that are sufficiently heavy that they cannot be supported by shallow foundations without excessive settlement, lateral movement, or rotation. Piles are commonly used to support bridge foundations including individual piers and/or abutments. They are occasionally used individually, but are more commonly driven in groups that are subsequently connected by a common pile cap to which structural loads are applied. This chapter provides a brief description of pile foundations and their design.

2.2 SINGLE PILE BEHAVIOR

Individual piles can support considerable vertical loads applied to its head when installed in competent soils. An individual pile may be loaded axially, laterally, and or with an overturning moment. A number of procedures by which the response of individual piles to various combinations of these loads are available.

2.2.1 Axial (Downward) Load Response

Piles are most commonly used to resist downward-acting vertical loads. Such loads typically result from gravity and may be divided into dead and live loads. These loads are resisted by a combination of bearing pressure on the base of the pile (tip resistance) and shear stress along the vertical sides of the pile (skin resistance). Several procedures are available for estimating the capacity of a pile foundation – the capacity may be estimated based on the properties of the pile and soil in which it is embedded, on the basis of recorded driving resistance during installation, and on the basis of pile load tests. These different procedures have different levels of accuracy and result in capacities with different levels of uncertainty.

2.2.1.1 Capacity Estimation from Pile and Soil Properties

Mobilization of pile capacity is a process that involves mobilization of the shear strength of the soil beneath and along the sides of the pile. As such, procedures for estimation of pile capacity based on pile geometry and soil strength were developed in the early days of foundation engineering and are still used in practice today. These procedures are generally divided into those addressing tip resistance, Q_t, and skin resistance, Q_s, so that the total capacity, Q_{ult}, is expressed as the sum

$$Q_{ult} = Q_t + Q_s \tag{2.1}$$

The tip resistance of a pile is a function of the tip bearing pressure and the cross-sectional area of the tip of the pile. The tip resistance can be estimated from deep bearing capacity theory using an expression of the general form

$$Q_t = c\,N_c^* + q'_v\,N_q^* \tag{2.2}$$

where c is the cohesive strength of the soil, q'_v is the original vertical effective stress in the soil at a depth equal to that of the tip of the pile, and N_c^* and N_q^* are bearing capacity factors. The bearing capacity factors are functions of the friction angle of the soil and the geometry of the failure surface; different researchers have proposed different failure mechanisms with different failure surface geometries, so a number of different expressions for N_c^* and N_q^* are available in the literature. Skin resistance results from the shear strength of the interface between the perimeter surface of the pile and the adjacent soil. The pile/soil interface is assumed to have strength characteristics similar to that of soil and is typically modeled as behaving according to the Mohr-Coulomb failure criterion. The unit skin resistance, f_s, therefore, can be described as

$$f_s = c_a + \sigma'_h \tan\delta \tag{2.3}$$

where c_a is the adhesion, σ'_h is the horizontal effective stress, and δ is the pile-soil interface friction angle. The adhesion can be estimated in different ways, the most common being by means of the so-called α method in which

$$c_a = \alpha c \tag{2.4}$$

where α is a factor that depends on c and c is the cohesive strength of the soil on the interface. Expressions for α can be found in numerous foundation design textbooks (e.g., Coduto, 2001; Salgado, 2007). The horizontal effective stress, σ'_h, is usually taken as being proportional to the vertical effective stress with the constant of proportionality depending on the type of pile; piles that displace a relatively large volume of soil (displacement piles), such as concrete piles, have a higher constant of proportionality than soils that displace relatively little soil (non-displacement piles) such as H-piles. The interface friction angle is taken as being proportional to the soil friction angle, ϕ, with the constant of proportionality depending on the nature of the pile material (i.e., steel, concrete, timber, etc.).

Estimates of axial load capacity based on pile and soil shear strength characteristics have been found to be significantly uncertain when compared against the results of pile load tests. As a result, such capacity estimates have been treated with relatively low resistance factors in LRFD design procedures.

2.2.1.2 Capacity Estimation from Driving Resistance

The process of driving a pile into the ground requires at least momentary exceedance of the instantaneous pile capacity to allow penetration to occur. This fact has been exploited in the development of several forms of pile capacity estimation procedures. The earliest such approach resulted in the Engineering News-Record, or *ENR*, formula for allowable load

$$Q_{all} = \frac{W_r h}{FS(s + C)} \tag{2.5}$$

where W_r is the weight of the hammer ram, h is the height of ram drop, FS is the factor of safety applied in an allowable strength design (ASD) format, s is the penetration per blow of the pile, and C is an energy loss term (note that Q_{all} and W_r must be in the same units of force, and that h, s, and C must be in the same units of displacement). A factor of safety of 6 was proposed for use with the original *ENR* formula.

A number of other pile driving formulae have been proposed based on calibrations against various datasets of pile driving resistance and load test results. The FHWA modified the original Gates (1957) formula to obtain the expression

$$Q_{ult} = 1.75\sqrt{E}\log(10N) - 100 \tag{2.6}$$

where E is the developed hammer energy (kinetic energy at point of impact) and N is the number of blows per inch of pile penetration. Finding that the FHWA formula overestimated pile capacity at low capacity levels, Allen (2005a) developed the WSDOT pile driving formula, which can be expressed as

$$Q_{ult} = 6.6F_{eff}E\ln(10N) \tag{2.7}$$

where F_{eff} is a hammer efficiency factor, E is developed energy at impact, and N is the penetration resistance expressed in hammer blows/inch averaged over the last four inches of driving. The value of F_{eff} is different for different types of hammer (e.g., 0.55 for air/steam, 0.37 for open-ended diesel hammers with concrete and timber piles), 0.47 for open-ended diesel hammers and steel piles, and 0.35 for all piles driven with a closed-ended diesel hammer. The WSDOT formula has also been expressed as

$$Q_{ult} = F \cdot E\ln(10N) \tag{2.8}$$

where F is a factor depending on the same quantities as F_{eff}. Details on the development of the WSDOT pile driving formulae, and values of the various factors, can be found in Allen (2005a, 2007).

When compared with the results of pile load tests, pile capacity estimates from driving resistance have been shown to be inaccurate relative to other available capacity estimation procedures. Although attractive in principle, the methods do not properly account for all factors affecting pile driving and combinations of pile-soil conditions that differ from those upon which the various driving resistance-based formulae are based. The driving formulae do not account for pile setup, variability in rated pile driving efficiency, cushion characteristics (and changes in those characteristics during driving), pile flexibility, and dynamic effects.

2.2.1.3 Capacity Estimation from Wave Equation Analysis

Pile driving formulae assume the pile to be rigid so that it moves equally along its entire length. Piles are not rigid and the sharp nature of the contact between the hammer and the pile means that part of the pile may be moving while another part is not. The flexibility of the pile, and its effect on driving, can be accounted for by simulating the driving process using wave equation analysis.

In a wave equation analysis, the pile is divided into a series of discrete masses connected by springs and dashpots of stiffness consistent with the modulus of elasticity and damping characteristics of the pile. The masses are connected to the surrounding soil by nonlinear (frequently elastic-perfectly plastic) springs and dashpots that simulate the interaction between the pile and the soil during driving. The characteristics of the springs and dashpots are related to the properties of the soil.

The pile driving process is simulated by imposing a velocity pulse equal to that imposed on the pile by the hammer at the top of the pile. The pulse travels as a wave down the pile with resistance being provided by inertia of the masses and relative pile-soil spring deflections. If the resistance in the upper portion of the pile is high, the amplitude of the wave reaching the lower part of the pile will be smaller due to the work done by movement of the pile, as would actually occur in the field. By computing the response of the discretized pile elements, the displacements and mobilized resistances of all elements can be computed for each blow of the hammer. In this manner, the wave equation analysis simulates the actual driving process in a manner that makes its predictions of capacity more accurate than those of pile driving formulae which assume rigid-body behavior of the pile. Wave equation analyses also allow estimation of driving stresses under various conditions, which can aid in selection of pile driving hammers, cushions, etc. to optimize pile drivability.

2.2.1.4 Capacity Estimation from Pile Driving Analysis

A more sophisticated method of pile capacity estimation based on driving characteristics can be used when a pile is instrumented prior to driving. By placing an accelerometer and strain gauge near the head of the pile, force and velocity signals can be computed from the measured strain and acceleration values. The Case method makes certain assumptions about the manner in which the soil resistance is mobilized and uses a wave propagation approach to compute a total capacity from the amplitudes of the downward-traveling stress wave (just after the hammer strike) and the upward-travelling stress wave that reflects off the bottom of the pile. By assuming that all of the capacity comes from the base of the pile, the dynamic component of the total capacity can be computed and subtracted from the total capacity, thereby yielding the desired static capacity. The Case method, therefore, provides an estimated capacity that reflects the driving conditions encountered by a specific pile in the field.

The Case method makes simplifying assumptions about the pile-soil behavior in order to compute a pile capacity from stress wave amplitude measurements. By combining the wave measurements with a wave equation analysis, the entire measured force and velocity waveforms can be used to identify a distribution of skin and tip resistances that would produce the same force and velocity waveforms. The capacity predicted by this more sophisticated approach has been shown to match measured capacities more accurately than the previously described procedures. A computer program, CAPWAP, is generally used to perform the waveform-matching calculations.

2.2.1.5 Capacity Estimation from Pile Load Test Results

The most reliable procedure for estimating the capacity of a single pile is to perform a field load test on the pile at the site of interest. Pile load tests involve applying an increasing vertical load to a pile and measuring the downward movement of the head of the pile. Various forms of

instrumentation, such as strain gauges, may be installed on the pile to aid in the evaluation of load transfer, but are not always used. The load-deflection behavior of the pile is measured and recorded. In some cases, the pile is loaded to "failure" (i.e., unacceptably large displacements) and in other cases to some multiple of the previously estimated capacity as a "proof" test. Examples of load-deflection behavior measured in load tests of piles in clay and sand profiles are shown in Figure 2.1.

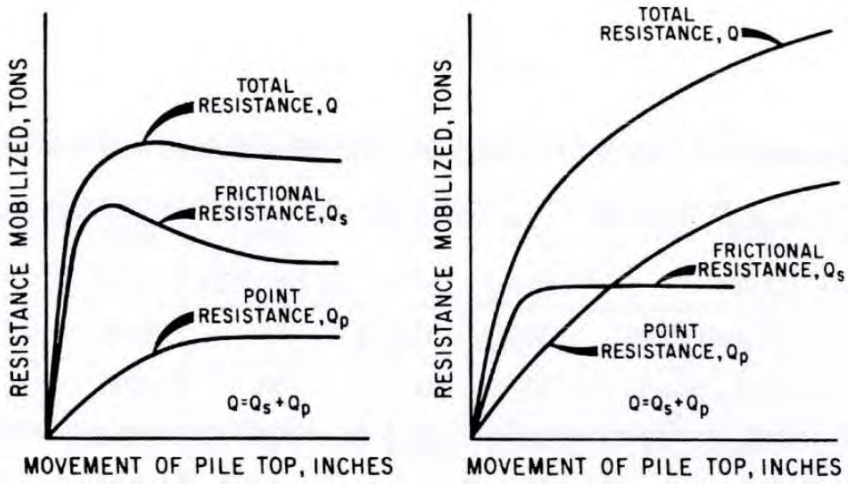

Figure 2.1. Load vs. vertical pile head settlement from load tests on piles in (a) clay and (b) sand (after Vijayvergiya, 1997).

Determination of pile capacity from load test results is not always straightforward. The results of many load tests show load-deflection diagrams with an initially linear portion followed by the onset of nonlinear behavior. The slope of the load-deflection diagram decreases as the load level increases. As shown in Figure 2.1, the slope drops more quickly for the load test in the clay profile than in the sand profile – this type of behavior is characteristic of deep foundations in clay and sand. A pile in clay will generally exhibit a maximum resistance after which it cannot resist significant additional load and may, as in Figure 2.1(a), even suffer some reduction in resistance. A pile in sand, on the other hand, will show a slowly increasing resistance to pile deflection levels that are well beyond those tolerable in typical applications.

Because of this behavior, procedures for evaluation of pile capacity based on pile head settlement during load tests are commonly utilized. The most common approach of this type is the Davisson procedure, which defines the point of "failure" (i.e., of capacity mobilization) as the intersection of an offset, sloping line with the load-deflection curve as shown in Figure 2.2. The line intercepts the settlement axis at a value related to the diameter of the pile and is inclined at a slope that reflects the elastic compression of the pile itself. The failure point is used to define the failure load, Q_f, and failure displacement, w_f. It should be noted that the failure load is displacement-related and should not be taken to imply that collapse, or plunging, of the pile is necessarily imminent.

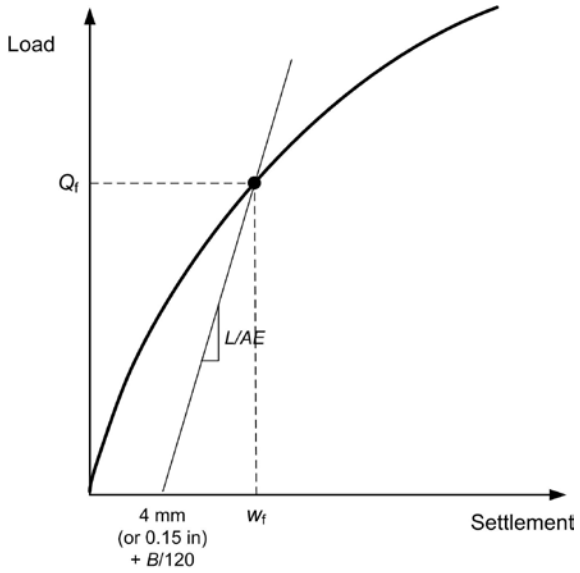

Figure 2.2. Schematic illustration of Davisson procedure for evaluating vertical capacity from pile load test.

2.2.1.6 Mobilization of Capacity

The preceding sections described a number of procedures by which the capacity of pile foundations can be estimated. Since the capacity develops as the shear strength of the soil adjacent to and below the pile is mobilized, some level of pile displacement occurs as the soil strains in response to the stresses imposed on it. As a result, the pile must move relative to the soil to mobilize its capacity.

The amount of pile movement required to mobilize skin and tip resistance is different. Mobilization of skin resistance occurs as a result of straining in a thin zone of soil around the perimeter of the pile. Since the zone is so thin, very little pile displacement (typically less than 1 cm), is required to produce shear strains sufficient to mobilize the skin resistance. Mobilization of the tip resistance involves deformation of the soil in a relatively large zone of soil beneath the tip of the pile. In order to develop sufficient strain to mobilize the shear strength of the soil throughout this zone, a relatively large amount of pile tip displacement, typically on the order of 10% of the pile diameter, is required.

The mobilization of skin resistance for pile foundations can be modeled using the *t*-*z* method. In a manner analogous to the representation of lateral resistance by *p*-*y* curves, the development of skin resistance can be modeled by *t*-*z* curves that relate unit skin resistance to pile displacement. A number of researchers have proposed procedures for developing *t*-*z* curves. According to Vijayvergiya (1997), the mobilized skin resistance in sands and clays can be expressed by

$$f = f_{\max}\left(2\sqrt{\frac{z}{z_c}} - \frac{z}{z_c}\right) \tag{2.9}$$

where f is the unit skin friction, f_{max} is the maximum unit friction obtained from Equation 2.3, and z_c is the critical displacement corresponding to f_{max}. The critical displacement, z_c, is usually between 0.2 and 0.3 inches for both sand and clays. A normalized *t-z* curve based on this approach is shown in Figure 2.3.

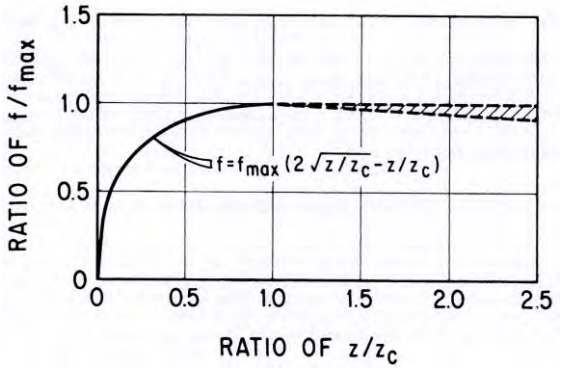

Figure 2.3 Normalized *t-z* curve for clay and sand (after Vijayvergiya, 1997)

The mobilization of tip resistance can be modeled by discrete elements whose load-displacement behavior is described by Q-z curves. Vijayvergiya (1997) proposed that the mobilized tip resistance in sands and clays could be expressed by a cube-root relationship up to the point of full capacity mobilization, i.e.,

$$Q = \left(\frac{z}{z_c}\right)^{1/3} Q_{max} \le Q_{max} \tag{2.10}$$

where q is the tip resistance for a value of z/z_c, Q_{max} is the maximum tip resistance obtained from Equation 2.8, and z_c is the critical displacement corresponding to Q_{max}. The critical displacement, z_c, is approximately 3% to 9% of the diameter for clays and sands (or 0.04*D* for clay to 0.06*D* for sand). A normalized *Q-z* curve is shown in Figure 2.4.

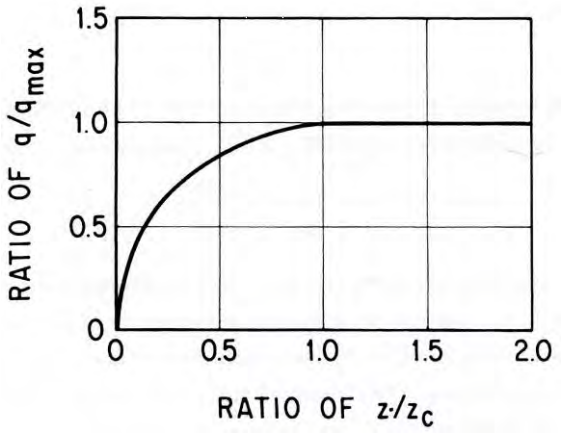

Figure 2.4 Normalized *Q-z* curve for clay and sand (after Vijayvergiya, 1997)

2.2.2 Axial (Uplift) Load Response

Piles may also be subjected to upward-acting loads. For bridge foundations, this situation normally occurs in piles near the edge of a group that is subjected to high overturning moments. The effect of the overturning moment is to increase the downward-acting loads on one side of a pile group while pulling upward on the piles on the opposite side of the group. When overturning moments are acting in two orthogonal directions, piles in the corners of a pile group may be subjected to significant upward-acting loads. If the upward-acting load is high enough and of long enough duration, the pile can be pulled out of the soil. Under earthquake loading conditions, when the overturning moments, and hence upward-acting loads, are transient, the momentary exceedance of pullout capacity will lead to increased rotation of the pile cap.

The capacity of a single pile to upward-acting loads is derived solely from its skin resistance. The bearing pressure due to the upward load would be negative and, although some suction could exist temporarily between the bottom of the pile and the soil immediately below it if the soil is saturated, it cannot be relied upon for design purposes. As a result, the pullout capacity is usually computed as the skin friction capacity reduced by a factor to account for the direction of loading.

2.2.3 Lateral Load Response

Piles can also be subjected to static and dynamic lateral loads. Static lateral loads may result from the structural configuration or the presence of sloping ground. Dynamic lateral loads can come from wind, traffic, water, and collisions in addition to earthquakes. Because piles are so much more flexible in bending than when subjected to axial loading, lateral load capacity is much more difficult to predict using the types of limit analysis approaches that have proven useful for prediction of axial capacity.

2.2.3.1 Lateral Load Capacity

Early analytical methods for designing laterally loaded foundations assumed that the foundations were perfectly rigid (i.e., infinite flexural stiffness, *EI*). Operating under this assumption, the required depth of embedment for lightweight foundations, such as those for streetlights or highway signs, can be calculated using the following equations according to the Uniform Building Code [UBC 1806.8.2] and the International Building Code [IBC 1805.7.2].

For the free-head condition, the minimum depth of embedment, $D_{\min}$, can be calculated by

$$D_{\min} = \frac{A}{2}\left(1+\sqrt{\frac{4.36h}{A}}\right) \tag{2.11}$$

where

$$A = \frac{2.34V}{S_1 B}$$

For fixed-head conditions, the required depth of embedment can be calculated as

$$D_{\min} = \sqrt{\frac{4.25Vh}{S_3 B}} \tag{2.12}$$

where V is the applied shear load, h is the vertical distance from the ground to the point of application, B is the foundation diameter, S_1 is the allowable soil pressure at $z = D_{\min}/3$, S_3 is the allowable soil pressure at $z = D_{\min}$, and z is the depth below the ground surface.

For many foundations, such as those that include long slender piles, the foundation does not behave perfectly rigidly, and a simple rigid analysis which neglects flexural bending in the pile is not accurate. Instead, the soil interaction problem is often modeled using non-rigid analytical techniques to model the lateral behavior of piles. The evaluation of the lateral capacity of piles involves soil-structure interaction in which the responses of both the pile and the soil must be evaluated in the same analysis. The behavior of the pile depends on soil resistance and soil resistance depends on the behavior of the pile.

2.2.3.2 Pile-Soil Interaction

Evaluation of the lateral load-deflection behavior of a pile foundation must consider the flexural rigidity of the pile, the response of the soil, and soil-pile interaction effects. Finite element methods that account for these aspects are used to analyze the pile response. Complete evaluation requires the use of (3-D) finite element analyses that include advanced constitutive models to capture soil response and robust contact elements to capture interaction effects. Complete finite element analyses can be computationally expensive. Instead, a simpler and more commonly used approach to model soil resistance is to use *p-y* method, also known as the Beam-on-Nonlinear-Winkler-Foundation (BNWF) method. Though simple, this method has worked well for predicting pile response and can be applied to seismic soil-pile interaction problems.

Beam-on-Nonlinear-Winkler-Foundation (BNWF) Models

In a typical BNWF model, as shown in Figure 2.5(a), the soil resistance is modeled by a beam supported by a series of independent horizontal nonlinear springs distributed along its length.

During an earthquake a pile will be subjected to both kinematic and inertial loads. Kinematic loads are imposed along the length of the pile by the displacement of the surrounding soil, and inertial loads are imposed on the top of the pile by the vibration of the structure. The soil motion near the pile, where nonlinear, inelastic soil-pile interaction occurs, is called near-field motion. The soil motion that occurs far enough from the pile to be uninfluenced by nonlinear, local interaction is called far-field or free-field motion. In a dynamic BNWF analysis, the free-field motion is provided by the soil column and the soil-pile interaction occurs at the interface springs. As shown in Figure 2.5(b), this type of analysis is called in a coupled analysis because the soil and pile are coupled together by interface springs.

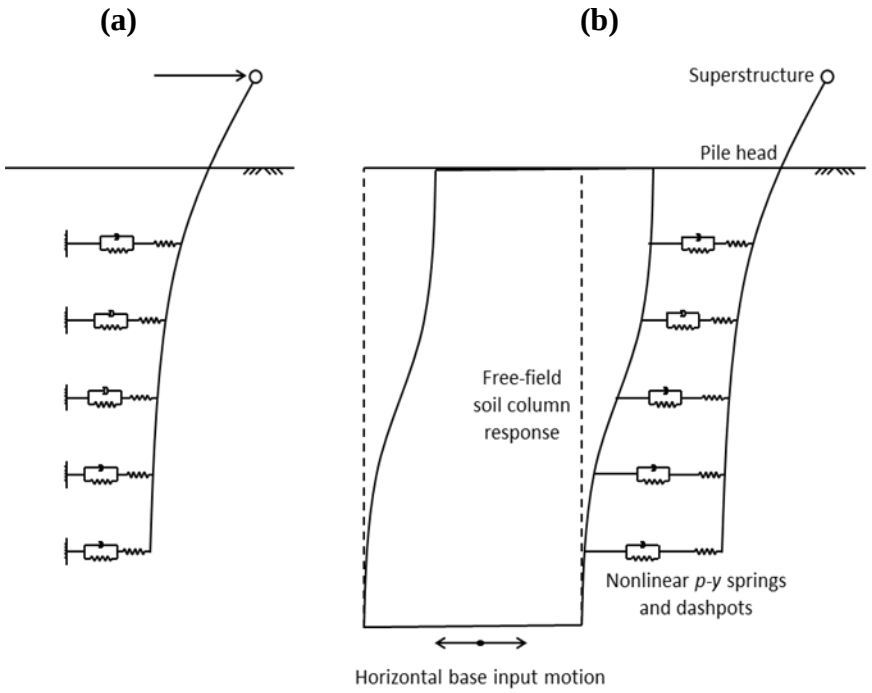

Figure 2.5 **Static and dynamic BNWF Models: (a) BNWF Model (after Shin, 2007), and (b) Dynamic BNWF model (after Boulanger et al., 1999)**

p-y Method of Analysis

The BNWF method is commonly called the *p-y* method, where *p* is the soil force per unit length and *y* is the lateral pile deflection relative to the soil movement. The BNWF model uses 1D structural elements to model the pile, and a series of independent nonlinear springs whose characteristics are based on *p-y* curves to model the soil. 1-D, 2-D, or 3-D finite difference analyses of the model can be performed. Figure 2.5 illustrates the model for a 1D analysis. Accurate *p-y* curves are a critical part of the definition of the BNWF model. For a model in which a pile is subjected to monotonic and cyclic loads at the pile head, *p-y* curves based on the initial stiffness and ultimate resistance of the soil are commonly used.

p-y Curves

Relationships between *p* and *y* can be developed based on field tests, laboratory model tests, and analytical solutions. The lateral response of piles can be described by combining these *p-y* relationships together with beam elements in BNWF models. The pile displacement and soil resisting force per unit length can be back-calculated from measured or calculated bending moments by double-differentiating and double-integrating the governing equilibrium differential equation. The basic beam-on-elastic-foundation equation is represented by

$$\frac{d^2M}{dz^2} + Q\frac{d^2y}{dz^2} - p = 0 \tag{2.13}$$

where M is the pile bending moment and z is depth. For the case of a pile with no vertical load, i.e., $Q = 0$

$$p = \frac{d^2}{dz^2} M(z) \tag{2.14}$$

Assuming linear bending behavior,

$$M = EI \frac{d^2 y}{dz^2} \tag{2.15}$$

so

$$p = EI \frac{d^4 y}{dz^4} \tag{2.16}$$

where EI is the flexural rigidity of the pile. When a lateral load test is performed, pairs of strain gauges can be used to measure the curvature, ϕ, at any point during the test. Therefore, values of p and y can be computed as

$$p = EI \frac{d^2 \phi}{dz^2} \tag{2.17}$$

and

$$y = \iint \phi dz \tag{2.18}$$

p-y Curves for Sand, Stiff Clay, and Soft Clay

Several different *p-y* criteria have been proposed for sand and clay. The main components of each criterion are the initial stiffness and ultimate soil resistance, which typically increase with depth and depend on soil type, loading condition, and location of groundwater. Figures 2.6 and 2.7 show static and cyclic *p-y* curves from sand and stiff clay profiles. For both sand and stiff clay, the cyclic *p-y* curves are softer and the ultimate lateral soil resistance is lower than for static loading. The main difference between the response of sand and stiff clay is the ultimate resistance in stiff clay decreases after a peak value has been reached.

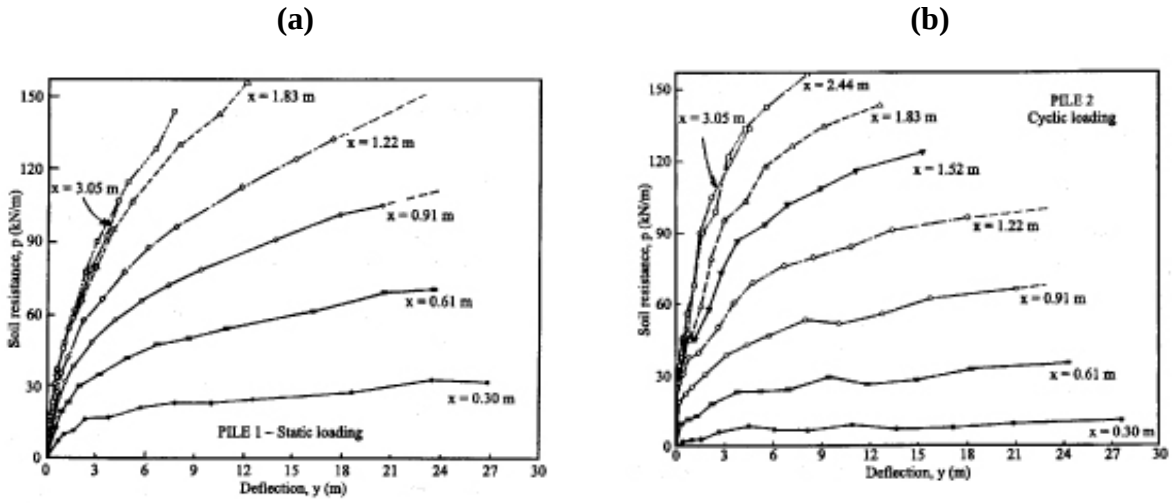

Figure 2.6 **Back-calculated p-y curves for sand from field tests: (a) static, and (b) cyclic (after Reese et al., 1975)**

Cyclic loading causes a softening of the *p-y* curves as shown by the *p-y* curves in Figure 2.8(b). Pile foundations subjected to cyclic loading in soft clays may have a reduced frictional capacity due to a loss of contact between the pile and the soil at shallow depths. This loss of contact is shown by the horizontal portion of the curves where resistance goes to zero. As shown in Figure 2.8(a), gaps can form between the pile and the upper portion of a clay layer. This behavior is not observed for sands.

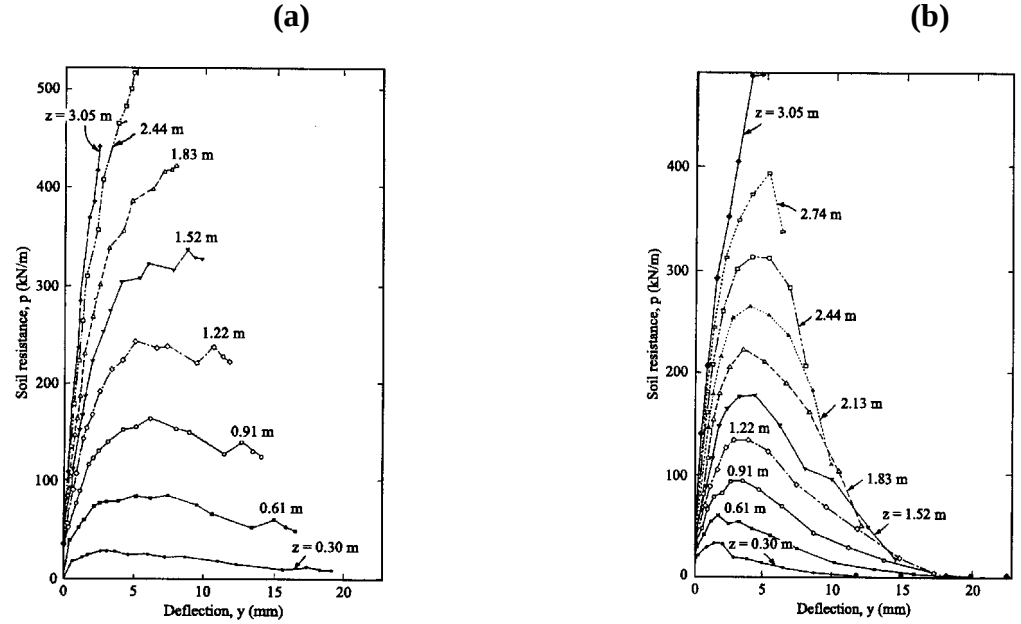

Figure 2.7 **Back-calculated p-y curves for stiff clay from field tests: (a) static, and (b) cyclic (after Reese et al., 1975)**

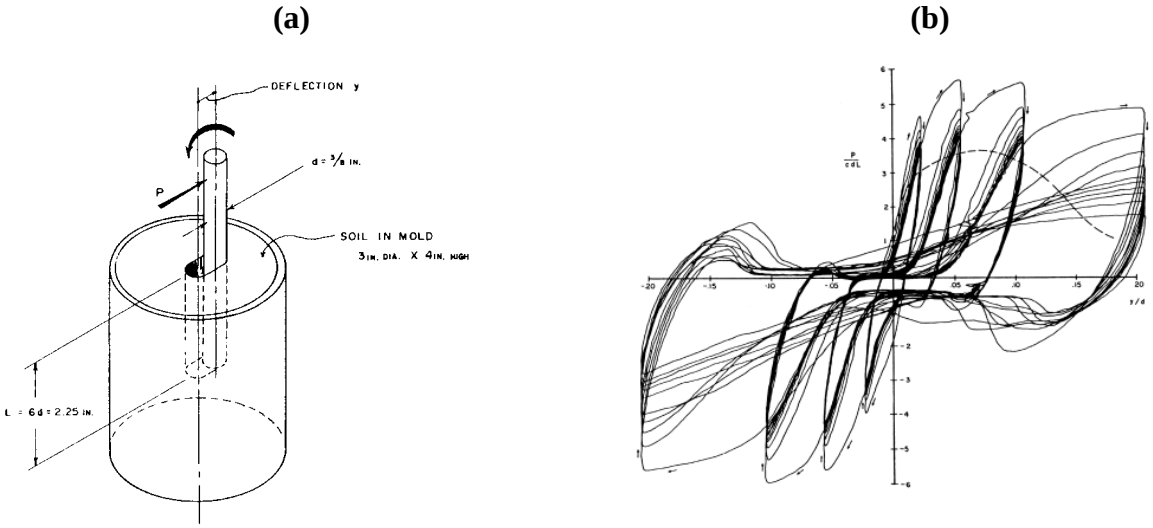

Figure 2.8 **Cyclic response of a rigid pile in soft clay: (a) test setup, and (b) cyclic p-y curves of clay (after Matlock, 1970)**

From many experimental observations, several methods for constructing *p-y* curves have been made, e.g. Matlock (1970) for soft clay, Reese et al. (1974) for sand, Reese et al. (1975) for stiff clay below the ground water table, Reese et al. (1981) for stiff clays above the ground water table. In this research, the construction of *p-y* curves was performed according to procedures outlined in API (1993).

Initial Stiffness of *p-y* Curves

For cohesionless soils, the initial stiffness can be expressed indirectly by a reference deflection, y_{50}, taken as that corresponding to one-half the ultimate soil resistance. The API (1993) method for sand is based on Reese's sand criteria, but uses a smooth hyperbolic function to construct *p-y* curves.

$$p = Ap_{ult} \tanh\left(\frac{kz}{Ap_{ult}} y\right) \tag{2.19}$$

where A is a factor to account for cyclic or static loading evaluated as

$$A = \begin{cases} \max\left[3.0 - 0.8z/D, 0.9\right] & \text{for static loading} \\ \\ 0.9 & \text{for cyclic loading} \end{cases} \tag{2.20}$$

and p_{ult} is the ultimate bearing resistance at depth, z, and k is the initial modulus of subgrade reaction determined as a function of relative density. After calculating the ultimate resistance and rearranging Equation 2.17, y_{50} can be obtained from

$$y_{50} = \frac{Ap_{ult}}{kz} \tanh^{-1}\left(\frac{0.5p}{Ap_{ult}}\right) \tag{2.21}$$

For cohesive soils, y_{50} is usually defined as

$$y_{50} = 2.5\varepsilon_{50}D \tag{2.22}$$

where ε_{50} is the strain corresponding to one-half the undrained strength and D is the pile diameter. Typical values for ε_{50} are given in Tables 2.1 and 2.2.

Table 2.1. Representative values of ε_{50} for normally consolidated clays (Peck et al., 1974 – after Reese and Van Impe, 2001)

Clay	Average undrained shear strength, (kPa)	ε_{50}
Soft clay	< 48	0.020
Medium clay	48 – 96	0.010
Stiff clay	96 – 192	0.005

Table 2.2. Representative values of ε_{50} for overconsolidated clays (after Reese and Van Impe, 2001)

Average undrained shear strength, (kPa)	ε_{50}
50 – 100	0.007
100 – 200	0.005
200 – 400	0.004

In many cases of static and cyclic loading, accurate definition of the initial stiffness is not critical (Reese and Van Impe, 2001). When a pile is subjected to lateral loading, most of the reaction occurs in the near surface soils. In this shallow region, the actual resistance mobilized is usually very close to or at the ultimate resistance and therefore, beyond the displacement at which initial stiffness could have an effect. For dynamic loading, however, the stiffness at low deflection levels can be more important.

Ultimate Resistance of *p-y* Curves

The ultimate soil resistance, p_{ult}, is calculated according to the idealized failure mechanism assumed to develop in the soil. For near-surface *p-y* curves, wedge failure, in which a three-dimensional sliding surface develops (Figure 2.9), is considered. For deeper *p-y* curves, below a critical depth, flow failure occurs in which a two-dimensional flowing soil failure mode around

the pile in a horizontal plane is considered. In both cases, the ultimate resistance is a function of pile diameter, depth, and soil strength parameters.

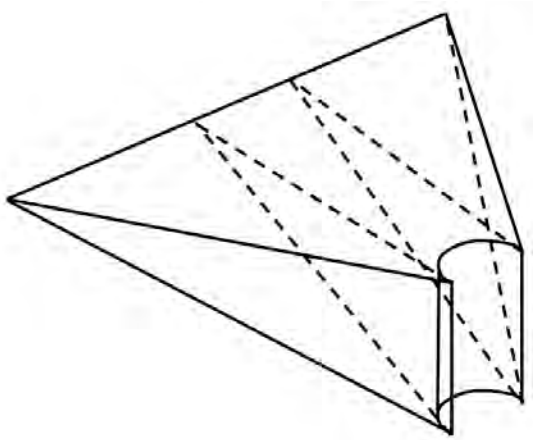

Figure 2.9. Shape of passive wedge controlling ultimate resistance at shallow depths

For cohesionless soils, the ultimate resistance is the smaller of the ultimate resistance at shallow depths, P_{us}, and the ultimate resistance at deeper depths, P_{ud}. According to API (1993) procedures, the ultimate resistance at shallow depths (through the wedge mechanism) can be calculated as

$$P_{us} = \left(C_1 z + C_2 D\right)\gamma' z \tag{2.23}$$

and the ultimate resistance at deeper depths (from the flow mechanism) can be calculated as

$$P_{ud} = C_3 D \gamma' z \tag{2.24}$$

where C_1, C_2, and C_3 are coefficients determined from API (1993) charts as shown in Figure 2.10 where values are correlated to angle of internal friction of the soil.

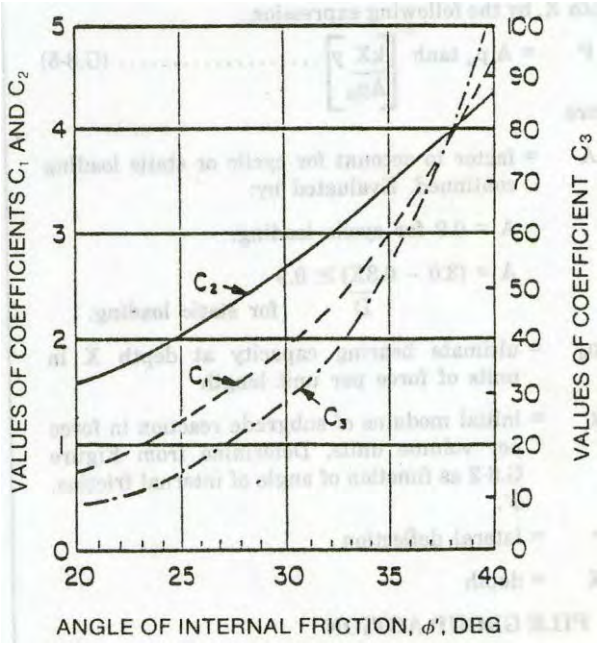

Figure 2.10 Coefficients as functions of friction angle (API, 1993)

For soft clays, p_{ult} increases from 3c to 9c as depth increases from 0 to z_R, where

$$z_R = \frac{6D}{\frac{\gamma D}{c} + J} \tag{2.25}$$

where c is the undrained shear strength, and J is a dimensionless empirical constant with values ranging from 0.25 to 0.5. The ultimate resistance is calculated by the smaller of the values given by the following equations. For shallow depths, when $z < z_R$, the ultimate resistance can be calculated as

$$p_{ult} = 3c + \gamma z + \frac{Jcz}{D} \tag{2.26}$$

For deeper depths, when $z \geq z_R$, the ultimate resistance can be calculated by

$$p_{ult} = 9c \tag{2.27}$$

Figure 2.11 illustrates the mobilization of the ultimate lateral resistance with depth for a laterally loaded pile in sands and clays. For sands, the critical depth, z_{cr}, represents the point at which the failure mechanism transitions from wedge failure in shallow soils to flow failure in deeper soils.

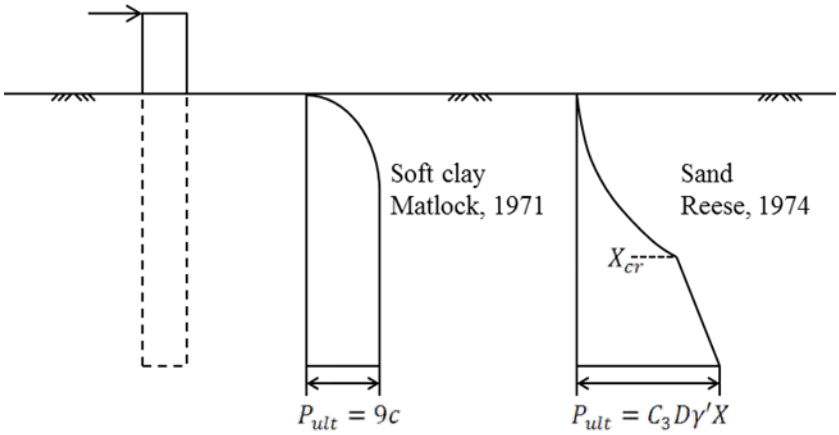

Figure 2.11 Comparison of the ultimate soil resistance of soft clay (after Matlock, 1970), and sand (Reese et al., 1974)

2.2.4 Pile Head Moment Response

Piles can also be subjected to moments applied at the ground surface, usually in conjunction with lateral loads applied at some height above the ground surface. The response of a single pile to pure moment loading (moment with no lateral or vertical load) involves rotation at the ground surface that produces lateral movements of the pile below the ground surface. Below a peak lateral movement, the amplitude of the lateral movement decreases with depth below the ground surface. The mechanism of resistance to rotation, therefore, has components related to the flexural stiffness of the pile itself, and to the lateral load (e.g., *p-y*) resistance of the soil. When a pile foundation is expected to subjected to large moments, a pile group will often be used to resist those moments more efficiently.

2.3 PILE GROUP BEHAVIOR

For large structures, column loads are often larger than the available resistance of a single pile. In such cases, the loads are generally supported by groups of piles connected by a common pile cap. The pile cap distributes the column loads to the individual piles, which then transmit the loads to the supporting soil. The behavior of a pile group can be influenced by the spacing of the piles within the group. The use of closely-spaced piles reduces the cost of the pile cap, but can cause the stressed zones of soil associated with the individual piles to interact with each other leading to a reduction in pile group capacity.

2.3.1 Vertical Load Response

The basic nature of pile group response to vertical loading is similar to that of a single pile. Each pile within a pile group is loaded vertically by the pile cap. Under purely vertical loading, the distribution of loads to the individual piles depends on the stiffness of the pile cap, but it is common to assume that the pile cap is sufficiently stiff that all piles are loaded equally.

Computation of pile group capacity requires consideration of group failure mechanisms. With widely-spaced piles, failure will generally be initiated by failure of an individual pile, either due to local weakness of the soil surrounding and beneath that particular pile or due to non-uniformly high load applied to that particular pile. In this case, group capacity, Q_{group}, is generally taken as the sum of the capacities of the individual piles within the group multiplied by a pile group efficiency factor that depends on the configuration (e.g., pile-to-pile spacing) of the group, i.e.,

$$Q_{group} = \eta \sum_{i=1}^{N} Q_i \tag{2.28}$$

where η is the pile group efficiency and Q_i is the capacity of the i^{th} of N piles comprising the group. A number of procedures for estimating pile group efficiency are available; perhaps the best-known is the Converse-Labarre formula

$$\eta = 1 - \frac{(n-1)m + (m-1)n}{90mn}\theta \tag{2.29}$$

where n and m are the numbers of piles in two orthogonal directions, $\theta = \tan^{-1}(B/s)$ in degrees, B is pile diameter, and s is pile center-to-center spacing.

For very closely spaced piles, it is possible that the soil between the piles moves with the piles upon loading. If a pile does not move relative to the surrounding soil, it cannot develop skin resistance so the capacity of the group can be markedly lower than the sum of the individual pile capacities. In such cases, the capacity of the pile group can be estimated by assuming a block failure mechanism in which the zone of soil and pile bounded by the outer dimensions of the pile group is assumed to act as a rigid block. The block failure mechanism is only significant for pile groups whose tip resistance is low relative to skin resistance – in sands, for example, the bearing capacity at the base of a large rigid block would be so large that the failure mechanism would likely never develop.

2.3.2 Lateral Load Response

When subjected to the same lateral load, a pile that is a member of a group will respond differently than a single isolated pile. Typically, a pile group will deflect more and resist less force per pile than a single pile. The pile group response depends on the individual pile capacity, pile spacing, group configuration, pile installation method, pile cap resistance, pile cap connection, and other factors. Of these, pile spacing and pile cap resistance are the most significant. Methods for accounting for pile spacing and cap resistance are discussed in the following sections.

When loaded in the lateral direction, the difference in the response of a single pile and a group of piles can be significant. Typically, a pile group will deflect more and resist less force per pile than a single pile. The difference in the pile group response can be attributed to three main aspects: the interference that occurs through the supporting soil between adjacent piles of the pile group, the additional rotational resistance provided by the restraint of the pile cap connection and vertical skin resistance of the piles, and the additional lateral resistance provided

by the pile cap (when buried). The overall effect of these differences must be taken into consideration when designing pile foundations to resist lateral loads.

2.3.2.1 Group Effect

In a group a pile is less efficient due to pile-soil-pile interaction effects. When a pile is loaded laterally a shear zone develops within the adjacent soil. When piles are closely spaced together, interference between shear zones of adjacent piles (Figure 2.12) causes a loss of soil resistance and, consequently, greater deflection for a given lateral load per pile. This reduction of soil resistance due to the overlap of shear zones is known as shadowing. The degree to which shadowing reduces capacity of the pile depends primarily on pile spacing and pile location within the group.

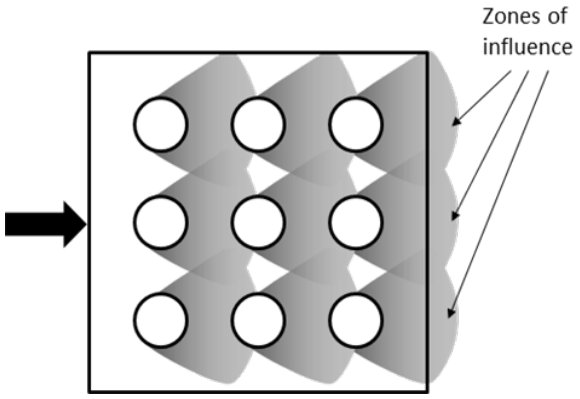

Figure 2.12 Soil zones of influence for a laterally loaded pile group

Shadowing affects piles that are in line with the direction of loading and causes the leading pile to take a greater load than its trailing piles. For example, the pile group in Figure 2.13 can be divided into three rows. When the lateral load acts from left to right, the leading row is the first row on the right (labeled Row 1). The rows following the leading row, from right to left, are typically described as the 1st trailing row, the 2nd trailing row, and so on.

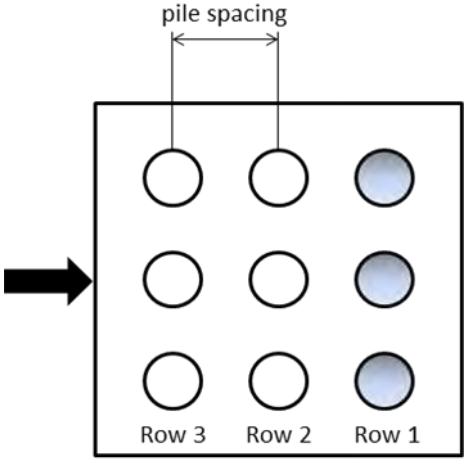

Figure 2.13 Schematic of pile alignment in a group

The *p-y* method can be easily adapted to approximate group interaction effects. To capture the response of piles in a group, group efficiency factors are included in the analysis and act to reduce the ultimate lateral resistance. A popular method to account for "shadowing" is to include *p*-multipliers (Brown et al., 1988). Researchers have performed experimental tests on pile groups varying the number of rows, number of piles per row, pile spacing, soil type and density to define these *p*-multipliers. Mokwa (1999) observed that pile spacing is the dominant factor affecting pile group interaction. Closer spaced piles develop greater interference and a greater reduction in resistance. Mokwa (1999) discovered that group effects for in-line alignments, were negligible when the pile spacing is greater than 6 pile diameters. Figure 2.14 shows *p*-multipliers for leading and trailing rows developed by Mokwa (1999).

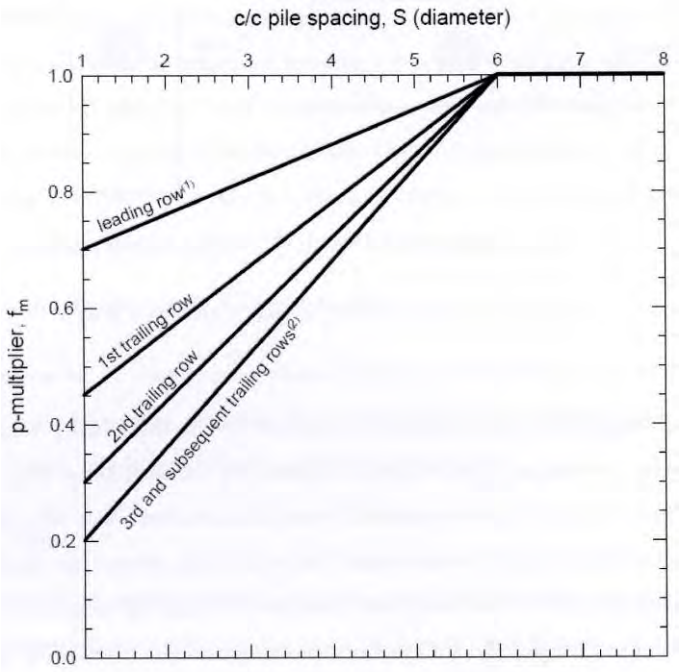

Notes:
(1) The term row used in this chart refers to a line of piles oriented perpendicular to the direction of applied load.
(2) Use the f_m values recommended for the 3rd trailng row for all rows beyond the third trailing row.
(3) Bending moments and shear forces computed for the corner piles should be adjusted as follows:

side by side spacing	corner pile factor
3D	1.0
2D	1.2
1D	1.6

Figure 2.14 *p*-multipliers design curves (Mokwa, 1999)

For static lateral loading, accounting for the difference in response using p-multipliers is critical. For dynamic lateral loading where the lateral load oscillates and leading rows become trailing rows (and vice versa), accounting for group effects is not as critical.

2.3.3 Overturning Moment Response

A pile group subjected to an overturning moment will resist that moment primarily through axial resistance developed in the piles. In much the same manner as bearing pressures vary across the face of a shallow foundation subjected to an overturning moment, the vertical loads in a pile group subjected to an overturning moment also vary with position. For an arbitrary pile located at position x_i, y_i from the centroid of a pile group subjected to vertical load, Q, and overturning moments, M_x and M_y, the axial load transmitted from a rigid pile cap would be given by

$$Q_i = \frac{Q_{group}}{N} + \frac{M_y x_i}{\sum_{j=1}^{N} x_j^2} + \frac{M_x y_i}{\sum_{j=1}^{N} x_j^2} \tag{2.30}$$

Note that the effect of the overturning moments will be to increase the downward-acting force on piles at positive x- and y-values, and to decrease that force on piles at negative x- and y-values. If a pile group is subjected to a relatively low vertical load, Q_{group}, and high overturning moments, some of the piles may be loaded in tension. Pullout failure can occur when uplift loading exceeds the available uplift resistance.

2.4 PILE CAP RESISTANCE

Deep foundations that support bridges often consist of groups of piles connected by concrete pile caps. These pile caps can be massive and are often buried. They can contribute significantly to the rotational and lateral resistance of the pile group system and, therefore, should be accounted for in design. In some cases, the lateral resistance provided by the pile cap can be as much as 50% of the total lateral resistance (Mokwa, 1999; Beatty, 1970).

The pile cap strongly affects the rotational capacity of the pile group. When a lateral force is applied to a pile group, the tendency of the group to rotate is resisted by vertical soil resistance along the piles and at the pile tips as shown in Figure 2.15. Pile axial resistance can therefore significantly affect the rotational resistance of the pile group.

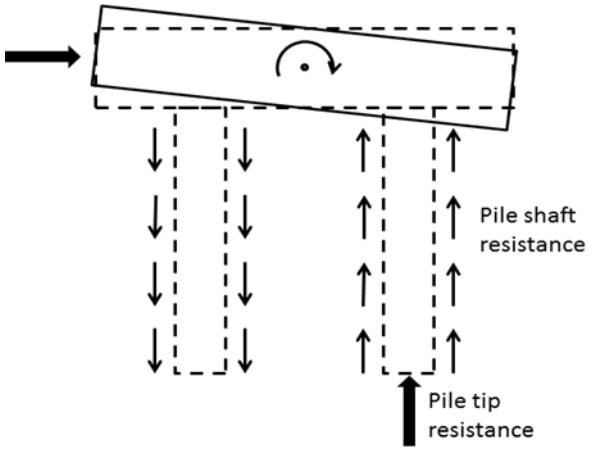

Figure 2.15 Schematic of rotational soil resistance due to pile cap rotation (after Shin, 2007)

The pile cap strongly affects the lateral capacity of the pile group. Passive earth pressure on the front of the cap, sliding resistance on the bottom and sides, and active earth pressure on the back contribute to the lateral resistance. Compared to the passive resistance, however, sliding and active resistance are usually quite small and are commonly ignored.

Mokwa (1999) developed a method for computing cap resistance based on passive earth pressures. Three components contribute to the passive earth pressure: soil weight and friction, soil cohesion, and surcharge. The passive earth pressure on the face of the cap can be calculated by

$$E_p = \frac{1}{2}\gamma H_c^2 K_p + 2cH_c\sqrt{K_p} + q_s H_c K_p \tag{2.31}$$

where K_p *is determined from log spiral theory, qs is the surcharge,* γ *is the unit weight, and* H_c *is the height of pile cap.*

Equation 2.31 gives the resulting earth pressure force if the passive region is two-dimensional. Considering a three-dimensional passive region, the resulting ultimate earth pressure force for cohesionless soils can be calculated by

$$p_{ult} = RE_p b \tag{2.32}$$

where b is the pile cap width and *R* is a factor that accounts for the three-dimensional geometry of the passive zone. In a real pile cap, as shown in Figure 2.16, the passive zone extends beyond the edges of the front face of the pile cap.

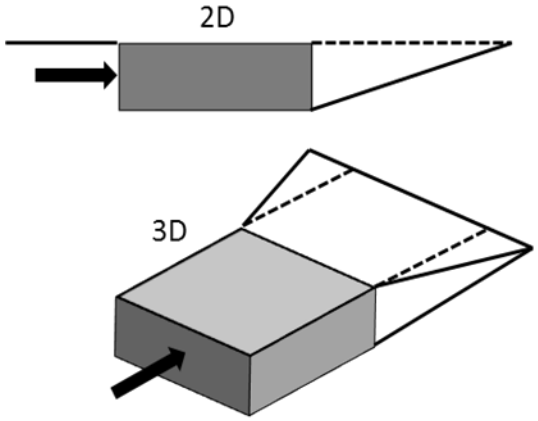

Figure 2.16 2-D and 3-D lateral earth pressure wedges

To investigate the three-dimensional effect, Ovesen (1964) conducted model tests on anchor blocks embedded in granular soils and developed empirical expressions for predicting the three-dimensional resistance. From Ovesen (1964), a three-dimensional modifying factor, *R*, can be calculated as

$$R = 1 + (K_p - K_a)^{2/3}\left[1.1E^4 + \frac{1.6B}{1+5b/H}\right] + \frac{0.4(K_p - K_a)E^3B^2}{1+0.05b/H} \tag{2.33}$$

where B=1 for a single pile cap, E = 1-H/(z_c+H), and z_c is the embedment depth from the ground surface to the top of the pile cap.

For cohesive soils ($\phi = 0$), the ultimate pressure force is calculated as

$$p_{ult,cap} = \frac{cbH}{2}\left(4 + \frac{\gamma H}{c} + \frac{0.25H}{b} + 2\alpha\right) \tag{2.34}$$

where α is the adhesion between the cohesive soil and the wall.

In this method, only the passive resistance on the front of the cap is considered. The contribution of the frictional resistance on the sides and bottom of the cap were not accounted for because their magnitudes are insignificant relative to the passive resistance.

2.5 DYNAMIC RESPONSE OF PILE FOUNDATIONS

Pile foundations are also expected to resist dynamic loads from different sources that produce a wide range of amplitudes, frequency contents, and durations. When subjected to dynamic loading, pile groups will respond dynamically with some pattern and amplitude of deformations. In most cases, dynamic loading is of relatively low amplitude, so the stiffness and damping characteristics of the foundation will control its deformations. A considerable literature on the dynamic response of pile foundations exists and charts for estimation of pile impedance, a quantity that accounts for both stiffness and damping characteristics, are readily available. If a pile cap is rigid, the piles can be replaced by springs and dashpots arranged in such as way as to model the horizontal, vertical, and rotational impedance of the foundation (Figure 2.17).

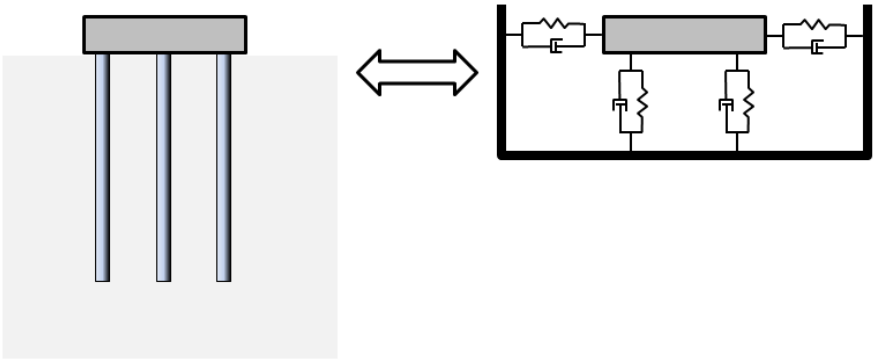

Figure 2.17. Schematic illustration of equivalent springs and dashpots for modeling vertical/horizontal/rotational impedance of pile group.

For the purposes of soil-structure interaction analysis, the dynamic stiffness of the foundation is of primary interest. The dynamic stiffness of a single pile is usually expressed as the product of its static stiffness and a dynamic stiffness factor. Piles themselves are generally quite stiff when loaded axially, so the entire pile tends to move vertically in phase and by essentially the same amount. When loaded laterally, however, piles can be quite flexible and

will tend to deflect more near the point of load application than farther away. For most pile dynamics problems, the loads are applied at the head of the pile so only a portion of the pile, usually termed the "active length" deflects significantly. The active length depends on the relative flexural stiffness of the pile and soil and is usually on the order of 10- TO 20-pile diameters (Randolph, 1981; Gazetas, 1991).

The dynamic response of pile groups is complicated. Piles tend to interact with each other under dynamic as well as static loading. The type of elastic solutions from which impedance functions are typically derived show that the individual piles within a group produce stress waves that emanate from their perimeters as they move laterally with respect to the surrounding soil. When linear elastic behavior is assumed, these waves can push an adjacent pile on one side and pull an adjacent pile on the other side. The result is a complex set of interactions that depend on frequency, pile spacing, number of piles, and other factors. Examples of the dynamic stiffness and damping behavior of 2x2, 3x3, and 4x4 pile groups are shown in Figure 2.18.

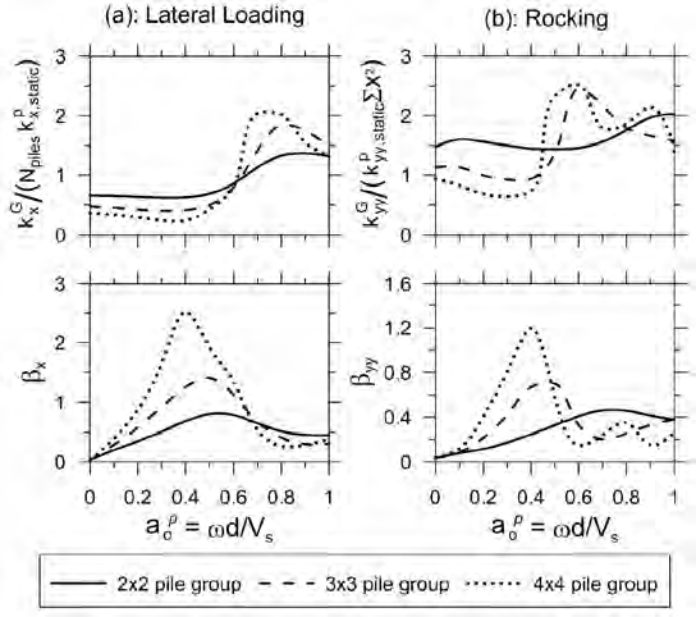

Figure 2.18. Dynamic stiffness and damping behavior of pile groups subjected to (a) lateral load at pile cap, and (b) overturning moment applied to pile cap. Stiffness expressed as ratio of dynamic stiffness to static stiffness (after Stewart and Mylonakis, 2011)

A number of chart-based procedures of the type illustrated in Figure 2.17 are available for estimation of pile group stiffness. The computer program, DYNA4 (Novak et al., 1993) uses elastic solutions to develop frequency-dependent stiffness and damping coefficients for arbitrarily-shaped pile groups. DYNA4 can provide a 6x6 impedance matrix that defines the stiffness and damping characteristics of a pile group with respect to three translational and three rotational degrees of freedom. These calculations generally assume linear, viscoelastic soil

behavior but can be used in an iterative, equivalent linear format to approximate nonlinear behavior.

2.6 SUMMARY

The response of individual piles to seismic loading is influenced by the characteristics of the pile, the soil, and the structure supported by the pile. The pile can loaded by forces from the structure, which include vertical and horizontal loads and moments, or by movement of the soil along the length of the pile. As the pile moves in response to these loads, it develops resistance by mobilizing the shear strength of the soil that surrounds it. Several analytical techniques have been developed to model the three-dimensional soil-structure interaction problem. The most commonly used of these involve modeling the pile as a Winkler beam with the soil modeled by discrete, independent springs. The load-resistance behavior of these springs can be expressed graphically in the form of *p-y* curves for lateral loading and response, *t-z* curves for mobilization of skin resistance in response to axial loads, and *Q-z* curves for mobilization of tip resistance due to axial loads.

The response of pile groups to seismic loading is even more complex than the response of individual piles. Within a group, piles can interact with each other in a complicated manner that depends on the characteristics of the piles and the soil, and on the configuration of the group. These interactions can be addressed using group interaction factors developed from elastic solutions for relatively low-amplitude loading, but nonlinearity and inelasticity at high levels of loading make their use more difficult. Reduction factors can be applied to *p-y*, *t-z*, and *Q-z* curves to approximate group effects under stronger levels of loading.

3 Approaches to Seismic Response and Design

3.1 INTRODUCTION

Earthquake engineers are frequently required to evaluate the seismic performance of existing structures or to design new structures to achieve some desired level of performance. A number of different approaches to these activities have been taken over the years. With the increasing availability of high-speed computers, sophisticated analysis software, and case history data against which analytical tests can be calibrated, the engineer's ability to predict the response of soil-foundation-structure systems is much greater than in the past.

Previous notions of successful performance as the avoidance of collapse are giving way to more refined measures of performance at damage levels well short of collapse. Multi-level design procedures have been used for a considerable period of time and have been formalized in different ways. For bridge design, load and resistance factor (LRFD) principles have been used to establish design requirements for different limit states – serviceability, ultimate, and extreme. In recent years, more explicit consideration of performance has been encapsulated in performance-based earthquake engineering, which has the potential to provide more consistent and rational designs in areas of widely-varying seismicity.

This chapter presents a review of uncertainties that can affect seismic design, and describes how they are accounted for in allowable stress, LRFD, and performance-based frameworks.

3.2 SEISMIC PERFORMANCE

The development and implementation of performance-based design requires that earthquake professionals be able to define performance in terms that are understandable and useful to the wide range of technical and non-technical professionals who make decisions on the basis of performance predictions. The term "performance" can mean different things to different people. To a seismologist, spectral acceleration may be a good descriptor of the potential performance of a building subjected to earthquake shaking. To an engineer, plastic rotation would likely be a better descriptor of performance. To an estimator preparing a bid for repairs, crack width and spacing could be more useful measures of performance. Finally, to an owner, the economic loss associated with earthquake damage could be the best measure of performance.

These different notions of performance lead to an intuitive way of viewing the earthquake process. As illustrated in Figure 1, an earthquake produces ground motion, which leads to dynamic response of a structure. That response can lead to physical damage, and that damage leads to losses. The prediction of losses, therefore, requires the ability to predict ground motion intensity, system response, and physical damage. If losses are the ultimate measure of, the performance evaluations in an ideal implementation of performance-based design should focus on predicting losses as accurately, consistently, and reliably as possible. The following sections describe the progression of events that lead to earthquake losses.

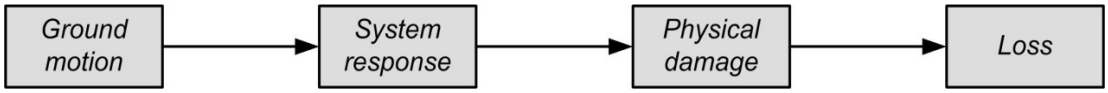

Figure 3.1. Schematic illustration of the progression that leads to earthquake losses.

3.2.1 Ground Motion

The rupture of crustal rock that produces an earthquake releases energy that propagates outward from the fault in all directions. As the energy spreads out over a greater and greater volume, its flux (energy per unit area) decreases and it is refracted, or scattered, by inhomogeneities in the crust. Some of the elastic wave energy is absorbed anelastically by the crustal material along the path from the fault to the site. At the site, the local geology further modifies the wave field, influencing the amplitude, frequency content, and duration of the ground motion.

Earthquake engineers characterize the intensity of ground motions using intensity measures (or *IM*s) such as peak acceleration, spectral acceleration, Arias intensity, etc. The response of a compliant system can vary dramatically from one earthquake to another and from one location to another in the same earthquake, because of differences in those ground motion characteristics. The most useful ground motion parameters are those to which the response of the system of interest is most closely related. The optimum parameters for predicting response should be recognized as being different for different types of structures and different types of response. In bridge design, spectral acceleration is the most commonly used *IM*, and spectral acceleration at the fundamental period of the bridge, $S_a(T_o)$, is likely the single most useful predictor of response.

3.2.2 System Response

Structures, whether comprised of steel, concrete, or soil, have mass and are compliant, and therefore respond more strongly at some frequencies than others. They exhibit generally linear behavior at very low levels of loading but can become highly nonlinear and inelastic at higher levels of shaking. Their stiffnesses can change dramatically from the beginning of an earthquake to the end and even, as in the cases of liquefiable soils and damaged reinforced concrete elements, within a given cycle of loading. Response to earthquake loading depends on the mass, geometry, stiffness, and damping characteristics of the structure and its foundation, and on the

amplitude, frequency content, and duration of the ground motion. Response can be expressed in terms of forces and stresses or displacements and strains, and are frequently characterized by engineering demand parameters, or *EDP*s. When the response is excessively high, damage will occur. In order to accurately predict the damage associated with structural response, it is necessary to identify the measures of response that are most closely related to damage, and to be able to predict the response caused by earthquake ground motion. In bridge foundation design, deflections (displacements and/or rotations) have historically been the most useful measures of response.

3.2.3 Physical Damage

The response of a structure may or may not result in physical damage depending on the structure's capacity to resist damage. The capacity may be viewed as a level of response beyond which some level of physical damage can be expected to occur. Many different types of damage can occur during an earthquake – some can be related to the structure itself, some to physical systems within the structure, and some to the contents of the structures. Consider a bridge, for example, subjected to earthquake shaking of various intensities. At low levels of shaking, the bridge may respond essentially elastically with light hairline cracking and negligible damage occurring. At stronger levels of shaking, cover concrete can spall and expansion joint seals may fail. At even stronger levels of shaking, columns/girders/beams can crack, joints can fail, foundations can rock and settle, and rebar can buckle. At very strong levels of shaking, ground movement can occur, foundations can fail, welded connections can fracture, columns can lose capacity and collapse can occur – such severe physical damage can lead to extremely high losses. In order to predict the losses associated with these and other forms of physical damage, it is necessary to identify the specific form(s) of physical damage, quantified by damage measures, or *DM*s, that contribute most strongly to the losses of interest, and to be able to predict the physical damage associated with the response of the system of interest.

3.2.4 Losses

Physical damage to structures and their contents result in losses. Losses can have many components – deaths and injuries, repair and replacement costs, and loss of utility for extended periods of time. Decisions regarding risk reduction through retrofitting, insurance protection, etc. are usually made on the basis of expected losses, so those losses are often characterized by decision variables, or *DV*s.

The prevention of death and serious injury has been the fundamental basis of seismic design since it was first attempted. The economic losses associated with earthquake damage are many, but can be divided into two categories – direct and indirect losses. Direct losses are those associated with the repair and/or replacement of structures and facilities damaged by earthquake shaking. Indirect losses include those associated with delayed or lost business, environmental damage, compromised infrastructure, etc. Downtime, which refers to the period of time in which structures or facilities are unavailable for their intended use, is among the most important of indirect economic losses and can produce, for critical systems, losses that far exceed direct losses. The loss of a major bridge in a non-redundant system, for example, can lead to inefficiencies in moving goods, services, and people that have very real, and very high, economic consequences.

3.3 UNCERTAINTY IN GEOTECHNICAL DESIGN

A design procedure should ensure some adequate margin of safety against failure. This objective, which requires a balance of safety and cost, is best accomplished with careful consideration of the sources and levels of uncertainty in the design problem.

Geotechnical design, in comparison with many other engineering disciplines, must deal with numerous sources of significant uncertainty and, as a result, higher margins of safety have historically been incorporated in geotechnical design. The following sections discuss the primary sources of uncertainty in capacity and demand with respect to geotechnical engineering problems.

3.3.1 Sources of Uncertainty in Demand (Loading)

For typical geotechnical engineering applications, the uncertainty in capacity is much greater than the uncertainty in the demand. However, in the case of rare but extreme loading, such as that produced by earthquakes, the uncertainty in demand can be great.

The primary loads on a structure are usually categorized into dead and live loads. These loads often control design because they occur in nearly all structures during normal operating conditions. In foundation design, applied dead and live loads are typically transmitted by the superstructure. The load transfer to substructures is not always well understood, which therefore adds uncertainty to foundation loading. For highway structures, gravity loads represent the main dead loads and traffic loads are the primary live loads. Gravity loads are quite predictable, and hence typically involve less uncertainty than live loads; traffic loads, for example, can vary over time scales ranging from hours to months. Nevertheless, the uncertainty in loading, in the absence of extreme events, is often lower than the uncertainty in resistance.

Extreme loading caused by wind, flowing water, earthquakes and vehicle impact must also be considered in the design of bridges and their foundations. Extreme loading occurs infrequently and typically for short durations but can be significant in magnitude. While a structure in a given area may be subject to multiple sources of extreme loading, it is highly unlikely that different extreme loading cases will occur at the same time. Therefore, different load combinations with different likelihoods of joint occurrence are considered. While primary dead and live loads usually act vertically, extreme loads frequently produce high lateral loads which may require special lateral load resisting systems to be incorporated in a structure. For bridges, strong wind, rapidly flowing water, earthquakes and possible vessel collisions can create high transient lateral forces.

Earthquake loading is an extreme event that requires special consideration in seismically active areas. Because earthquakes are unpredictable, seismic loading can easily be more uncertain than the resistance. The characteristics of earthquake ground motions cannot be predicted accurately and soil-pile-structure interaction is very complex. As lateral shaking occurs, the stiffness and strength of the soil changes and large lateral loads and overturning moments can be imposed on foundations. Also, limited strong ground motion data and site response effects contribute to the uncertainty in earthquake loads.

3.3.2 Sources of Uncertainty in Capacity (Resistance)

In the context of geotechnical design, the capacity of a system such as a foundation refers to its ability to resist some demand satisfactorily with respect to a specified performance objective. Traditionally, geotechnical engineers have considered stability as an ultimate performance objective; hence, capacity has been interpreted as the full mobilization of available resistance (in terms of forces and/or stresses), beyond which no additional loading can be resisted. However, capacity can be defined more generally – in addition to its traditional (ultimate) interpretation, it can also be interpreted in terms of response, physical damage, or loss.

To arrive at the ultimate capacity, ultimate material parameters such as soil shear strength are first estimated by laboratory or in situ testing, correlation to other parameters, or through knowledge and experience. The material parameters are then used as input to a model that predicts the capacity of the system of interest. As a result, the uncertainty in the ultimate capacity for a given level of loading depends on the uncertainty of the material parameters, the sensitivity of the capacity to those parameters, and the uncertainty of the model used to predict the capacity. Models used to predict the ultimate capacities of foundations may range from limit equilibrium procedures that require shear strength parameters as input to empirical procedures that may be based on parameters such as penetration resistance. In geotechnical engineering, many models are based on empirical data developed from regressions of field observations and/or experiments and knowledge of the phenomenon. These models can be based on limited data and make significant assumptions. On the other hand, measurements made during foundation construction, such as in the case of pile driving, can prove to be more reliable (i.e., less uncertain) than laboratory test data and theoretical calculations. Therefore, it is important to understand the limitations and appropriateness of the calculation model chosen.

Geotechnical material properties are notoriously difficult to determine accurately. Undisturbed samples are nearly impossible to obtain and empirical correlations to other measured quantities (e.g., insitu test parameters) are not perfect. Soils behave nonlinearly and their properties can depend on time, stress history and strain level. As a result, experience, geologic interpretation, and engineering judgment are frequently required to estimate geotechnical parameters, resulting in soil properties with a high degree of uncertainty.

The evaluation of soil properties is also made difficult by the spatial variability caused by the random nature of soil deposition processes. Spatial variability can be significant for bridge construction in river valleys, where sediments are eroded and deposited frequently. Due to seasonal flooding and meandering flow channels, the subsurface near rivers may include large debris, pockets of soft material and varying depths and thicknesses of good bearing soil. These variations can be very significant when considering the shaft length needed for a bridge pier. The level of spatial uncertainty depends on the amount of site exploration conducted. Every site exploration involves characterization of the soil properties at a limited number of discrete locations (e.g., boreholes, test pits, etc.). Soil properties at all other locations are estimated from the properties at these discrete locations with consideration of the geologic processes at work in the area. If many explorations are conducted, a site may be characterized quite well. However, for typical sites, cost and/or accessibility may limit the thoroughness of the exploration program resulting in a relatively unknown subsurface profile.

Because of construction effects and variations in installation procedures, the actual capacity achieved may differ from the calculated capacity. Properly accounting for these effects

helps to ensure that design capacity is similar to in situ capacity. For piles, the uncertainty in capacity depends on the amount of monitoring done during installation. When driving rate, embedment depth and other factors are not monitored it is difficult to know if the pile has gained adequate strength.

3.3.3 Allowable Stress Design

Allowable Stress Design (ASD), also known as Working Stress Design (WSD), has been the most commonly used method of design in civil engineering since the early 1800s and is still widely used in practice. ASD involves the comparison of the load, or demand, to the resistance, or capacity, through the use of a factor of safety.

3.3.3.1 Principles of Allowable Stress Design

In ASD, the estimated ultimate resistance, R, is reduced by a factor of safety, FS to obtain the allowable design load, Q_{all}. The basic load requirement of ASD is that the applied load, Q, must be less than or equal to the allowable design load.

$$Q \leq Q_{all} = \frac{R}{FS} \tag{3.1}$$

The factor of safety, therefore, is applied only to the estimated capacity with the implication that limiting the loading to some fraction of the estimated ultimate capacity will produce a desired level of performance.

3.3.3.2 Factors of Safety

ASD generally relies on a single, global, design factor of safety to account for uncertainties and consequences of failure (Allen, 2005b). The factor of safety, in reality, accounts for uncertainty due to variations in loads and resistances, inaccuracies of response models, the amount of observational information obtained during construction, the consequences of failure, and, to an extent, tradition and expedience. Because each of these factors can vary significantly from one project to another, the use of a single, standard factor of safety will rarely produce a consistent actual margin of safety.

The factor of safety is typically applied to the estimated capacity, and this greatly reduced resistance is then compared to the estimated load. Alternatively, a factor of safety could be applied to parameters that control capacity and those reduced parameters could then be used to calculate the resistance. The former approach has historically been more common in the United States, and the latter more popular in Europe.

In either case, the actual factor of safety is frequently much higher than the design factor of safety because soil strength data is usually interpreted conservatively, the design loads are estimated conservatively (actual service loads are likely less than the design loads), the as built dimensions of the foundation may be larger than planned and some analysis methods make conservative assumptions that produce conservative results.

For typical bearing capacity problems, geotechnical engineers frequently use a factor of safety between 2.5 and 3.5, but may use a value outside this range depending on factors such as soil type, soil variability, amount of site characterization data obtained, importance of structure and consequences of failure, and the likelihood of design load occurring during the lifetime of the structure.

The factor of safety applied to pile foundation design problems depends on the extent of analysis and control in construction and monitoring. A smaller factor of safety is used when a greater level of control is used, as illustrated by Table 3.1. The table assumes that subsurface exploration will be performed, and that conventional, limit equilibrium capacity calculations will be performed. If those efforts are supplemented by capacity estimates based on dynamic formulae, which are notoriously uncertain, a factor of safety of 3.5 is recommended. However, if a wave equation and CAPWAP analysis is performed, the recommended factor of safety drops to 2.25. If a pile load test is also performed a factor of safety of 1.9 is recommended. More construction control generally corresponds to a lower factor of safety and usually means a more economical design.

Table 3.1 Factor of safety on ultimate axial geotechnical capacity based on level of construction control (after AASHTO, 1997)

Basis for Design and Type of Construction Control	Increasing Design/Construction Control →				
Subsurface Exploration	X	X	X	X	X
Static Calculation	X	X	X	X	X
Dynamic Formula	X				
Wave Equation		X	X	X	X
CAPWAP Analysis			X		X
Static Load Test				X	X
Factor of Safety	3.50	2.75	2.25	2.00*	1.90

*For any combination of construction control that includes a static load test, FS = 2.0.

The design factor of safety is generally selected subjectively based on the knowledge, experience and judgment of the engineer. An experienced engineer working on projects in an area with which he is very familiar, may use his knowledge of what has worked and not worked in the past to adjust the design factor of safety downward (or upward, if necessary) to achieve some perceived level of confidence in the anticipated performance of the structure. In ASD, therefore, the design engineer has the flexibility to choose an appropriate factor of safety for the project. This freedom can be useful for unique projects, but it can also create ambiguity and inconsistency in design.

ASD has worked for many years and does have practical advantages. Engineers are familiar with ASD and it allows expedience and rapid implementation in design. However, the fact that ASD has worked for many years is not justification that it is good design. In ASD, uncertainties are accounted for only in a qualitative, and usually inconsistent, sense. A more rational approach would consider uncertainties individually and quantitatively, allowing for consistent design reliability and quantifiable design risk.

3.3.4 Reliability Based Design

The ambiguity caused by the subjective treatment of uncertainty in the ASD approach can be reduced by reliability-based design (RBD). Through the use of probabilistic methods, RBD provides a more rational and rigorous treatment of the uncertainties in design. RBD quantifies uncertainty so that risk can be accounted for objectively and consistently. Absolute reliability is unattainable in the presence of uncertainty. However, through the use of probability theory, RBD can provide a framework for developing design criteria that ensures a prescribed level of reliability. Reliability theory has been successfully used to calibrate and optimize many design codes.

3.3.4.1 Probability in Design

Probability concepts can be used to quantify uncertainties in loads and resistances for design problems. In practice, neither capacity nor demand are deterministic quantities. Therefore, it is appropriate to model each as random variables and to incorporate their variability into the design process through probabilistic means. Modeling and quantifying the uncertainties of random variables are the initial and essential steps in any risk-based analysis and design.

Assuming that they are normally distributed, the variations of load and resistance are completely described by their respective means, $\bar{Q}$and $\bar{R}$, and standard deviations. The factor of safety is taken as the ratio of the resistance to the loading. Using mean values, the central, or mean, factor of safety can be expressed as

$$FS_m = \frac{\bar{R}}{\bar{Q}} \tag{3.2}$$

The central factor of safety is affected by the relative distance between the mean values of load and resistance (i.e., the distance between the centers of the distributions), but is not affected by the dispersion in either load or resistance.

In reality, the actual load and capacity for a given case may differ from their respective mean values. In design, a nominal load, Q_n, and a nominal resistance, R_n, are often selected conservatively with respect to their mean values. The nominal resistance is typically a fraction of the standard deviation below the mean resistance and the nominal load is a fraction of the standard deviation above the mean load. The nominal factor of safety, FS_n can then be expressed as

$$FS_n = \frac{R_n}{Q_n} = \frac{\bar{R} - \lambda_R \sigma_R}{\bar{Q} + \lambda_Q \sigma_Q} \tag{3.3}$$

whereσ_Q andσ_R are the standard deviations of the load and resistance, respectively, and $\lambda_Q$andλ_R are constants that reflect bias in the nominal loads and resistances. The nominal factor of safety, therefore, provides a more conservative design when its value is equal to that of the central factor of safety. Using the above definitions,

$$FS_m = \frac{\bar{R}}{\bar{Q}} > FS_n = \frac{R_n}{Q_n} \tag{3.4}$$

as illustrated in Figure 3.2.

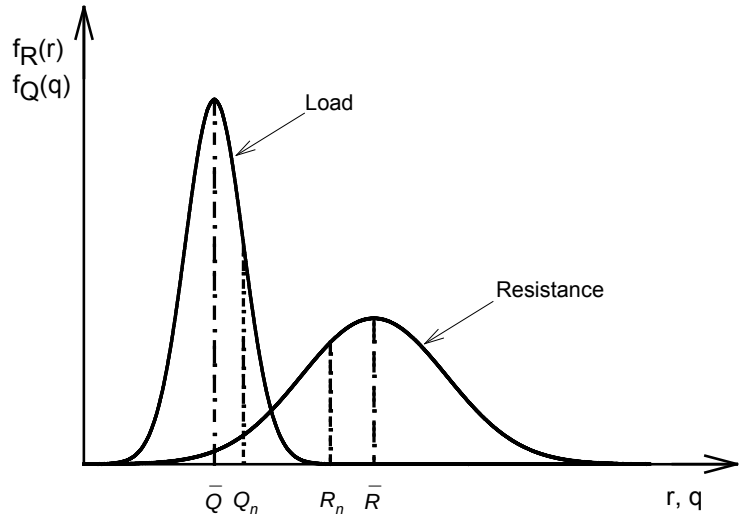

Figure 3.2. Illustration of mean and nominal loads and resistances.

3.3.4.2 Probability of failure

Design reliability is related to the probability that system performance is satisfactory or that some design criteria is achieved. On the other hand, design risk is related to the probability that system performance is unsatisfactory or that some design criteria is not achieved. In general, this probability of failure must be acceptably low to achieve the desired level of reliability.

After the uncertainty of the load and resistance has been quantified, the probability of failure can be estimated. Figure 3.3 shows that a region exists in which the load and resistance distributions overlap each other, i.e., where there is some non-zero probability that the load can exceed the resistance and thereby produce failure. The probability of failure is related (but not equal) to the area of the overlap of the load and resistance pdfs as shown by the shaded area in Figure 3.3. The actual probability of failure can be computed as

$$P_f = P[R < Q] = \int_0^\infty F_R(q)\, f_Q(q) dq \tag{3.5}$$

where $F_R(q)$ is the CDF of R evaluated at $Q = q$.

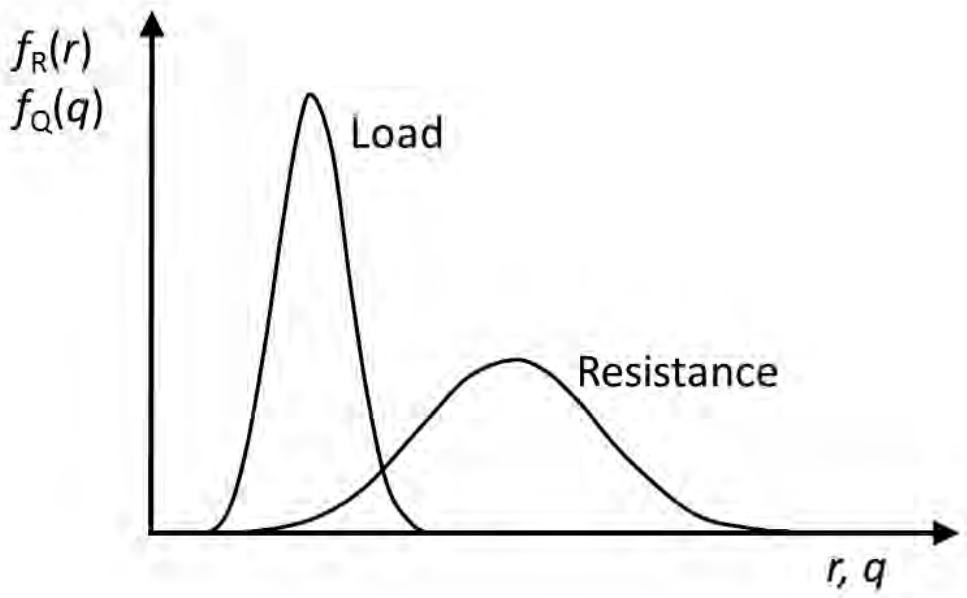

Figure 3.3 An illustration of the probability of failure for normally distributed variables.

The overlap of the load and resistance distributions shows that there is some probability that a higher-than-average load could combine with a lower-than-average resistance to produce failure. The probability of failure, therefore, is affected by the relative distance between the curves, the dispersion of the curves and the shapes of the curves. Safe design ensures that the area of the overlap is sufficiently small to produce an acceptable probability of failure.

This graphical characterization of load and resistance can be used to illustrate the value of the probability of failure as a design tool and the shortcomings of the central factor of safety in the ASD approach. Figure 3.4 shows two resistance distributions with the same mean resistance but different levels of dispersion about that mean resistance. An evaluation based on the central factor of safety would show that both have the same factor of safety, which many engineers would take to imply that the likelihood of failure is the same. However, the levels of overlap between resistance distributions R_1 and R_2 with the load distribution clearly indicate that a higher probability of failure would be expected for resistance distribution R_2 than for R_1. Therefore, the ASD central factor of safety does not accurately indicate a level of design risk.

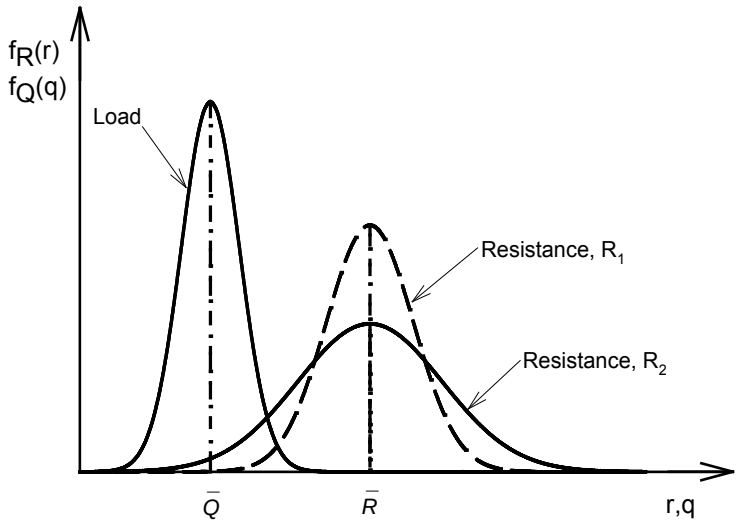

Figure 3.4. An illustration of the effect of the dispersion of resistance on factor of safety

Figure 3.5 shows another situation where the factor of safety used in ASD can provide a misleading indication of safety. The system with resistance, R_1, has a lower mean resistance but less dispersion than the system with resistance, R_2. The relative positions of the mean resistances (i.e., $\bar{R}_1 < \bar{R}_2$) and the load in Figure 3.5 implies that R_2 is safer than R_1 when safety is evaluated in terms of the central factor of safety. However, in reality $P_{f,2} > P_{f,1}$ due to the higher uncertainty in R_2. The use of a central factor of safety in this case is again misleading.

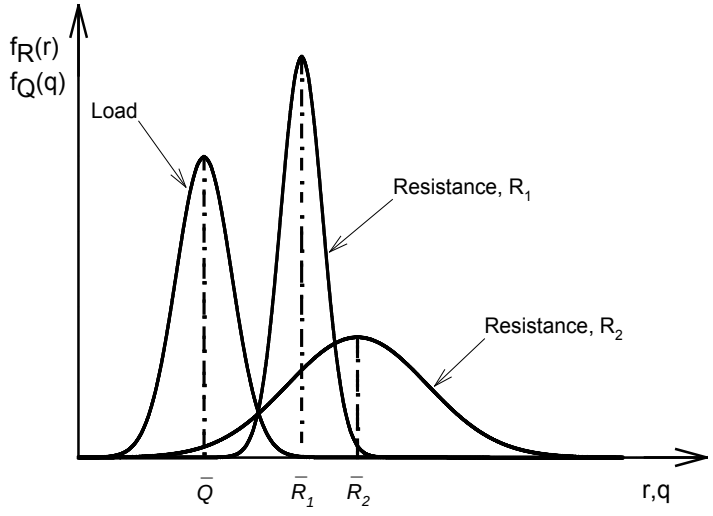

Figure 3.5. Illustration of the effect of the expected value and dispersion of resistance on factor of safety.

The use of the nominal factor of safety might reduce the types of inconsistency described in the preceding paragraphs; however, there is no prescribed method for selecting the nominal value so the use of a factor of safety remains ambiguous.

Equation 3.25 provides a means for computing the probability of failure for any distributions of Q and R. For certain specific distributions, closed-form analytical expressions can be derived. For example, if Q and R are normally distributed, failure will occur when $Z = R - Q$. Therefore, the probability of failure can be expressed as

$$P_f = P[Z < 0] = \Phi\left[\frac{0 - (\bar{R} - \bar{Q})}{\sqrt{\sigma_R^2 - \sigma_Q^2}}\right] = 1 - \Phi\left[\frac{\bar{R} - \bar{Q}}{\sqrt{\sigma_R^2 - \sigma_Q^2}}\right] \tag{3.6}$$

whereΦ is the CDF of the standard normal variate.

If R and Q are lognormally distributed with logarithmic mean, λ, and logarithmic standard deviation, ζ, then

$$P_f = 1 - \Phi\left[\frac{\lambda_R - \lambda_Q}{\sqrt{\zeta_R^2 + \lambda_Q^2}}\right] \tag{3.7}$$

Recognizing that (for a random variable, X),

$$\lambda_X = \ln X = \ln \mu_X - \frac{1}{2}\zeta_X^2 \tag{3.8}$$

$$\zeta_X = \sigma_{\ln X} = \sqrt{\ln 1 + \left(\frac{\sigma_X}{\mu_X}\right)^2} = \sqrt{\ln(1 + COV_X^2)} \tag{3.9}$$

the probability of failure can be written in terms of means and coefficients of variation as

$$P_f = 1 - \Phi\left[\frac{\ln\left[\frac{\mu_R}{\mu_Q}\sqrt{\frac{1 + COV_Q^2}{1 + COV_R^2}}\right]}{\sqrt{\ln(1 + COV_R^2)(1 + COV_Q^2)}}\right] \tag{3.10}$$

3.3.4.3 Reliability index

After a prescribed value is chosen for the probability of failure, design will proceed with the goal that all elements have a probability of failure less than or equal to the prescribed value.

For two independent, normally distributed random variables, $X_1$and X_2, the function $Z = X_1 - X_2$ will also be normally distributed with pdf given by

$$f_Z(z) = \frac{1}{\sqrt{2\pi\left(\sigma_{X_1}^2 + \sigma_{X_2}^2\right)}} exp\left[-\frac{1}{2}\left(\frac{z - (\bar{X}_1 - \bar{X}_2)}{\sqrt{\sigma_{X_1}^2 + \sigma_{X_2}^2}}\right)^2\right] \tag{3.11}$$

Letting $X_1 = R$and $X_2 = Q$, then assuming $Z = R - Q$ gives

$$f_Z(z) = \frac{1}{\sqrt{2\pi\left(\sigma_R^2 + \sigma_Q^2\right)}} exp\left[-\frac{1}{2}\left(\frac{z - (\bar{R} - \bar{Q})}{\sqrt{\sigma_R^2 + \sigma_Q^2}}\right)^2\right] \tag{3.12}$$

which indicates that $\bar{Z} = \bar{R} - \bar{Q}$ and $\sigma_z = \sqrt{\sigma_R^2 + \sigma_Q^2}$. Note that the standard deviation of Z depends on both σ_R and $\sigma_Q$and is greater than either $\sigma_R$or σ_Q. The failure state ($Z < 0$or $R < Q$) can be seen in Figure 3.6. to be β standard deviations below the mean, i.e., $\beta = \bar{Z}/\sigma_Z$. The quantity β is commonly referred to as the reliability index and is uniquely related to the probability of failure through the relationship

$$\beta = \Phi^{-1}\left(1 - P_f\right) \tag{3.13}$$

Or alternatively

$$P_f = 1 - \Phi(\beta) = \Phi(-\beta) \tag{3.14}$$

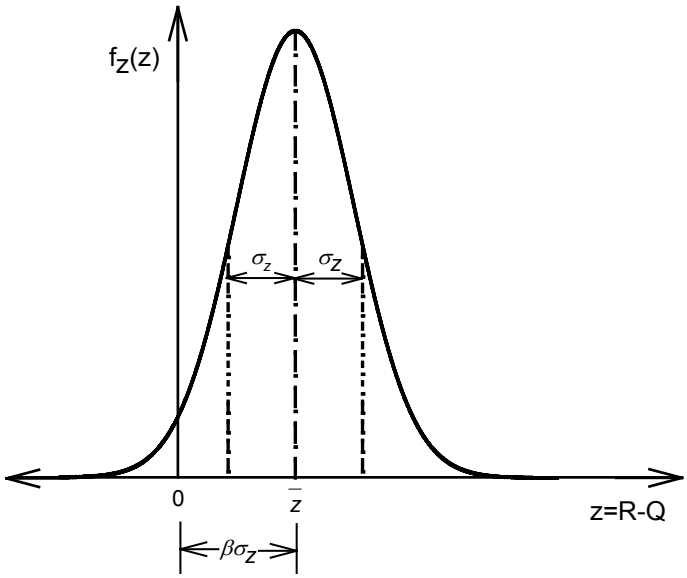

Figure 3.6. An illustration of a probability density function $R - Q$.

The reliability index, β, is usually a more convenient representation of the probability of failure, and is commonly used in risk-based design. The probability of failure decreases as β increases. Typical values of the reliability index and its corresponding level of performance are summarized in Table 3.2. Though the numbers can be of similar magnitude, the reliability index is not the same as the factor of safety from ASD.

Table 3.2. Relationship between Reliability Index and Probability of Failure (after U.S. Army Corps of Engineers, 1997).

Reliability Index, β	Probability of Failure, $P_f = \Phi(-\beta)$	Expected Performance Level
1.0	0.16	Hazardous
1.5	0.07	Unsatisfactory
2.0	0.023	Poor
2.5	0.006	Below average
3.0	0.001	Above average
4.0	0.00003	Good
5.0	0.0000003	High

Note: $\Phi(\cdot)$ = standard normal probability distribution

3.3.5 Load and Resistance Factor Design

As suggested by Becker (1996a), there are three basic levels of probabilistic design. Level III is the fully probabilistic method. It requires that the actual probability density functions for all variables be known. It is the most complex, time consuming and expensive method, and is generally only suitable for use on unique projects. Level II is the approximate probabilistic method. It does not require knowledge of the actual probability distributions of random

variables. Instead, only the shape and type of distribution needs to be defined. Level I is the semi-probabilistic method in which safety is represented by separate load and resistance factors which are determined from a second moment (Level II) reliability analysis.

RBD is most commonly implemented through the use of a practical framework called Load and Resistance Factor Design (LRFD). In LRFD, the global factor of safety used in ASD is replaced by separate load and resistance factors. LRFD (a Level I method) is a simplification of the rigorous RBD into a practical and easy to use design approach that can readily be codified. It is the end product of a shift in design philosophy to the use of probabilistic design as opposed to deterministic design. RBD is simplified into an LRFD format by defining a load factor, γ, and resistance factor, ϕ, that are applied to the nominal load and resistance, respectively, such that the following equation is satisfied:

$$\eta \sum \gamma_i Q_{n_i} \leq \phi R_n \tag{3.15}$$

where η is a factor that accounts for the ductility, redundancy, and importance of the system, γ_i is a load factor applicable to a specific load component, Q_{n_i} is a specific nominal load component and $\sum \gamma_i Q_{ni}$ the summation of the factored loads for the given loading condition applicable to the limit state being considered. This represents the sum of the factored load contributions. If only one load component is considered, Equation 3.48 can be shown as

$$\eta\gamma Q_n \leq \varphi R_n \tag{3.16}$$

whereQ_n is the nominal load and R_n is the nominal resistance. The product of the load factor and the nominal load, γQ_n, is referred to as the factored load and, likewise, the product of the resistance factor and the nominal resistance, ϕR_n, is referred to as the factored resistance. Generally, load factors are limited to values greater than one and therefore produce factored loads that are greater than the nominal load. Resistance factors are limited to values less than one and produce factored resistances that are lower than the nominal resistance.

The values of the load and resistance factors are determined, or calibrated, in such a way as to provide a desired level of reliability, which can be expressed in terms of a reliability index or probability of failure associated with some performance objective.

3.3.5.1 LRFD Calibration

Implementation of LRFD requires the specification of appropriate load and resistance factors, whose values must be determined through a calibration exercise. The fundamental goal of the calibration is to establish a set of load and resistance factors that are consistent with a desired probability of failure or reliability index for a given performance objective. In some cases, load

and resistance factors are selected to produce a design consistent with conventional (generally ASD-based) practice.

Although different procedures can be used for LRFD calibration, the main steps in a typical calibration process are described in the following subsections.

Identification of Limit States

LRFD has appropriately been referred to as Limit States Design (LSD) because it requires that all performance objectives be defined in terms of limit states. A limit state is a performance condition related to a design objective. Three basic limit states are commonly used in LRFD design. Ultimate (or strength) limit states represent states at which the ultimate capacity of a system (or its important components) is reached. Exceedance of an ultimate limit state, therefore, can have very serious consequences such as collapse of a structure. Serviceability limit states, on the other hand, relate to lower levels of damage that affect the operating characteristics of the system of interest. While the strength limit state is often most important, LRFD emphasizes checking both strength and serviceability limit states for compliance. Depending on geographic location and the potential for extreme cases of loading, an extreme limit state may also need to be checked. Each limit state may have a different probability of exceedance, so load and resistance factors have different values for different limit states.

Ultimate Limit State

The Ultimate Limit State (ULS) is used to ensure an appropriate margin of safety based on the ultimate strength of the materials. At the ULS, the strength of the soil and/or structure is fully mobilized and any additional stress or load would produce a failure mechanism that could lead to instability (collapse) of the structure. Exceedance of the ULS can lead to destruction of the structure and danger to people in, on, beneath, or near it. The requirement for ULS is usually expressed in terms of loads or stresses, as in Equation 3.49.

Serviceability Limit State

While the ULS deals with life safety and structural stability performance objectives, it is also desirable that a structure remain operational under lower levels of loading than those associated with the ULS. The Serviceability Limit State (SLS) is used to control the likelihood that deformations, vibrations and movements large enough to affect operability of a structure will occur under anticipated loading conditions. In geotechnical engineering, serviceability limit states can be defined with respect to settlement, lateral displacement, and overall stability. Pile lateral capacity design is controlled by the serviceability limit state. In this context, the notions of load and resistance typically expressed in terms of forces (and stresses) are not particularly useful. It has become common in structural engineering to use the terms "demand" and "capacity" in the place of "load" and "resistance." Demands, therefore, become a measure of the response of a system and can be expressed in terms of loads or displacements (structural engineers refer to "displacement demand," for example). The capacity, therefore, can be a measure of a system's ability to resist force, or to accommodate displacement without exceeding some acceptable level of damage. The performance requirement for SLS is normally expressed in terms of tolerable deformations (i.e., deformation $\leq$ tolerable deformation to remain serviceable, or deformation demand $\leq$ deformation capacity). In current LRFD procedures,

unacceptable deformation is compared to the deformation predicted using factored loads and the resistances.

Serviceability limit states have a higher likelihood of occurrence than ULS because they occur at lower, and consequently more frequent, levels of ground motion. In many geotechnical applications the SLS (settlement) is initially designed for, and the adequacy of design with respect to the ULS is checked subsequently.

Extreme Event Limit State

Structures may also, generally depending on their geographic location, be subjected to one or more forms of extreme loading. For bridges, extreme events could include major earthquakes or floods, collision with a vessel, vehicle or ice flow, or scour. The Extreme (Event) Limit State (ELS) is used to assure that catastrophic failure, which would have life safety implications, will not occur in extreme loading cases.

Develop Response Models

A response model must be developed for each limit state. The response model must predict the response parameter(s) of interest, typically force and/or stress for the ULS and displacement and/or strain for the SLS, given the appropriate loading. A response model for pile capacity, for example, could be the Gates model (Gates, 1957) that predicts capacity (in terms of force) as a function of driving resistance. On the other hand, a response model for pile displacement could involve finite element analysis of a pile embedded in a soil deposit. A number of different response models are typically available for a given problem.

Proper formulation, use, and interpretation of the response model is one of the most important aspects of design; it is imperative that the engineer use his/her knowledge and experience to identify all feasible failure modes and deformation mechanisms and to ensure that their development can be adequately captured by the response model(s) used in the design process.

Select Characteristic Values

Prior to establishing the load and resistance factors, it is critically important to clearly define the characteristic load and resistance values to which the load and resistance factors will be applied. Some implementations have used mean values and others have used more conservative nominal values; obviously, mixing factors with different characteristic values inconsistently can lead to substantially under- or over-conservative designs. AASHTO recommends that average measured values of relevant laboratory and/or insitu test data be used for individual geologic units when sufficient data to compute a stable average is available. Since the goal of LRFD is to produce designs with predictable reliabilities, the amount of conservatism (or statistical *bias*) in any characteristic load and resistance values must be carefully determined.

As previously described, nominal parameter values may differ, usually in a conservative manner, from mean values of the parameters. The ratio of the mean measured value to the predicted value is typically defined as the bias associated with the predicted value; obviously, predictions that match the mean values are unbiased.

Characterize Uncertainty in Response Model Parameters

A response model will have a number of input parameters that it uses to predict the response parameter(s) of interest. In most cases, these input parameters will not be known with complete certainty, so they can be treated as random. Characterization of a random variable can be performed at different levels, and can range from the use of a small number of statistical moments (e.g., mean and variance) to specification of a complete probability distribution.

It is a rare project for which sufficient data to perform a complete statistical characterization of soil properties is available. Consequently, it is frequently necessary to estimate the uncertainty in various soil properties using the results of data compilations from similar soil conditions (e.g., Phoon and Kulhawy, 1999a; 1999b; Jones et al., 2002). Such compilations, an example of which is shown in Table 3.3, generally present coefficients of variation for different properties for different soil types. Suggestions regarding the type of distribution that best represents the different soil properties may also be available; many soil properties have been shown to be approximately lognormally distributed, and it is common to assume that they are distributed in that manner. The lognormal distribution has the important property of not permitting negative parameter values, and is positively skewed in a manner similar to that frequently observed in soil property databases. With that assumption, knowledge of the mean and coefficient of variation is sufficient to define the entire lognormal distribution. It should be recognized, however, that the lognormal distribution is unbounded at the high end and may, therefore, assign non-zero probabilities to parameter values that may not be feasible or realistic.

Table 3.3. Coefficient of variation (C.O.V.) for typical geotechnical parameters (after Becker, 1996b).

Geotechnical parameter	C.O.V.	References
Index Properties		
Natural variability	0.05 – 0.15	Kay, 1993
Natural water content	(18)	Kulhawy, 1992; Phoon et al., 1993
Liquid and plastic limits	(0.11)	Kulhawy, 1992; Phoon et al., 1993
Unit weight	0.04 – 0.16 (0.07)	Cherubini et al., 1993; Kulhawy, 1992
Initial void ratio	(0.20)	Kulhawy, 1992
SPT *N* penetration resistance	0.15 – 0.50	Barker et al., 1991; Meyerhof, 1993; 1995
CPT q_c tip resistance	0.15 – 0.37	Barker et al., 1991; Meyerhof, 1993; 1995
Strength Properties		
Angle of internal friction		
From laboratory tests	0.05-0.25(0.13)	Cherubini et al. 1993; Meyerhof 1993, 1995; Kulhawy 1992; Manoliu and Marcu 1993
From CPT correlations for sand	0.15-0.25	Barker et al. 1991
Undrained shear strength	0.12-0.85(0.34)	Meyehoff 1993, 1995; Cherubini et al. 1993; Kulhawy 1992
Deformation properties		
Elastic modulus	0.2-0.5	Meyerhof 1993, 1995
Modulus of deformation	0.2-0.4	Meyerhof 1993, 1995
Compression index, C_c	0.17-0.55(0.37)	Cherubini et al. 1993; Meyerhof 1993, 1995; Kulhawy 1992

Values in parenthesis represent mean values

Characterize Model Uncertainty

A number of different response models are frequently available for a given problem. Some are relatively simple and easy to use, and some are quite detailed and complex. In general, the simpler models do not account for the mechanism(s) of response as well as the more detailed models, and therefore have a higher level of model uncertainty (or, potentially, model bias). Because model uncertainty and bias affect the probability of failure it is usually necessary to compute resistance factors for different models. When calibrated to achieve a particular reliability index (or probability of failure), the use of a less accurate (more uncertain) response model will require use of a lower resistance factor for the same level of bias. This situation, therefore, allows an owner or engineer to choose between using simple response models, which will lead to more expensive structures due to the lower resistance factor, and more complex response models, which will have higher engineering costs but lower construction costs by allowing the use of a higher resistance factor.

The quantity and quality of calibration data will both affect load and resistance factors. Ideally, a large data set indicating the response of the type of system of interest to significant ranges of the various variables that influence the response would be available. For each response model, then, analyses of the cases in the data set would be performed and the accuracies of the models would be interpreted in terms of the residuals (i.e., differences between model-predicted and observed values). These residuals would be affected by uncertainty in the input parameters and model uncertainty. Procedures are available for identification of model uncertainty given the total uncertainty and the parametric uncertainty; these procedures are typically based upon the generally reasonable assumption that model and parametric uncertainty are independent of each other, in which case the total variance is the sum of the parametric variance and the model variance. The model variance (and, hence, the model standard deviation) can be obtained by subtracting the parametric variance from the total variance.

Select Calibration Target

LRFD can be implemented in a number of different ways, each of which has philosophical and practical advantages and disadvantages. The decision on which approach to take for a given problem, may well be controlled by political or regulatory considerations rather than purely engineering considerations. The primary approaches are described briefly in the following paragraphs.

The original intent of reliability-based limit state design was to produce designs with a specified probability of successful performance. In that sense, calibrating load and resistance factors to produce a given reliability index is ultimately the most appropriate manner in which to implement LRFD. However, such calibration requires more performance data than is frequently available, and also requires specification of a particular reliability index, which may involve some level of subjective decision-making.

Another calibration target may be to produce designs of reliability consistent with the reliability of other components of a structure or system. The concept of consistent reliability is important for development of optimal designs. One of the drawbacks of ASD is that it frequently produces designs of variable (and unknown) reliability that can lead, for example, to a foundation with a much higher probability of failure than the structure it supports. In such cases, the money spent to provide the “extra” capacity of the structure is wasted because the structure

may still be destroyed if its foundation fails; in other cases, the reverse situation (foundation with higher capacity than structure) may occur. Therefore, a target level for calibration of an LRFD foundation design procedure may be specified as being equal to the reliability index used for the superstructure.

Finally, the introduction of any new design paradigm should, at least in the early stages of its use, produce designs that are not radically different from designs known to have performed satisfactorily in the past. For this reason, and for reasons relating to availability of data and historical precedent, LRFD calibrations for geotechnical problems have frequently been performed to produce designs consistent with typically-used ASD factors of safety. While this approach is not seen as the best ultimate use of LRFD principles, it offers a logical way to transition from ASD to reliability-based LRFD design procedures and is commonly used in practice. A detailed description of the development of current load and resistance factors for foundation design is presented in Allen (2005b).

Determine Load and Resistance Factors Consistent with Calibration Targets

The process of determining the load and resistance factors in an LRFD calibration exercise depends on the calibration target and on the nature of the problem of interest. In some cases, resistance factors may be desired for a single load case; in others, they may be desired for multiple load cases. It should be noted that load and resistance factors are not unique – there are an infinite number of combinations of load and resistance factors that can produce the same probability of failure (or reliability index). It is desirable, however, to constrain load factors to being greater than 1.0 and resistance factors to be less than 1.0, although there are special conditions under which that may not be possible. For relatively simple design problems, closed-form solutions for load and resistance factors may be available.

Load Factor

Load factors are generally more straightforward to determine than resistance factors since they depend primarily on factors that can often be measured for common load cases. Upon statistical characterization of the load, Q, a load factor to be applied to the mean load, $\bar{Q}$, (or $\lambda_Q Q_n$, if the nominal load is used) can be estimated as

$$\gamma = 1 + n_\sigma COV_Q \tag{3.18}$$

where n_σ is the desired number of standard deviations above the mean required to obtain the desired probability of exceedance and COV_Q is the coefficient of variation of the load. In practice, values of n_σ have been somewhat arbitrary (Allen et al., 2005b), but values of $n_\sigma = 2$ are common. With this approach, the factored load would be two standard deviations above the mean load. If normally distributed, the factored load would then have a 2.3% probability of being exceeded.

Resistance Factor

Once a load factor has been established, the resistance factor required to produce the desired probability of failure, or reliability index, can be determined. As indicated previously in

Equation 3.25, for the case of normally distributed load and resistance, the probability of failure can be computed as

$$P_f = 1 - \Phi^{-1}\left[\frac{\bar{R} - \bar{Q}}{\sqrt{\sigma_R^2 + \sigma_Q^2}}\right] \tag{3.19}$$

To develop an explicit expression for a risk-based design format, Equation 3.52 can be written as

$$\bar{R} \geq \bar{Q} + \Phi^{-1}\left[1 - P_f\right]\sqrt{\sigma_R^2 + \sigma_Q^2} \tag{3.20}$$

which, recognizing that $\beta = \Phi^{-1}\left[1 - P_f\right]$, allows the equality corresponding to the limit state boundary to be expressed as

$$\bar{R} = \bar{Q} + \beta\sqrt{\sigma_R^2 + \sigma_Q^2} \tag{3.21}$$

Substituting $\bar{R} = \bar{Q}\gamma/\phi$, $\sigma_R = \bar{R} \cdot COV_R$, $\sigma_Q = \bar{Q} \cdot COV_Q$, and $\gamma = 1 + n_\sigma COV_Q$, an expression for the resistance factor, ϕ, can be written as

$$\phi = \frac{1 + n_\sigma COV_Q}{1 + \beta\sqrt{(\gamma/\phi)^2 COV_R^2 + COV_Q^2}} \tag{3.22}$$

It should be noted that the resistance factor, ϕ, appears on both sides of Equation (2.15) so that an iterative approach may be required to compute its value.

If the calibration is to be performed for a target of consistency with a particular ASD central factor of safety, FS_m, Equation 3.54 can be modified by substituting $\bar{R} = FS_m \cdot \bar{Q}$ and solving for the value of β that is consistent with the specified factor of safety. That value of β can then be used with Equation 3.55 to determine the resistance factor, ϕ.

For the case of lognormally distributed load and resistance, the resistance factor can be expressed as

$$\phi = \gamma\frac{\sqrt{\left(1 + COV_Q^2\right)/\left(1 + COV_R^2\right)}}{\exp\left[\beta\sqrt{\ln\left[\left(1 + COV_Q^2\right)\left(1 + COV_R^2\right)\right]}\right]} \tag{3.23}$$

In this case, iteration is not required to compute the resistance factor.

The preceding examples are simple but show how the load and resistance factors are related to each other, to the reliability index, and to the uncertainties in both load and resistance. For design problems that are sufficiently complicated that they cannot be idealized or approximated as having normal or lognormal distributions, more complicated procedures such as Monte Carlo simulation may be required to identify load and resistance factors.

3.4 PERFORMANCE-BASED SEISMIC DESIGN

A complete prediction of performance requires prediction of the response, damage, and loss associated with one or more specific levels of ground shaking. This process can be illustrated schematically as shown in Figure 3.7. A response model is used to predict the response of a soil-structure system to earthquake shaking. The response model can range from an empirical algebraic equation to a detailed nonlinear finite element model. A damage model is used to predict physical damage from response levels. Finally, losses are predicted from damage by a loss model. The loss model may be a relatively straightforward combination of repair quantities and unit costs, or a complex financial model that considers indirect losses, future interest rates, etc. Alternatively, a loss model can be expressed in terms of downtime or increased traffic congestion due to temporary (or permanent) loss of one or more bridges.

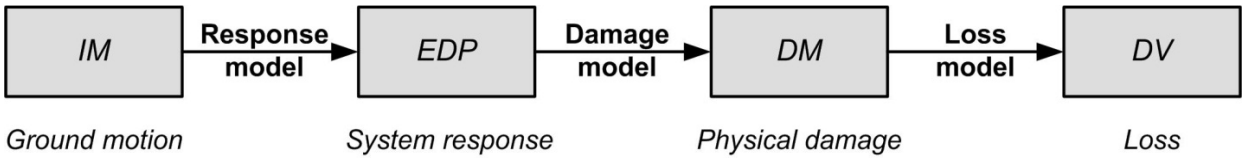

Figure 3.7. Schematic illustration of process by which response, damage, and loss are predicted.

3.4.1 History of Performance-Based Seismic Design

Early efforts at seismic design were scenario-based, i.e., based on the identification of one or more "design earthquakes" (e.g., maximum credible and maximum probable earthquakes) typically specified by source (fault), magnitude, and location. The ground motions associated with the design earthquakes were estimated deterministically using median values from early attenuation relationships. These median values generally neglected the now widely-recognized uncertainty inherent in ground motion estimation.

An important advance in seismic design came in the late 1970s with the publication of the ATC-3-06 (Applied Technology Council, 1978) report. ATC-3-06 built on the probabilistic seismic hazard analysis concepts of Cornell (1968) and the mapping work of Algermissen and Perkins (1976) to express design seismic loading in a probabilistic manner. Recognizing the dramatic differences in seismic activity across the United States, ATC-3-06 presented contour maps of effective peak acceleration (*EPA*) and effective peak velocity (*EPV*) which, together with soil profile coefficients, could be used to develop design response spectra for bridge structures. The use of these two measures of ground motion intensity accounted for differences

in the high- and low-frequency characteristics of ground motions, and the soil profile coefficient controlled spectral shape. ATC-3-06 recommended that design be based on a single level of ground shaking – that with a 10 percent probability of exceedance in a 50-yr period, i.e., a 475-yr return period. For structures, ATC-3-06 provided guidance for the allowance of inelastic behavior of components through the provision of ductility, and based performance on the relationship between estimated and allowable interstory drifts. The allowable story drifts were presented for four seismic performance categories in three seismic use groups. Thus, the use of deformation-based response and capacity measures was introduced.

Subsequent codes in various areas of the world have maintained the basic approach of ATC-3-06 but have refined many of the details. Instead of basing design spectra on *EPA* and *EPV*, some are now based on short-period (0.2 sec) and long-period (1.0 sec) spectral accelerations. Soil effects are accounted for by more refined soil classification systems with site class coefficients that account for basic effects of nonlinear response.

3.4.2 Discrete Hazard Level Approach

The first document widely recognized as establishing procedures for performance-based design of new structures was the Vision 2000 report (SEAOC, 1995). While developed for buildings rather than bridges, Vision 2000 described procedures intended to produce structures "of predictable performance" with respect to a series of discrete hazard levels. Figure 3.8 shows how Vision 2000 coupled four discrete performance levels (fully operational, operational, life safe, and near collapse) with four ground motion hazard levels (frequent, occasional, rare, and very rare) for structures with performance objectives for three categories of structures (basic, essential/hazardous, and safety critical). The Vision 2000 report described the general levels of damage to various building components and provided allowable inter-story drift limits associated with the four performance levels. These limits were expressed deterministically but were intended to be conservative; the degree of conservatism, however, is not known. Thus, Vision 2000 provided for design based on multiple levels of performance at multiple ground motion hazard levels, with performance related to deformation-related quantities (e.g., inter-story drift) that are closely related to damage.

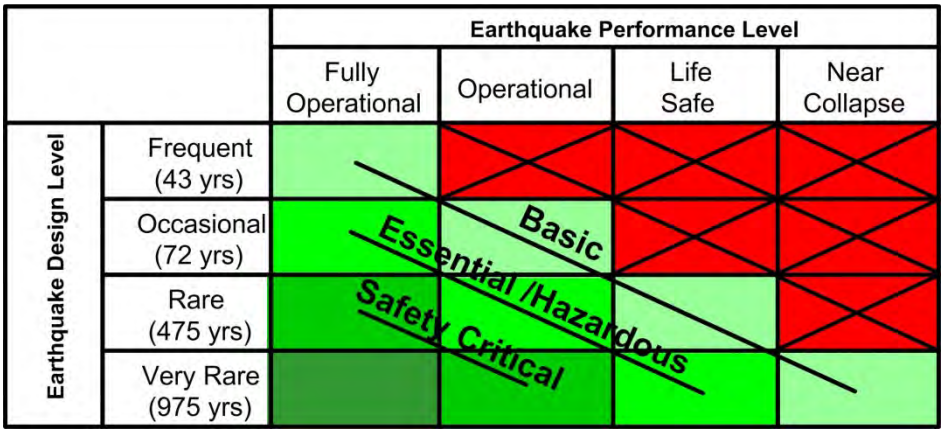

Figure 3.8. Combinations of earthquake hazard and performance levels proposed by Vision 2000 (SEAOC, 1995).

3.4.3 Integral Hazard Level Approach

The Pacific Earthquake Engineering Research Center (PEER) has proposed a framework for PBEE (Cornell and Krawinkler, 2000; Deierlein et al., 2003). The framework makes use of the previously described notation, and recognizes the fact that *IM*s, *EDP*s, *DM*s, and *DV*s, as well as the relationships between them, are all uncertain. The PEER framework is encapsulated in a "framing equation" formally presented in its most general form as

$$\lambda(\boldsymbol{DV}) = \iiint G(\boldsymbol{DV} \mid \boldsymbol{DM}) \left| dG(\boldsymbol{DM} \mid \boldsymbol{EDP}) \right| \left| dG(\boldsymbol{EDP} \mid \boldsymbol{IM}) \right| \left| d\lambda(\boldsymbol{IM}) \right| \tag{3.24}$$

In Equation (1), $G(a|b)$ denotes a complementary cumulative distribution function (CCDF) for a conditioned upon b (the absolute value of the derivative of which is the probability density function for a continuous random variable) and the bold type denotes vector quantities. From left to right, the three CCDFs result from loss, damage, and response models; the final term, $d\lambda(\boldsymbol{IM})$ is obtained from the seismic hazard curve. The framing equation implicitly assumes that the quantities used to describe ***IM***, ***EDP***, and ***DM*** are sufficient predictors of ***EDP***, ***DM***, and ***DV***, respectively.

The framing equation allows calculation of loss hazard (i.e., the mean annual rate of exceeding various levels of loss) by integrating over all levels of ground motion, response, and damage with the contributions of each of those variables weighted by their relative likelihoods of occurrence. The computed loss hazard can be viewed as the weighted average of all possible earthquake, ground motion, response, damage, and loss scenarios. It can account not only for location-dependent differences in tectonic environment but also for local differences in construction quality (as evidenced by capacities to resist damage), repair costs, and local indirect costs. It can therefore allow a uniform, objective, and consistent estimate of losses in different geographic regions.

3.4.3.1 Solution by Numerical Integration

This triple integral can be solved directly only for an idealized set of conditions, so it is solved numerically for most practical problems. When all variables are continuous, the numerical integration can be accomplished (assuming scalar parameters for simplicity) as

$$\lambda_{DV}(dv) = \sum_{k=1}^{N_{DM}} \sum_{j=1}^{N_{EDP}} \sum_{i=1}^{N_{IM}} P[DV > dv \mid DM = dm_k] \times P[DM > dm_k \mid EDP = edp_j] \times P[EDP > edp \mid IM = im_i] \Delta \lambda_{IM}(im_i) \tag{3.25}$$

where $P[a|b]$ describes the probability of a given b, and where N_{DM}, N_{EDP}, and N_{IM} are the number of increments of *DM*, *EDP*, and *IM*, respectively.

The PEER framework has the useful benefit of being modular. The discretized framing equation (Equation 2) can be broken down into a series of components, e.g.,

$$\lambda_{EDP}(edp) = \sum_{i=1}^{N_{IM}} P[EDP > edp \mid IM = im_i] \Delta \lambda_{IM}(im_i) \tag{3.26a}$$

$$\lambda_{DM}(dm) = \sum_{j=1}^{N_{EDP}} P[DM > dm \mid EDP = edp_j] \Delta \lambda_{EDP}(edp_j) \tag{3.26b}$$

$$\lambda_{DV}(dv) = \sum_{k=1}^{N_{DM}} P[DV > dv \mid DM = dm_k] \Delta \lambda_{DM}(dm_k) \tag{3.26c}$$

which means that hazard curves can be computed for *EDP*, *DM*, and *DV* and interpreted in the same manner as the more familiar seismic hazard curve (for *IM*) produced by a PSHA.

Using numerical integration, The PEER framing equation can be solved for arbitrary response, damage, and loss relationships. Considering the response, a response hazard curve can be obtained, using Equation 3(a), for any *IM* hazard curve, any form of *EDP* = *f*(IM), and any distribution of *EDP* values given *IM*. Because integration occurs over $\lambda_{IM}(im)$, the PEER framework considers *the entire ground motion hazard curve* rather than just a single point as is done in conventional seismic design. This allows consistent prediction of response hazards in different seismic/tectonic environments ranging from low/weak (e.g., Sacramento) to moderately frequent/strong (e.g., Seattle) to frequent/very strong (e.g., Los Angeles) to rare/extremely strong (e.g., Aberdeen). These benefits could also be applied at the national level where even more extreme variations in seismic activity exist.

3.4.3.2 Closed Form Solution for Response

Many seismic hazard curves are nearly linear on a log-log plot, at least over significant ranges of ground motion intensity (Department of Energy, 1994; Luco and Cornell, 1998), which implies a power law relationship between mean annual rate of exceedance and *IM* that can be expressed as

$$\lambda_{IM}(im) = k_0 (IM)^{-k} \tag{3.27}$$

In this expression, k_0 is the value of $\lambda_{IM}(im = 1)$ and k is the slope of the seismic hazard curve (in log-log space, in which Equation (3.27) plots as a straight line).

The response of a bridge foundation, expressed in terms of displacements and rotations, is a function of the earthquake ground motion, the dynamic response of the foundation, and the dynamic response of the structure supported by the foundation. The nature of the loading applied to a pile group, therefore, is strongly influenced by the dynamic response of the structure, which will be sensitive to the specific characteristics of the individual structure. In order to produce a more general solution, the PEER framework can be modified by the inclusion of a load measure, *LM*, that is a function of the ground motion and structural response, and is also a sufficient predictor of foundation response. If the loading model is assumed to be of power law form

$$EDP = a(IM)^b \tag{3.28}$$

with lognormal dispersion ($\beta_R = \sigma_{\ln EDP|IM}$), a closed-formy solution for the resulting *EDP* hazard curve can be expressed as

$$\lambda_{EDP}(edp) = k_0 \left[\left(\frac{EDP}{a} \right)^{1/b} \right]^{-k} \exp\left[\frac{k^2}{2b^2} \beta_R^2 \right] \tag{3.29}$$

This equation describes the mean annual rate of exceeding some level of response, $EDP = edp$, given the seismic hazard curve, which is the result of a probabilistic seismic hazard analysis and a probabilistic response model. It therefore considers *all* possible values of *IM* rather than only those corresponding to the small integer number of return periods considered in conventional design, and all levels of foundation loading given the various levels of ground shaking. Equation (8) is composed of two parts, the first of which is a function of *edp* and the constants (k_0, k, a, b) that describe the mean hazard curve and the median *EDP-LM* relationship (i.e., the response model). The second part depends on the slopes of the hazard curve and median response model relationship and, most significantly, on the uncertainty in the response model. The second term can be viewed as an "uncertainty multiplier" since its value is 1.0 when there is no uncertainty in the loading and response models and becomes progressively greater than 1.0 as the response model uncertainty increases. This result shows that the mean annual rate of exceedance of a particular *EDP* value increases with increasing uncertainty. Put another way, the *EDP* value corresponding to a given mean annual rate of exceedance (or return period) increases with increasing response model uncertainty.

3.5 A MODIFIED PERFORMANCE-BASED RESPONSE FRAMEWORK

Direct prediction of the response of a soil-foundation-bridge system from an earthquake ground motion would require development of a complete soil-foundation-structure model for the specific bridge of interest. Such an analysis would require either a single computer program capable of modeling the soil, foundation, and structure with appropriate levels of rigor, or a substructuring approach. Most computer programs used for direct seismic analysis model soil behavior or structural behavior rigorously, but few are capable of modeling both simultaneously. Furthermore, given the high levels of nonlinearity that exist in soil behavior (at moderate levels of shaking) and structural response (at higher levels of response), direct analyses must be performed in the time domain and are therefore computationally time-consuming. The substructuring approach involves performing a kinematic interaction analysis, in which the soil and foundation (with stiffness but no mass) are modeled in one analysis to obtain a foundation input motion, and then the structural response to the foundation input motion is computed in a second, inertial interaction analysis. The substructuring approach relies upon the principle of superposition and therefore implies linear (or equivalent linear) response.

In order for the investigation described in this report to produce results of sufficient generality to be useful and applicable to a wide variety of bridge, site, and foundation conditions, a modified performance-based framework was developed. The modified framework involves definition of an intermediate variable, referred to hereafter as a "load measure," *LM*, that is computed from the ground motion and used to compute the foundation response. Figure 3.9 schematically illustrates the role of the load measure in the response prediction process.

Figure 3.9. Schematic illustration of modified performance-based framework.

In the modified framework, a modular substructuring approach is used to separate the structural and foundation responses. The purpose of this approach is to allow more convenient consideration of a wide range of bridge structures and pile foundations. While the direct, coupled analysis of specific soil-foundation-structure systems is preferable to decoupled analysis, the decoupled approach provides a useful degree of flexibility in exploring the response of different systems.

3.5.1 Calculation of Response

Following the logic described in Section 3.3.3, a general expression for response hazard including the load measure intermediate variable can be written as

$$\lambda(\boldsymbol{EDP}) = \iint G(\boldsymbol{EDP} \mid \boldsymbol{DM}) \left| dG(\boldsymbol{LM} \mid \boldsymbol{IM}) \right| \left| d\lambda(\boldsymbol{IM}) \right| \tag{3.30}$$

For practical purposes, a scalar response hazard curve can be obtained by numerical integration of the form

$$\lambda_{EDP}(edp) = \sum_{j=1}^{N_{EDP}} \sum_{i=1}^{N_{IM}} P[EDP > edp \mid LM = lm_j] \times P[LM > lm_j \mid IM = im_i] \Delta \lambda_{IM}(im_i) \tag{3.31}$$

The modified response prediction can also be performed in modular fashion with a *LM* hazard curve being computed from a ground motion hazard curve, and a response hazard curve computed using the *LM* hazard curve.

$$\lambda_{LM}(lm) = \sum_{i=1}^{N_{IM}} P[LM > lm \mid IM = im_i] \Delta \lambda_{IM}(im_i) \tag{3.32a}$$

$$\lambda_{EDP}(edp) = \sum_{j=1}^{N_{LM}} P[EDP > edp \mid LM = lm_j] \Delta \lambda_{LM}(lm_j) \tag{3.32b}$$

Regardless of whether the response hazard curve is computed directly or in modular form, the preceding equations can be applied to ground motion hazard curve, load, and response models with any characteristics. The accuracy of the response hazard will depend on the number of *IM* and *LM* increments over which the numerical integration is accomplished.

3.5.2 Closed Form Solution for Response

The closed-form solution for response is also based on assumption of a power law relationship between mean annual rate of exceedance and *IM* described in Equation 3.4. The response of a bridge foundation, expressed in terms of displacements and rotations, is a function of the earthquake ground motion, the dynamic response of the foundation, and the dynamic response of the structure supported by the foundation. The nature of the loading applied to a pile group, therefore, is strongly influenced by the dynamic response of the structure, which will be sensitive to the specific characteristics of the individual structure. In the modified framework, the load measure, *LM*, is a function of the ground motion and structural response. If the loading model is assumed to be of power law form

$$LM = a(IM)^b \tag{3.33}$$

with lognormal dispersion ($\beta_L = \sigma_{\ln LM|IM}$), a closed-form solution for the resulting *LM* hazard curve can be expressed as

$$\lambda_{LM}(lm) = k_0 \left[\left(\frac{lm}{a} \right)^{1/b} \right]^{-k} \exp\left[\frac{k^2}{2b^2} \beta_L^2 \right] \tag{3.34}$$

If the response model is also assumed to be of power law form

$$EDP = d(LM)^e \tag{3.35}$$

with lognormal dispersion ($\beta_R = \sigma_{\ln EDP|LM}$), a closed-form solution for the resulting *EDP* hazard curve can be expressed as

$$\lambda_{EDP}(edp) = k_0 \left[\frac{1}{a} \left(\frac{edp}{d} \right)^{1/e} \right]^{-k/b} \exp\left[\frac{k^2}{2b^2 e^2} \left(e^2 \beta_L^2 + \beta_R^2 \right) \right] \tag{3.36}$$

This equation describes the mean annual rate of exceeding some level of response, *EDP* = *edp*, given the seismic hazard curve, which is the result of a probabilistic seismic hazard analysis, a probabilistic loading model, and a probabilistic response model. It therefore considers *all* possible values of *IM* rather than only those corresponding to the small integer number of return periods considered in conventional design, and all levels of foundation loading given the various levels of ground shaking. The right side of Equation (3.36) is composed of two parts, the first of which is a function of *edp* and the constants (k_0, *k*, *a*, *b, d, e*) that describe the mean hazard curve, median *LM-IM* relationship (i.e., the load model), and the median *EDP-LM* relationship (i.e., the response model). The second part depends on the slopes of the hazard curve, median loading model relationship, median response model relationship and, most significantly, on the uncertainty in the loading and response models. The second term can be viewed as an "uncertainty multiplier" since its value is 1.0 when there is no uncertainty in the loading and response models and becomes progressively greater than 1.0 as the loading and/or response model uncertainty increases. This result shows that the mean annual rate of exceedance of a particular *EDP* value increases with increasing uncertainty. Put differently, the *EDP* value corresponding to a given mean annual rate of exceedance (or return period) increases with increasing loading and/or response model uncertainty.

3.6 SUMMARY

This chapter has presented a discussion of seismic performance and a probabilistic framework for seismic performance evaluation. With this framework, the return periods of various levels of response, damage, and loss can be predicted in a probabilistically rigorous manner, i.e., with consideration of uncertainties in ground motions, seismic response, physical damage, and loss estimation.

The performance-based framework described in this chapter can be viewed as an extension of probabilistic seismic hazard analysis (PSHA), a technology that has become widely accepted for seismic design. Rather than designing for a deterministically-obtained level of response from a probabilistically-defined ground motion, a probabilistic representation of response given some ground motion can be combined with a probabilistic representation of ground motion hazards to obtain a fully probabilistic representation of response.

Design based on the fully probabilistic representation of response, as described in Chapter 6, allows more accurate, objective, and consistent prediction of performance in areas of different seismicity and using design procedures of different reliability.

4 Numerical Model of Pile Group Response

4.1 INTRODUCTION

To evaluate the seismic performance of pile foundations, a series of analyses of a pile group were performed using two types of numerical models. First, a structural model was used to predict the pile cap loading given the response of a simplified bridge structure to an applied input motion. Next, a soil-foundation model was used to predict the displacements and rotations of the pile foundation in response to the pile cap loading.

The details of the numerical models and overall pile group modeling concept are discussed in this chapter. Input and output parameters, and the strategies used to measure seismic response of the pile group are included in this discussion. First, a more detailed description of the pile foundation model is provided. Next, the numerical modeling framework (OpenSees) that was used to simulate response is introduced. To validate the numerical model, evidence in the form of comparisons with a full-scale static load test and dynamic centrifuge testing is presented.

4.2 SOIL-FOUNDATION-BRIDGE MODELING CONCEPT

As discussed in Chapter 3, there are an infinite number of different combinations of bridge types, pile group configurations, and soil conditions. Each combination will have a unique response, so predicting the response of a particular system requires a complete soil-foundation-bridge model for that system. For maximum accuracy, that model should be developed using software that represents soil and structural response, and the interaction between them, with high and equal rigor. Few software packages currently available have such capabilities, and their use is very time-consuming. The results of such analyses would correspond to the particular details of the soil-foundation-structure system being modeled, and generalization of the computed response to other conditions would be difficult. For the purposes of this project, which seeks to provide pile foundation design guidance for a wide range of soil, foundation, and structure characteristics, such an approach is not tenable.

For this project, a framework with the ability to create response models for many different pile group configurations in many different soil profiles was developed. The framework is basically that of a substructuring approach to soil-foundation-structure interaction. The soil-foundation-structure system is broken down into two systems – the structure and the foundation – each of which is analyzed separately. The purpose of the structural analysis is to compute realistic loading histories at the top of the pile cap. The second analysis then computes the response of the pile cap to the imposed loading.

The following sections describe the basic aspects of the structural and pile group models and present typical results from both models.

4.2.1 Bridge Modeling

The structural model used to represent a bridge was kept simple in order to provide foundation loading histories general enough to be applicable to bridges with different characteristics. The bridge structure was idealized as a lumped mass at the top of a single distributed-mass column. The column was modeled in OpenSees as having both lateral and axial stiffness through the use of a fiber model. As a result, the bridge would respond dynamically to all three components of input ground motions.

4.2.1.1 Structural Model

A schematic illustration of the structural model is shown in Figure 4.1. The characteristics of the structure were developed to be consistent with typical highway bridges of the types that might be designed by agencies such as WSDOT and Caltrans. Based on discussions with Caltrans and WSDOT engineers, structures with fundamental periods of 0.5 sec and 1.0 sec were analyzed. The supported mass was chosen to produce a desired level of initial static vertical load in the pile group of interest. The column sections were chosen to be consistent with those used in ATC-49. Finally, the heights of the columns were selected to produce the desired fundamental period with the selected supported mass and column flexural stiffness.

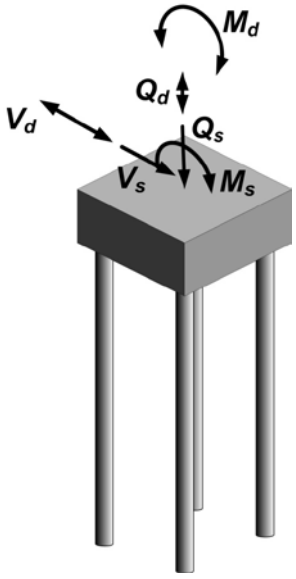

Figure 4.1 **Schematic illustration of forces and moments acting on pile cap. Subscripts 's' and 'd' refer to static and dynamic loads, respectively. Loads and moments for only one horizontal directions is shown here for clarity – the same loads and moments exist in the orthogonal horizontal direction.**

In order to evaluate the influence of column yielding on pile foundation response, a number of analyses were performed using nonlinear column models. These models used fiber models that could produce a desired column yield moment.

4.2.1.2 Foundation Model

The base of the column was assumed to be connected to a pile group with a rigid pile cap embedded in a soil profile of interest. In the OpenSees model, however, the pile group and pile cap were represented by equivalent springs and dashpots whose properties were computed using the DYNA4 computer program (Novak et al., 1993). DYNA4 allows consideration of the contributions of the piles and pile caps to pile group stiffness and damping. The OpenSees model was developed with springs and dashpots representing translational and rocking degrees of freedom at the base of the column; rotation about the vertical axis, i.e., torsion, was not modeled as it was not considered to produce a significant level of response in the types of typical bridge structures that are the subject of this research.

4.2.1.3 Equivalent Linear Analysis Procedure

DYNA4 assumes linear elastic behavior of the soil and the foundation elements, and computes stiffness and damping coefficients as functions of frequency. Since soils are known to exhibit nonlinear behavior, an equivalent linear procedure was used to approximate the effects of soil nonlinearity. DYNA4 analyses were performed for different soil shear moduli to account for the softening associated with nonlinear soil behavior. The results of these analyses were used to express the spring and dashpot coefficients as functions of pile cap displacement/rotation.

The structural model was then analyzed by applying three components of ground motion to the ends of the spring-dashpot assemblies at the base of the column in the OpenSees structural model. The response of the model was computed, including the displacements and rotations of the base of the column. These displacements and rotations were compared with the values corresponding to the foundation impedances used in the analysis. If the displacements and rotations differed by more than 2%, new impedance factors corresponding to the computed displacements and rotations were substituted for the original impedance factors and the analysis repeated. This procedure was repeated until the computed displacements and rotations of the pile cap were compatible with the impedance factors.

4.3 NUMERICAL MODELING USING OPENSEES

To simulate the seismic response of a pile foundations, both structural and geotechnical models that account for soil-structure interaction for a range of input parameters must be included in the model. The Open System for Earthquake Engineering Simulation (OpenSees) is a finite element program developed by the Pacific Earthquake Engineering Research (PEER) Center that is well suited to capture the seismic response of pile foundations (http://opensees/berkeley.edu).OpenSees is capable of modeling 1D, 2D and 3D nonlinear structural and geotechnical systems using a variety of different structural and geotechnical material models.

A finite element model of a pile group and pile cap system was constructed in OpenSees. This pile group system was subjected to multiple static load states and multiple dynamic load states as calculated in the structural dynamic analysis. All dynamic loads were applied to the pile cap. The response that was measured included horizontal displacements, vertical displacements, and rocking rotations (e.g. δ_x, δ_y, δ_z, θ_x, θ_y, θ_z).

4.3.1 Dynamic BNWF Model

The Beam-on-Nonlinear-Winkler-Foundation (BNWF) method is commonly used for simulating soil-pile interaction. In a BNWF model, the pile is modeled by a beam supported by a series of independent horizontal and vertical springs distributed along its length. A 1-D shear beam soil column can be used to provide free-field (far-field) motion and interface springs (p -y , t -z , and q -z) can be used to model soil-pile-structure interaction (near-field). It is also possible to attach a structural model to the top of the pile in a BNWF model.

A schematic of the OpenSees response model used in this research is shown in Figure 4.2. The superstructure and free-field soil motion were not modeled. The soil profiles considered in this investigation did not have strong impedance contrasts and did not contain liquefiable soils. As a result, kinematic interaction effects were expected to be negligible. Dynamic loading occurred only at the pile cap and p -y , t -z , and q -z springs provided soil resistance.

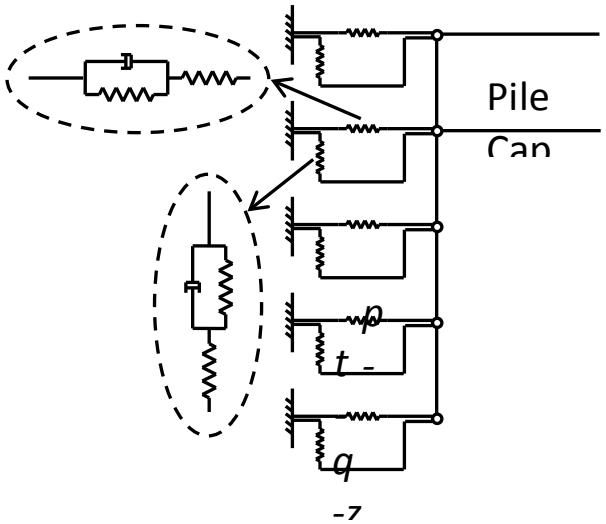

Figure 4.2. Schematic of BNWF model with interface springs (after Shin, 2007)

4.3.2 Material Models

To capture the response of the pile group system, specific material models were used in OpenSees to model piles, pile cap, p -y springs, t -z and q -z springs, and pile cap springs.

P -y springs were included to account for the lateral soil-pile interaction. The interface springs included elastic, plastic, and gap components connected in series. The p -y backbone curves for sand were based on the sand relation of API (1993). The ultimate lateral soil resistance, p_{ult}, and the deflection at one-half the ultimate soil resistance,y_{50}, were calculated according to procedures outlines in API (1993). The p -y backbone curves for clay were based on the soft clay relation of Matlock (1970). The inputs, p_{ult} and y_{50} were also calculated based on Matlock (1970.

To account for the vertical soil-pile interaction, the relationship between frictional shaft resistance and local deflection was modeled using t-z springs. The t-z backbone curves were based on Reese and O'Neill (1987)'s relation for piles in clay and Mosher (1984)'s relation for piles in sand (Reese and O'Neill, 1987; Mosher, 1984). q-z springs were used to model the relationship between point resistance and deflection at the bottom of the pile. The q-z backbone curves were based on Reese and O'Neill (1987)'s relation for drilled shafts in clay and Vijayvergia's relation for piles in sand (Vijayvergiya, 1977). Input values of q_{ult}, t_{ult}, and y_{50} were calculated according to procedures outlined in API (1993).

To capture the response of the pile group, pile elements were modeled using elastic beam elements. The pile cap consisted of very stiff elastic beam elements. Both pile and pile cap elements were massless.

4.4 MODEL VALIDATION

The use of the OpenSees framework as a response model for the seismic evaluation of pile foundations is validated by comparison with model test and field load test behavior. Shin (2007) showed that numerical modeling strategies used in OpenSees were capable of modeling soil-pile-structure interaction well. Shin's results validated the use of OpenSees to model the seismic performance of pile foundations.

Based on Shin's results, a pile group model was developed in OpenSees for use in this research. To verify the accuracy of the pile group model under static conditions, the results of a comparison between the OpenSees model and a case history of a large scale lateral load test are presented and discussed (Brown et al., 1988). To illustrate the ability of OpenSees to accurately simulate the response under seismic conditions, the results of simulations performed by Shin (2007) are also reviewed.

4.4.1 Static Loading

The OpenSees framework may be a sound approach to the seismic design of pile foundations, but numerical simulations are only useful if they can consistently predict response to an acceptable degree of accuracy. The results of a large-scale load test on a pile group reported by Brown, et al. (1988) were used to validate the accuracy of the static response of the model used in this research. The load test was modeled in OpenSees to show that the model is capable of producing accurate results that are consistent with current design practices.

A study was conducted at the University of Texas concerning the behavior of a closely spaced group of piles in sand when subjected to cyclic lateral loading (Brown et al., 1988). The research included a large-scale lateral load test of a group of nine steel pipe piles in sand as well as a load test of a single isolated pipe pile for comparison. The configuration is shown in Figure 4.3. Piles were founded in soil consisting of 9.5 ft (2.9 m) of medium dense sand underlain by very stiff clay. Because the sand extended to a depth slightly greater than 10 pile diameters, the response of the piles to lateral loading was dominated by the sand. Results from direct shear tests on the sand indicated an angle of internal friction of 38.5 degrees and a dry density of 98.5 lb/ft^3 (1.58 g/cm^3). Piles consisted of 10.75 in. (27.3 cm) outside diameter piles, with 0.365 in. (9.27 mm) wall thickness. The pile group was arranged in a 3x3 configuration with a center-to-

center spacing of 3 diameters. The piles were instrumented to measure the load on the top of each pile and the distribution of bending stresses along the length of each pile.

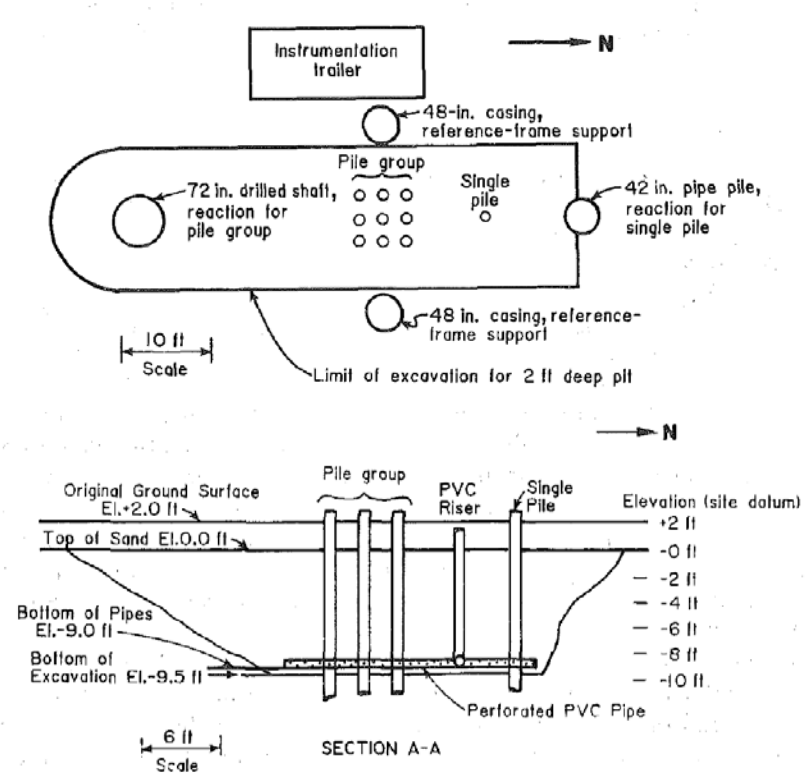

Figure 4.3. Site layout and test set up (Brown et al., 1988)

OpenSees simulations were performed to model the full scale test for both a single pile and the pile group. The focus of the comparison was not only to check the general level of agreement between predicted and measured response, but also to calibrate p -multipliers to account for group effects. A quick comparison of results shows that a general consistency between measured results and numerical results in OpenSees can be obtained.

4.4.1.1 Single Pile

A comparison of the behavior of a single isolated pile was made. Figure 4.4 shows the lateral load vs. deflection for the single pile. Circles (SP actual) represent actual measured values from the field test. In the field test, the single pile was less stiff than the group piles. To make the single pile behavior comparable to the group pile behavior, Brown et al. (1988) applied a correction factor to account for the reduced stiffness in the single pile. The solid line (SP stiff) represents the projected curve after the correction was made. The projected response (solid lines) from Brown et al. (1988) agrees well with the simulated response (dotted line) from OpenSees (OS). Figure 4.5 shows the bending moment in the pile vs. depth for a single pile. Again, the measured values closely match the numerical values.

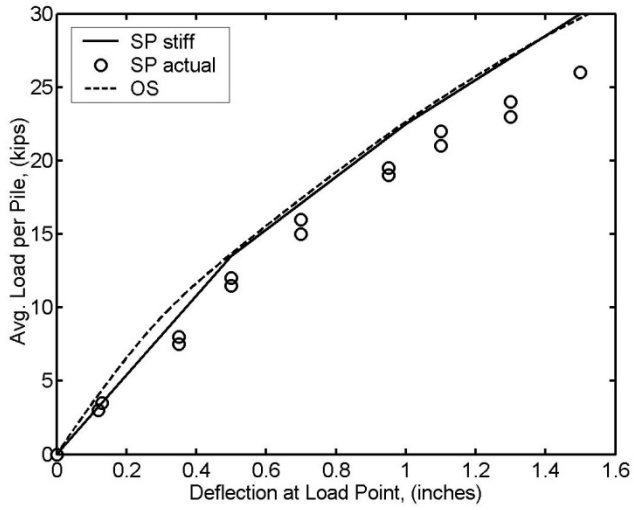

Figure 4.4. Lateral load vs. deflection for a single pile in sand

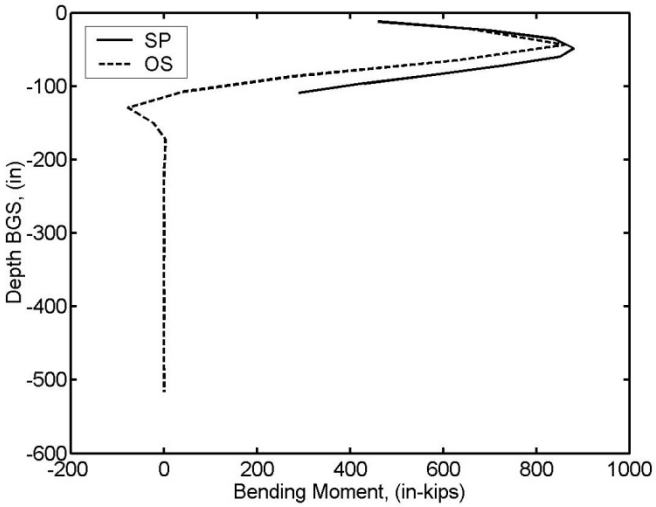

Figure 4.5. Bending moment vs. depth for a single pile in sand

4.4.1.2 Pile Group

When loaded to a similar average per pile load, the group piles deflected more than the single isolated pile. This is shown Figure 4.6 by the relative position of the curve for the single pile (SP) compared to the curves for a pile in the leading row (LR), a pile in the middle row (MR), and a pile in the back row (BR) of the pile group. That is, with the pile group there is a reduction in resistance at a given displacement level that needs to be accounted for. For example, the piles in the leading row of a pile group subjected to lateral loading will be significantly stiffer than piles in trailing rows due to group effects. To account for the reduced capacity, *p*-multipliers were introduced to the OpenSees model.

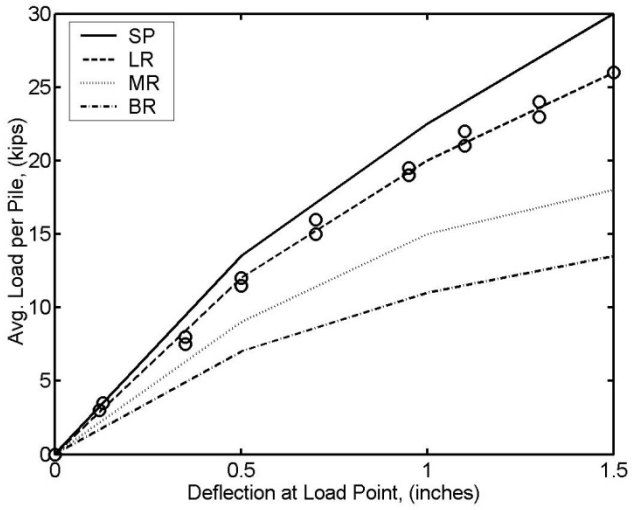

Figure 4.6. Load vs. deflection for single pile and pile group by row (after Brown et al., 1988)

Typical p -multipliers of 0.8, 0.4, and 0.3 were used for the leading, first trailing, and second trailing rows, respectively (Brown and Bollman, 1993; Hannigan et al., 1997). The *p-y* curves for sand were based on the sand relation of API (1993). Figure 4.7 shows the computed load-transfer relationships at a depth of one meter in sand for leading, first trailing, and second trailing rows of the pile group. These curves are representative of all curves that were obtained.

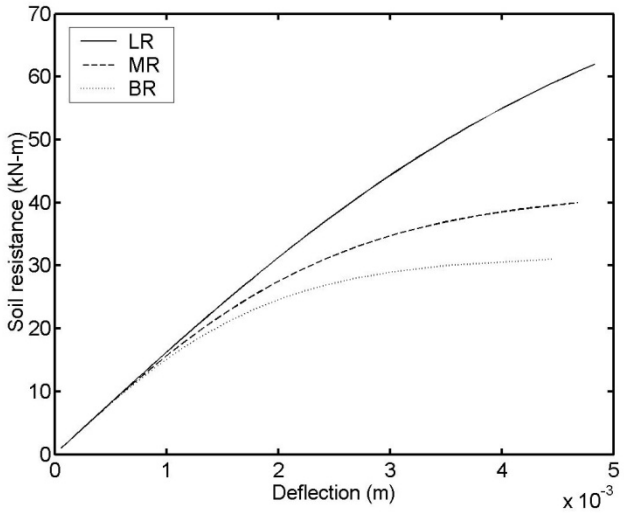

Figure 4.7. Typical *p-y* curves by row position for piles in group

Brown et al. (1988) compared measured data from the load test to predicted response from analytical methods. Brown noted that due to increased shear strength produced by densification, computed p -y curves significantly underpredicted soil resistance when compared to large-scale load test data. Brown et al. (1988) varied input soil parameters so that computed p -y curves matched measured p -y curves and obtained back-calculated soil parameters, and

found that an increase in friction angle from 38.5 to 50 degrees was required to account for the densification that apparently occurred during driving. Therefore, to simulate the measured response of the laterally loaded pile group, the same back-calculated soil properties used in OpenSees. Figure 4.8 shows a comparison of computed load-transfer relationships using actual and back-calculated soil properties.

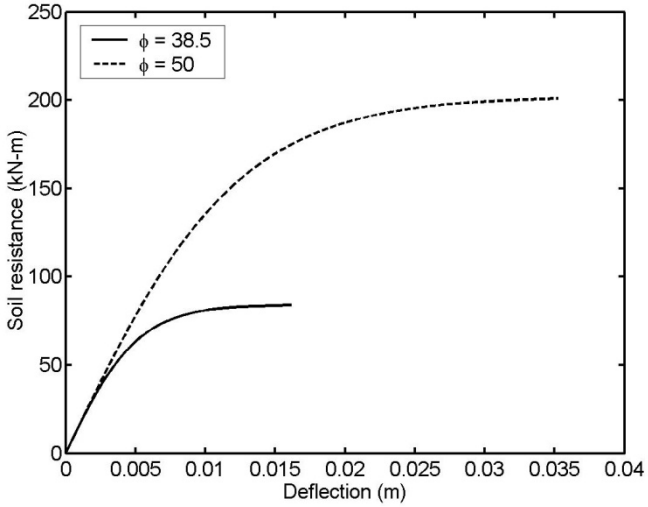

Figure 4.8. Comparison of experimental and computed *p-y* curves for a single pile

Using p -multipliers of 0.8, 0.4, and 0.3 for the leading, first trailing, and second trailing rows, respectively, and back-calculated soil properties, good agreement between simulated response from OpenSees and measured response from Brown et al. (1988) was obtained as shown in Figures 4.9 to 4.14.

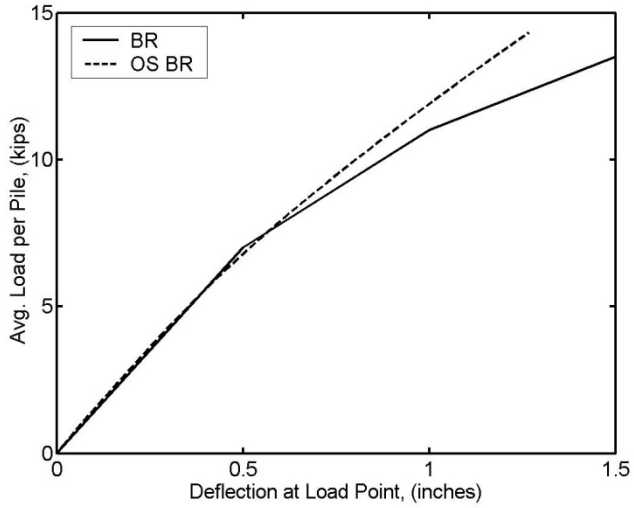

Figure 4.9. Plot of pilehead load vs. deflection for the second trailing row of a 3x3 pile group – comparison of OpenSees response (OS BR) to measured response (BR)

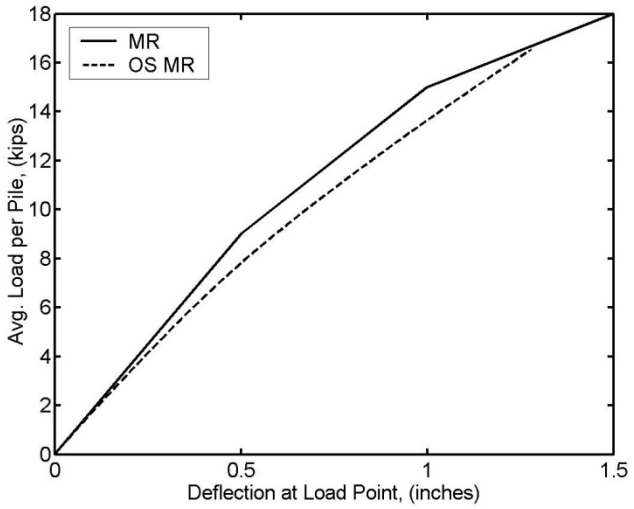

Figure 4.10. Plot of pilehead load vs. deflection for the first trailing row of a 3x3 pile group – comparison of OpenSees response (OS MR) to measured response (MR)

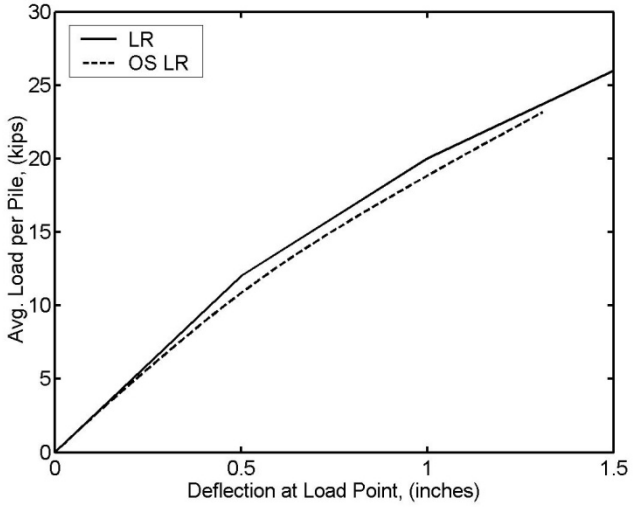

Figure 4.11. Plot of pilehead load vs. deflection for the leading row of a 3x3 pile group – comparison of OpenSees response (OS LR) to measured response (LR)

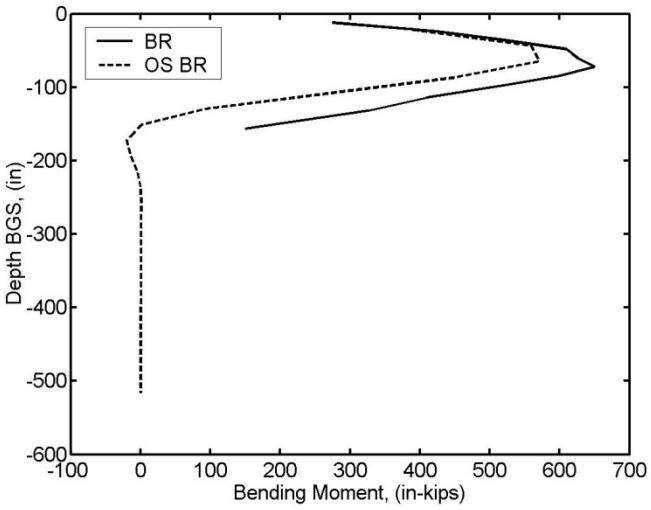

Figure 4.12. Plot of bending moment vs. depth for the second trailing row of a 3x3 pile group – comparison of OpenSees response (OS BR) to measured response (BR)

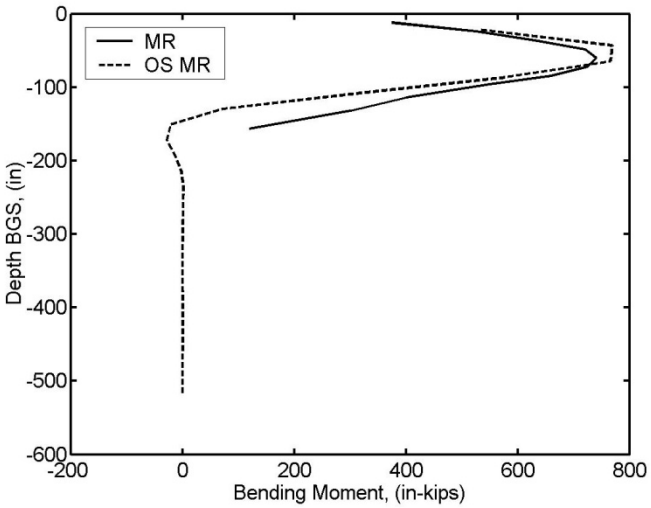

Figure 4.13. Plot of bending moment vs. depth for the middle row of a 3x3 pile group – comparison of OpenSees response (OS MR) to measured response (MR)

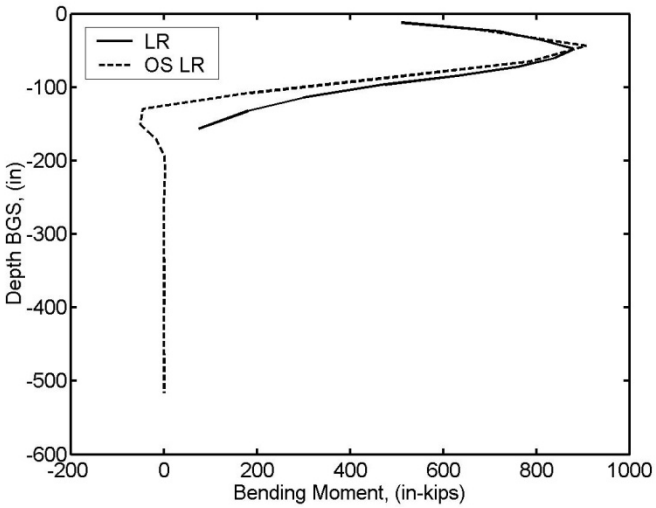

Figure 4.14. Plot of bending moment vs. depth for the leading row of a 3x3 pile group – comparison of OpenSees response (OS LR) to measured response (LR)

4.4.2 Dynamic Loading

Shin (2007) showed that the OpenSees framework could predict the measured dynamic response of model pile foundations to an acceptable degree of accuracy. To understand and validate numerical modeling strategies to capture soil-pile-structure interaction of bridge structures, Shin first performed a set of instrumented centrifuge experimental tests at UC Davis. The test setup, shown in Figure 4.15, included multiple pile lengths, stiffnesses, and group configurations that were subjected to multiple motions at multiple intensity levels.

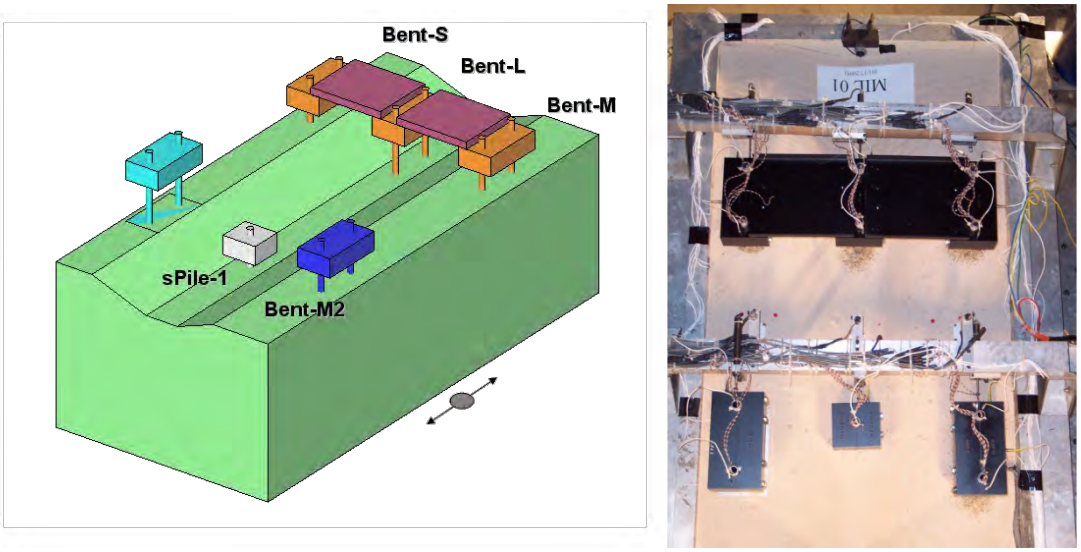

Figure 4.15. Schematic drawing and test setup for single pile, two-pile bents, and two span bridge (Shin, 2007)

The centrifuge experiments were modeled in OpenSees using dynamic Beam-on-Nonlinear-Foundation (BNWF) models based on conventional p -y springs for typical earthquake scenarios. In his research, Shin validated the OpenSees BNWF model by comparing centrifuge responses with numerical responses for a bent, a single pile, and a two span bridge. The comparison showed that the measured centrifuge response under dynamic conditions could be captured well by simulations in OpenSees.

4.4.2.1 Dynamic Response of a Pile Bent Structure

The dynamic response of the two-column bent structure, Bent-M2 from Figure 4.17, and its corresponding simulated response were compared. The measured centrifuge response and the simulated response were in good agreement for moderate shaking levels as shown by the comparison of acceleration time histories in Figure 4.16 and the comparison of pile bending moments in Figure 4.17.

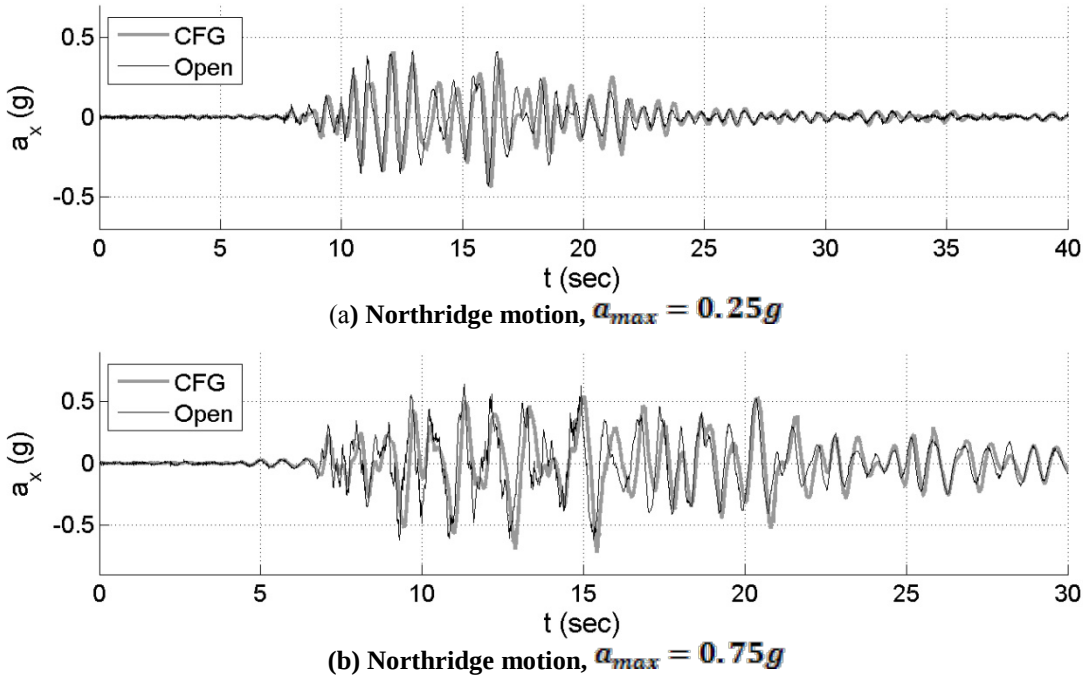

(a) **Northridge motion, $a_{max} = 0.25g$**

(b) Northridge motion, $a_{max} = 0.75g$

Figure 4.16. Superstructure acceleration time histories for Bent-M2 obtained from centrifuge test and numerical simulations (Shin, 2007)

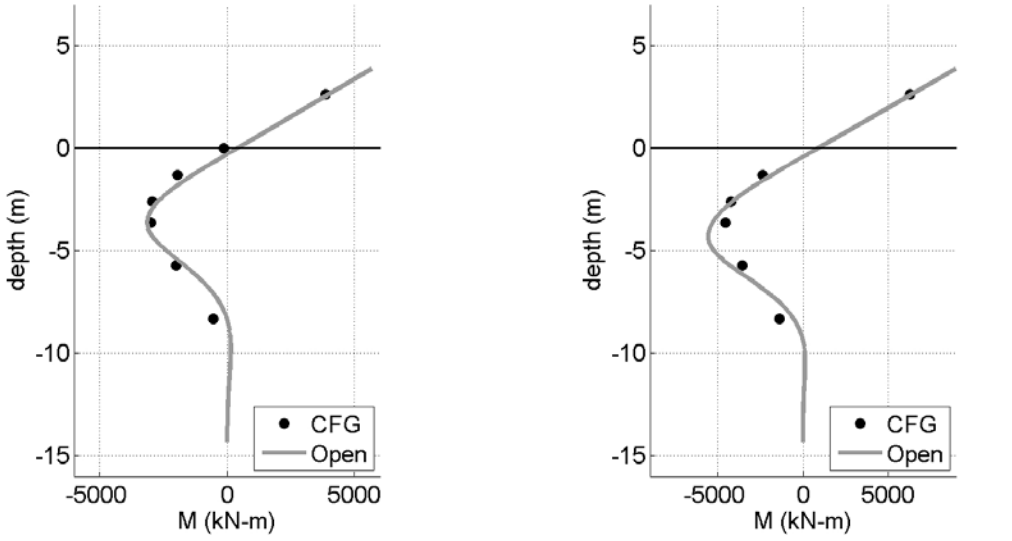

(a) **Northridge motion, $a_{max} = 0.25g$** **(b) Northridge motion, $a_{max} = 0.75g$**

Figure 4.17. Maximum pile bending moments for Bent-M2 obtained from centrifuge test and numerical simulations (Shin, 2007)

4.4.2.2 Dynamic Response of a Two-Span Bridge

The centrifuge test results and numerical response of the two-span bridge can also be compared. The two-span bridge had three foundations, labeled Bent-S, Bent-L, and Bent-M as shown in Figure 4.17, that supported columns of short, long, and medium heights. The differing stiffnesses of the columns caused more complex soil-foundation-structure interaction than would have occurred with constant column heights. Nevertheless, the measured centrifuge response and the simulated response were in good agreement for moderate shaking levels as shown by the comparison of acceleration time histories in Figure 4.18 and the comparison of pile bending moments in Figure 4.19.

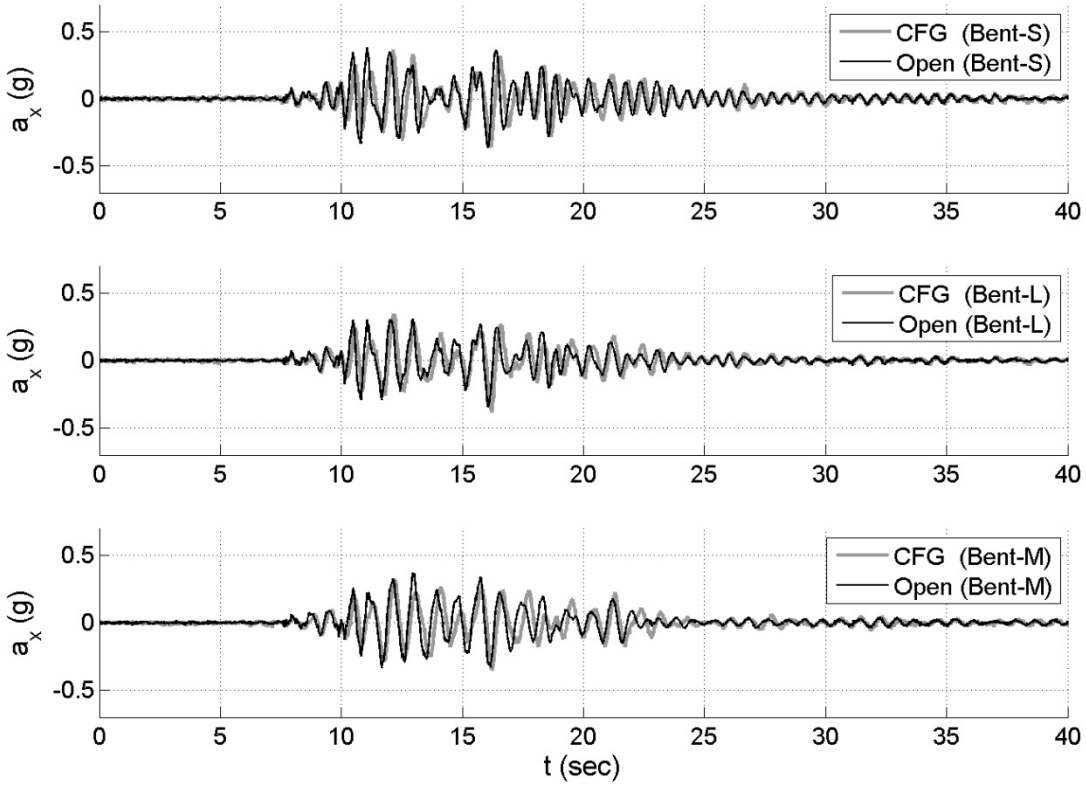

Figure 4.18. Centrifuge and OpenSees bridge deck acceleration time histories at three bent locations for Northridge event, $a_{max} = 0.25g$ (Shin, 2007)

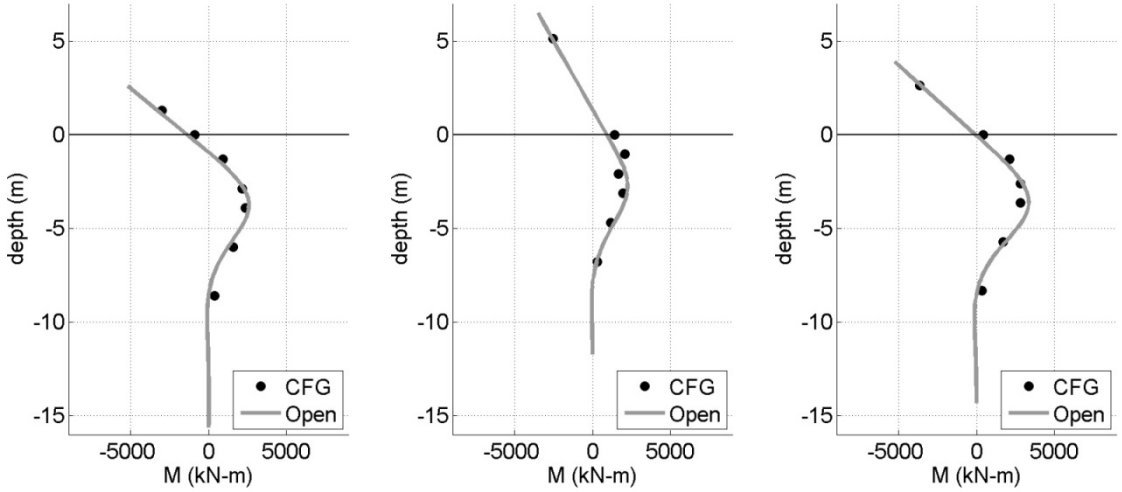

(a) Bent-S **(b) Bent-L** **(c) Bent-M**

Figure 4.19. Centrifuge and OpenSees pile bending moments for Northridge event, a_{max} = 0.25g (Shin, 2007)

4.5 SUMMARY

In this chapter, the numerical models used in this research to evaluate seismic performance of pile foundations were introduced and described in detail. The numerical modeling framework (OpenSees) that was used to simulate response was introduced and validated. To validate the numerical model, evidence in the form of comparisons with a full-scale static load test and dynamic centrifuge testing was presented. Comparisons of results obtained from experimental tests and OpenSees numerical simulations showed good agreement. The BNWF models based on conventional p-y springs captured the dynamic response of the centrifuge tests fairly well. Therefore, using similar modeling strategies, OpenSees simulations can be used to evaluate the seismic design of pile foundations.

5 OpenSees Modeling of Bridge Foundation Response

5.1 INTRODUCTION

As discussed in Chapter 3, an infinite number of possible combinations of bridge types, pile group configurations, and soil conditions must be considered when developing general design procedures for bridge foundations. Each combination will produce a unique response, so predicting the response of a particular system would require analysis of a complete soil-foundation-bridge model for that system. For maximum accuracy, that model should be developed using software that represents soil and structural response, and the interaction between them, with high and consistent levels of rigor. Few software packages currently available have such capabilities, and their use is generally very time-consuming. The results of such analyses would correspond to the particular details of the soil-foundation-structure system being modeled, and generalization of the computed response to other conditions would be difficult. For the purposes of this project, which seeks to provide pile foundation design guidance for a wide range of soil, foundation, and structure characteristics, such an approach is not tenable.

To evaluate the general seismic performance of pile groups used as bridge foundations, a series of analyses were performed using two types of numerical models. To maximize the generality of the process, the structural and foundations models were kept relatively simple and straightforward. The modeling process made use of the intermediate load measure variable introduced in Section 3.x in order to allow foundation response to be computed from the response of different structural responses.

5.2 SOIL-FOUNDATION-BRIDGE MODELING CONCEPT

For this project, a framework with the ability to create response models for many different pile group configurations in many different soil profiles was developed. The framework is basically that of a substructuring approach to soil-foundation-structure interaction, as illustrated in Figure 5.1. The soil-foundation-structure system is broken down into two systems – the structure and the foundation – each of which is analyzed separately. First, a structural model was used to predict the pile cap loading (i.e., the load measure, *LM*, introduced in Chapter 3) given the response of a simplified bridge structure to an applied input motion. Next, a soil-foundation model was used to predict the displacements and rotations of the pile foundation in response to the pile cap loading. The purpose of the structural analysis is to compute realistic loading histories at the top of the pile cap. These histories are consistent with the recorded ground motions used to compute them and with the dynamic characteristics of a bridge. While they

correspond to the response of a very simple structure, they account for realistic response characteristics including correlations between the various components of loading applied to pile groups. The second analysis then computes the response of the pile cap to the imposed loading.

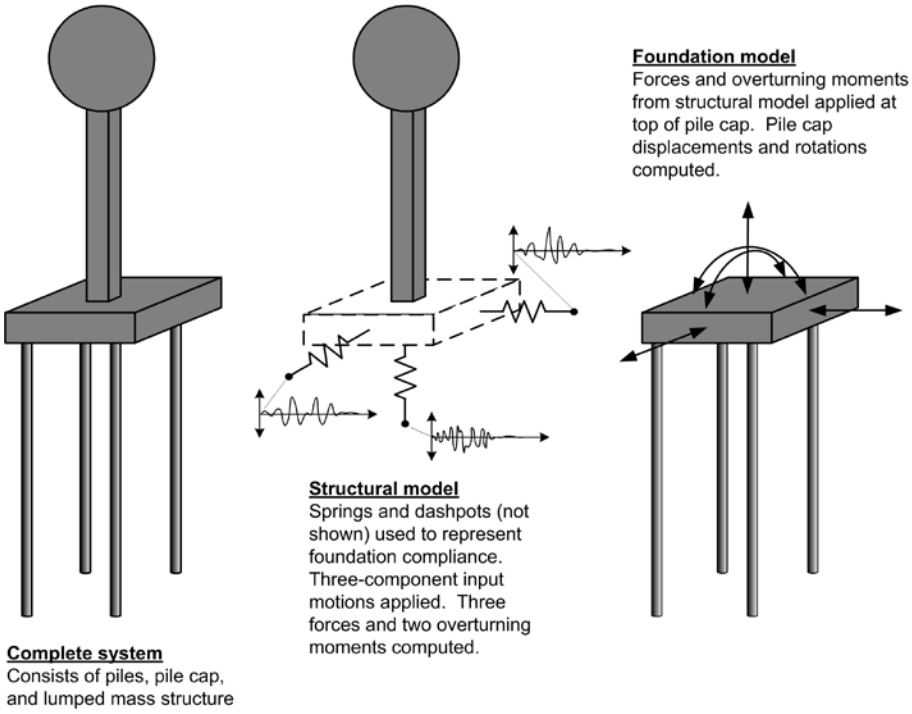

Figure 5.1 Schematic illustration of substructuring process used to separate response analysis into structural and geotechnical components. Note that rotational springs used in analysis are not shown.

The following sections describe the basic aspects of the structural and pile group models and present typical results from both models.

5.2.1 Bridge Structure Modeling

The structural model used to represent a bridge was kept simple in order to provide foundation loading histories general enough to be applicable to bridges with different characteristics. Two approaches were taken over the course of the research. Initially, structural analyses were performed using the SAP2000 computer program, a program widely used for dynamic analysis of bridges and other structures. Later, the same calculations were performed in OpenSees, a more general finite element package that has strong soil as well as structural modeling capabilities; the results of the OpenSees analyses were confirmed as being consistent with those obtained using SAP2000. The results presented in this report are based on the OpenSees analyses.

The bridge structure was idealized as a concentrated mass at the top of a single distributed-mass column. The column was modeled as having both lateral and axial stiffness

through the use of a fiber model. As a result, the bridge structure responds dynamically to all three components of input ground motions. Five components of loading – vertical load, Q, lateral loads, V_x and V_y, in the x- and y-directions, and overturning moments, M_x and M_y, about the y- and x-axes – were recorded in each analysis.

5.2.1.1 Structural Model

The characteristics of the model structure were developed to be consistent with typical highway bridges of the types that might be designed by agencies such as WSDOT and Caltrans. Based on discussions with Caltrans and WSDOT engineers, structural models with fundamental periods of 0.5 sec and 1.0 sec were analyzed. The supported mass was chosen to produce a desired level of initial static vertical load in the pile group of interest. The column sections were chosen to be consistent with those used in ATC49, a set of LRFD guidelines developed by the Applied Technology Council and the Multidisciplinary Center for Earthquake Engineering Research. The column sections were circular with 48-inch diameters, variable lengths, and a flexural stiffness of 5.9×10^9 k-in^2. The heights of the columns were selected to produce the desired fundamental period with the selected supported mass and column flexural stiffness. In order to evaluate the influence of column yielding on pile foundation response, a number of analyses were performed using nonlinear column models. These models used fiber models (Section 4.2.2) that would produce a desired column yield moment. Table 5.1 summarizes the characteristics of the structural models used in the analyses.

Table 5.1 Characteristics of model bridge structure

Pile Group Configuration										
	3x3		3x5		3x7		5x5		7x7	
Property	$T_o = 0.5$	$T_o = 1$	$T_o = 0.5$	$T_o = 1$	$T_o = 0.5$	$T_o = 1$	$T_o = 0.5$	$T_o = 1$	$T_o = 0.5$	$T_o = 1$
W (k)	687	687	1145	1145	1603	1603	1908	1908	3740	3740
A (in^2)	1810	1810	1810	1810	1810	1810	1810	1810	1810	1810
I (ft^4)	79.419	79.419	79.419	79.419	79.419	79.419	79.419	79.419	79.419	79.419
E (ksi)	3605	3605	3605	3605	3605	3605	3605	3605	3605	3605
L (ft)	32	53	28	44	25	40	24	38	19	30

5.2.1.2 Foundation Compliance

The base of the column was assumed to be connected to a pile group with a rigid pile cap embedded in a soil profile of interest. Because the response of the structure, which produces the computed pile cap loading, is affected by the dynamic behavior of the foundation, the compliance of the structural foundation was taken into account. In the OpenSees structural model, the pile group and pile cap were represented by discrete equivalent springs and dashpots at the base of the column. The properties of these elements were computed using the DYNA4 soil-structure interaction computer program (Novak et al., 1993). DYNA4 allows modeling of the response of piles and pile caps in layered elastic profiles. DYNA4 provided 5x5 impedance matrix functions from which spring and dashpot coefficients for translational (3) and rocking (2) degrees of freedom of the pile cap could be extracted; rotation about the vertical axis, i.e., torsion, was not modeled as it was not considered to produce a significant level of response in the types of typical bridge structures that are the subject of this research.

5.2.1.3 Equivalent Linear Analysis Procedure

DYNA4 assumes linear elastic behavior of the soil and foundation elements, and computes pile group impedances as functions of frequency. Examination of the DYNA4 output showed that stiffness and damping varied only weakly with frequency in the frequency range of interest. Since soils are known to exhibit nonlinear behavior, however, an equivalent linear procedure was used to approximate the effects of soil nonlinearity. DYNA4 analyses were performed for different soil shear moduli to account for the softening associated with nonlinear soil behavior. The results of these analyses were used to express the spring and dashpot coefficients as functions of pile cap displacement/rotation.

The structural model was then analyzed by applying three components of ground motion to the ends of the spring-dashpot assemblies at the base of the column in the OpenSees structural model. The response of the model was computed, including the displacements and rotations of the pile cap. These displacements and rotations were compared with the values corresponding to the foundation impedances used in the analysis. If the displacements and rotations differed by more than 1%, new impedance factors corresponding to the computed displacements and rotations were substituted for the original impedance factors and the analysis repeated. This procedure was repeated until the computed displacements and rotations of the pile cap were compatible with the impedance factors. Five components of pile cap load – Q, V_x, V_y, M_x, and M_y – were recorded for each analysis; these loading histories were saved for use in the foundation response analyses and for computation of load measures.

5.2.2 Foundation Modeling

The combination of structural and soil models available in OpenSees allows modeling of pile foundations in a number of ways. While it is possible to model piles as three-dimensional structural elements embedded in three-dimensional soils with interface elements, such models have so many degrees of freedom that their use is impractically time-consuming for the purposes of this research. A common compromise between rigor and computational efficiency is provided by the use of discrete, zero-length elements to describe the interaction between pile foundations and the surrounding soil. The general behavior of OpenSees pile group models was described in Chapter 4. The following sections describe the main components of the specific OpenSees foundation models used in this investigation.

The OpenSees pile group models were subjected to the loading histories computed in the structural response analyses. Each structural analysis produced time histories of vertical load, Q, lateral loads, V_x and V_y, and overturning moments, M_x and M_y. These loads were applied at the center of the upper surface of the pile cap as illustrated schematically in Figure 5.2. For each analysis, five components of pile cap movement – vertical displacement, w, lateral displacements, u and v, in the x- and y-directions, and rocking rotations, θ_x and θ_y, about the y- and x-axes – were recorded.

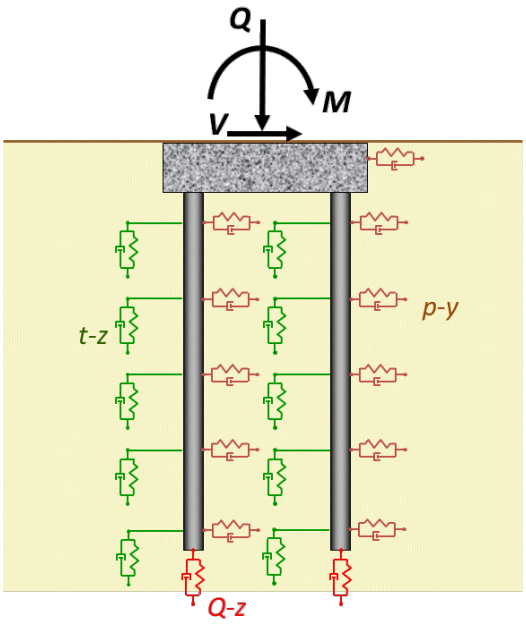

Figure 5.2. Schematic illustration of OpenSees pile group model showing only three loading components and one plane of *p-y* elements.

5.2.2.1 Piles

The response analyses performed in this research are based on 60-ft-long, 24-inch diameter steel pile piles with ½-inch thick walls. In OpenSees, the piles were modeled with a series of 18 3.33-ft-long fiber beam elements connected end-to-end. *P-y* and *t-z* elements were attached to the piles at 3.33-ft increments along their entire lengths. A *Q-z* spring was attached to the base of each pile.

5.2.2.2 Pile Groups

The basic pile group model consisted of a pile cap supported by a group of *N*x*M* piles where *N* is the number of piles in the *x*-direction and *M* is the number of piles in the *y*-direction. A pile group generator program was written so that piles could be spaced at arbitrary center-to-center distances, Δx and Δy. A variety of pile group configurations, including 3x3, 3x5, 3x7, 5x5, and 7x7, were used in the foundation response analyses.

5.2.2.3 Pile Caps

The pile caps were modeled as being virtually rigid using a frame of rigidly connected beam elements. Two levels of beam element frames connecting the piles in both the *x*-direction and the *z*-direction were rigidly attached by a 3.5-foot-long beam element in the *y*-direction. The piles were assumed to be rigidly connected to the pile cap. Since the top of the pile cap is flush with the ground surface, *p-y* springs were used to model the relationship between passive earth pressures and the movement of the pile cap.

5.3 SOIL CONDITIONS

To develop generally applicable results, the analyses were performed assuming the piles were installed in different soil profiles. Pile foundations are known to behave differently when installed in cohesive and cohesionless soil profiles, and procedures for prediction of pile response often use parameters that are divided into those two categories. Therefore, the pile foundations modeled in this study were assumed to be embedded into two profiles – a sand profile and a clay profile. Modification of the pile capacities, intended to represent variability in soil profile characteristics, were included in some of the analyses.

5.3.1 Sand Profile

The sand profile was assumed to consist of a deep deposit of medium-dense dry sand with a unit weight of 125 pcf. The sand was assumed cohesionless with a friction angle of 36^o and to correspond to an SPT resistance, $(N_1)_{60} \sim 20$. A shear wave velocity profile for the sand profile is plotted in Figure 5.3.

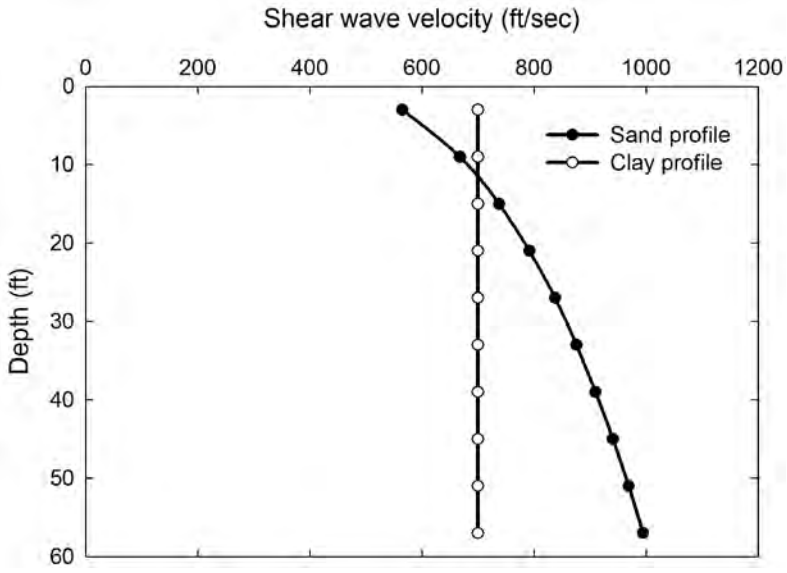

Figure 5.3 Shear wave velocity profiles for sand and clay soil profiles.

5.3.2 Clay Profile

The clay profile was assumed to consist of a deep deposit of medium stiff, uniform clay with an undrained strength of 3,000 psf. The shear wave velocity of the clay was assumed to be proportional to undrained strength, and therefore constant with depth as shown Figure 5.3.

5.4 STATIC LOADING CONDITIONS

A given pile group supporting a bridge will be subjected to some set of static loads prior to the occurrence of an earthquake. These static loads can include virtually any combination of vertical load, lateral loads (in two orthogonal directions), and overturning moments (about two

orthogonal axes). The relative magnitudes of these loads depend on the individual characteristics of the bridge, the site at which it is constructed, and on its foundations. When an earthquake occurs, additional dynamic loads are imposed upon the pile group – these include all five components (three loads and two overturning moments) and also depend on the specific characteristics of the bridge and foundation.

5.4.1 Static Load Response

A pile group supporting a bridge column will displace and/or rotate as loads are applied to it during construction. The OpenSees pile group model allows calculation of such displacements for any combination of static vertical, lateral, and overturning loads. The static design of pile foundations seeks, directly or indirectly, to prevent displacements from becoming excessively large. Large pile group movements under static loading can induce high bending and shear demands in a bridge structure, and in the pile group itself.

5.4.1.1 Reference Loads

To denote the proximity of the initial static load state to "failure," the notion of a reference load is introduced. The conventional idea of a pile group "capacity" implies that some dramatic effect is likely to occur if an applied load exceeds that capacity. In reality, exceeding a particular load capacity will lead to some additional pile group movement, the amount of which may be small or relatively large depending on the nature of the load-displacement behavior of the foundation. A reference load will be defined, for the purposes of this research, as a load level beyond which the accumulation of pile cap displacements becomes increasingly undesirable. The reference loads for this project were defined as:

Vertical loading: Q_{ref} = load corresponding to static capacity as determined from simulation of a pile group load test using Davisson (ref) criterion.

Lateral loading: V_{ref} = lateral load producing lateral displacement equal to 10% of pile diameter in simulations of pile group lateral load test.

Overturning: M_{ref} = moment applied in one direction causing vertical movement of any pile equal to that corresponding to Q_{ref}.

Reference load values for pile groups of different configurations are shown for the sand and clay profiles in tables 5.2 and 5.3.

Table 5.2 Sand profile reference loads

Vertical Reference Loads (kN)			
N_x/N_y	3	5	7
3	43676	72793	101911
5	72793	121322	-
7	0	-	237791

Horizontal Reference Loads (kN)			
N_x/N_y	3	5	7
3	10850	17820	24790
5	20238	33704	-
7	28392	-	66192

Reference Moments (kN-m)			
N_x/N_y	3	5	7
3	43870	55102	62827
5	113612	160699	-
7	221353	-	411509

Table 5.3 Clay profile reference loads

Vertical Reference Loads (kN)			
N_x/N_y	3	5	7
3	7778	12964	18149
5	13352	22254	-
7	18211	-	42493

Horizontal Reference Loads (kN)			
N_x/N_y	3	5	7
3	17882	29806	41728
5	29806	49673	-
7	41728	-	97360

Reference Moments (kN-m)			
N_x/N_y	3	5	7
3	28028	38230	46911
5	69550	102147	-
7	128418	-	259323

5.4.1.2 Reference Displacements

Reference displacements and rotations were simply defined as the displacements and rotations corresponding to the reference loads and moments. The reference vertical displacement, w_{ref}, is the displacement corresponding to the capacity obtained from the Davisson (1972) procedure. The reference lateral displacements, u_{ref} and v_{ref}, are both equal to 10% of the pile diameter. The reference rotations, $\theta_{x,ref}$ and $\theta_{y,ref}$, are the rocking angles that correspond to a maximum pile displacement of w_{ref}; those angles will depend on the width of the pile group as well as the value of w_{ref}. Reference load values for pile groups of different configurations are shown for the sand and clay profiles in tables 5.4 and 5.5.

Table 5.4 Sand profile reference displacements

Vertical Reference Displacement (m)			
N_x/N_y	3	5	7
3	0.0277	0.0277	0.0277
5	0.0277	0.0277	-
7	0.0277	-	0.0277

Horizontal Reference Displacement (m)			
N_x/N_y	3	5	7
3	0.061	0.061	0.061
5	0.061	0.061	-
7	0.061	-	0.061

Reference Rotation (degrees)			
N_x/N_y	3	5	7
3	0.9812	0.4906	0.3271
5	0.9812	0.4906	-
7	0.9812	-	0.3271

Table 5.5 Clay profile reference displacements

Vertical Reference Displacement (m)			
N_x/N_y	3	5	7
3	0.0167	0.0167	0.0167
5	0.0167	0.0167	-
7	0.0167	-	0.0167

Horizontal Reference Displacement (m)			
N_x/N_y	3	5	7
3	0.061	0.061	0.061
5	0.061	0.061	-
7	0.061	-	0.061

Reference Rotation (degrees)			
N_x/N_y	3	5	7
3	0.6166	0.3083	0.2055
5	0.6166	0.3083	-
7	0.6166	-	0.2055

5.4.1.3 Normalized Loads and Displacements

The reference loads will obviously be different for pile groups of different sizes and numbers of piles. One might expect, however, for pile groups loaded at similar fractions of their respective reference loads, to exhibit similar behavior. To allow comparison of the response of different pile groups, normalized loads and displacements will be defined as:

$$Q_n = Q/Q_{ref} \qquad w_n = w/w_{ref}$$
$$V_{xn} = V_x/V_{x,ref} \qquad u_n = u/u_{ref}$$
$$V_{yn} = V_y/V_{y,ref} \qquad v_n = v/v_{ref}$$
$$M_{xn} = M_x/M_{x,ref} \qquad \theta_{yn} = \theta_y/\theta_{y,ref}$$
$$M_{yn} = M_y/M_{xy,ref} \qquad \theta_{xn} = \theta_x/\theta_{x,ref}$$

It should be noted that normalized loads and displacements can be defined for different loading conditions, e.g., static, pseudo-static, and dynamic.

5.4.1.4 Computed Response

The normalized load-displacement behavior for vertical loading of 3x3, 5x5, and 7x7 pile groups is shown in Figure 5.4. Because the axial resistances of the individual piles are modeled by identical *t-z* and *Q-z* elements, the normalized vertical load responses are identical. The responses of the pile groups in sand are relatively linear up to normalized loads of about 0.7, and the pile groups continue to resist load with significant stiffness at normalized loads greater than

1.0. The pile groups in the clay profile show relatively linear behavior up to normalized loads of 0.7-0.8 but then become strongly nonlinear at higher normalized loads. Under static loading, the vertical displacements of the pile groups in the clay profile increase rapidly as the normalized vertical load approaches 1.0.

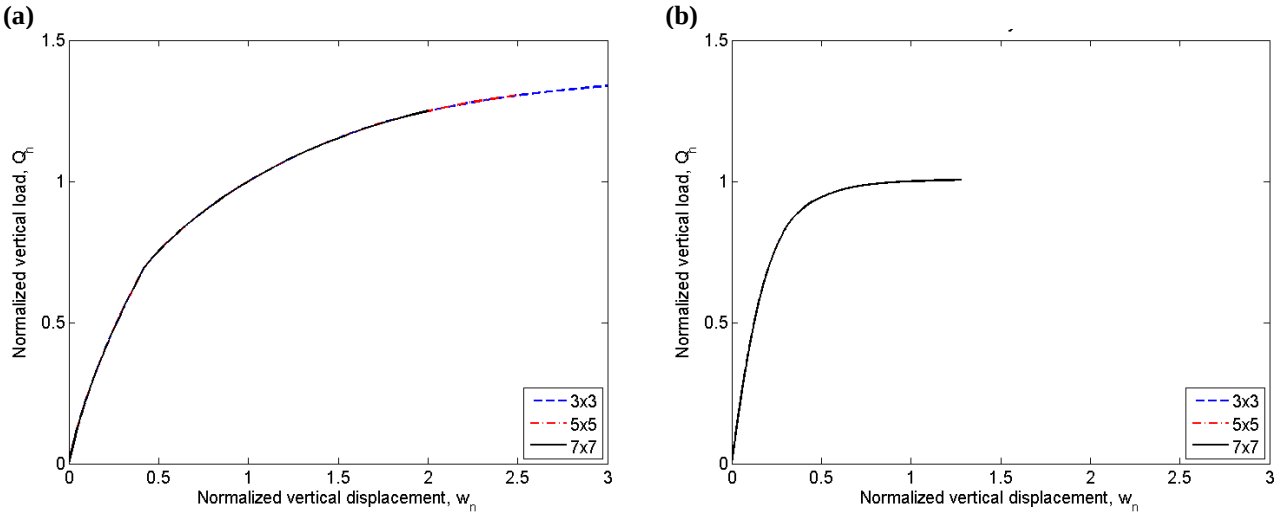

Figure 5.4. Normalized vertical load response for 3x3, 5x5, and 7x7 pile groups: (a) sand profile, (b) clay profile.

Figure 5.5 shows the normalized lateral load response of 3x3, 5x5, and 7x7 pile groups in the sand and clay profiles. The normalized curves for the three pile groups are very consistent across a broad range of response levels. The normalized response can be seen to exhibit more nonlinearity at low loading levels than the vertical loading curves of Figure 5.4. The response in sand is somewhat more linear than that in clay, and the pile groups in sand tend to exhibit slightly greater stiffness at normalized loads greater than 1.0. The responses of the pile groups to lateral loading in the sand and clay profiles are much more similar than in the case of vertical loading.

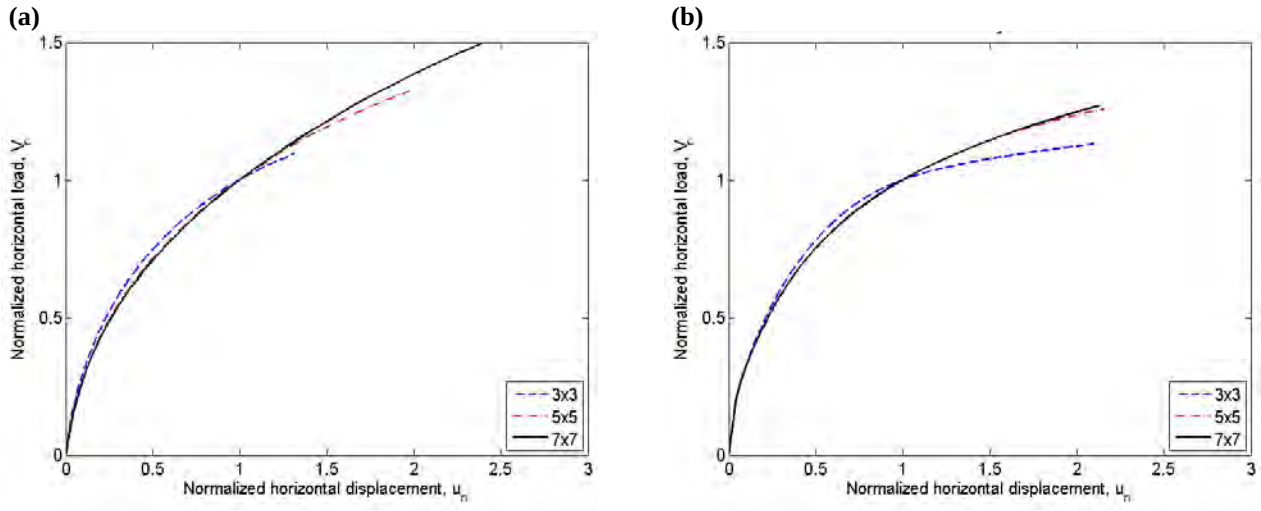

Figure 5.5. Normalized horizontal load response for 3x3, 5x5, and 7x7 pile groups: (a) sand profile, (b) clay profile.

The normalized responses of 3x3, 5x5, and 7x7 pile groups to overturning moments are shown in Figure 5.6. Because the resistance to overturning of a pile group comes from mobilization of axial resistance of the individual piles, the responses of the pile groups to overturning moments shares some of the characteristics of the responses to vertical loading. The pile groups exhibit relatively linear moment-rotation behavior to normalized moments of about 0.7-0.8 in the sand profile and 0.8-0.9 in the clay profile. The static curves are also quite consistent at normalized moments up to about 1.05; at higher normalized moments, the curves diverge with the normalized rotation for a given normalized moment increasing with increasing pile group size. This effect is more pronounced for the pile groups in the clay profile than in the sand profile.

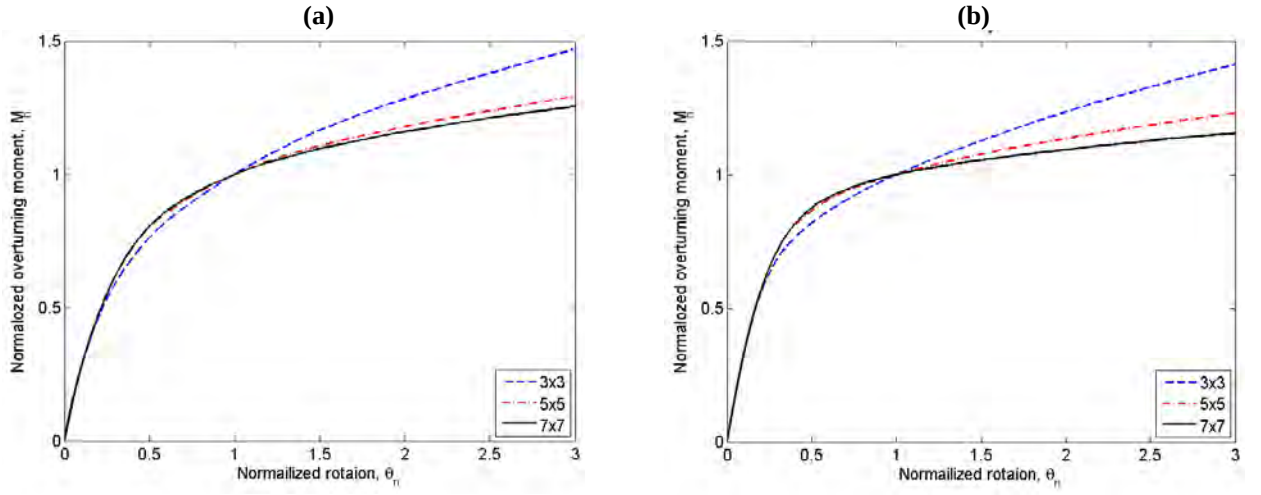

Figure 5.6. Normalized overturning moment response for 3x3, 5x5, and 7x7 pile groups: (a) sand profile, (b) clay profile.

The results of these analyses show that normalization of pile group response is effective to normalized static loads/moments of at least 1.05 for pile groups of different sizes in both the sand and clay profiles. The normalized responses in the sand and clay profiles, however, are significantly different. Because pile foundations are generally designed to support loads that are significantly lower than their failure loads, the normalized static loads that exist in actual pile foundations prior to earthquake shaking can be expected to be well below 1.0, in which case normalization of load-displacement (and moment-rotation) behavior is very effective.

5.4.2 Static Load Combinations

In order to produce general results that would cover a wide range of possible bridge configurations, a suite of initial static loading states was analyzed. The initial load states were intended to cover a very broad range of initial conditions ranging from relatively low static loads to cases where the static loads were significantly higher than would be expected in normal design practice. This wide range allowed development of pile group response relationships that covered displacements ranging from very small to quite large. Table 5.6 presents the normalized static loads used in this study. Static vertical loads, for example, ranged from 20% of the reference load (implying $FS \approx 5$) to 90% of the reference load ($FS \approx 1.1$). Lateral loads ranged from zero to 67% of the reference load, and overturning moments from zero to 60% of the reference moment. The analysis of all combinations of these static load levels would result in 4 x3 x3 = 36 initial load states. The horizontal loads and moments were applied in both the *x*- and *y*-directions.

Table 5.6 Initial static load states used in analyses.

$Q_{sn} = Q_s/Q_{ref}$	$V_{sn} = V_s/V_{,ref}$	$M_{sn} = M_s/M_{,ref}$
0.20	0.00	0.00
0.40	0.33	0.30
0.67	0.67	0.60
0.90		

5.5 GROUND MOTIONS

The analyses were performed with a suite of 50 three-component ground motions selected to represent a wide range of potential seismic hazards. The motions were obtained from the PEER NGA database by the following process:

1. Sort database and extract motions recorded at stations with V_{s30} values between 270 m/sec and 560 m/sec. This process led to a set of 2,029 candidate ground motions.
2. Divide motions into the following nine magnitude-distance (*M*-*R*) bins:

$M_w < 6.5$ $r_{jb} < 20$ km	$M_w < 6.5$ 20 km $< r_{jb} <$ 50 km	$M_w < 6.5$ $r_{jb} > 50$ km
$6.5 < M_w < 7.5$ $r_{jb} < 20$ km	$6.5 < M_w < 7.5$ 20 km $< r_{jb} <$ 50 km	$6.5 < M_w < 7.5$ $r_{jb} > 50$ km
$M_w > 7.5$ $r_{jb} < 20$ km	$M_w > 7.5$ 20 km $< r_{jb} <$ 50 km	$M_w > 7.5$ $r_{jb} > 50$ km

where M_w = moment magnitude and r_{jb} = Joyner-Boor distance measure.

3. Divide motions within each *M*-*R* bin into 10 amplitude bins based on geometric mean $S_a(T = 0.5)$ and $S_a(T = 1.0)$.
4. Compute ε values for $S_a(T = 0.5)$ and $S_a(T = 1.0)$. The mean of the median values of the Abrahamson-Silva, Boore-Atkinson, Campbell-Bozorgnia, and Chiou-Youngs models were used to calculate ε.
5. For each amplitude bin, select five motions with low ε values and consistent $S_a(T = 0.5)$ and $S_a(T = 1.0)$ values.

This process led to a suite of 50 motions that were (a) well-behaved in term of having $S_a(T = 0.5)$ and $S_a(T = 1.0)$ values that were consistent with those predicted by NGA attenuation relationships (b) well-behaved in terms of being consistent with each other, and (c) relatively uniformly distributed over a wide range of amplitudes. The response spectra for the 50 motions are plotted in Figures 5.7 – 5.9.

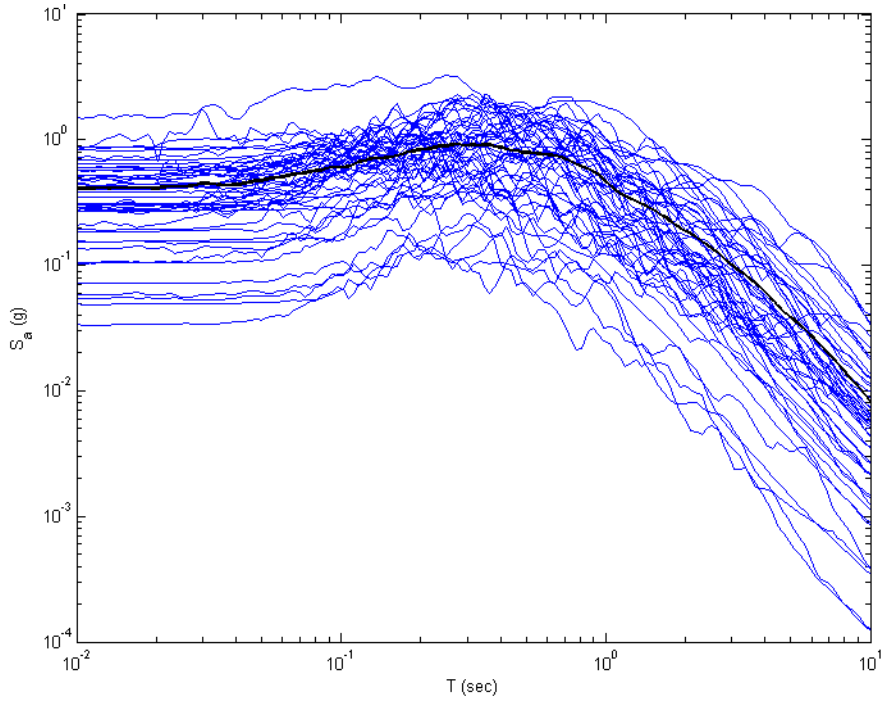

Figure 5.7 Response spectra for fault normal components of ground motions.

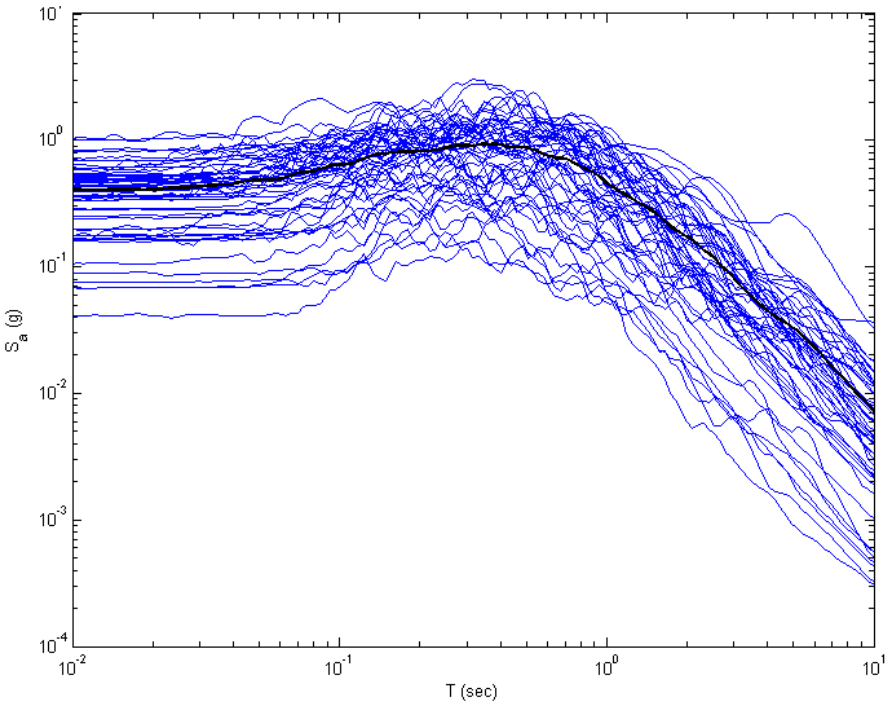

Figure 5.8 **Response spectra for fault parallel components of ground motions.**

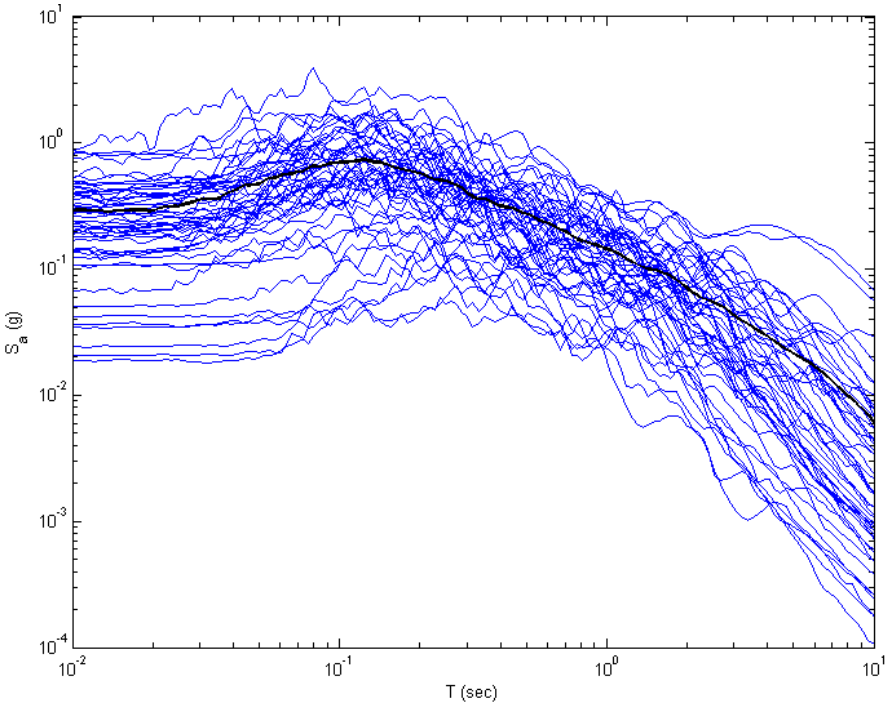

Figure 5.9 **Response spectra for vertical components of ground motions.**

Some of the motions were processed by removing long periods of leading or trailing zeros or by increasing the time step of the motion in order to improve computational efficiency. All processed motions were baseline-corrected and compared with the original motions to ensure that spectral accelerations in the range of periods of greatest interest (approximately 0.25 – 2 sec) were not significantly affected by the processing. A list of the records used in the analyses is presented in Table 5.7.

Table 5.7. Ground motions used in response analyses.

Earthquake	Record	Earthquake	Record
Northridge-01	Sylmar - Olive View Med FF	Northridge-01	Sun Valley - Roscoe Blvd
Loma Prieta	LGPC	Kocaeli, Turkey	Duzce
Chi-Chi, Taiwan	CHY028	Imperial Valley-06	SAHOP Casa Flores
Northridge-01	Beverly Hills - 14145 Mulhol	Erzican, Turkey	Erzincan
Kobe, Japan	Takarazuka	Parkfield	Cholame - Shandon Array #5
Loma Prieta	BRAN	Landers	Joshua Tree
Northridge-01	Rinaldi Receiving Sta	Imperial Valley-06	Chihuahua
Cape Mendocino	Rio Dell Overpass - FF	Whittier Narrows-01	San Gabriel - E Grand Ave
Northridge-01	Simi Valley - Katherine Rd	Northridge-01	LA - Brentwood VA Hospital
Duzce, Turkey	Bolu	Chi-Chi, Taiwan	NST
Chi-Chi, Taiwan	TCU074	Northridge-01	LA - N Faring Rd
Loma Prieta	Corralitos	Northridge-01	LA - UCLA Grounds
San Salvador	Geotech Investig Center	Whittier Narrows-01	LA - Obregon Park
San Salvador	National Geografical Inst	Cape Mendocino	Eureka - Myrtle & West
Northridge-01	Castaic - Old Ridge Route	Kern County	Taft Lincoln School
Cape Mendocino	Cape Mendocino	Coalinga-01	Parkfield - Gold Hill 2E
Northridge-01	Jensen Filter Plant Generator	Morgan Hill	Gilroy Array #3
Chi-Chi, Taiwan	TCU072	Northridge-01	LA - W 15th St
N. Palm Springs	Whitewater Trout Farm	San Fernando	LA - Hollywood Stor FF
Northridge-01	Canyon Country - W Lost Cany	Sierra Madre	San Marino - SW Academy
Northridge-01	Pacoima Kagel Canyon	Hector Mine	Salton City
Loma Prieta	Capitola	Northridge-01	San Bernardino - CSUSB Gr
Duzce, Turkey	Duzce	N. Palm Springs	Winchester Page Bros R
Managua, Nicaragua-01	Managua, ESSO	Chi-Chi, Taiwan-05	KAU054
Morgan Hill	Anderson Dam (Downstream)	Friuli, Italy-01	Conegliano

5.6 RESPONSE OF REPRESENTATIVE PILE GROUP

To illustrate the performance of the OpenSees pile group model, the results of a series of analyses of a representative pile group are presented. The response to monotonically increasing static loading was presented in Section 5.4.1. Examples of the response to dynamic loading are presented in the following sections.

5.6.1 Representative Pile Group

The representative pile group is a 3x3 group in the sand profile. The piles were spaced at 5 ft (i.e., 2.5*D*) center-to-center, and were connected to a 13 ft x 13 ft x 3.25 ft thick pile cap. The top of the pile cap was assumed to be flush with the ground surface.

5.6.2 Representative Loading Histories

The dynamic response of a pile group is influenced by both the static and dynamic loading applied to the foundation. For a given static load state, pile group displacements can be expected to increase with increasing dynamic loads. Also, for a given level of dynamic loading, displacements (particularly permanent displacements) will increase with increasing static loads.

5.6.2.1 Response to Harmonic Loading

The general reasonableness of the OpenSees pile group model can be illustrated using simple harmonic loads applied to the pile group. One should expect that application of a static vertical load will result in some vertical settlement of the pile cap, and that cyclic vertical loads superimposed on the static loads would cause additional displacement of an amount that depends on the cyclic load amplitude. Figure 5.10 shows the response of the representative pile group to cyclic vertical loads of different amplitudes when applied after application of normalized static vertical loads of $Q_{sn} = 0.2$ (upper row) and $Q_{sn} = 0.4$ (lower row). The amplitudes can be seen to increase with increasing cyclic load amplitude and to be higher for the case with $Q_{sn} = 0.4$ than for the case with $Q_{sn} = 0.2$.

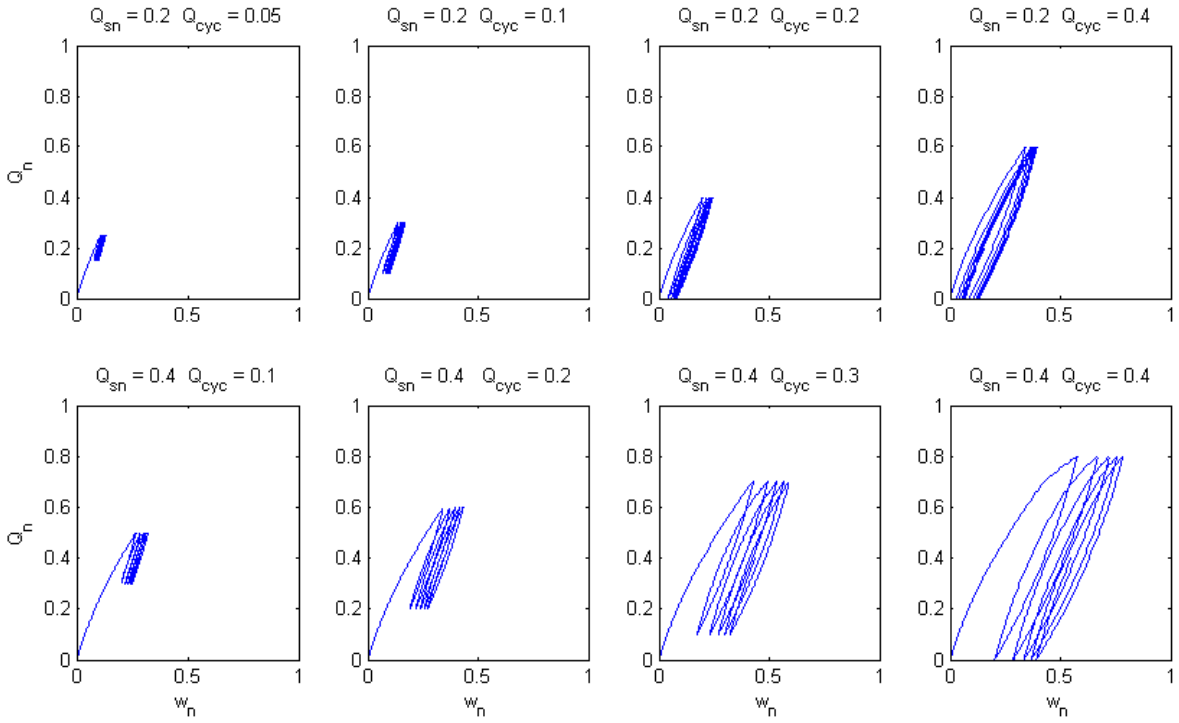

Figure 5.10. Response of pile groups subjected to harmonic vertical loading.

Figure 5.11 illustrates the response of the representative pile group to lateral loading. Dynamic loads of different amplitude are superimposed upon normalized static loads of 0.33 and 0.67. The horizontal displacement amplitude can be seen to increase with increasing dynamic load amplitude and to be higher for the cases with $V_{sn} = 0.67$ than for $V_{sn} = 0.33$. The results for the lateral load and overturning moment loading were analogous to those described for the vertical loading.

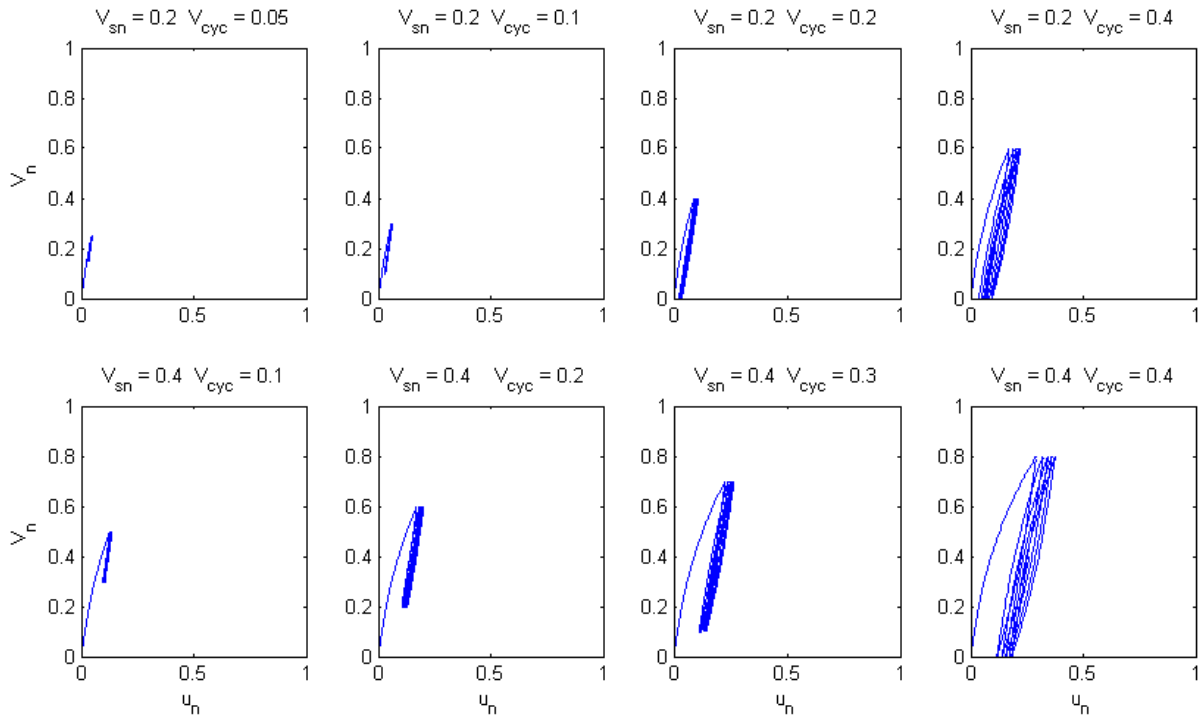

Figure 5.11. Response of pile groups subjected to harmonic lateral loading.

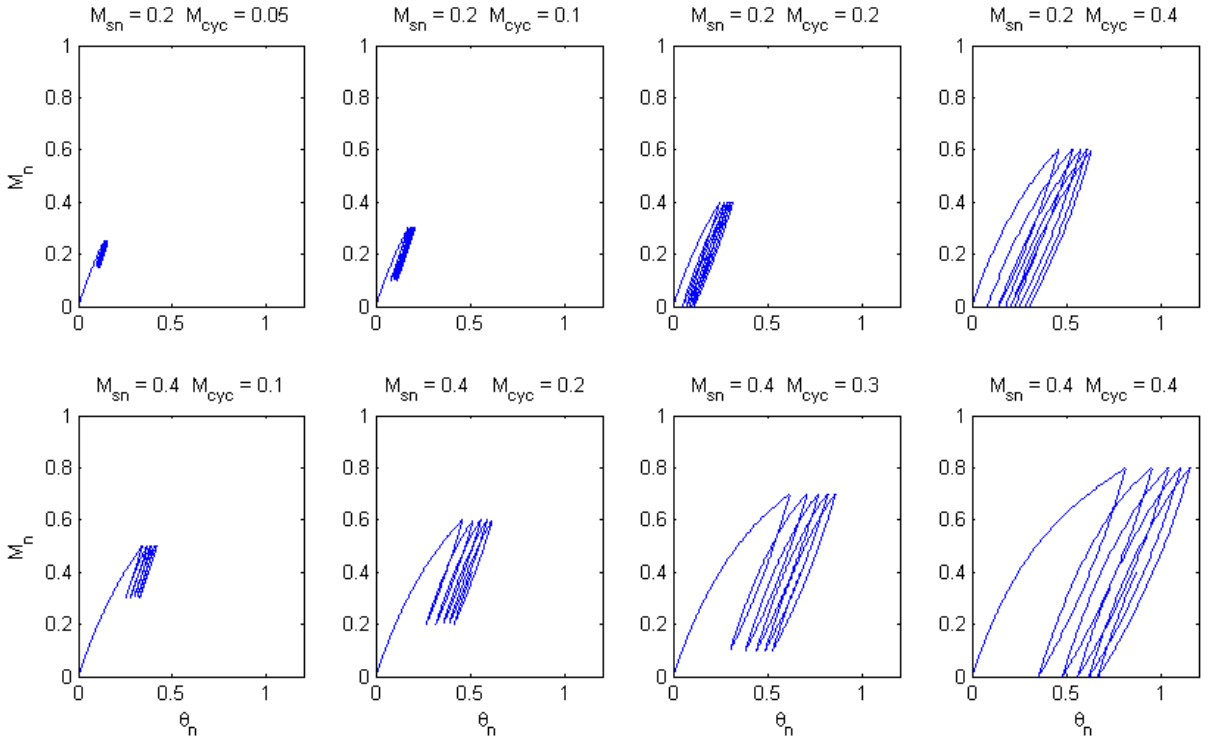

Figure 5.12. Response of pile groups subjected to harmonic overturning moment.

The interaction of different loading components can also be illustrated using relatively simple harmonic loading. Figure 5.13 shows the effects of rocking on the accumulation of vertical displacement. Although they are plotted to different scales, the vertical settlement can be seen to increase with increasing cyclic rotation amplitude, and to be higher for the case with $Q_{sn} = 0.4$ than for the case with $Q_{sn} = 0.2$. Such analyses show that rocking, in addition to cyclic vertical loading, has an important effect on the settlement of pile groups.

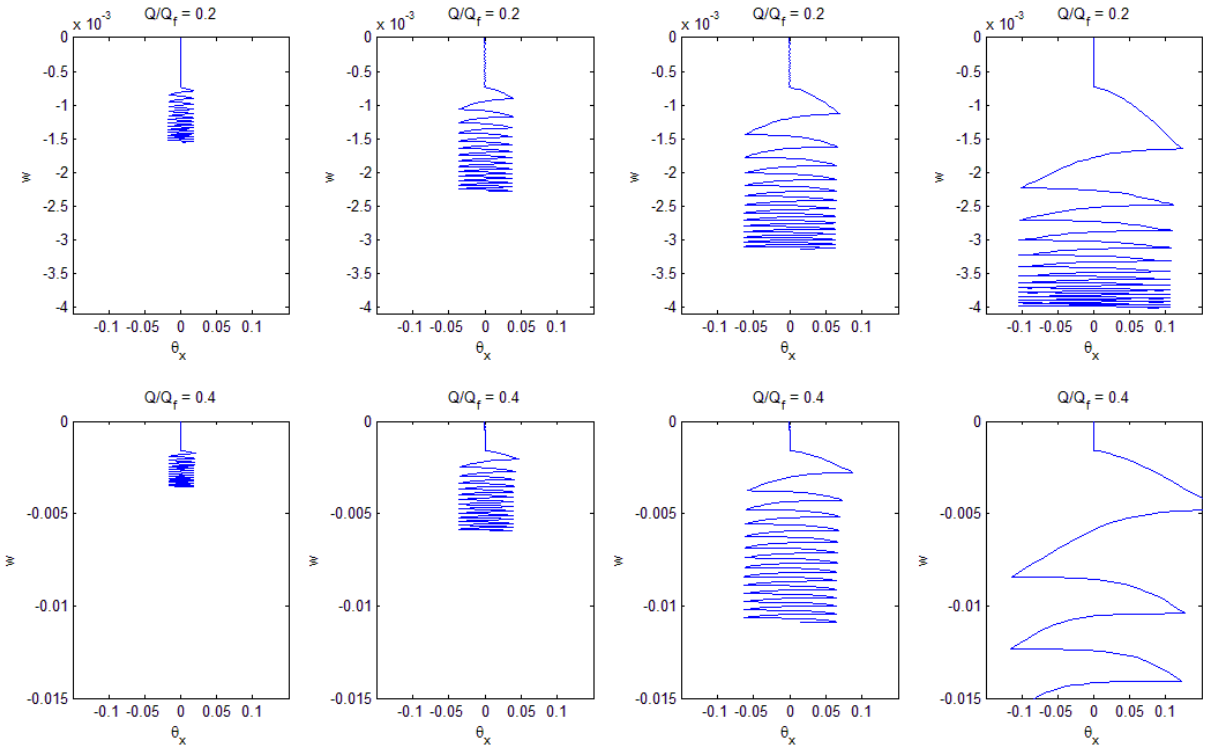

Figure 5.13. Settlement-rotation (w-θ_x) response of pile groups subjected to harmonic overturning moments under different levels of static, vertical loading.

5.6.2.2 Response to Transient Loading

In more realistic situations, transient loads are expected to be applied to pile foundations by earthquakes and other types dynamic loads. Figure 5.14 shows the response of a 3x3 pile group in sand with two different initial static load combinations. Static Load Case 1: $Q/Q_{ref} = 0.2$ and $V_x/V_{x\,ref} = 0.0$ and Static Load Case 2: $Q/Q_{ref} = 0.2$ and $V_x/V_{x\,ref} = 0.33$ to earthquake loading. The acceleration time history from the Parkfield earthquake was applied to both cases.

The response (Figure 5.14) can be seen to be complicated, as the dynamic loads combine with the static loads to produce both cyclic and permanent displacements (vertical and horizontal) and rotations. Static Load Case 2, in which 33% of the horizontal reference load was applied statically, accumulates significant horizontal displacement and rotation compared with Static Load Case 1, which had no static lateral load. Vertical displacements accumulated for both cases, but the displacement for Static Load Case 1 are greater than those for Static Load

Case 2. Figure 5.15 shows the relationships between the pile cap movements (vertical, horizontal, and rocking), which can be seen to increase together but in a complicated manner.

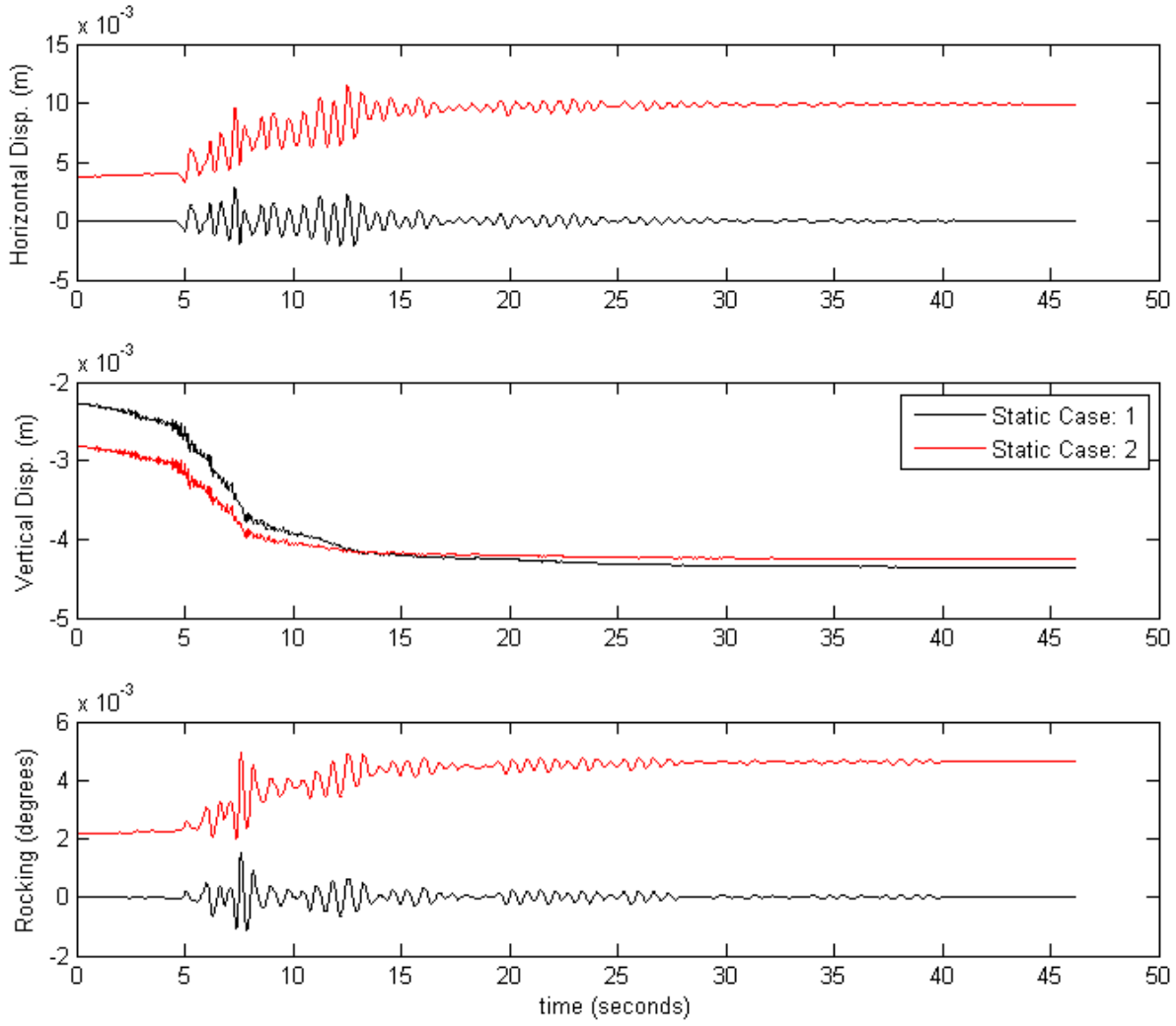

Figure 5.14 **Response of pile group to transient motions. Static Load Case 1: Q_{ns} = 0.2 and V_{ns} = 0.0 and Static Load Case 2: Q_{ns} = 0.2 and V_{ns} = 0.33.**

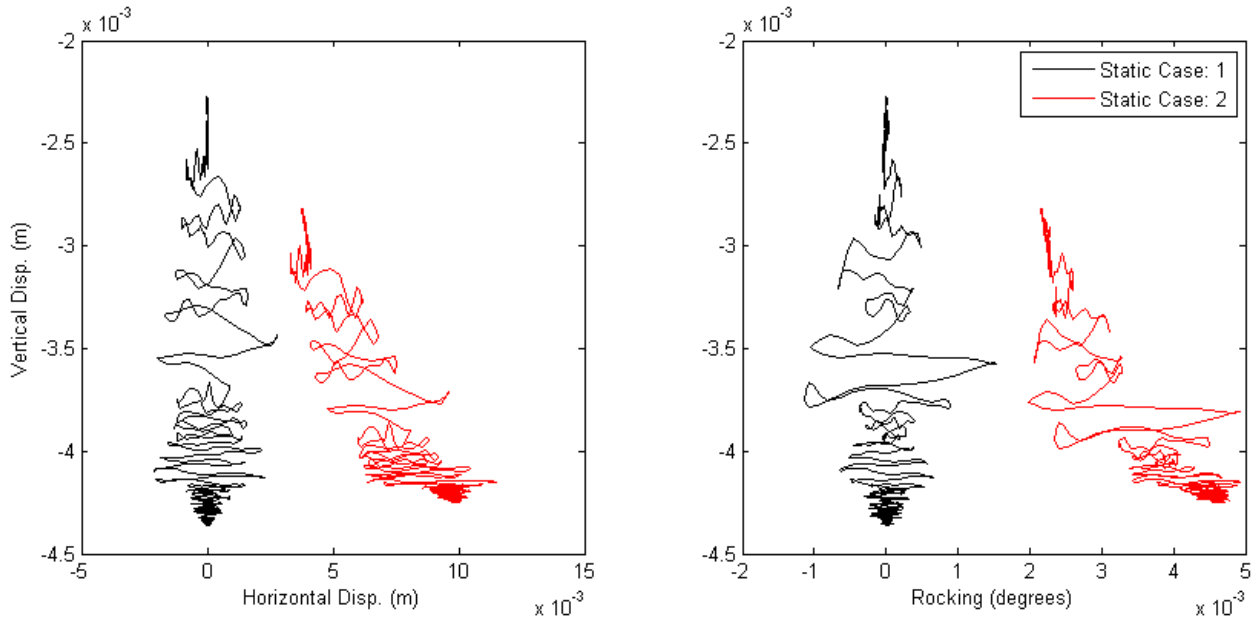

Figure 5.15 **Response of pile group to transient motions. Static Load Case 1: Q_{sn} = 0.2 and V_{sn} = 0.0 and Static Load Case 2: Q_{sn} = 0.2 and V_{sn} = 0.33**

5.7 AGGREGATE RESPONSE

An extensive series of production analyses was performed. These analyses considered different structural characteristics, different pile group configurations, sand and clay soil profiles, many different initial static load states, both linear and nonlinear column behavior (with multiple column yield moments), different pile capacities, and different pile cap stiffnesses. For the great majority of the different combinations of conditions that were analyzed, all 50 ground motions were applied to the model; for several cases intended to explore a particular aspect of pile group behavior, a subset of 10 ground motions were applied in order to reduce processing time.

The following sections present the results of the soil-foundation-structure interaction analyses. The results are presented in terms of scatter plots, each point on which represents the peak absolute response for a particular input motion. The peak values are taken individually and do not necessarily occur at the same time. Representative plots are shown to illustrate basic trends in the response with respect to different variables or parameters. The entire data set was used in the regression analyses performed to interpret the results of the tests; the regression analyses are described in Section 5.7.

5.7.1 Normalization of Loading and Response

The concept of normalized loads and response was introduced in Section 5.4.1.3. Figure 5.16 shows the benefits of describing pile group response using normalized variables. Figure 5.16(a) illustrates the vertical displacements of 3x3, 5x5, and 7x7 pile groups supporting a linear structure with T_o = 0.5 sec in the sand profile in response to all 50 input motions. Figure 5.16(b) shows the same results plotted in terms of normalized loads and displacements – the normalized

displacements fall into a much narrower band that is closely related to the normalized load, which suggests that normalized displacements of all three pile group sizes can be predicted as a function of normalized loads without a great loss of accuracy.

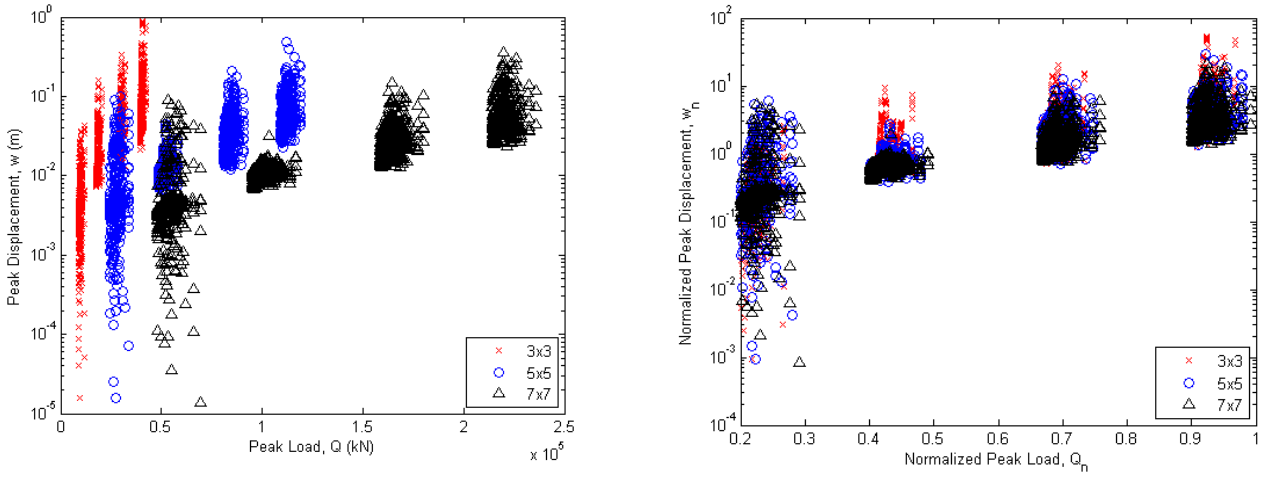

Figure 5. 16. Response of pile groups in sand profile with Q_{sn} = 0.40, V_{sn} = 0.33, and M_{sn} = 0.30 to earthquake loading: (a) peak vertical displacement vs. peak vertical load, and (b) normalized vertical displacement vs. normalized vertical load.

Figure 5.16 illustrates the benefits of expressing both loading and response in terms of normalized variables. Similar results were observed for horizontal displacement and rocking rotation; in these cases, normalization of displacement/rotation results in consistent relationships to normalized load/moment. All results presented in the remainder of this chapter will be presented in terms of normalized loads and displacements. Furthermore, the interpretation of results described in the subsequent section will also be expressed in terms of normalized loads and displacements.

It should be recognized, however, that the uncertainty in displacement shown in figure 5.16 is quite high even after normalization. The displacement ordinates in Figure 5.16 cover six orders of magnitude.

5.7.2 Effects of Structural Period

Discussions with WSDOT and Caltrans engineers indicated that bridges with fundamental periods ranging from 0.5 – 1.0 sec would be of greatest interest for development of a performance-based design framework. Soil-foundation-structure interaction analyses were performed for structures with fundamental periods of 0.5 sec and 1.0 sec. Comparison of the results of analyses based on the two different structural periods showed that the period had relatively little effect on the normalized response. Figure 5.17 shows the effects of structural period on the normalized response of a 5x5 pile group in the sand profile. The data can be seen to virtually overlie each other, indicating that the normalized displacements and rotations are insensitive to structural period. Figure 5.18 shows the same behavior for a 5x5 pile group in the clay profile This trend was seen consistently in the data; in subsequent plots, the results from analyses based on T_o = 0.5 sec and T_o = 1.0 sec are combined. In both Figures 5.17 and 5.18, the

responses to horizontal load and overturning moment show generally consistent response, but both show a significant number of data points with lower displacement/rotation than the majority of the data. These cases correspond to initial load cases with zero static lateral force/moment; this behavior will be observed in many of the following plots as well.

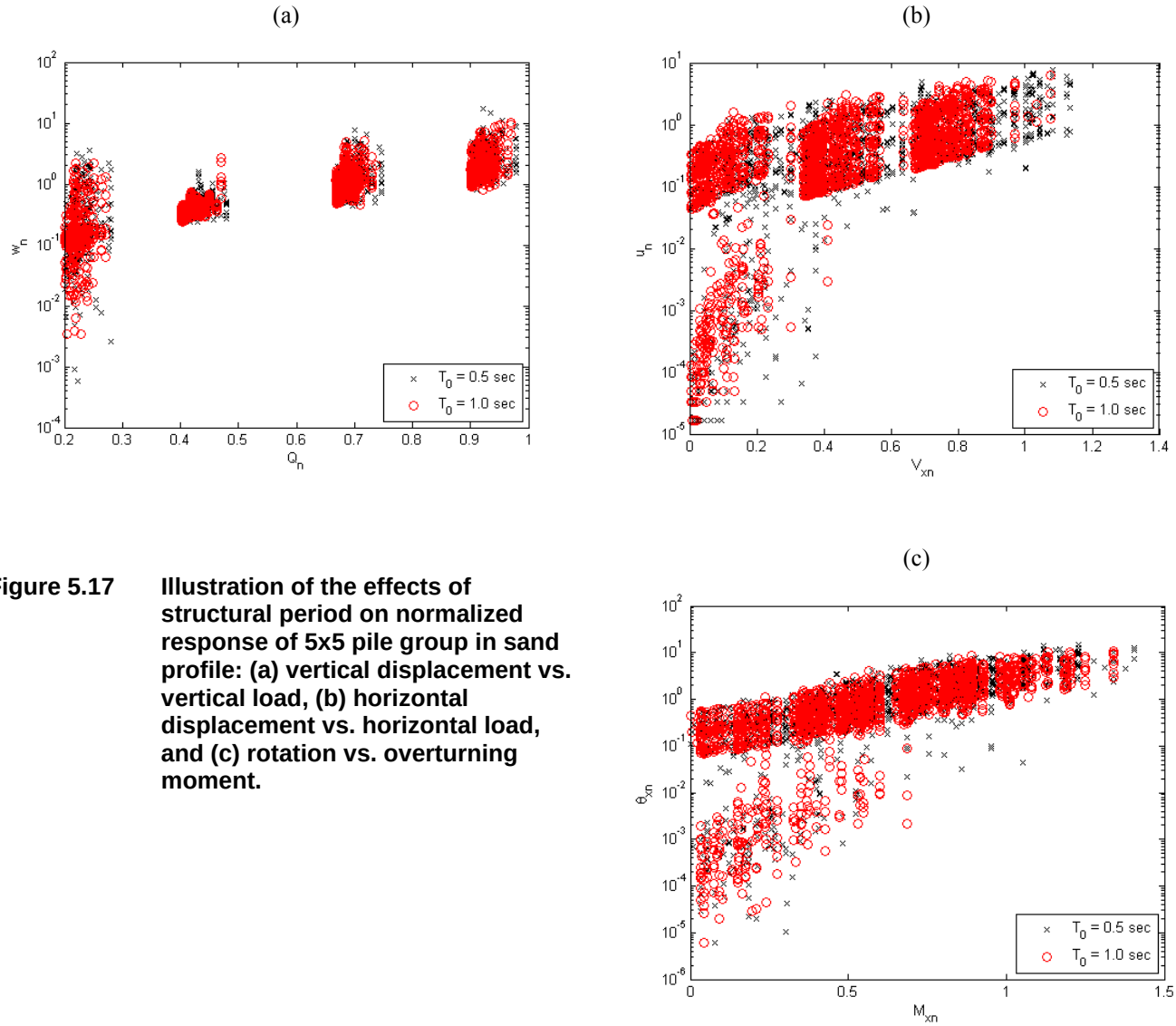

Figure 5.17 **Illustration of the effects of structural period on normalized response of 5x5 pile group in sand profile: (a) vertical displacement vs. vertical load, (b) horizontal displacement vs. horizontal load, and (c) rotation vs. overturning moment.**

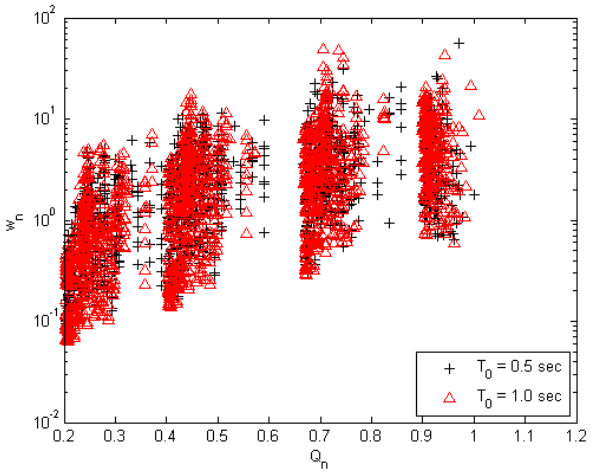

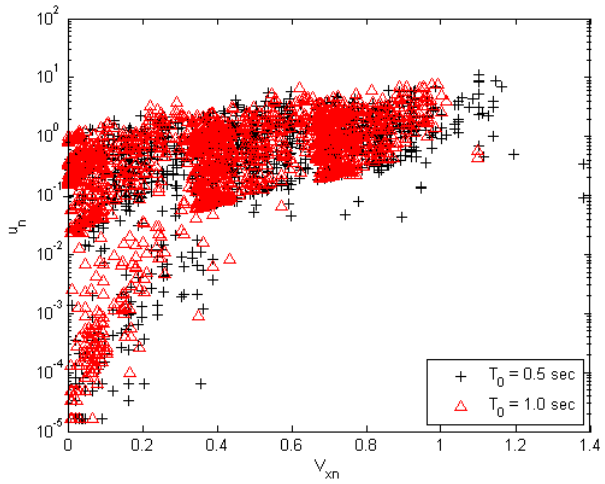

(c)

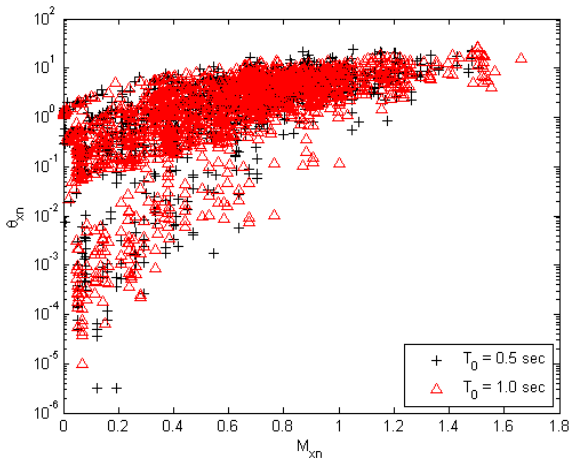

Figure 5.18 **Illustration of the effects of structural period on normalized response of 5x5 pile group in clay profile: (a) vertical displacement vs. vertical load, (b) horizontal displacement vs. horizontal load, and (c) rotation vs. overturning moment.**

5.7.3 Effects of Pile Group Size

As indicated in Figure 5.16 for a particular initial, static load state, the size of a "square" pile group, i.e., one that has the same number of piles in both horizontal directions, affects load-displacement response strongly in an absolute sense, but only weakly when normalized by the reference loads/moments and displacements/rotations. The results in Figure 5.16 correspond to a particular initial, static load state. When all static load states are considered, the normalized displacements are related to normalized loads as shown for 3x3, 5x5, and 7x7 pile groups in figures 5.19 (sand profile) and 5.20 (clay profile).

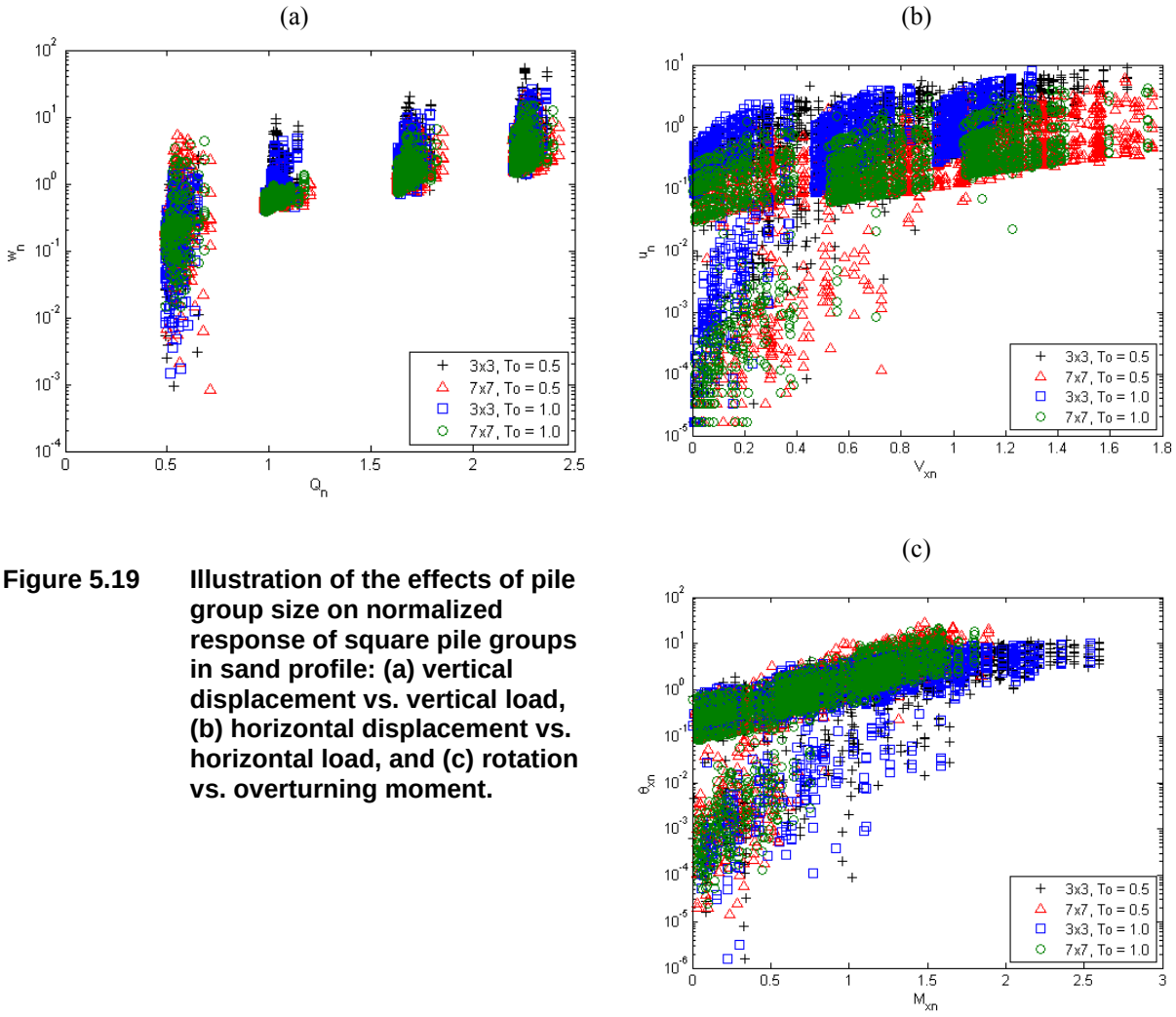

Figure 5.19 **Illustration of the effects of pile group size on normalized response of square pile groups in sand profile: (a) vertical displacement vs. vertical load, (b) horizontal displacement vs. horizontal load, and (c) rotation vs. overturning moment.**

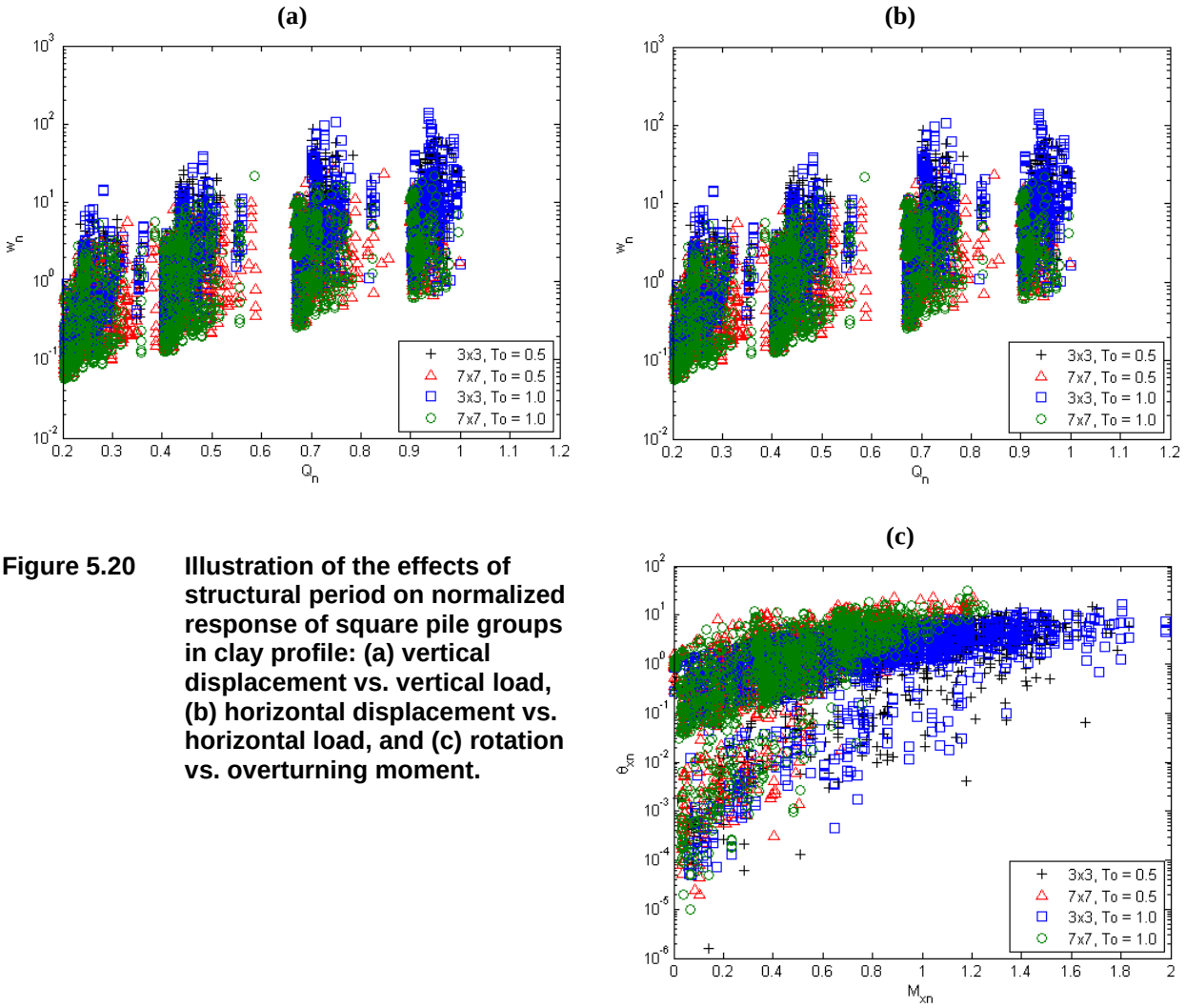

Figure 5.20 **Illustration of the effects of structural period on normalized response of square pile groups in clay profile: (a) vertical displacement vs. vertical load, (b) horizontal displacement vs. horizontal load, and (c) rotation vs. overturning moment.**

Additional analyses were performed to investigate the behavior of rectangular pile groups. In addition to the 3x3 groups already mentioned, both 3x5 and 3x7 pile groups were analyzed. Figure 5.21 shows the computed response of 3x3, 3x5, and 3x7 pile groups with respect to all five components of loading and movement; the plots are organized so that the y-direction is the long direction of the rectangular pile groups. These plots show that the normalized vertical displacements are insensitive to pile group configuration – the data for the 3x3, 5x5, and 7x7 pile groups lie virtually on top of each other. The normalized lateral load response shows some sensitivity to pile group configuration with the normalized lateral displacement decreasing with increasing pile group aspect ratio. The normalized lateral displacements are approximately equal for horizontal loading along the long and short axes of the pile group. The normalized rotation behavior, however, is significantly different in the two directions; greater normalized rotations are observed about the short axis of the pile group. It should be noted, however, that the number of pile is also changing with aspect ratio in these plots.

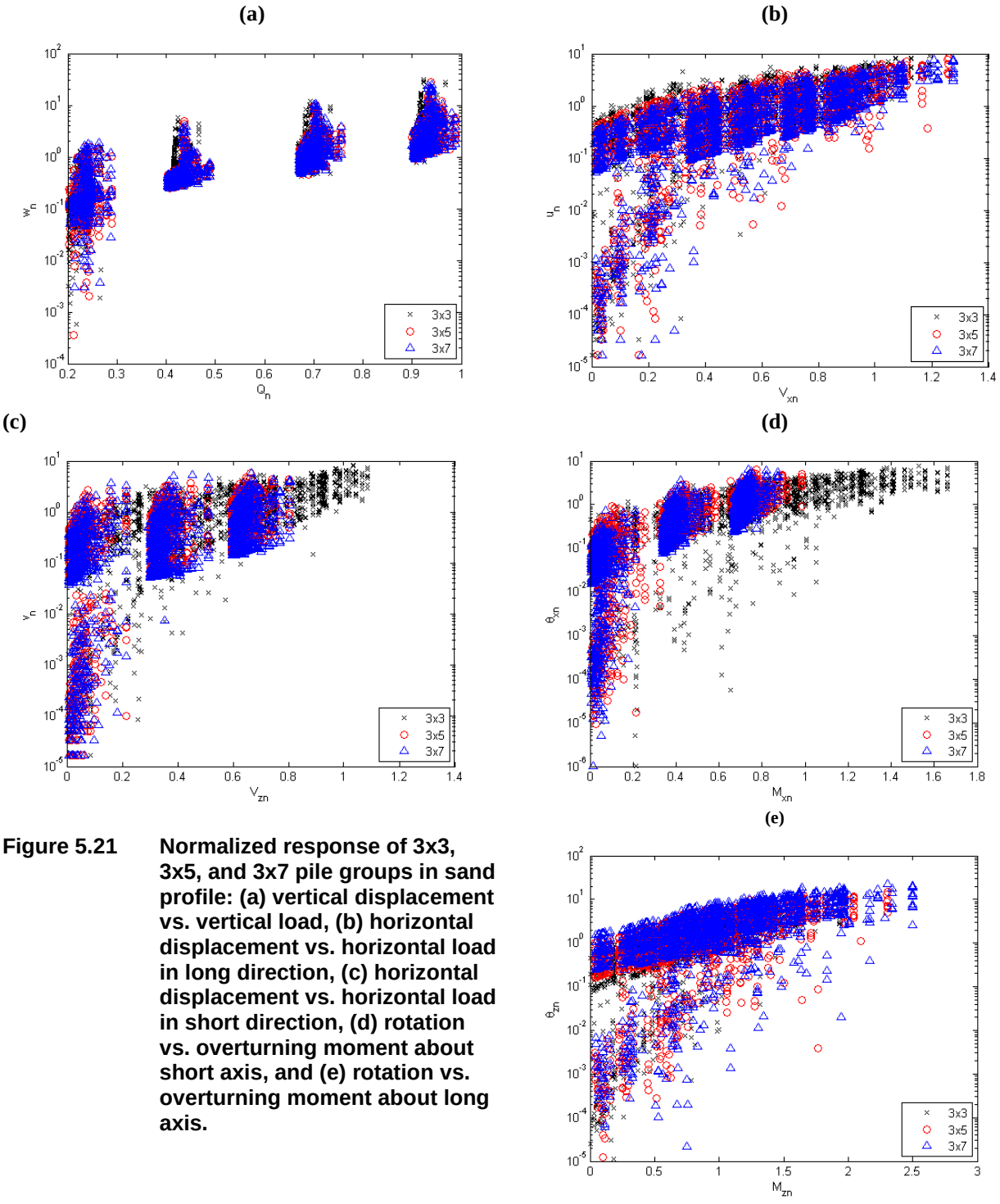

Figure 5.21 **Normalized response of 3x3, 3x5, and 3x7 pile groups in sand profile: (a) vertical displacement vs. vertical load, (b) horizontal displacement vs. horizontal load in long direction, (c) horizontal displacement vs. horizontal load in short direction, (d) rotation vs. overturning moment about short axis, and (e) rotation vs. overturning moment about long axis.**

5.7.4 Effect of Yield Moment

Bridge columns may be designed to yield plastically to limit the amplitudes of the loads applied to foundations supporting them. Numerous analyses were performed with nonlinear column properties selected to allow development of limiting plastic moments in the structural column;

the effects of these limiting moments were to cap the overturning moment and lateral loads applied to the top of the pile cap. Figure 5.22 shows time histories of all five *LM* components due to application of an input motion to the structural model with a limiting moment. With the exception of a very brief numerical "overshoot," the lateral force and overturning moment reach maximum values at several points during the time history. Depending on the nature of the input motion, the moments and lateral forces may stay at their limiting values for a period of time before dropping down into the elastic range of behavior.

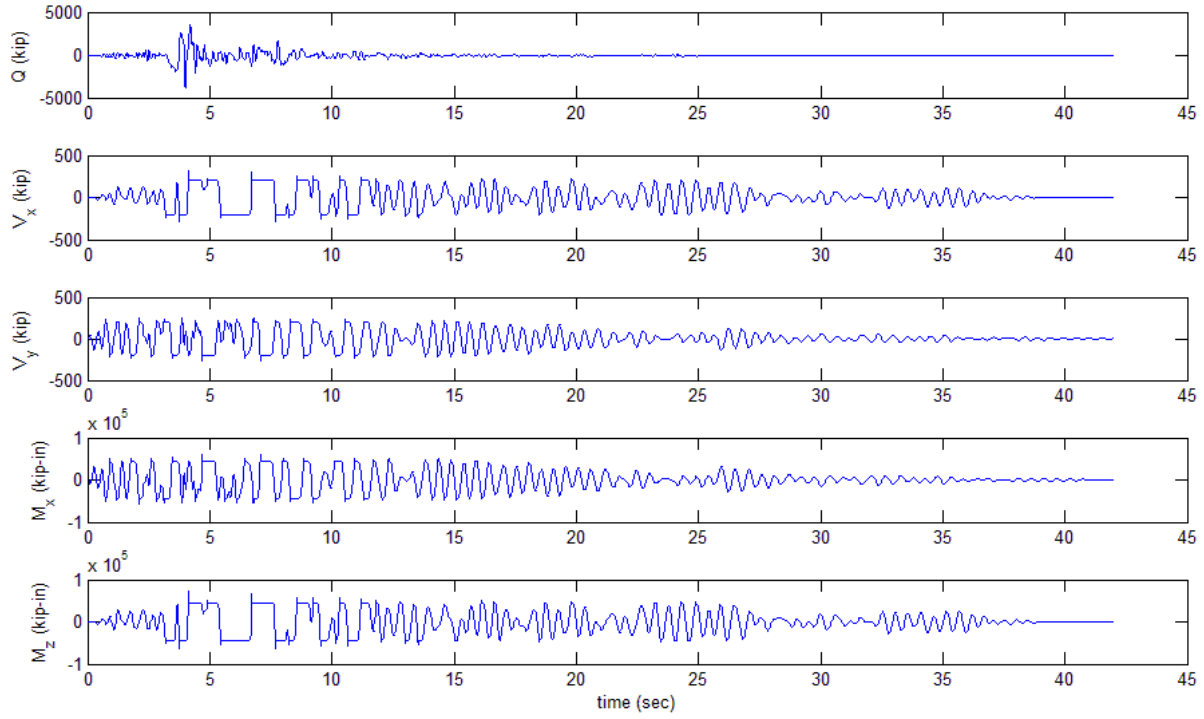

Figure 5.22 Effects of yield moment on loads and moments applied to pile cap.

Figure 5.23 shows the computed response of a 5x5 pile group supporting a T_o = 0.5 sec structure in the sand profile subjected to loading influenced by three different yield moment levels. The figure shows that the load normalization procedure appears to allow consideration of the effects of column yielding within the same framework as that of non-yielding columns. Figure 5.24 shows that the same general behavior was observed for a 5x5 pile group in the clay profile.

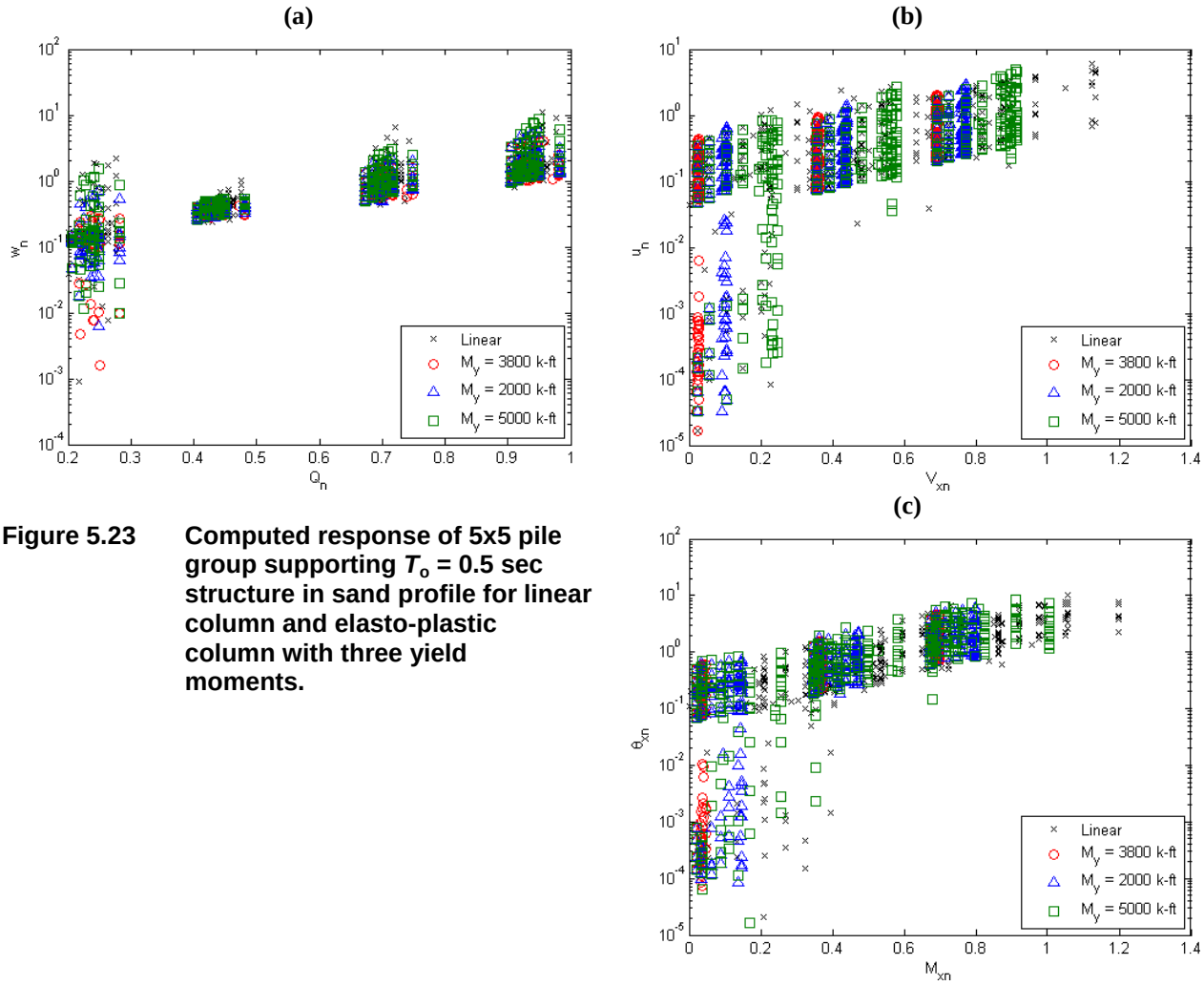

Figure 5.23 **Computed response of 5x5 pile group supporting T_o = 0.5 sec structure in sand profile for linear column and elasto-plastic column with three yield moments.**

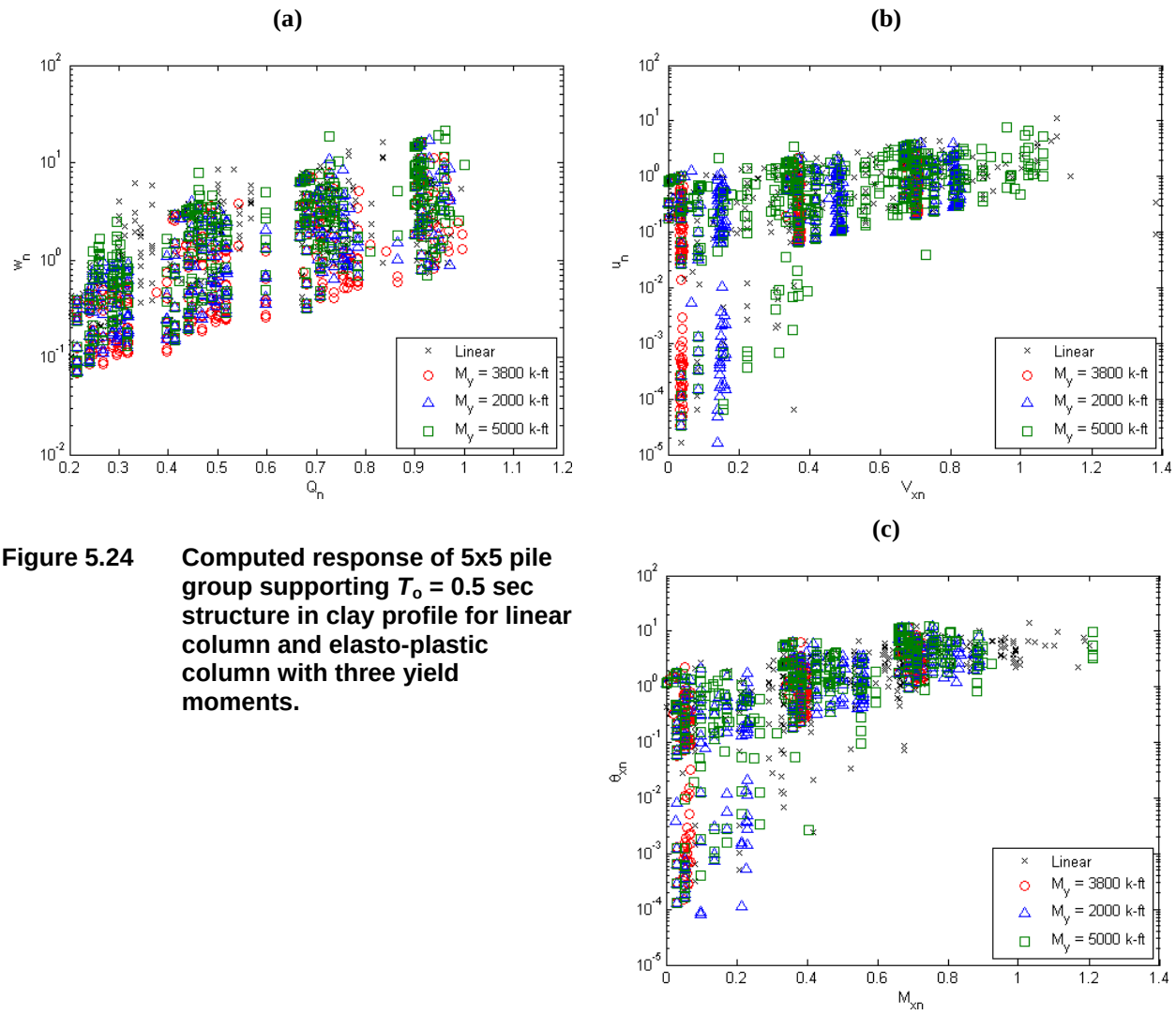

Figure 5.24 **Computed response of 5x5 pile group supporting T_o = 0.5 sec structure in clay profile for linear column and elasto-plastic column with three yield moments.**

5.7.5 Effect of Pile Cap Passive Resistance

A pile cap can provide a significant component of resistance to lateral loads under earthquake loading conditions. To investigate the sensitivity of pile cap response to pile cap resistance, analyses were performed with the stiffness of the pile cap passive resistance springs doubled and halved. Figures 5.24 and 5.25 show the computed response of pile caps with three levels of pile cap stiffness in sand and clay profiles, respectively. The stiffness of the pile cap lateral spring has virtually no effect on the settlement behavior of the pile group, which is not unexpected. The stiffness of the passive pile cap resistance also appears to have a relatively small effect on horizontal displacement and rotation, which may indicate that the pile cap stiffness represents a relatively small fraction of the total lateral resistance. The effect could be larger for a pile group in which the cap attracts a larger fraction of the lateral load.

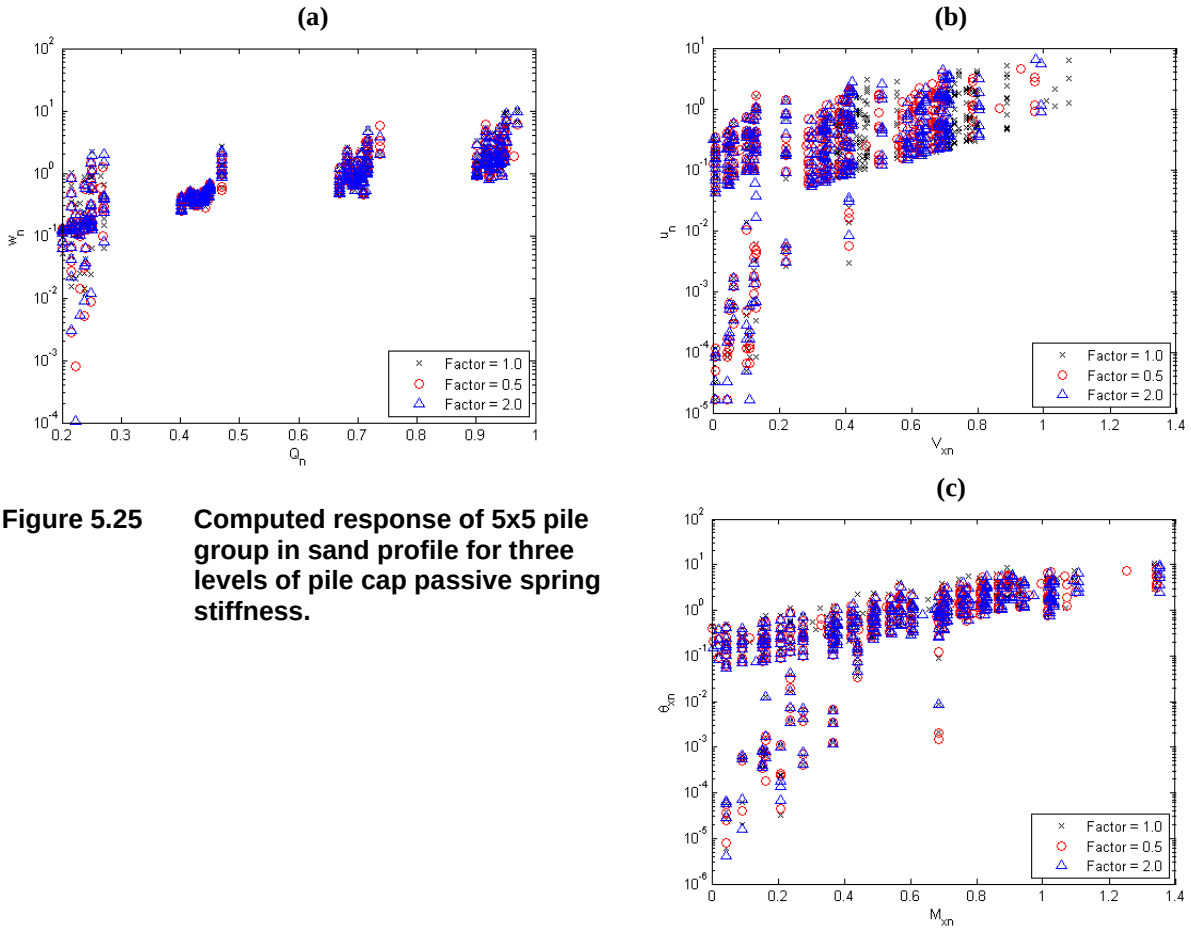

Figure 5.25 **Computed response of 5x5 pile group in sand profile for three levels of pile cap passive spring stiffness.**

5.7.6 Effect of Soil Shear Strength

To determine the sensitivity of normalized displacement/rotations to variations in capacities that result from variations in soil properties, a series of analyses were performed with soil shear strength values divided by factors of 1.5 and 3.0. The reduced shear strengths led to reduced pile capacities, hence also to reduced vertical reference loads and reference displacements. Figures 5.26 and 5.27 show the computed normalized displacements and rotations for different shear strengths in the sand and clay profiles, respectively. The results indicate that the normalization process generally takes care of the effects of soil shear strength so that normalized response is not particularly sensitive to variations in shear strength.

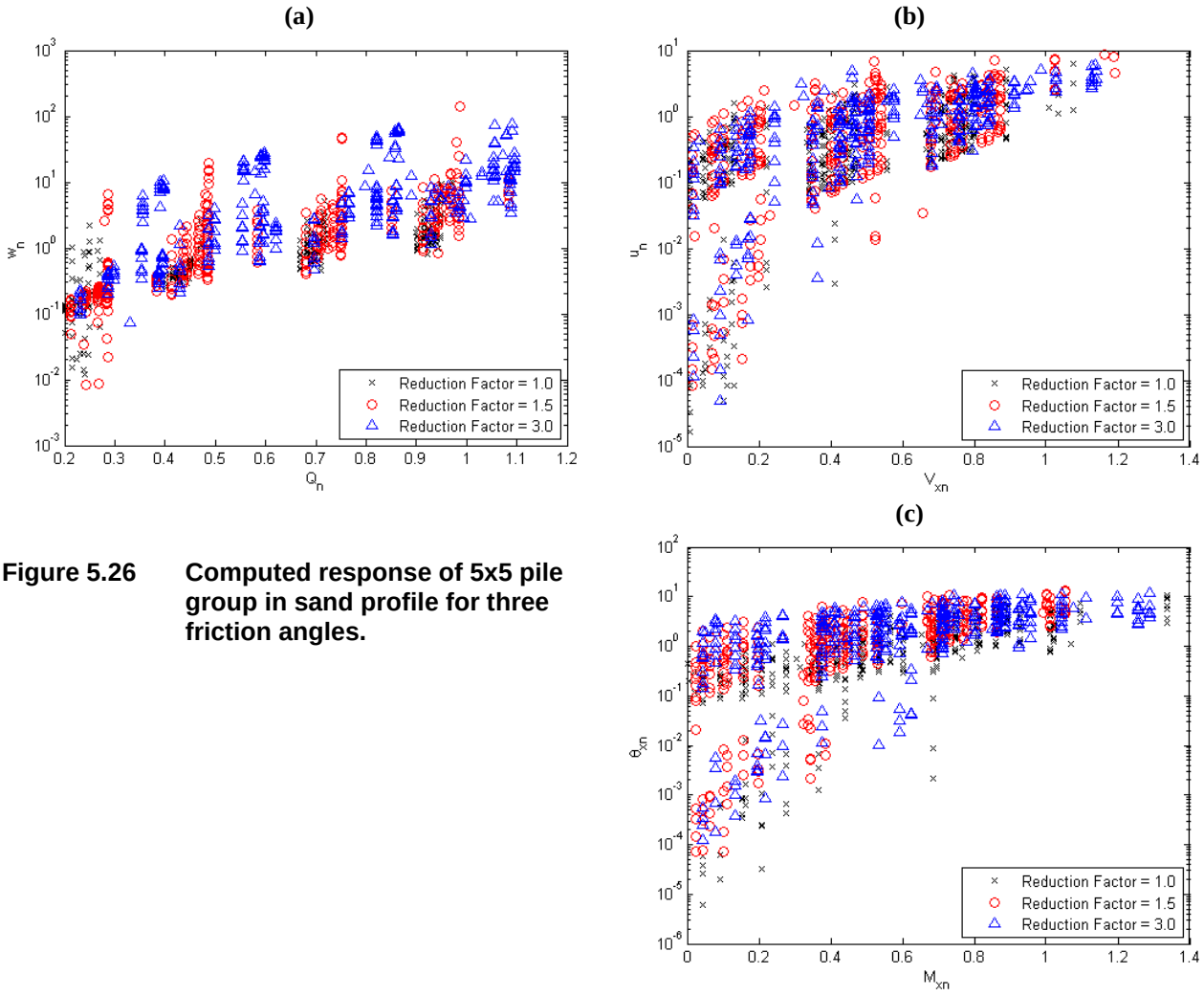

Figure 5.26 **Computed response of 5x5 pile group in sand profile for three friction angles.**

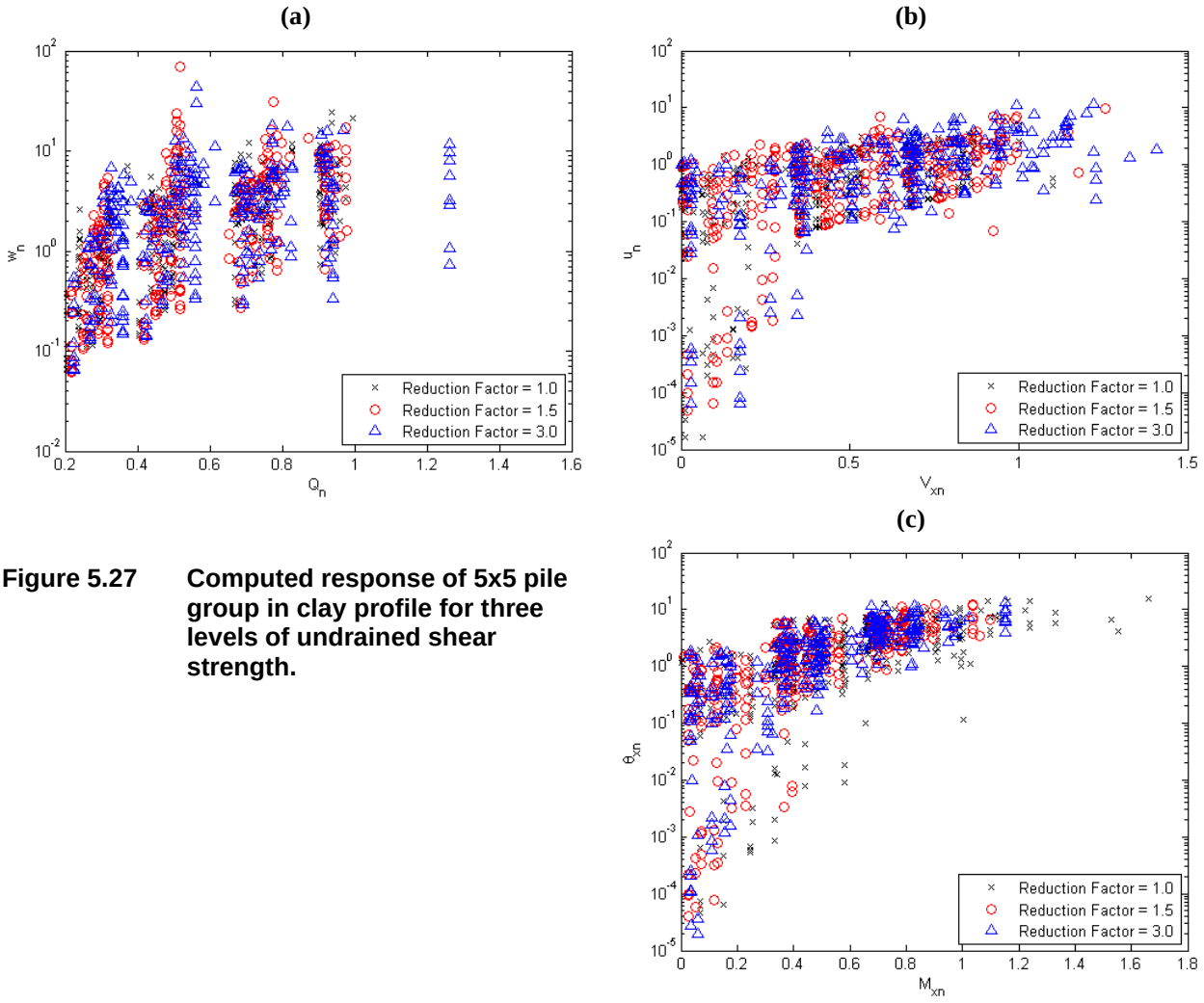

Figure 5.27 **Computed response of 5x5 pile group in clay profile for three levels of undrained shear strength.**

5.7.7 Discussion

The OpenSees model of pile group response was shown in Chapter 4 to predict response consistent with that observed in full-scale static load tests, and to predict the response of pile groups subjected to dynamic loading in centrifuge model tests. The model makes use of discrete elements, such as *p*-*y*, *t*-*z*, and *Q*-*z* elements, to represent three-dimensional soil-pile interaction and passive pile cap resistance. These elements are not claimed to model response perfectly, but they do capture the primary effects of soil-pile interaction and treat them in a consistent manner.

The normalization procedures described in this section are not perfect, but they are very useful. For a given set of analysis conditions, the uncertainty in computed response is caused primarily by differences in the characteristics of the input motions, often referred to as record-to-record variability, is quite high. As a result, differences in the mean responses under various conditions may be so small relative to record-to-record variability that lumping the responses together through the normalization process is acceptable.

5.8 INTERPRETATION OF PILE GROUP RESPONSE

As indicated in the preceding sections, thousands of OpenSees analyses were performed resulting in tens of thousands of data points. The primary objective of the analyses was to develop relationships for predicting pile group displacements and rotations as functions of pile group loads and moments.

5.8.1 Normalization

To make the results of the dynamic pile group analyses as general and useful as possible, the concept of combining data from multiple analyses by normalizing both forces/moments and displacements/rotations was investigated. As indicated in Section 5.6.1, normalization proved to be effective in bringing the median response levels to common, consistent values even when other variables (e.g., pile group size or shape) were changed. Differences between median curves were so small compared to the scatter in response about the respective medians that separating the different cases for individual consideration provided no significant benefit.

5.8.2 Regression Analyses

A series of regression analyses were performed to develop models that would predict normalized displacements from normalized loads. The displacements (including rotations) were expressed in terms of a five-component displacement ratio vector, $DR = \{u, v, w, \theta_x, \theta_y\}$ and the loads in terms of a five-component load ratio vector, $LR = \{Q, V_x, V_y, M_x, M_y\}$.

Anticipating that LRFD-like "checks" would likely be performed on individual load or displacement components (rather than checking the joint occurrence of all five components), individual component models were investigated. These models were of the form

$$w_n = f_w\left(Q_n, V_{xn}, V_{yn}, M_{xn}, M_{yn}\right)$$
$$u_n = f_u\left(Q_n, V_{xn}, V_{yn}, M_{xn}, M_{yn}\right)$$
$$v_n = f_v\left(Q_n, V_{xn}, V_{yn}, M_{xn}, M_{yn}\right)$$
$$\theta_{xn} = f_{\theta_{xn}}\left(Q_n, V_{xn}, V_{yn}, M_{xn}, M_{yn}\right)$$
$$\theta_{yn} = f_{\theta_{yn}}\left(Q_n, V_{xn}, V_{yn}, M_{xn}, M_{yn}\right)$$

The models were developed in an incremental, methodical manner. Each normalized displacement had an associated primary normalized load. For example, the vertical load, Q_n, is the primary *LR* component for the vertical displacement, w_n. Initially, each *DR* component was modeled as a sole function of its primary *LR* component. An example, for the case of normalized lateral displacement, u_n, is shown in Figure 5.28. The fitted curve can be seen to pass generally through the middle of the data as plotted, but the uncertainty, expressed in terms of the standard deviation of the (logarithmic) residuals, $\sigma_\varepsilon = \sigma_{\ln DR|LR} = 1.203$, which is very high. The residuals were then plotted as functions of other potential predictor variables. Figure 5.29 shows the residuals plotted against the other four *DR* components. Figure 5.29(a) shows a modest trend in residuals with vertical load, indicating that differences in vertical load level are responsible for some of the uncertainty in the initial model. Figure 5.29(b) shows no trend in

residuals given the perpendicular horizontal load, V_y, and figures 5.29(c) and 5.29(d) show a strong trend in the residuals with both overturning moments, M_x and M_y.

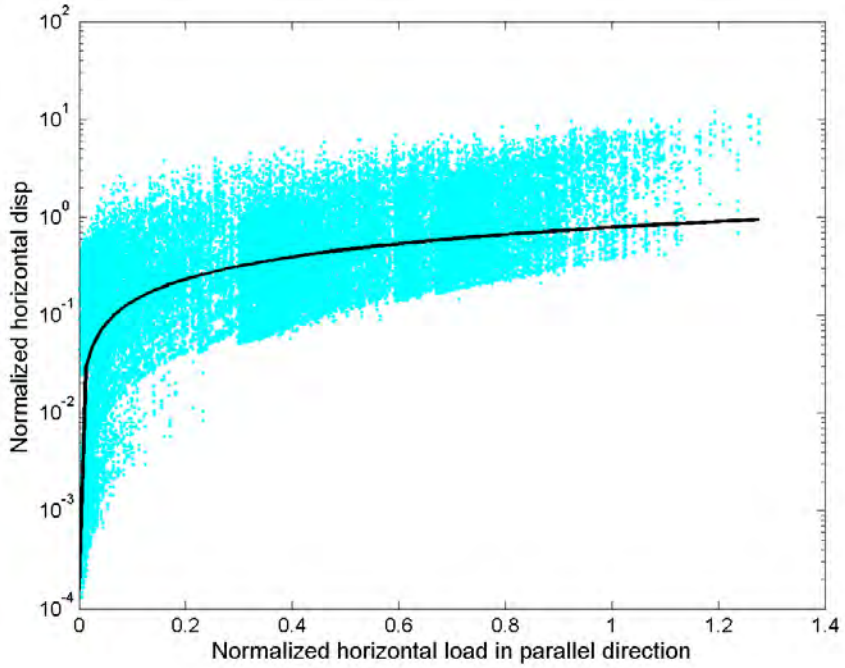

Figure 5.28 **Initial model for prediction of normalized horizontal displacement, u_n, as a function of normalized horizontal load, V_{xn}.**

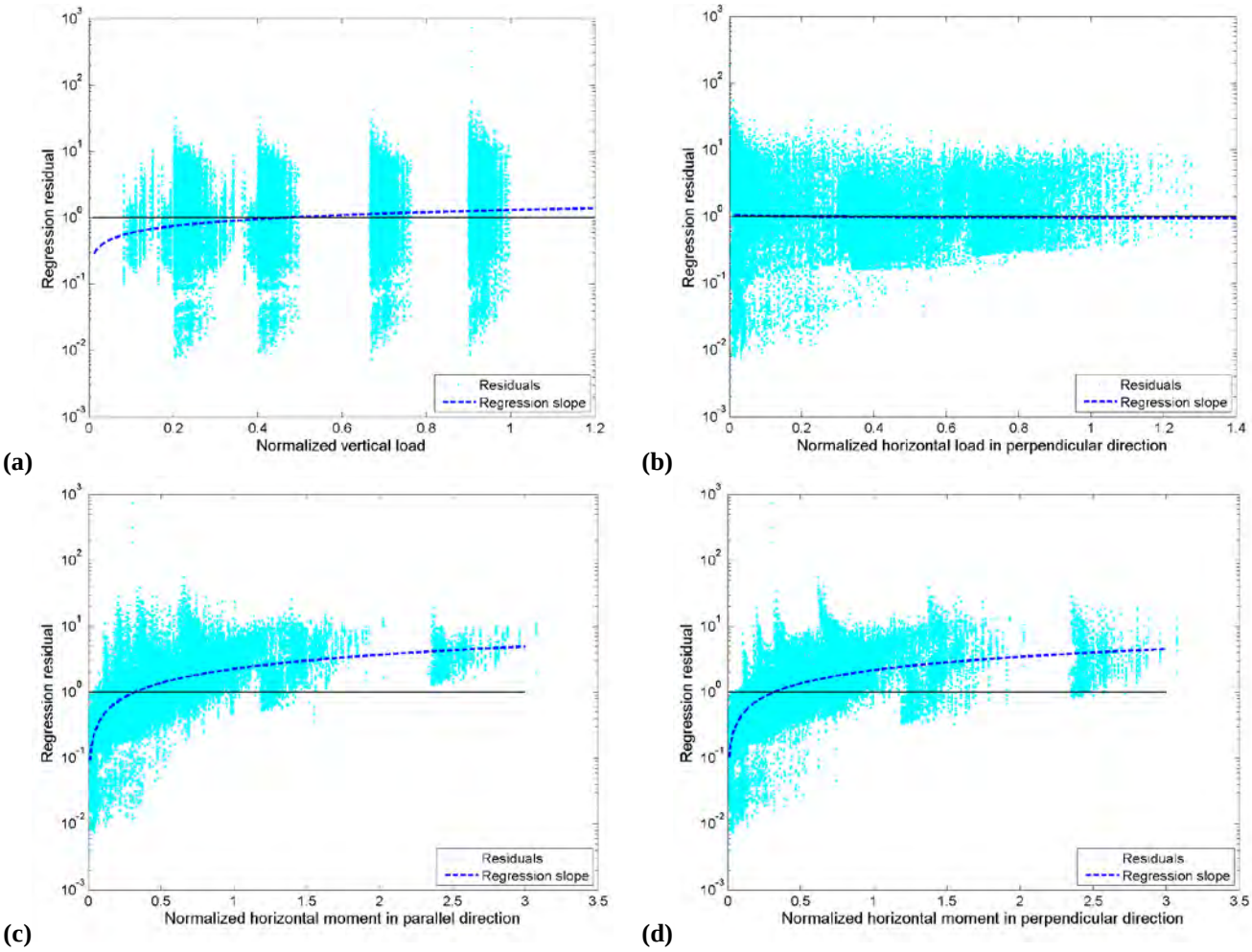

Figure 5.29 **Variation of residuals with secondary predictive variables for initial horizontal displacement, u_n, model: (a) vertical load, Q_n, (b) perpendicular horizontal load, V_{yn}, (c) moment about perpendicular axis, M_{yn}, and (d) moment about parallel axis, M_{xn}.**

The residuals plots indicated that overturning moments were the most influential of the secondary predictive variables, so M_x and M_y terms were added to the predictive equation and the residuals from the updated equation examined for remaining trends. Vertical load was still found to be influential and was then added to the model. A number of different model formulations were investigated, including different ways (e.g., sums, products, etc.) of combining lateral load and moment components, with the objective of balancing predictive power with model simplicity. In the end, a model of the form

$$\ln u_n = 0.191 + 0.364Q_n + 0.990V_{xn} - 0.320V_{yn} + 0.796\ln(M_x + M_y)$$

was obtained. The value of u_n from this equation is the median normalized horizontal displacement in the x-direction. The standard deviation of the logarithmic residuals was $\sigma_\varepsilon = \sigma_{\ln DR|LR} = 0.749$, a value that is high but much lower than that of the original model. The residuals are shown in Figure 5.30. The inclusion of additional variables, such as number of piles, and

other refinements such as separating static and dynamic components of loading, was not found to offer benefits in terms of reduction of uncertainty that were sufficient to justify the increased model complexity. More highly nonlinear relationships were also investigated and found not to produce significantly improved predictions.

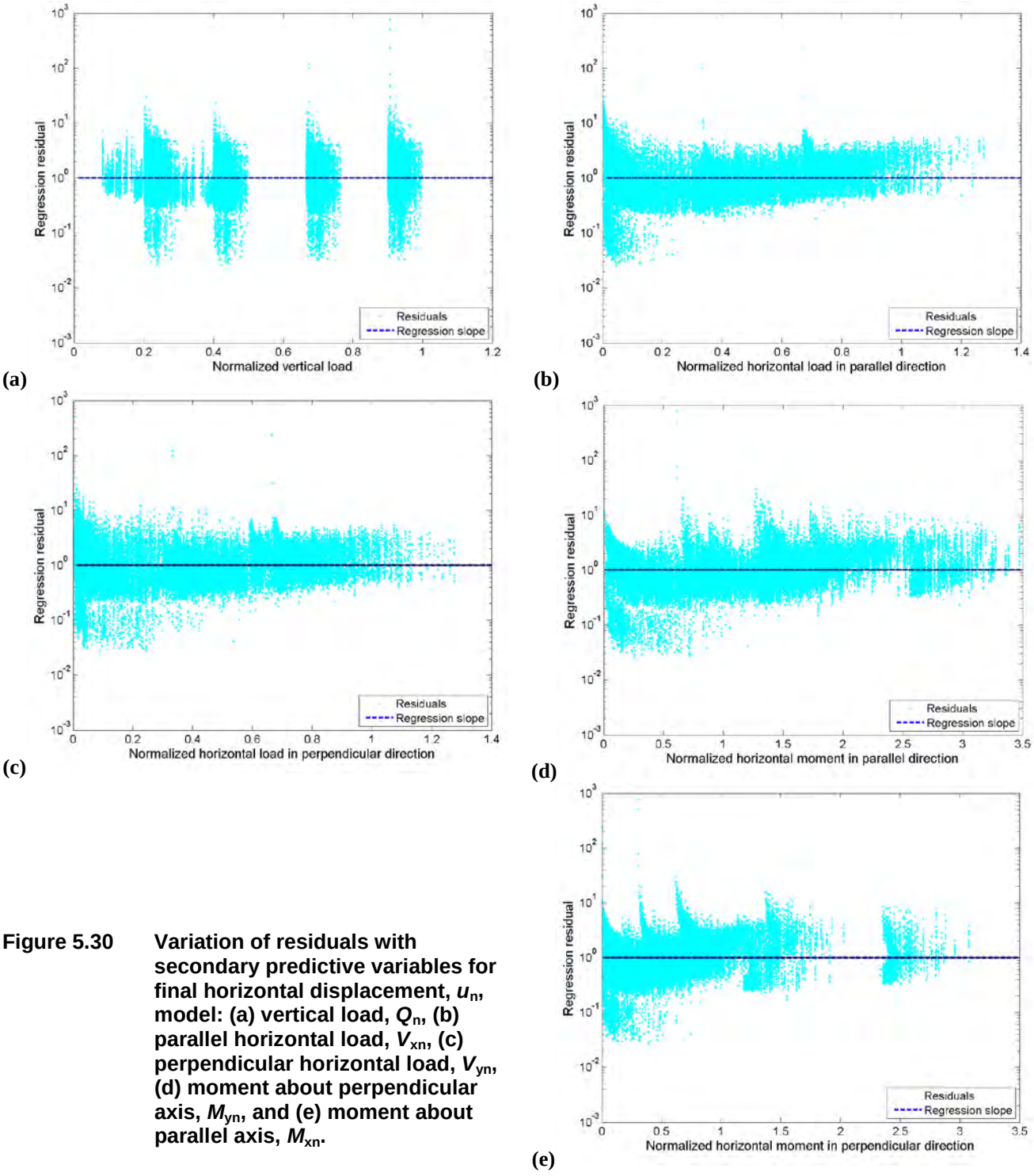

Figure 5.30 **Variation of residuals with secondary predictive variables for final horizontal displacement, u_n, model: (a) vertical load, Q_n, (b) parallel horizontal load, V_{xn}, (c) perpendicular horizontal load, V_{yn}, (d) moment about perpendicular axis, M_{yn}, and (e) moment about parallel axis, M_{xn}.**

This process was repeated systematically for all of the *DR* variables using the data from the sand and clay profiles. Fundamental differences in the constitutive behavior of sands and clays produced sufficient differences in response that a unified model that applied to both was not feasible. The final models, with their accompanying uncertainties, are listed in Table 5.8.

Table 5.8 Final predictive models for normalized displacements/rotations.

Soil	Equation	σ_ε
Sand	$\ln w_n = 0.777 + 1.648 \ln Q_n + 0.103 \ln(V_{xn} + V_{yn}) + 0.203 \ln(M_{xn} + M_{yn})$	0.434
	$\ln u_n = 0.191 + 0.364 \ln Q_n + 0.990 V_{xn} - 0.320 V_{yn} + 0.796 \ln(M_{xn} + M_{yn})$	0.749
	$\ln v_n = 0.191 + 0.364 \ln Q_n - 0.320 V_{xn} + 0.990 V_{yn} + 0.796 \ln(M_{xn} + M_{yn})$	0.749
	$\ln \theta_{xn} = 0.674 + 0.401 nQ_n - 0.672 \ln V_{xn} + 1.127 \ln V_{yn} + 0.904 \ln(M_{xn} + M_{yn})$	0.740
	$\ln \theta_{yn} = 0.674 + 0.401 \ln Q_n + 1.127 \ln V_{xn} - 0.672 \ln V_{yn} + 0.904 \ln(M_{xn} + M_{yn})$	0.740
Clay	$\ln w_n = 0.386 + 2.317 \ln Q_n + 0.197 \ln(V_{xn} + V_{yn}) + 0.667 \ln(M_{xn} + M_{yn})$	0.635
	$\ln u_n = 0.329 + 0.843 \ln Q_n + 0.826 V_{xn} - 0.297 V_{yn} + 0.947 \ln(M_{xn} + M_{yn})$	0.976
	$\ln v_n = 0.329 + 0.843 \ln Q_n - 0.297 V_{xn} + 0.826 V_{yn} + 0.947 \ln(M_{xn} + M_{yn})$	0.976
	$\ln \theta_{xn} = 1.113 + 0.955 \ln Q_n - 0.501 \ln V_{xn} + 0.873 \ln V_{yn} + 1.084 \ln(M_{xn} + M_{yn})$	1.012
	$\ln \theta_{yn} = 1.113 + 0.955 \ln Q_n + 0.873 \ln V_{xn} - 0.501 \ln V_{yn} + 1.084 \ln(M_{xn} + M_{yn})$	1.012

5.8.3 Discussion

The predictive models are based on the OpenSees analyses that were described earlier in the chapter. Those analyses were performed on a simple, single-mass structural model subjected to three-dimensional input motions, and on a limited number of soil-foundation configurations. The model was intended to represent the first-order behavior of a bridge structure for the purpose of building and testing a performance-based framework for seismic LRFD. The model was not intended to capture all elements of the seismic response of a particular bridge structure, and may exhibit behavior that is not representative of the behavior of an actual bridge. It is expected that the framework would be used with the results of analyses of actual structures.

Similarly, the pile groups analyzed in this project were limited to a relatively narrow range of geometries, materials, and soil conditions. As a result, the predictive models described in the preceding section may be somewhat limited. They are sufficient, however, for the purpose of developing and using the performance-based framework for seismic LRFD.

6 A Performance-Based Design Framework

6.1 INTRODUCTION

As indicated in Chapter 3, developing a design framework considering the virtually infinite number of combinations of bridge type, geometry, and material properties, the virtually infinite number of possible site and subsurface conditions, and the very large number of combinations of different pile types, lengths, and group configurations requires a procedure that can produce results general enough to be applicable to different combinations of these conditions.

Chapter 3 described a performance-based framework for evaluating the response of a pile group subjected to dynamic loading. Design, however, involves both demand and capacity and the development of a procedure that allows the probability that demand exceeds capacity to be quantified and kept below some user-specified level. This chapter describes a performance-based design framework that provides the basis for selection of load (demand) and resistance (capacity) factors consistent with a specific return period of limit state exceedance. Two alternative procedures are developed – one based on forces and moments and the other based on displacements and rotations. This framework required consideration of the intermediate load measure variable and of correlations between various loads and deformations.

Seismic design involves an element of time that does not exist in most LRFD frameworks. While the loading considered in static design (e.g., dead loads and live loads) exist for extended, if not indefinite, periods of time, earthquakes produce short and infrequent periods of intense loading. As a result, performance levels in seismic design are more appropriately related to targeted rates of occurrence (or exceedance) of failure rather than targeted probabilities of failure. Such rates can be expressed in terms of mean annual rates of exceedance, return periods, or (under a generally reasonable assumption) mean annual probabilities.

A force-based design framework, in which uncertainties in loads and capacities are accounted for by load and resistance factors, is presented. In this framework, the load and resistance factors are tied to user-specified mean annual rates of exceedance, or return periods.

Because pile group performance is closely related to displacements, a displacement-based design procedure is also presented. It provides factors by which median response and capacities can be multiplied to achieve a user-specified probability that the pile group displacement would not exceed a user-specified limit state displacement in a user-specified average period of time. The procedure considers uncertainties in earthquake ground motions, structural response, pile group response, and limit state displacements for all five components of pile cap displacement. This approach could potentially form the basis for the development of serviceability limit states for extreme events.

6.2 CAPACITY

The capacity of a foundation can be thought of as a limiting level of response beyond which performance of the foundation is considered to be unsatisfactory in some way. Therefore, the specification of capacity requires choice of a response metric, definition of acceptable performance, and identification of the response metric value that defines the onset of unacceptable performance. Two basic forms of response metric, force-related and displacement-related have been used in engineering practice. The development of a framework that can handle both is described in the remainder of this chapter.

6.2.1 Allowable Load as Capacity

The design of pile foundations has historically been force-based, in that the forces imposed on the foundations have been compared with force-based pile capacities to infer performance. The results of force-based analyses have usually been expressed in terms of factors of safety, with values greater than one implying successful performance and values less than one implying failure. In this approach, design factors of safety are usually specified as being greater than one by a factor sufficient to account for uncertainty and consequences of failure.

In many cases, pile foundations are designed using force-based LRFD procedures in which a single factor of safety is replaced by load and resistance factors that account separately for uncertainties in loading and capacity. In a force-based design, the capacity is expressed in terms of resisting forces (for vertical and horizontal loads) and resisting moments (for overturning). These capacities can be obtained by any of the methods described in Chapter 2.

Because of spatial variability, measurement error, model uncertainty, and other factors, the capacity of a foundation is uncertain. This uncertainty is accounted for in static LRFD design through the use of resistance factors whose values decrease as uncertainties in capacity increase and conservatism in the capacity estimate decreases. Table 6.1 presents resistance factors for pile foundations – the values for the most reliable capacity estimation procedures, such as load tests, are relatively close to 1.0 while values for less reliable procedures are well below 1.0.

Table 6.1 Resistance factors for pile capacity by dynamic analysis and static load tests (after AASHTO, 2010)

Condition/Resistance Determination Method		Resistance Factor
Nominal Bearing Resistance of Single Pile—Dynamic Analysis and Static Load Test Methods, φ_{dyn}	Driving criteria established by successful static load test of at least one pile per site condition and dynamic testing* of at least two piles per site condition, but no less than 2% of the production piles	0.80
	Driving criteria established by successful static load test of at least one pile per site condition without dynamic testing	0.75
	Driving criteria established by dynamic testing* conducted on 100% of production piles	0.75
	Driving criteria established by dynamic test with signal matching at beginning of redrive (BOR) conditions only of at least one production pile per pier, but no less than the number of tests per site provided in Table 10.5.5.2.3-3.	0.65
	Wave equation analysis, without pile dynamic measurements or load test, at end of drive conditions only	0.40
	FHWA-modified Gates dynamic pile formula (End of Drive condition only)	0.40
	Engineering News Record (as defined in Article 10.7.3.8.5) dynamic pile formula (End of Drive condition only)	0.10

6.2.2 Allowable Displacement as Capacity

The actual serviceability of pile foundations is much more closely related to displacements than to forces. In this sense, the term "capacity" can also be expressed in terms of "allowable" deformation-related quantities such as settlement, lateral displacement, and rotation. Displacement capacities can be specified for various limit states that correspond to different levels of performance. Displacement-based capacities are newer than force-based capacities, and procedures for estimating allowable displacements are not as advanced or well-developed as those for estimating force-based capacities. As a result, displacement-based capacities are likely to be more uncertain than force-based capacities.

6.3 LIMIT STATE CONCEPT

Performance-based seismic design seeks to produce structures that will achieve user-specified levels of performance with a specified level of reliability. Performance levels can be defined in many different ways. Regardless of what metric is used to describe performance, that metric will have one or more levels that are considered to mark the boundary between acceptable and unacceptable performance. These levels can be described as "limit states" that quantify the boundary between acceptable and unacceptable performance. Limit states can be expressed in terms of force (e.g., as a pile resistance or deformations (e.g., as an acceptable settlement).

In current practice, limit states are effectively defined as limiting response levels beyond which various levels of damage and loss are assumed to occur. The response levels can be expressed in terms of force- or displacement-related quantities. In conventional practice, design limit states usually represent conservative, but deterministic, estimates of limiting response. The

level of conservatism in the allowable response value is generally not standardized or quantified, and likely varies from one designer to another.

In reality, limit states should be recognized as being uncertain, and the level of uncertainty as depending on the procedure(s) used to define them. Rather than characterizing allowable response conservatively and deterministically, it is desirable to characterize the distribution of allowable response as accurately and objectively as possible and to include its uncertainty in the performance evaluation.

6.3.1 Calculation of Limit State Exceedance Rate

An allowable level of response, whether expressed in terms of load or resistance, can be described as a limit state that marks the boundary between two levels of performance. Limit states can be expressed explicitly in terms of consequences, which could be expressed in terms of physical damage (ranging, say, from concrete cracking to structural collapse) or expected losses (repair cost, downtime, or some other measure). Seismic design, then, requires identification of appropriate limit states and acceptable rates (or annual probabilities) of their exceedance.

6.3.1.1 Force-Based Limit State

Force-based limit states for foundations are related to ultimate strength and moment resistance, which are compared with force and moment demands generally obtained through dynamic structural analyses. The capacities themselves must be considered to be uncertain. Letting C represent a random variable that describes a force-based capacity, the mean annual rate at which a scalar value of that capacity, $C = c$, representing a particular limit state would be exceeded by a given load measure, LM, is given by

$$\lambda_{LM}(c) = \nu \sum_{i=1}^{N_{IM}} P[LM > c \mid IM = im_i] P[IM = im_i] \tag{6.1}$$

where ν is the mean annual rate of earthquakes exceeding some minimum magnitude. If C is uncertain, the mean annual rate of the capacity exceedance limit state, i.e., $LS = LM > C$, would be given by

$$\lambda_{LS} = \int_0^\infty \lambda_{LM}(c) f_C(c) dc \tag{6.2}$$

Thus, a hazard curve for force-based limit state exceedance, which considers the capacity and its uncertainty, can be evaluated from the IM hazard curve, the (probabilistic) relationship between IM and LM, and the uncertainty in capacity.

6.3.1.2 Displacement-Based Limit State

For foundations, displacement-based limit states consist of maximum acceptable displacements and rotations, which can be characterized as EDPs. These quantities are often difficult to determine and must be assumed to be uncertain. From Equation (3.8), the mean annual rate of exceeding a response level, $EDP = edp_k$, can be expressed as

$$\lambda_{EDP}(edp_k) = \nu \sum_{i=1}^{N_{IM}} \sum_{j=1}^{N_{LM}} P\left[EDP > edp_k \mid LM = lm_j\right] P[LM = lm_j \mid IM = im_i] P\left[IM = im_i\right] \quad (6.3)$$

Letting C represent the maximum acceptable response (i.e., displacement) level for a given damage state, the mean annual rate at which a specific capacity, C=c, is exceeded can then be computed as

$$\lambda_{EDP}(c) = \nu \sum_{i=1}^{N_{IM}} \sum_{j=1}^{N_{LM}} P\left[EDP > c \mid LM = lm_j\right] P[LM = lm_j \mid IM = im_i] P\left[IM = im_i\right] \quad (6.4)$$

Accounting for the fact that the capacity is also uncertain, a hazard curve for the limit state, $LS = EDP \geq C$, can be expressed as

$$\lambda_{LS} = \int_0^\infty \lambda_{EDP}(c)\, f_C(c) dc \quad (6.5)$$

Equation 6.5 can be integrated numerically to compute the mean annual rate (or return period) of limit state exceedance. The computed rates depend on the *IM* hazard curve, the (probabilistic) relationship between *IM* and *LM*, the (probabilistic) relationship between *LM* and *EDP*, and the uncertainty in displacement capacity.

6.3.2 Closed-Form Solution for Limit State Exceedance Rates

Consideration of a closed-form solution, despite its restriction to the previously discussed assumptions regarding hazard curve, loading, and response relationships can provide useful insight into the development and behavior of load and resistance factors. With the assumption of capacity lognormality, the previous closed-form response relationships can be extended to obtain closed-form limit state exceedance relationships.

6.3.2.1 Force-Based Limit States

A closed-form expression for the mean annual rate of *LM* exceedance was given in Equation 3.34. The rate at which some load capacity, $C = c$, would be exceeded is then

$$\lambda_{LM}(c) = k_0 \left[\left(\frac{c}{a}\right)^{1/b}\right]^{-k} \exp\left[\frac{1}{2}\frac{k^2}{b^2}\beta_L^2\right] \quad (6.6)$$

Using Equation 6.5 to account for uncertainty in load capacity

$$\lambda_{LS} = \int_0^\infty k_0 \left[\left(\frac{c}{a}\right)^{1/b}\right]^{-k} \exp\left[\frac{1}{2}\frac{k^2}{b^2}\beta_L^2\right] f_C(c) dc \quad (6.7)$$

Extracting c from the first term and moving capacity-independent terms out of the integral,

$$\lambda_{LS} = k_o a^{k/b} \exp\left[\frac{1}{2}\frac{k^2}{b^2}\beta_L^2\right]\int_0^\infty c^{-k/b} f_C(c)dc \tag{6.8}$$

The term inside the integral is, by definition, the mean value of $c^{-k/b}$. Since the expected value of a lognormal random variable, *Y*, with median, $\hat{Y}$, and dispersion, $\beta_Y = \sigma_{\ln Y}$, raised to the power α is given by

$$E(Y^\alpha) = E(e^{\alpha \ln Y}) = \left(\hat{Y}\right)^\alpha \exp\left[\frac{1}{2}\alpha^2 \beta_Y^2\right] \tag{6.9}$$

Equation (6.8) becomes

$$\lambda_{LS} = k_o a^{k/b}\left(\hat{C}\right)^{-k/b} \exp\left[\frac{1}{2}\frac{k^2}{b^2}\beta_L^2\right]\exp\left[\frac{1}{2}\frac{k^2}{b^2}\beta_C^2\right] \tag{6.10}$$

which can be simplified to

$$\lambda_{LS} = k_o\left(\frac{\hat{C}}{a}\right)^{-k/b} \exp\left[\frac{1}{2}\frac{k^2}{b^2}\beta_L^2\right]\exp\left[\frac{1}{2}\frac{k^2}{b^2}\beta_C^2\right] \tag{6.11}$$

The mean annual rate of load capacity exceedance can be seen to increase with increasing uncertainty in capacity as well as uncertainty in loading.

6.3.2.2 Displacement-Based Capacity

A similar approach can be taken to obtain a closed-form expression for displacement-based capacity exceedance rate. This expression must account for uncertainty in *LM*, *EDP*, and capacity. Following the closed form expression of Equation (3.13), the mean annual rate of exceeding some known capacity level, $C = c$, is given by

$$\lambda_{EDP}(c) = k_0\left[\frac{1}{a}\left(\frac{c}{d}\right)^{1/e}\right]^{-k/b} \exp\left[\frac{1}{2}\frac{k^2}{b^2 e^2}\left(e^2\beta_L^2 + \beta_R^2\right)\right] \tag{6.12}$$

If the capacity is assumed to be lognormally distributed with median, $\mu_{\ln C}$, and logarithmic standard deviation, $\beta_C = \sigma_{\ln C}$, the mean annual rate of exceeding the capacity can be expressed as

$$\lambda_{LS} = \int_0^\infty k_o\left[\frac{1}{a}\left(\frac{c}{d}\right)^{1/e}\right]^{-k/b} \exp\left[\frac{1}{2}\frac{k^2}{b^2 e^2}\left(e^2\beta_L^2 + \beta_R^2\right)\right] f_C(c)dc \tag{6.13}$$

Again, extracting *c* from the first term and moving capacity-independent terms out of the integral, Equation (6.13) can be written as

$$\lambda_{LS} = k_o \left[\frac{1}{a} \left(\frac{1}{d} \right)^{1/e} \right]^{-k/b} \exp\left[\frac{1}{2} \frac{k^2}{b^2 e^2} \left(e^2 \beta_L^2 + \beta_R^2 \right) \right] \int_0^\infty c^{-k/be} f_C(c) dc \tag{6.14}$$

The term inside the integral is the expected value of $c^{-k/be}$. By the same logic used in the preceding section, Equation (6.14) becomes

$$\lambda_{LS} = k_o \left[\frac{1}{a} \left(\frac{1}{d} \right)^{1/e} \right]^{-k/b} \left(\hat{C} \right)^{-k/be} \exp\left[\frac{1}{2} \frac{k^2}{b^2 e^2} \left(e^2 \beta_L^2 + \beta_R^2 \right) \right] \exp\left[\frac{1}{2} \frac{k^2}{b^2 e^2} \beta_C^2 \right] \tag{6.15}$$

which can be simplified to

$$\lambda_{LS} = k_o \left[\frac{1}{a} \left(\frac{\hat{C}}{d} \right)^{1/e} \right]^{-k/b} \exp\left[\frac{1}{2} \frac{k^2}{b^2 e^2} \left(e^2 \beta_L^2 + \beta_R^2 \right) \right] \exp\left[\frac{1}{2} \frac{k^2}{b^2 e^2} \beta_C^2 \right] \tag{6.16}$$

The first part of Equation 6.16 represents the limit state exceedance rate without the effects of uncertainty, and the latter two parts (i.e., the exponential terms) represent the uncertainty in loading/response and capacity, respectively. Thus, the mean annual rate of capacity exceedance is affected by uncertainty in the capacity as well as uncertainties in the loading and response models.

6.4 LOAD AND RESISTANCE FACTOR FRAMEWORK

The preceding section described procedures by which the mean annual rate of exceeding some limit state, interpreted as an exceedance of capacity, could be computed. Such procedures allow for the element of time, in the form of rates of different levels of earthquake shaking, to be accounted for. However, design for exceedance rate is not a familiar concept to geotechnical and foundation engineers, so some benefits can be obtained by casting performance-based seismic design in a more familiar format. Jalayer and Cornell (2003) developed a demand-and-capacity-factor-design format for structural design.

Load and resistance factors are intended to account for uncertainties in loads and resistances, respectively. For seismic design, loads are induced by ground motions so the total uncertainty in loading depends on the uncertainty in ground motion and the uncertainty in structural loading given the level of ground motion. Capacities, and their uncertainties, are generally independent of loads.

Uncertainty in design ground motion level is typically handled through probabilistic seismic hazard analyses, the results of which are usually expressed in terms of design response spectra. Different procedures for development of design spectra are available, but they all produce spectra associated with some mean annual rate of exceedance, or return period. If a design check is performed using ground motions developed from probabilistic seismic hazard analyses, the only uncertainty that need be represented by the load factor is the uncertainty in load given the intensity measure used to characterize ground motion at the design return period. This uncertainty will generally include a component of "record-to-record variability" that describes the variability of *LM* found in the predictions of analyses using input motions scaled to

the same *IM*, and model uncertainty. Model uncertainty for force predictions is likely to be significantly lower than model uncertainty for displacement predictions.

6.4.1 Calculation of Load and Resistance Factors

If the uncertainty in *LM*|*IM* is zero, a deterministic *LM* hazard curve can be expressed in a relatively straightforward manner. If the mean load measure can be related to the ground motion intensity by $LM = f(IM)$, the zero-uncertainty mean load measure is

$$LM_0 = f(IM) \tag{6.17}$$

Letting $im_{\text{lm}} = f^{-1}(lm)$, the zero-uncertainty *LM* hazard curve can therefore be expressed as

$$\lambda_{LM_0}(lm) = \lambda_{IM}\left(im^{lm}\right) \tag{6.18}$$

which means that the value of *LM* at a particular return period is just the value of *LM* computed deterministically using the value of *IM* at the same return period.

With consideration of uncertainty in load given ground motion level, the hazard curve for *LM* can be obtained from Equation 3.34. For a given return period, the value of *LM* from this hazard curve can be expressed as LM_1. When uncertainty in *LM*|*IM* and capacity are both considered, as described in Equation 6.8, the *LM* at a particular return period can be expressed as LM_2. With this notation, load and resistance factors can be defined as

$$LF = \frac{LM_1}{LM_0} \tag{6.19a}$$

and

$$RF = \frac{LM_1}{LM_2} \tag{6.19b}$$

Graphically, the load and resistance factors would be interpreted as indicated in Figure 6.1. For a given return period, the value of LM_0 is that which would be computed deterministically using the median *IM* value for the same return period. The product of the load factor and that deterministic load is equal to the nominal load, LM_1. For the same return period, the load capacity including uncertainty in capacity is given by LM_2. The product of the load capacity and the resistance factor is the nominal resistance, which is also LM_1.

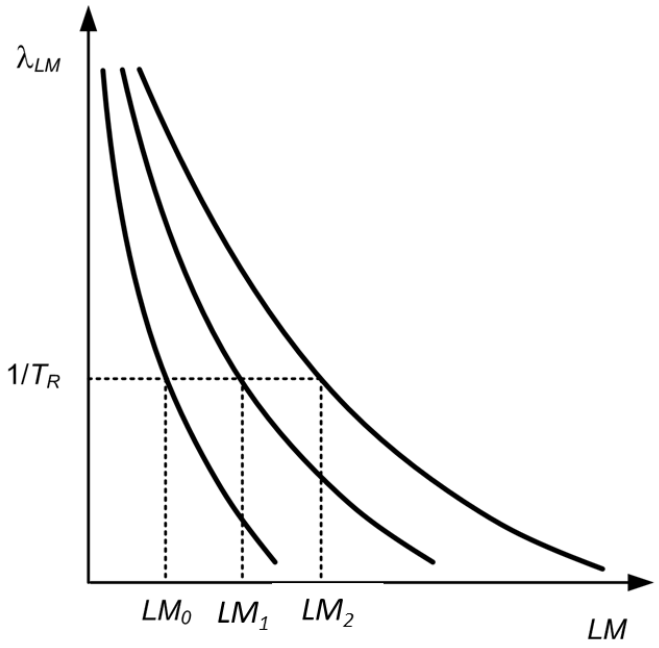

Figure 6.1. Schematic illustration of load measure hazard curves for cases of no uncertainty, uncertainty in load given ground motion intensity, and uncertainties in load given ground motion intensity and capacity.

A seismic hazard curve can easily be combined with the Poisson model to estimate the probability of exceeding a particular *IM* level in a finite time interval. From the Poisson model, the probability of exceedance of $IM = im$ in a time period, t, is

$$P[N \geq 1] = 1 - e^{-\lambda_{IM}(im)t} \tag{6.20}$$

Expanding in a Taylor series and eliminating high-order terms shows that

$$P[N \geq 1] = \lambda_{IM}(im)t + \frac{(\lambda_{IM}(im)t)^2}{2} + \frac{(\lambda_{IM}(im)t)^3}{6} + \cdots \approx \lambda_{IM}(im)t \tag{6.21}$$

for small values of λt (or, equivalently, small values of t/T_R), which are typical for seismic design. This result is often used to approximate the annual (t = 1 yr) probability of exceedance as being equal to λ_{IM}. Letting im^p represent the *IM* value corresponding to a mean annual probability of exceedance, p (or $T_R = 1/p$), a design that satisfies the condition

$$LF \cdot \hat{L}_p \leq RF \cdot \hat{C}$$

where $\hat{L}_p$ is the load measure computed deterministically from $IM = im^p$ and $\hat{C}$ is the median capacity would result in a mean annual probability of limit state exceedance of p.

6.4.2 Closed-Form Solution

The development of a closed-form expression for the mean annual rate of capacity exceedance was described in Section 6.3.2.1. The LRFD framework is intended to produce load and resistance factors that will be consistent with a user-specified mean annual rate of limit state exceedance (or return period or mean annual probability). If the target mean annual probability is *p*, the design must satisfy $\lambda_{LS} \le p$. Using Equation 6.11, and solving for $\hat{C}$,

$$\hat{C} \le a\left(\frac{p}{k_0}\right)^{-b/k} \exp\left[\frac{1}{2}\frac{k}{b}\beta_L^2\right]\exp\left[\frac{1}{2}\frac{k}{b}\beta_C^2\right] \tag{6.22}$$

In this expression, the term $\left(p/k_0\right)^{-1/k}$ is the *IM* value associated with the mean annual probability, *p*. Representing that quantity as im^p, the design must satisfy

$$\hat{C} \le a\left(im^p\right)^b \exp\left[\frac{1}{2}\frac{k}{b}\beta_L^2\right]\exp\left[\frac{1}{2}\frac{k}{b}\beta_C^2\right] \tag{6.23}$$

In this expression, $a\left(im_p\right)^b$ is the median *LM* value corresponding to $\lambda_{LS} = p$, or $\hat{L}_p$. Grouping the loading terms on the left and the resistance terms on the right produces an equation that states that the factored load must be smaller than the factored resistance.

$$\hat{L}_p \cdot \exp\left[\frac{1}{2}\frac{k}{b}\beta_L^2\right] \le \hat{C} \cdot \exp\left[-\frac{1}{2}\frac{k}{b}\beta_C^2\right] \tag{6.24}$$

This equation can be written in a more common LRFD format as

$$LF \cdot \hat{L}_p \le RF \cdot \hat{C} \tag{6.25}$$

where the load factor

$$LF = \exp\left[\frac{1}{2}\frac{k}{b}\beta_L^2\right] \tag{6.26a}$$

is applied to the median load measure and the resistance factor,

$$RF = \exp\left[-\frac{1}{2}\frac{k}{b}\beta_C^2\right] \tag{6.26b}$$

is applied to the median capacity.

6.4.3 Randomness and Uncertainty

The LRFD framework is inherently probabilistic. The need for probabilistic treatment in seismic design is evident from previous discussion of the accuracy with which ground motions, loads, response, and capacities can be predicted. The term "uncertainty" is usually used in discussions of statistical parameters and probabilistic models, but it can be helpful to distinguish between

randomness and uncertainty when developing, implementing, and interpreting probabilistic design models.

Randomness, which is frequently described by the term "aleatory uncertainty," refers to the inherent or intrinsic variability of some quantity or phenomenon; as a result, it cannot be reduced by additional data or more thorough investigation. Randomness can manifest itself, for example, in the variability of response produced by different ground motions, even when scaled to the same *IM*. This record-to-record variability, which results from the apparently random, unpredictable nature of earthquakes, is a very significant component of the overall uncertainty in a typical PBEE investigation. Uncertainty due to lack of data or knowledge concerning the quantity or phenomenon is frequently referred to as "epistemic uncertainty." Epistemic uncertainty differs from aleatory uncertainty in that it can be reduced by the acquisition of new information, e.g., by additional data, more extensive investigation, or by new research.

The distinction between aleatory and epistemic uncertainties can be difficult, ambiguous, and confusing. In practice, the distinction often depends as much on pragmatic as theoretical concerns. While arguments can be made that all uncertainty is epistemic, practical considerations require that some be treated as aleatory; one could, for example, gain knowledge of the inherent variability of a natural soil deposit by drilling and sampling the entire site with boreholes on a six-inch spacing – an action so obviously impractical (and destructive) that it illustrates why such variability is treated as aleatory. The assignment of aleatory vs. epistemic uncertainty can also be situation-dependent. For example, uncertainty in the shear wave velocity of an existing earth dam would be characterized as epistemic if it is possible to measure it using various geophysical techniques; the shear wave velocity of a future earth dam, however, would be characterized as aleatory if the source of the fill material from which it is to be constructed is not known.

The nature of the models used to predict performance will also affect the aleatory-epistemic distinction. All predictive models should be recognized as mathematical idealizations of reality – they are not perfect. Model uncertainty, i.e., errors in model predictions, have two primary components: (a) the effect of missing predictive variables, and (b) the effects of inaccurate model form. Missing variables may be those not recognized as being influential or those that cannot be measured or otherwise characterized. Inaccurate model form may result from practical consideration of computational complexity/effort or lack of understanding of the basic physics of the problem. Both components of model uncertainty can potentially be reduced, by including additional predictive variables and/or the use of improved mathematical expressions, but there will usually be a limit to the number of variables that can be identified and/or measured or to the understanding of the physics of the problem of interest that will limit the degree to which uncertainty can be reduced. Therefore, model uncertainty will generally have both aleatory and epistemic components. The fact that different models are frequently of different form and use different predictive variables means that they will predict different output values. The variability of mean (or median) predictions from different plausible models, therefore, represents another component of epistemic uncertainty. This situation is familiar in the context of PSHA where different attenuation relationships, for example, are used with their weighted contributions accounted for through a logic tree. To properly account for epistemic uncertainty in response, damage, and loss predictions, multiple predictive models, where available, should also be used.

The need for distinguishing between aleatory and epistemic uncertainty depends on the manner in which the results of the PBEE analysis will be used. The final result of the PEER PBEE framework is a mean annual rate of exceedance (or corresponding return period) of some loss level; the mean value is invariant with respect to the characterization of uncertainty as aleatory or epistemic. As such, that characterization doesn't matter in the end – the numerical value of the loss hazard will be the same regardless of whether some component of uncertainty is treated as aleatory or epistemic – what matters is properly capturing the total uncertainty. It should be noted that the aleatory/epistemic distinction can become important if design or evaluation is to be based on some percentile (rather than mean) loss value. In such cases, the value of interest can be sensitive to the manner in which uncertainty is divided into aleatory and epistemic components, and care must be taken to ensure that this division can be justified as fair and objective (i.e., not influenced by economic or competitive factors).

Even when the mean hazard is used, however, it is still useful to consider which components of uncertainty can and cannot be reduced and the costs and benefits of doing so. As will be illustrated shortly, increasing uncertainty tends to drive the ground motions, response, damage, and losses for a given return period higher in a performance-based evaluation. The ability to show the benefits of increased investment, for example, in additional subsurface investigation or more sophisticated response modeling, represents a tremendous opportunity for geotechnical earthquake engineering practitioners. Randomness and uncertainty can be distinguished and accounted for separately in the closed-form solution. Assuming random and uncertain components to be statistically independent, the total dispersions of load and resistance can be expressed as

$$\beta_L = \sqrt{\beta_{LR}^2 + \beta_{LU}^2} \tag{6.27a}$$

and

$$\beta_C = \sqrt{\beta_{CR}^2 + \beta_{CU}^2} \tag{6.27b}$$

where the subscript 'R' refers to randomness and the subscript 'U' to uncertainty.

6.5 RESPONSE AND CAPACITY FACTOR DESIGN FRAMEWORK

In contrast to conventional load-based procedures, i.e. load-and-resistance-factor-design (LRFD), the format described in Section 6.4 can be expressed in terms of response (displacement) and capacity (allowable displacement) levels and will be referred to here as a demand-and-capacity-factor design (DCFD) approach following the terminology of Jalayer and Cornell (2003). Expressions for response and capacity factors are developed in the following sections using an approach that accounts for the intermediate *LM* variable.

Together, demand and capacity factors can play a role similar to that of the factor of safety so commonly used in geotechnical engineering practice over the past 50+ years. They can, however, be calibrated in such a way that they allow mapping from the results of a deterministic response analysis to those of a performance-based response analysis.

In LRFD-based design, the load and resistance factors are intended to account for uncertainty in loads and resistances, respectively, and to allow design for a specific (and generally very low) probability that loads will exceed resistances. In a displacement-based DCFD design, the demand factor would account for uncertainties in pile group loading by the supported structure, response (e.g., pile group displacement), and the capacity factor for uncertainties in pile group limit state (e.g., allowable displacement). For seismic design purposes, the demand and capacity factors need to be tied to a particular limit state exceedance rate (or return period, or mean annual probability).

6.5.1 Calculation of Demand and Capacity Factors

The DCFD format can be developed in both a general form and an alternative form based on the closed-form solutions described in the preceding section. Its development can be simplified by the introduction of certain notation and relationships. Several are introduced in the following sections. The general form follows the approach taken for the development of general load and resistance factors in Section 6.4.1.

If the loading measure is taken as a deterministic (i.e., perfectly certain) function of ground motion intensity, $LM = f(IM)$, and the response measure is taken as a deterministic function of loading, $EDP = g(LM)$, then the response in the absence of uncertainty can be expressed as

$$EDP_o = g\left(f(IM)\right) \tag{6.28}$$

With respect to the closed-form solution, the load and response model relationships of Equations (6.5) and (6.7) can be inverted to express the ground motion intensity measure associated with a given level of response, i.e.,

$$im^{edp} = f^{-1}\left(g^{-1}(edp)\right) = \left(\frac{edp}{da^e}\right)^{\frac{1}{be}} \tag{6.29}$$

Thus, im^{edp} is the *IM* value that produces a median *EDP* value of *edp*. The variable, EDP_0, therefore will be taken to represent the response level that exists in the absence of uncertainty in loads or response. With no uncertainty in *LM*|*IM* or *EDP*|*LM*, the *EDP* exceedance probability,

$$P\left[EDP_0 > edp\right] = P\left[IM > f^{-1}\left(g^{-1}(edp)\right)\right] = P\left[IM > im^{edp}\right] \tag{6.30}$$

which means that the mean annual rate of exceeding a particular level of response is equal to the mean annual rate of exceeding the intensity measure that produces that response in the absence of uncertainty. The mean annual rate of exceedance of EDP_o is then given by

$$\lambda_{EDP_o}(edp) = \lambda_{IM}(im^{edp}) \tag{6.31}$$

Considering the uncertainty in displacement given the uncertainties in load and displacement conditional upon *IM*, the hazard curve for *EDP* can be computed using Equation 6.31. For a given return period, the value of *EDP* from this hazard curve will be referred to as EDP_1. A third hazard curve can be defined by adding the effects of uncertainty in displacement

capacity using Equation 6.5. The *EDP* value from this curve at a particular return period will be referred to as EDP_2. With the goal of relating the response computed deterministically to that computed considering uncertainties in load, demand, and capacity, i.e., of relating EDP_o to EDP_2, demand and capacity factors can be defined as

$$DF = \frac{EDP_1}{EDP_o} \tag{6.32a}$$

and

$$CF = \frac{EDP_1}{EDP_2} \tag{6.32b}$$

A design based on the requirement that

$$DF \cdot \hat{D}_p \le CF \cdot \hat{C} \tag{6.33}$$

where $\hat{D}_p$ is the value of *EDP* computed deterministically from $IM = im^p$ and $\hat{C}$ is the median capacity, would correspond to an annual probability of limit state exceedance less than or equal to *p*. The inequality can also be written as

$$\hat{R}_p \le \frac{CF}{DF} \cdot \hat{C} = \frac{EDP_1/EDP_2}{EDP_1/EDP_o} \cdot \hat{C} = \frac{EDP_0}{EDP_2} \cdot \hat{C} \tag{6.34}$$

If the ratio of median capacity to median response is viewed as being analogous to a factor of safety, the factor of safety would be given by EPD_2/EDP_0 for a given return period.

6.5.2 Closed-Form Solution

The objective of the RCFD development process is to identify resistance and capacity factors that, when used together, will ensure that the mean annual rate of limit state exceedance, λ_{LS} is lower than some desired value, *p*. This objective would require satisfaction of the inequality, using Equation (6.16),

$$\lambda_{IM}(im^{\hat{C}}) \exp\left[\frac{1}{2}\frac{k^2}{b^2 e^2}\left(e^2\,\beta_L^2 + \beta_R^2\right)\right] \exp\left[\frac{1}{2}\frac{k^2}{b^2 e^2}\beta_C^2\right] \le p \tag{6.35}$$

where, from Equation (6.16), the mean annual rate at which *IM* exceeds the value of *IM* that produces the median capacity, $\hat{C}$, is

$$\lambda_{IM}(im^{\hat{C}}) = k_0 \left[\frac{1}{a}\left(\frac{\hat{C}}{d}\right)^{1/e}\right]^{-k/b} \tag{6.36}$$

Substituting Equation (6.35) into Equation (6.36) gives

$$k_0\left[\frac{1}{a}\left(\frac{\hat{C}}{d}\right)^{1/e}\right]^{-k/b}\exp\left[\frac{1}{2}\frac{k^2}{b^2e^2}\left(e^2\,\beta_L^2+\beta_R^2\right)\right]\exp\left[\frac{1}{2}\frac{k^2}{b^2e^2}\beta_C^2\right]\le p \tag{6.37}$$

Solving Equation (6.37) for the median capacity allows determination of the median capacity that is consistent with an annual probability, p, of limit state exceedance.

$$\hat{C}\le d\left[a\left(\frac{p}{k_o}\right)^{-b/k}\right]^{e}\exp\left[\frac{1}{2}\frac{k}{be}(e^2\,\beta_L^2+\beta_R^2)\right]\exp\left[\frac{1}{2}\frac{k}{be}\beta_C^2\right] \tag{6.38}$$

Making use of Equation (6.32)

$$\hat{C}\le d\left(a(im^p)^b\right)^e\exp\left[\frac{1}{2}\frac{k}{be}(e^2\,\beta_L^2+\beta_R^2)\right]\exp\left[\frac{1}{2}\frac{k}{be}\beta_C^2\right] \tag{6.39}$$

In this expression, the term $d\left(a(im^p)^b\right)^e$ is the median *EDP* value for $IM = im^p$, or $\hat{R}_p$. Making this substitution and rearranging,

$$\hat{R}_p\exp\left[\frac{1}{2}\frac{k}{be}(e^2\,\beta_L^2+\beta_R^2)\right]\exp\left[\frac{1}{2}\frac{k}{be}\beta_C^2\right]\le\eta_C \tag{6.40}$$

Now, grouping the demand-related terms on the left and the capacity-related terms on the right,

$$\hat{R}_p\exp\left[\frac{1}{2}\frac{k}{be}(e^2\,\beta_L^2+\beta_R^2)\right]\le\eta_C\exp\left[-\frac{1}{2}\frac{k}{be}\beta_C^2\right] \tag{6.41}$$

which represents the final form of the DCFD format. The left side can be interpreted as a factored demand and the right side as a factored capacity. The factored demand is equal to the median demand resulting from a motion associated with a user-determined probability level multiplied by a factor that depends on the uncertainty in demand given the ground motion intensity; that factor is always greater than or equal to 1.0. The factored capacity is equal to the median capacity multiplied by a factor that depends on the uncertainty in the capacity; that factor is always less than or equal to 1.0. The factored demand is analogous to a factored load in a load-based LRFD format and the factored capacity is analogous to a factored resistance. Equation (6.41) can be rewritten in a form familiar to LRFD designers as

$$RF\cdot\hat{R}_p\le CF\cdot\hat{C} \tag{6.42}$$

where $\hat{R}_p$ is the median displacement demand given $IM = im^p$, $\hat{C}$ is the median capacity, the response factor is

$$RF=\exp\left[\frac{1}{2}\frac{k}{be}(e^2\,\beta_L^2+\beta_R^2)\right], \tag{6.43a}$$

and the capacity factor is

$$CF = \exp\left[-\frac{1}{2}\frac{k}{be}\beta_C^2 \right] \tag{6.43b}$$

Note that this derivation assumes that the hazard curve can be expressed as a power function (i.e., that it is linear in log-log hazard space), that the response model can also be expressed as a power function, and that the response variable (*EDP*) is lognormally distributed. While these requirements are approximately satisfied for a number of seismic design situations, they are not generally satisfied over wide ranges of *IM* and *EDP* values. However, they may represent an adequate approximation of actual behavior over ranges of *IM* and *EDP* that are significant from a practical design standpoint. If that is the case, the design problem can be locally linearized to fit the *IM* and *EDP* behavior in the range of greatest interest and thereby be used to develop practical response and capacity factors.

6.6 COMPUTATIONAL APPROACH

The process of identifying appropriate demand and capacity factors involves the performance of a probabilistic seismic hazard analysis (PSHA), combining its results with those of probabilistic load and response analyses, followed by integration over capacity distributions in order to obtain the desired factors. The process is complicated by the fact that the load measure, *LM*, and response measure, *EDP*, are both five-component vectors and that the components can be correlated to each other. The calculations involved in these analyses are voluminous and can be quite time-consuming.

A computer program, pgDF (pile group Design Factors), was written to perform the required analyses. This Fortran program requires the user to provide basic input on ground motion hazards, structural loads, pile group characteristics, and allowable displacements. The program then performs the calculations required to obtain the desired response and capacity factors. The general operation of the program is illustrated in Figure 6.2 with details on each of the primary components described in the following sections.

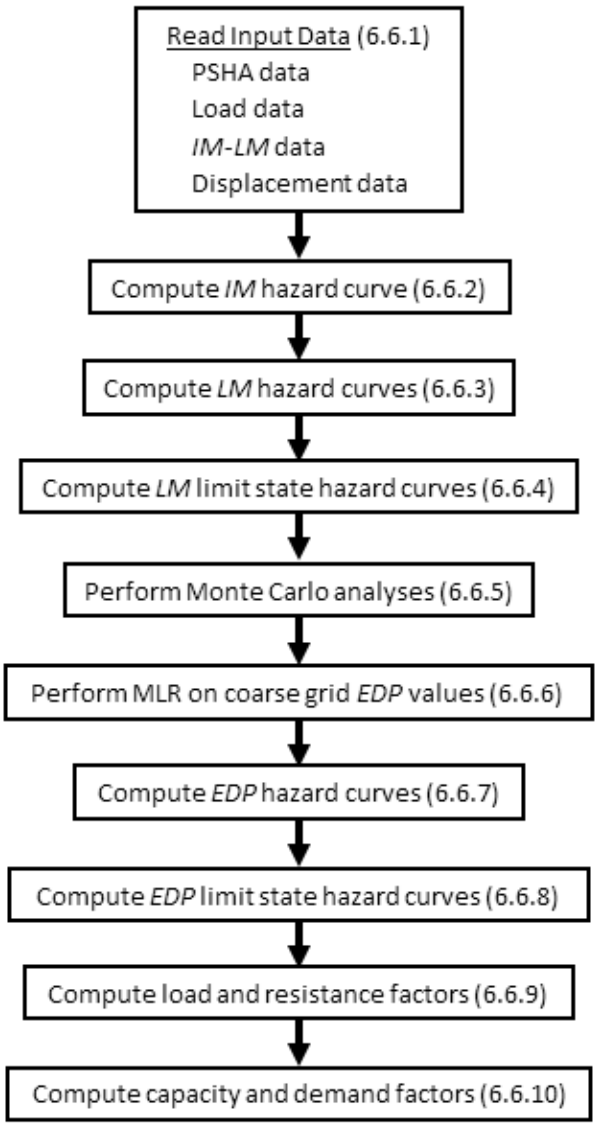

Figure 6.2. Schematic illustration of main components of pgDF. Descriptive section numbers in parentheses.

6.6.1 Read Input Data

The pgDF program was written to allow exploration of the effects of different inputs on demand and capacity factor values. Toward that end, the user is required to provide certain input data. This allows the user to investigate the sensitivity of the demand and capacity factors to various conditions and assumptions. The primary data supplied by the user include:

1. Seismic hazard data – in order to develop capacity and demand factors that account for local seismicity, the user is allowed to enter a seismic hazard curve for the site of interest. The intensity measure for the seismic hazard curve must be same intensity measure that the load measure is defined in terms of. The intensity measures are entered with their corresponding return periods; up to 15

return periods may be specified. For example, the pile group loads are generally expressed as functions of the fundamental period spectral acceleration, i.e., $S_a(T_o)$. Therefore, the hazard curves must be expressed in terms of $S_a(T_o)$. For bridges, fundamental periods of 0.5 – 1.0 sec are common.

2. Load data – the user provides static (i.e., pre-earthquake) loads and reference loads. All five load components (vertical and two horizontal loads, and two overturning moments) must be provided and the user may specify correlation coefficients between all combinations of loads. The reference loads used in the OpenSees analyses were defined as:

   Vertical – load capacity obtained from Davisson (1973) procedure
   Horizontal – load corresponding to pile load deflection of 0.1*D*.
   Overturning – moment that produces vertical load equal to vertical load capacity in any pile under unidirectional moment loading.

   To account for uncertainties in static, dynamic, and reference loads, a series of Monte Carlo simulations are performed. The user is asked to specify coarse and fine load measure grids. Due to time and memory constraints, the time-consuming Monte Carlo simulations are performed on a relatively coarse grid of dynamic load levels. The Monte Carlo results are then interpolated to the fine *LM* grid over which subsequent performance-based integration calculations take place.

3. Structural response data – the structural loads (i.e., vertical and two horizontal loads, and two overturning moments) are assumed to be related to the ground motion intensity measure used to define the ground motion hazard curve. The program allows the user to enter an *IM-LM* relationship defined by median *LM* values corresponding to different *IM* values, and a corresponding dispersion, $\beta_L = \sigma_{ln\ LM|IM}$. This relationship would typically be defined by structural response analyses. The *IM-LM* data are entered as pairs of discrete points; the behavior between the entered points is interpolated linearly in log-log space. This arrangement allows the load measures to vary nonlinearly with ground motion intensity. For example, the effects of column hinging can be accounted for with a nonlinear *IM-LM* relationship.

4. Displacement data – the program requires entry of the reference displacements, i.e., the displacements corresponding to the reference loads, and the displacement capacity (i.e., allowable displacement) for each of the five components of displacement. Displacement capacities are assumed to be lognormally distributed and are therefore expressed in terms of a median value, $\hat{C}$, and dispersion, $\beta_C = \sigma_{\ln C}$, for each component of displacement.

6.6.2 Compute *IM* Hazard Curves

The ground motion hazard data is generally provided by the user at a small integer number of return periods; the USGS National Seismic hazard Mapping website, for example provides ground motion hazard data at six return periods – 108, 224, 475, 975, 2,475, and 4,975 years. While return periods beyond the boundaries of this data are rarely used for design of civil structures, motions with lower or higher hazard levels may still provide some contribution to pile response in a performance-based framework. Therefore, extrapolation to return periods less than 108 years and greater than 4,975 years is required. This extrapolation was performed using the logic developed by Mayfield (2007). At the high hazard (low return period) level, the hazard curve was extrapolated linearly in $\log IM - \log T_r$ space to pass through a point where T_R = 0.000001 yr was assigned to IM = 0.000001. At the low hazard (long return period) level, a quadratic equation was fit to the ground motion hazard data at return periods of 975, 2,475, and 4,975 years in log-log space and used to extrapolate to longer return periods. A maximum return period of 1,000,000 years was used when integrating ground motion hazards.

6.6.3 Compute *LM* Hazard Curves

Load measure hazard curves are computed for vertical load, Q, horizontal loads, V_x and V_y, and overturning moments, M_x and M_y, using the *IM* hazard curve and probabilistic *IM-LM* relationships provided by the user. The *LM* hazard behavior is computed using the numerical integration process described in Equation 6.3(a). Two *LM* hazard curves are computed – a curve that neglects all uncertainty and represents the median load measure, LM_0, for a given return period, and a curve that includes the effects of uncertainty in static load, reference load and load measure given ground motion, which is encapsulated in the load measure, LM_1,

6.6.4 Compute *LM* Limit State Hazard Curves

The *LM* hazard curves are then integrated over the load capacity distributions, as indicated in Equation 6.1, to develop force-based limit state hazard curves. These calculations are performed for all five load measure components; for each, the hazard curve that includes capacity and its uncertainty, as represented by the load measure, LM_2, is obtained.

6.6.5 Perform Monte Carlo Simulation of *LM-EDP* Response

The response of the pile group to the applied dynamic loads, with consideration of all uncertainties, is estimated using Monte Carlo simulation based on the results of the pile group-soil-structure interaction analyses described in Chapter 5. In order to provide a complete indication of pile group response, all combinations of *LM* components are evaluated on a coarse grid of *LM* values. With five *LM* components, the number of *LM* combinations is 5^n where n is the number of *LM* increments. Load and displacement ratios for all components need to be stored in pgDF, which leads to 6-dimensional load and displacement arrays with $5n^5$ elements (e.g., 38,800 elements for n = 6). To avoid exceeding RAM memory limits, the Monte Carlo simulations are performed on a relatively coarse grid with subsequent interpolation for the finer grid that is required for accurate numerical integration in the probability calculations. The main steps in the Monte Carlo simulation procedure are:

1. Definition of static loads – static load data consisting of median values and logarithmic standard deviations are provided by the user. These values are used to compute five randomized *LM* vectors.

2. Establishment of a coarse *LM* array – the user-specified *LM* values are used to develop a 5-dimensional array that consists of all possible combinations of coarse-grid *LM* values.

3. Looping through all possible combinations of *LM* values – for each combination, the following steps are performed:

    a. Randomized static, reference, and dynamic loads are computed. User-specified load component correlations are achieved using the eigenvalue/eigenvector approach described by Haldar and Mahadevan (2000).
    b. Resulting randomized load ratio (normalized *LM*) values are computed. The load ratios include the effects of uncertainties in static loads, reference loads, and dynamic loads.
    c. Displacement ratios are computed for all combinations of randomized load ratio values. The displacement ratios are computed from the regression relationships described in Chapter 5, and account for the correlated uncertainties in all components of the *LM* vector.
    d. Displacement ratio values are statistically characterized. Median and logarithmic standard deviation values are computed from the simulated displacement ratio distributions.

This process results in median and logarithmic standard deviation values for all combinations of load measures on the coarse *LM* grid.

6.6.6 Perform Multiple Linear Regression Analyses on Coarse Grid *EDP* Data

The displacement ratio values computed in the previous step correspond to the coarse *LM* grid. Since subsequent performance-based calculations will require integration over all of the *LM* values, achieving adequate accuracy will require probabilistic characterization (i.e., availability of median and logarithmic standard deviation data) on a finer *LM* grid. The median normalized displacement value can be thought of as consisting of a component predicted by the normalized *LM-EDP* regression relationships and a component that results from the uncertainty in that relationship and its various input variables. The first component of median normalized displacement can be computed directly from the available regression equations. The second component does not fluctuate significantly over the range of load ratios, and is therefore evaluated as a continuous function of the various *LR* components using multiple linear regression analyses. The logarithmic standard deviation values are also relatively stable and are therefore represented as a continuous function of the *LR* components using multiple linear regression.

With the multiple linear regression analyses, the pgDF program can compute all components of displacement ratio for any combination of fine-grid normalized load components. This procedure removes the need for five-dimensional interpolation between the coarse grid *DR* values.

6.6.7 Compute *EDP* Hazard Curves

Displacement hazard curves are obtained from the *LM* hazard curves and the Monte Carlo simulation-based normalized *LM-EDP* relationships. The curves are obtained by numerical integrations of the form shown in Equation 6.3(b) over a fine grid of *LM* values. The median *LM* values on the fine grid were taken as the sum of the median value from the *LR-DR* regression relationship and the multiple linear regression-based median increment function described in Section 6.6.5. The logarithmic standard deviation values were obtained from the multiple linear regression-based fit to the coarse grid dispersion data. The normalized displacement ratios were transformed to *EDP* values (vertical displacement, two horizontal displacements, and two rocking rotations) using the reference displacement values.

The integrations required to determine the EDP values are performed over five dimensions (each of the load measure components) for each EDP. The approach used to perform this integration required modification of the basic PEER PBEE integral. Consider the PEER integral for a scalar value, X, related to another scalar, $Y = g(X)$. In its conventional form, the PEER PBEE integral would be written as

$$\lambda_Y(y) = \int_0^\infty P[Y > y \mid X = x] d\lambda_X(x) \tag{6.44}$$

This integral can easily be rewritten as

$$\lambda_Y(y) = \int_0^\infty P[Y > y \mid X = x] \frac{d\lambda_X(x)}{dx} dx \tag{6.45}$$

Integrating Equation (6.47) by parts ($\int udv = uv - v\int du$) gives

$$\lambda_Y(y) = P[Y > y \mid X = x]\lambda_X(x)\Big|_0^\infty - \int_0^\infty \lambda_X(x) dP[Y > y \mid X = x] \tag{6.46}$$

For the first term in Equation (6.46), $P[Y > y \mid X = x] = 0$ when $x = 0$ and $d\lambda_X(x) = 0$ when $x = \infty$, which means that the term outside the integral is zero. Therefore,

$$\lambda_Y(y) = \int_0^\infty \lambda_X(x) dP[Y > y \mid X = x] \tag{6.47}$$

which can also be written as

$$\lambda_Y(y) = \int_0^\infty \lambda_X(x) \frac{dP[Y > y \mid X = x]}{dx} dx \tag{6.48}$$

The multi-dimensional equivalent would be

$$\lambda_Y(y) = \int_0^\infty \int_0^\infty \cdots \int_0^\infty \lambda_X(x) dP[Y > y \mid X_1 = x_1, X_2 = x_2, \ldots X_n = x_n] \tag{6.49}$$

where the incremental probability can be computed as

$$dP[Y > y \mid X_1 = x_1, X_2 = x_2, \ldots X_n = x_n] = \frac{\partial P[Y > y \mid X_1 = x_1, X_2 = x_2, \ldots X_n = x_n]}{\partial x_1} dx_1 + \frac{\partial P[Y > y \mid X_1 = x_1, X_2 = x_2, \ldots X_n = x_n]}{\partial x_2} dx_2 + \cdots + \frac{\partial P[Y > y \mid X_1 = x_1, X_2 = x_2, \ldots X_n = x_n]}{\partial x_n} dx_n \tag{6.50}$$

or

$$dP[Y > y \mid X_1 = x_1, X_2 = x_2, \ldots X_n = x_n] = \sum_{i=1}^{n} \frac{\partial P[Y > y \mid X_1 = x_1, X_2 = x_2, \ldots X_n = x_n]}{\partial x_i} dx_i \tag{6.51}$$

Therefore

$$\lambda_Y(y) = \int_0^\infty \int_0^\infty \cdots \int_0^\infty \lambda_X(x) \sum_{i=1}^{n} \frac{\partial P[Y > y \mid X_1 = x_1, X_2 = x_2, \ldots X_n = x_n]}{\partial x_i} dx_i \tag{6.52}$$

The integrations and partial differentiation need to be performed numerically. Writing it all out for the five-dimensional case (in which *X* represents *LM* and *Y* represents *EDP*),

$$\lambda_Y(y) = \sum_{m=1}^{N_{X_5}} \sum_{l=1}^{N_{X_4}} \sum_{k=1}^{N_{X_3}} \sum_{j=1}^{N_{X_2}} \sum_{i=1}^{N_{X_1}} \lambda_{X_1, X_2, X_3, X_4, X_5}(x_{1i}, x_{2j}, x_{3k}, x_{4l}, x_{5m}) [dP] \tag{6.53}$$

where

$$\begin{aligned}[dP] = {} & P[x_1 + \Delta x_1/2, x_2, x_3, x_4, x_5] - P[x_1 - \Delta x_1/2, x_2, x_3, x_4, x_5] + \\ & P[x_1, x_2 + \Delta x_2/2, x_3, x_4, x_5] - P[x_1, x_2 - \Delta x_2/2, x_3, x_4, x_5] + \\ & P[x_1, x_2, x_3 + \Delta x_3/2, x_4, x_5] - P[x_1, x_2, x_3 - \Delta x_3/2, x_4, x_5] + \\ & P[x_1, x_2, x_3, x_4 + \Delta x_4/2, x_5] - P[x_1, x_2, x_3, x_4 - \Delta x_4/2, x_5] + \\ & P[x_1, x_2, x_3, x_4, x_5 + \Delta x_5/2] - P[x_1, x_2, x_3, x_4, x_5 - \Delta x_5/2\end{aligned}$$

This form allows convenient implementation of the assumption that

$$\lambda_{X_1, X_2, X_3, X_4, X_5}(x_{1i}, x_{2j}, x_{3k}, x_{4l}, x_{5m}) \approx \min\left\{\lambda_{X_1}(x_{1i}), \lambda_{X_2}(x_{1j}), \lambda_{X_3}(x_{1k}), \lambda_{X_4}(x_{1l}), \lambda_{X_5}(x_{1m})\right\}$$

These calculations are performed both with and without uncertainty to obtain hazard curves for the zero-uncertainty response measures, EDP_0, and the response measure, EDP_1, that includes the effects of uncertainty.

6.6.8 Compute *EDP* Limit State Hazard Curves

The *EDP* hazard curves are then integrated over the displacement capacity distributions, as indicated in Equation 6.4, to develop displacement-based limit state hazard curves. These calculations are performed for all five response measure components; for each, the hazard curve that includes capacity and its uncertainty, as represented by the load measure, EDP_2, is obtained.

6.6.9 Compute Load and Resistance Factors

With all three *LM* hazard curves computed, load and resistance factors are computed using Equations 6.19. This process requires interpolation to find *LM* values at consistent return periods; the interpolations are performed linearly in log-log space.

6.6.9.1 Compute Demand and Capacity Factors

With all three *EDP* hazard curves computed, load and resistance factors are computed using Equations 6.21. This process requires interpolation to find *EDP* values at consistent return periods; the interpolations are performed linearly in log-log space.

6.7 VALIDATION OF DCFD ANALYSES

Validation of the computational model was difficult and time-consuming , largely because of the complexity of the five-dimensional nature of the *LM* and *EDP* vectors, the multiple uncertain and nonlinear relationships that affect its results, and the lack of any specific solution against which to verify the accuracy of the full model. As indicated previously and derived in Chapter 3 and earlier in this chapter, a closed-form solution can be developed for specific assumptions about the loading and response behavior – however, this solution is only available for scalar relationships, i.e., a single *LM* and a single *EDP*. The assumptions required for the closed-form solutions (i.e., power law hazard and response curves with lognormal uncertainties) are somewhat restrictive with respect to the actual conditions involved in bridge and pile foundation evaluation and design, but still can play an important role in showing that the basic form of the computational model is correct under those conditions.

The philosophy of the validation process was to first show that the computational model could predict the results obtained by the closed-form solution for a variety of conditions. Following validation of the basic computational approach by comparison with closed-form solutions for conditions under which the closed-form solutions are applicable, deviations from the closed-form assumptions were instituted with the results examined for logic and reasonableness. Parametric analyses illustrating the behavior and sensitivities of the model to various factors were performed.

6.7.1 Comparison with Closed-Form Solutions

The closed-form solution assumes power law relationships between *IM* and *LM* and between *LM* and *EDP*, and assumes lognormal dispersion of the *IM-LM* and *LM-EDP* relationships. The power law functions can describe linear and various degrees of nonlinear behavior, and the dispersion relationships can be used to model different degrees of uncertainty. Analyses were performed using multiple perturbations of a basic structure-foundation model with the results compared with the closed-form solution results. In these analyses, the full five-dimensional integration was performed but the five loads and displacements were assumed to develop independently – for example, the vertical displacement was assumed to be affected only by the vertical load with no contribution from lateral loads or overturning moments

An extensive series of analyses, a portion of which are described in this section of the report, were performed to confirm that the program accurately reproduced the results given by the closed-form solution. These analyses considered a variety of relationships between *IM*, *LM*, and *EDP*, ranging from linear to nonlinear, and a variety of different levels of uncertainty in those relationships. The initial analyses considered deterministic systems, after which the effects of uncertainty were evaluated.

6.7.1.1 Base Case System

The closed-form solutions were developed for a simple, base-case system in which the seismic hazard curve for 0.5-sec spectral acceleration was defined as

$$\lambda_{S_a(0.5)} = 0.00117\left(S_a(0.5)\right)^{-2.626} \tag{6.54}$$

where $S_a(0.5)$ is expressed as a fraction of gravity. The *IM-LM* relationships were initially set at

$$LM = 8487\, S_a^{0.9} \tag{6.55}$$

for all of the load measures. This relationship indicates that loads are a mildly nonlinear function of spectral acceleration. Finally, the *LM-EDP* relationships were assumed to be independent and given by

$$\ln EDP = -0.5 + LM \tag{6.56}$$

or

$$EDP = 0.000016702\, LM^{1.0} \tag{6.57}$$

The various relationships between *IM*s, *LM*s, and *EDP*s are shown in Figure 6.3. The seismic hazard curve of Figure 6.3(a) is similar to the USGS hazard curve for San Francisco, California. The *IM-LM* relationship is representative of a linear or slightly nonlinear single-mass system similar to that described in Section 5.2.1, and the *LM-EDP* relationship is an arbitrary linear relationship. Note that the base case system has little nonlinearity; the actual values of the parameters describing the *IM-LM-EDP* relationships are not important for the purpose of showing that the computer model can reproduce the closed-form results under the conditions required for applicability of the closed-form solution.

6.7.1.2 Results of Closed-Form Comparative Analyses

The results of the comparative analyses will be expressed in terms of computed response hazard curves, since they are the basic elements of the LRFD calculations. Calculation of load and resistance factors, and of demand and capacity factors, is a straightforward extension of the hazard curve calculation – the hazard curve calculation is the demanding part of the process and the one in which calculation errors or inconsistencies are most readily seen. Hence, numerically computed hazard curve values that match values from the closed-form solution are taken as evidence of the adequacy of the calculations for the considered conditions.

Because the performance-based load and response calculations involve Monte Carlo simulation of pile group response and repeated numerical integration over multiple loading and response dimensions, significant trade-offs between computational effort and accuracy exist. The use of small integration increments, particularly the increments of load over which the response parameters are integrated, will lead to more accurate solutions. They will also, however, lead to more time-consuming calculations. Halving the integration increments will, for example, increase computation time by a factor of approximately $2^5 = 16$. With the calculations for a relatively coarse integration grid taking 2-3 hours on a computer of moderate capabilities, such potential increases can be very costly.

6.7.1.3 Purely Deterministic Analysis

The first test was performed deterministically, i.e., with the assumption of no uncertainty in any of the variables. Dispersion values (i.e., logarithmic standard deviations) were all set to values of 0.001. This condition is actually one of the most difficult to model numerically because the probability of exceeding a particular variable value changes instantaneously from 0 to 1 when the median value of the variable is exceeded – more formally, the cumulative distribution function for the variable is a step function. The extent to which a perfect step function can be modeled numerically depends on the size of the integration increment; the numerical approximation takes the form of a "ramp" function that approximates the step function more accurately as the number of integration increments increases, but can only be exact in the limit as the number of integration increments becomes infinite.

The results of the closed-form analyses will be presented in terms of vertical displacements which, in the scalar manner required by the closed-form solution, result purely from vertical loads. Figure 6.3 shows the results of Test 1, in which the closed form solution is shown with a smooth solid curve and the numerically predicted values as discrete points at different vertical displacement levels. The computed values can be seen to generally coincide well with the closed-form solution, although the points at very low settlement values (and very short return periods) do not match well, and the numerical results appear to fluctuate a bit with respect to the closed-form solution at higher settlement values. The underprediction of response (settlement) at low response levels is related to the size of the response increment selected. In this case, the response increment was 0.05 m (about 2 inches). It should be noted that the numerically-modeled points for the deterministic case, the case of load model uncertainty, and the case of load and resistance model uncertainty (i.e., the curves representing LM_0, LM_1, and LM_2 in Equation 6.21) all plot on top of each other, as they should for the assumed conditions.

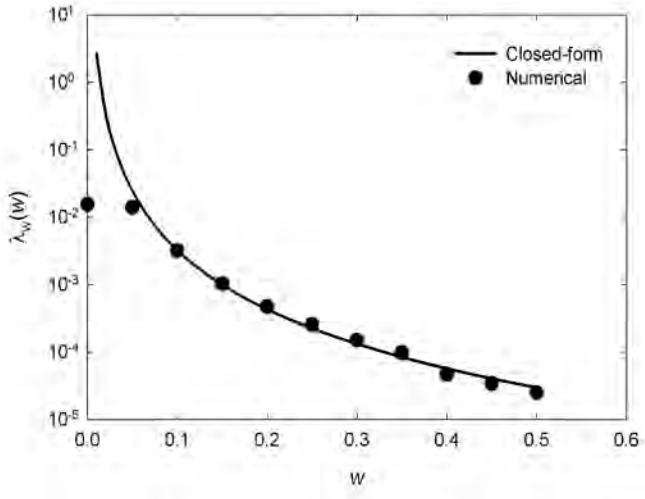

Figure 6.3 Comparison of closed-form and numerical solutions for deterministic base case vertical settlement problem and relatively coarse settlement increment.

The use of a smaller response increment would produce better agreement between the numerical and closed-form results at low response levels, but would increase the total number of increments for which calculations would need to be performed, thereby increasing the execution time. For this particular case, the agreement becomes poor at mean annual rates of exceedance greater than about 0.01 yr^{-1}, or return periods shorter than about 100 yrs. Since seismic design is based on return periods much longer than 100 yrs, some degree of inaccuracy at these short return periods is not considered problematic. It should be noted that the numerical values are consistent with the closed-form values to return periods of about 50,000 yrs, which is much greater than design-level return periods.

6.7.1.4 Variation of IM Hazard Curve

To confirm that the numerical analysis could properly account for variations in the position and slope of the seismic hazard curve, deterministic analyses were performed for several different spectral acceleration hazard curves. Figure 6.4 shows the results of closed-form and numerical analyses for the base case hazard curve and for another hazard curve (Test 2) given by

$$\lambda_{S_a(0.5)} = 0.0011\left(S_a(0.5)\right)^{-1.5} \tag{6.58}$$

The mean annual rates of settlement exceedance based on the second S_a hazard curve also agree well with those given by the closed-form solution. For this deterministic analysis, the numerical points for all three curves fell on top of each other. Again, some deviation was observed at low settlement levels for the settlement increment used in these analyses. These results indicate that the numerical model can properly account for differences in seismicity.

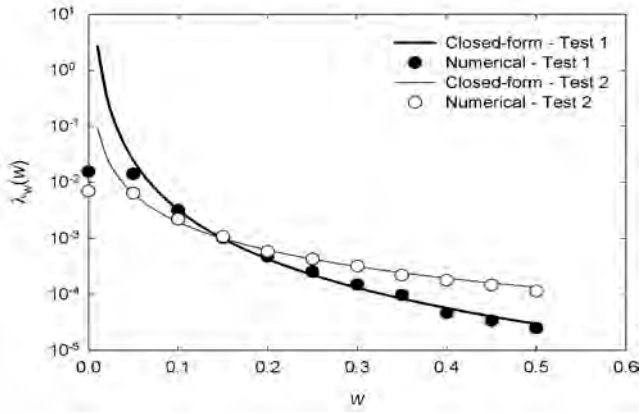

Figure 6.4 Comparison of closed-form and numerical solutions for deterministic base case problem with different *IM* hazard curves.

6.7.1.5 Variation of Load Model

The ability of the numerical model to account for differences caused by different load models was evaluated in a series of analyses. While the base case analysis assumed that vertical load was directly proportional to spectral acceleration, additional analyses were performed with different *IM-LM* relationships. Figure 6.5 presents the results of the base case analysis along with another analysis identical to the base case analysis except for the load model, which was assumed to be strongly nonlinear,

$$Q = 4000\left(S_a(0.5)\right)^{0.5} \tag{6.59}$$

The numerical results can be seen to track the closed-form solution well over a range of return periods that span far beyond the range of return periods used for design. The return periods at which the numerical values deviate significantly from the closed-form values are well above or below the range considered for design. These results indicate that the computational model can properly account for differences in structural response, as reflected in a load model.

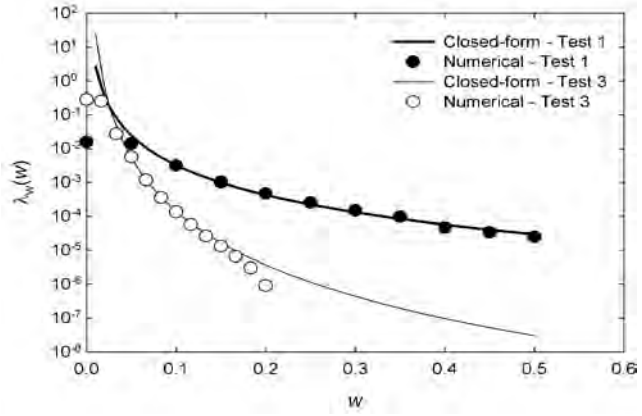

Figure 6.5 Comparison of closed-form and numerical solutions for deterministic base case problem with different *IM-LM* relationships.

6.7.1.6 Variation of Response Model

The response of a pile group to the loading applied to it is of critical importance for foundation design. To isolate the effects of the response model, analyses were performed for the base case condition modified only by alternate *LM-EDP* relationships. Figure 6.6 presents the results of analyses for the base case and another system for which settlement was a nonlinear function of vertical load,

$$w = 0.0001Q^{0.8} \tag{6.60}$$

Again, the numerical model was able to predict mean annual rates of exceedance that matched the closed-form solution well. Deviations between the two approaches occurred outside the range of interest for design.

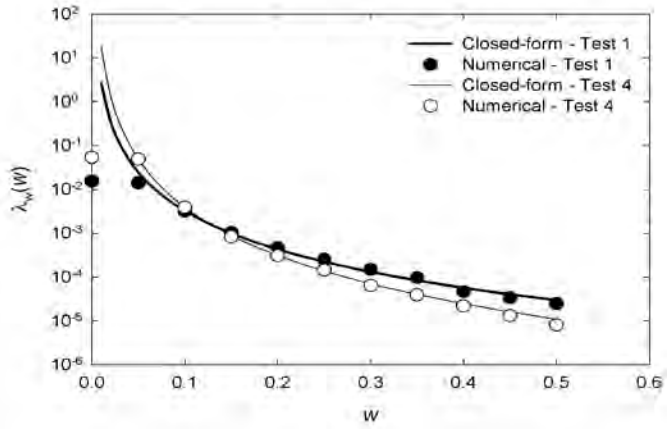

Figure 6.6 Comparison of closed-form and numerical solutions for deterministic base case problem with different *LM-EDP* relationships.

6.7.1.7 Inclusion of Load Model Uncertainty

The preceding sections have shown that the computational model is capable of representing different modeling relationships under deterministic conditions. Without uncertainties in loads, displacements, or capacities, all design factors (load, resistance, demand, and capacity) have values of 1.0. One primary purpose of the performance-based framework, however, is to account for uncertainties in the development of design factors. The closed-form framework allows consideration of uncertainties in load and response, which were isolated in a series of analyses. When uncertainty in the load model, i.e., in the load given the ground motion intensity, is included, the load factor should be expected to increase to a value above 1.0 and the resistance factor to remain at 1.0. Figure 6.7 shows the results of analyses in which the dispersion in vertical load, $\beta_Q = \sigma_{\ln Q|S_a}$, was set at a value of 0.3. Careful examination shows that, at a given hazard level, $Q_1 = Q_2 > Q_0$ and $w_1 = w_2 > w_0$, as should be expected. The computed load and resistance factors agree very well with those given by the closed-form solution.

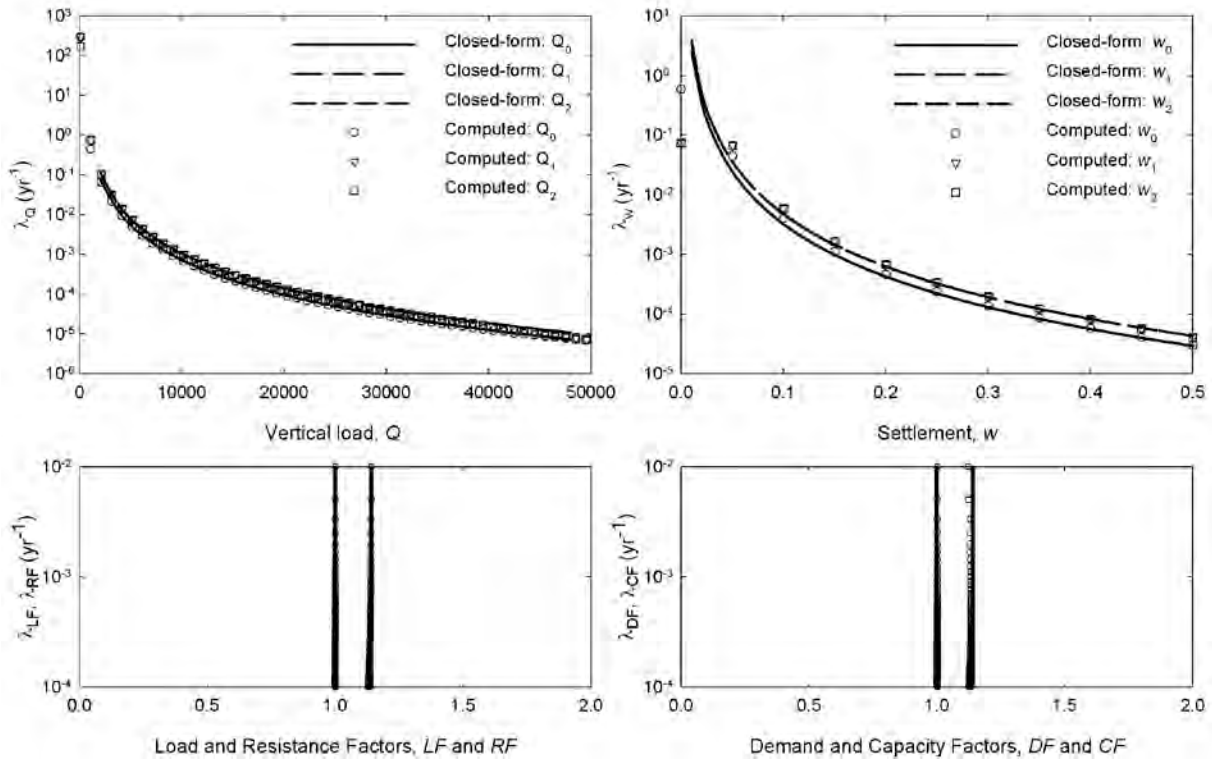

Figure 6.7 **Comparison of closed-form and numerical load and response curves and load, resistance, demand, and capacity factors including the effects of load model uncertainty. Load and demand factors are greater than resistance and capacity factors in each plot.**

6.7.1.8 Inclusion of Response Model Uncertainty

Uncertainty also exists in the prediction of pile group response, i.e., displacement given applied loading. To isolate the effects of uncertainty in response, analyses were performed in which the dispersion in vertical settlement, $\beta_w = \sigma_{\ln w|Q_a}$, was set at a value of 0.5. The results of this analysis are shown in Figure 6.8. Careful examination shows that, at a given hazard level, $Q_1 = Q_2 = Q_0$ (since zero uncertainty in loading was assumed) and $w_1 = w_2 > w_0$, as should be expected. The computed load and resistance factors agree very well with those given by the closed-form solution.

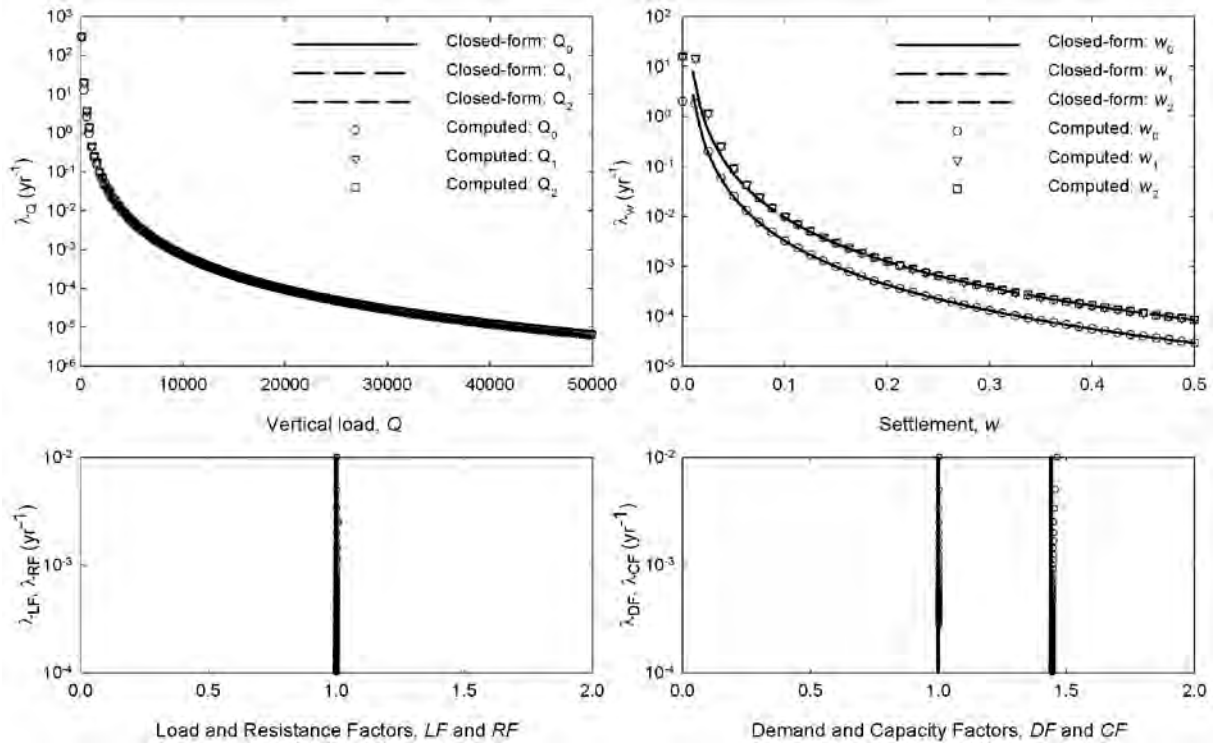

Figure 6.8 Comparison of closed-form and numerical load and response curves and load, resistance, demand, and capacity factors including the effects of response model uncertainty. Load and demand factors are greater than resistance and capacity factors in each plot.

6.7.1.9 Inclusion of Load and Response Model Uncertainty

When uncertainties in load and response exist, the computational model must be able to properly account for both even though their effects are computed in different manners. An analysis was performed with the load and response uncertainties of the preceding two cases both applied simultaneously, i.e., $\beta_Q = \sigma_{\ln Q|S_a} = 0.3$ and $\beta_w = \sigma_{\ln w|Q_a} = 0.5$. Uncertainties in capacities were still assumed to be zero. Figure 6.9 shows the results of analyses with both components of uncertainty. Again, the load and demand factors are greater than 1.0, as they should be when uncertainties in load and displacement demand are considered. The resistance and capacity factors remain at 1.0 due to the deterministic treatment of force and displacement capacities.

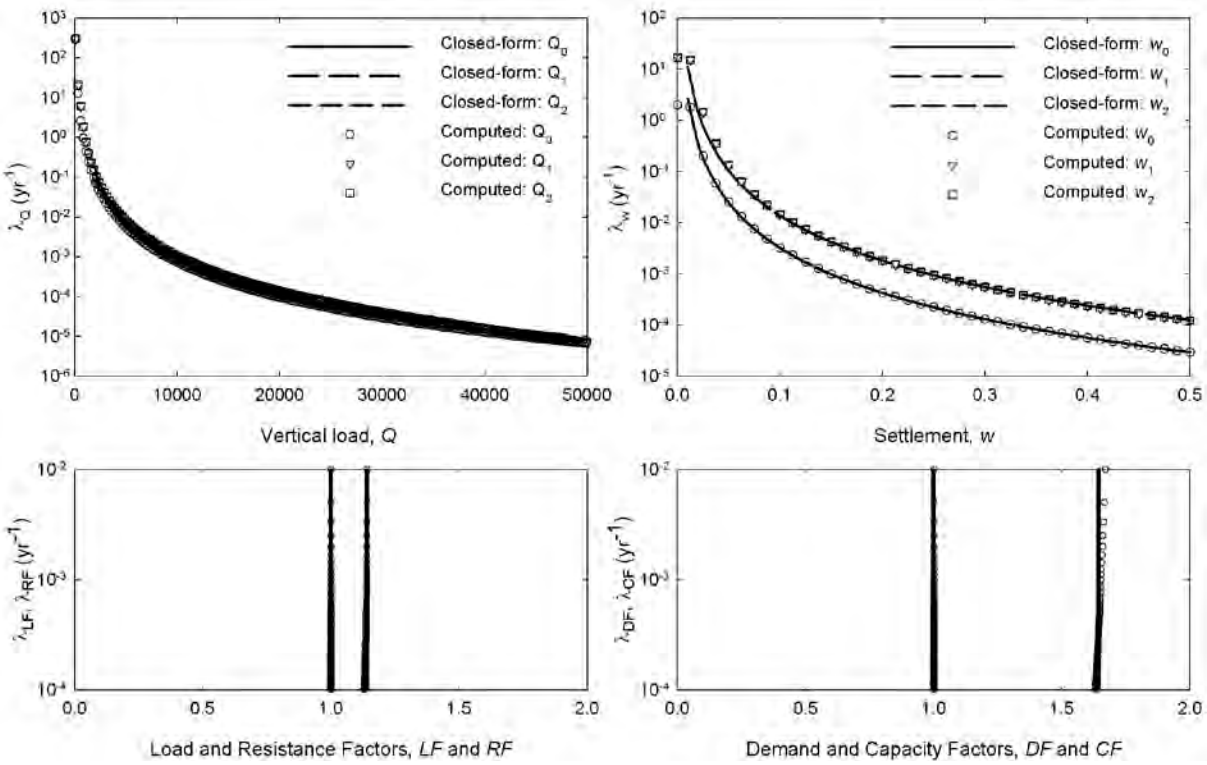

Figure 6.9 Comparison of closed-form and numerical load and response curves and load, resistance, demand, and capacity factors including the effects of both load and response model uncertainty. Load and demand factors are greater than resistance and capacity factors in each plot.

6.7.1.10 Inclusion of Load Model, Response Model, and Capacity Uncertainty

Adding uncertainties in force and displacement capacities can be expected to cause resistance and capacity factors to drop below 1.0. A series of analyses were performed with uncertainties in force capacity alone, displacement capacity alone, and force and displacement capacity together. The results of these analyses, shown in Figures 6.10 through 6.12, show that the computational model is able to reproduce the closed-form solution for each of these specific cases.

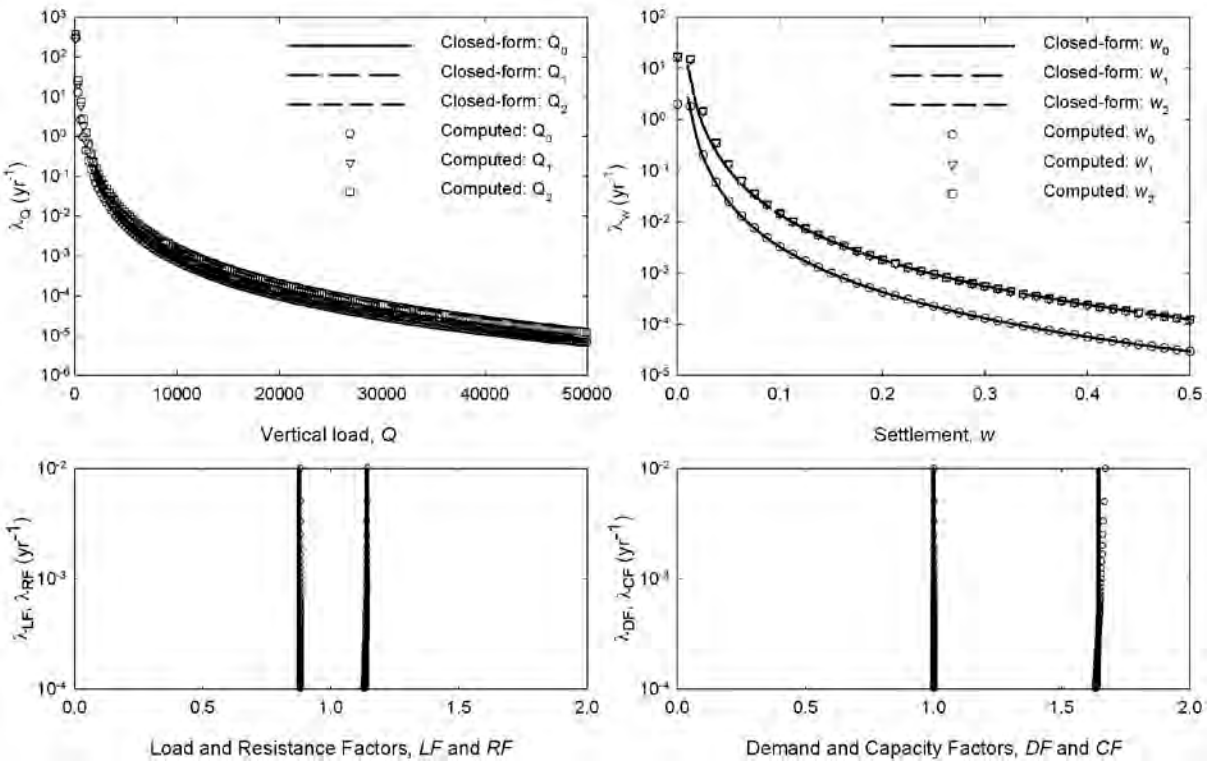

Figure 6.10 Comparison of closed-form and numerical load and response curves and load, resistance, demand, and capacity factors including the effects of force capacity uncertainty. Load and demand factors are greater than resistance and capacity factors in each plot. Legends in upper figures also apply to lower figures.

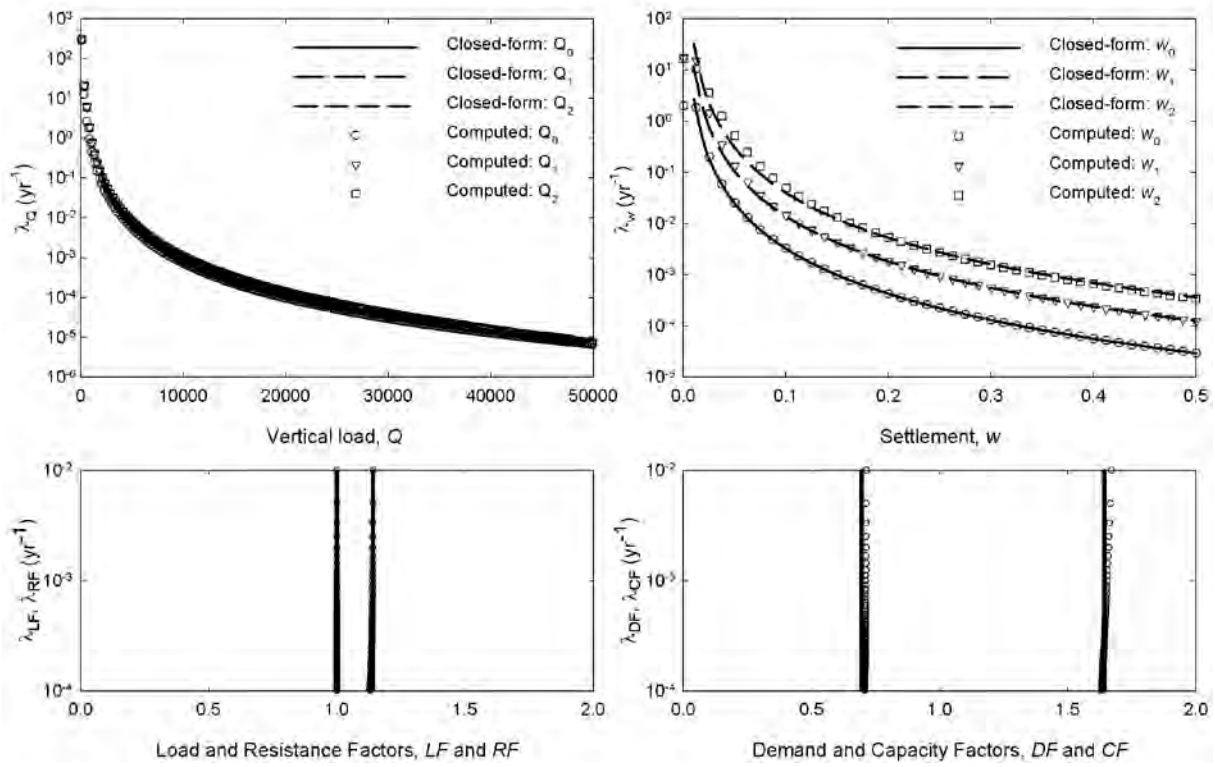

Figure 6.11 Comparison of closed-form and numerical load and response curves and load, resistance, demand, and capacity factors including the effects of response capacity uncertainty. Load and demand factors are greater than resistance and capacity factors in each plot. Legends in upper figures also apply to lower figures.

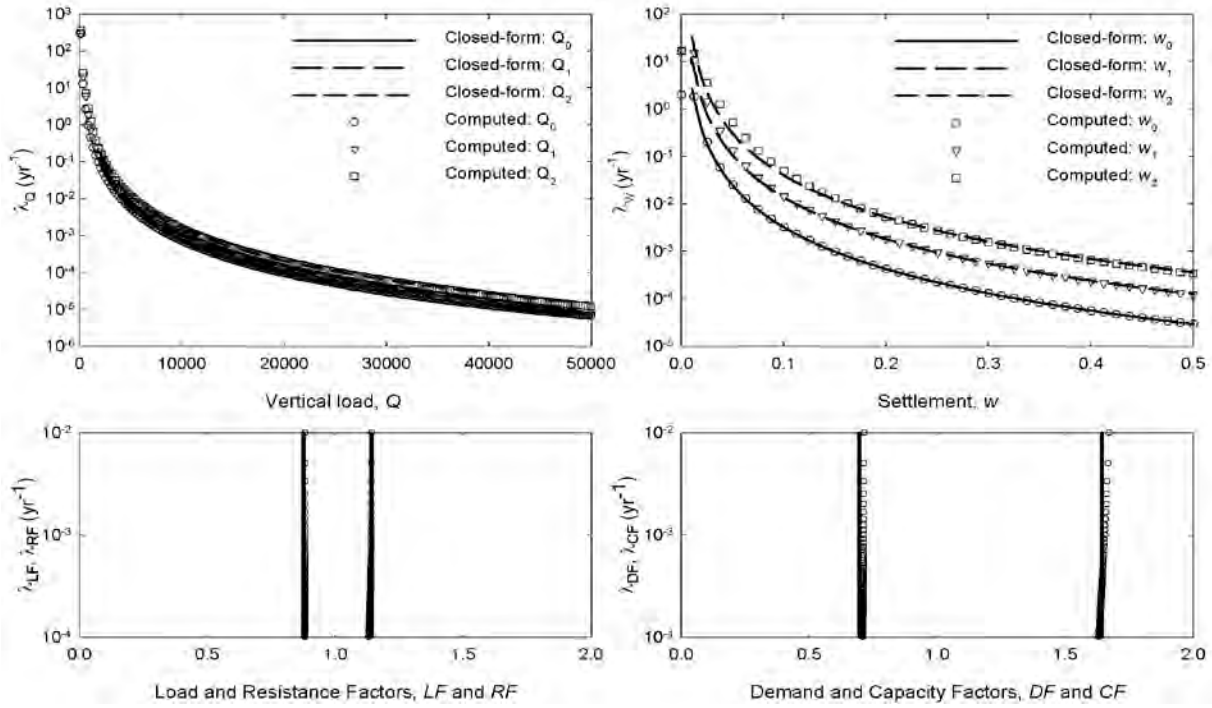

Figure 6.12 Comparison of closed-form and numerical load and response curves and load, resistance, demand, and capacity factors including the effects of both force and response capacity uncertainty. Load and demand factors are greater than resistance and capacity factors in each plot. Legends in upper figures also apply to lower figures.

6.7.1.11 Discussion

The preceding results illustrate the ability of the computational model to accurately replicate closed-form results for the conditions under which the closed-form solution are applicable. Those conditions are generally consistent with potential seismicity, structural response, and foundation response, but the relationships they are based on are simpler than the relationships that best represent actual behavior. Furthermore, the closed-form solutions are applicable only to scalar (i.e., single variable) loading and response relationships. The computational model was checked for each of the five pairs of loading and response variables, Q-w, V_x-u, V_y-v, M_x-θ_y, M_y-θ_x, and each individual relationship was found to behave in the manner illustrated by vertical load and settlement in the preceding paragraphs.

As discussed earlier in this chapter, the LRFD and DCFD frameworks compute load, resistance, demand, and capacity factors based on ratios of *LM* and *EDP* values at equal mean annual rates of exceedance (or return periods). The numerical integration process can be seen in the previous figures to provide close approximations to the closed-form solution, but the approximate nature of the numerical integration prevents them from being exact. As a result, the individual load and response hazard curve data points do not necessarily provide a smooth fit to the smooth closed-form curves. The effects of these relatively small fluctuations about the smooth curve, however, lead to a more pronounced lack of smoothness in their ratios, hence in the design factors. As a result, the load, resistance, demand, and capacity factors should be

interpreted in terms of gradual trends rather than the rapid fluctuations that may appear in some of the subsequently presented numerically-computed results.

6.7.2 Incremental Testing of Multiple Components

With the ability of the program to match the results of closed-form solutions for individual components demonstrated, the problem dealing with multiple components must be addressed. The OpenSees analyses described in Chapter 5 clearly showed that various components of pile group displacement were influenced, to varying degrees, by multiple components of loading. These dependencies were accounted for, at least in an average sense, in the regression relationships shown in Table 5.7. The simulations and integrations required for the vector problem should be recognized as being much more complicated than those required for comparison with the closed-form solutions; many more variables and relationships are required. These relationships are generally nonlinear with a complexity greater than that assumed for the closed-form solution. With the final results influenced by so many intermediate relationships and variables, the checking of numerical results becomes extremely difficult – the analysis has so many "moving parts" that isolation of the cause of a particular aspect of behavior becomes extremely difficult.

In order to develop confidence that the full model is producing reasonable results, many analyses were performed and studied. An example of one series of analyses is presented in the following paragraphs. The purpose of the series of analyses was to incrementally invoke the various capabilities of the model with examination of the reasonableness of the results after each increment. The results of the analyses reported here are presented in terms of vertical loads and settlements; these results are representative of those observed for the other loading and response variables.

The initial analysis was performed with no uncertainty in any of the variables or relationships, and with the settlement assumed to be a factor of vertical load alone – the coefficients associated with V_x, V_y, M_x, and M_y in the sand profile load-settlement relationship in Table 5.7 were all set to zero. For these conditions, all three vertical load hazard curves and all three settlement hazard curves are expected to be coincident, and all load, resistance, demand, and capacity factors are expected to be 1.0. Figure 6.13 presents the results of this analysis, and shows that the anticipated results were achieved. With the settlement depending only on the vertical load, and with no uncertainty considered, the settlement hazard is quite low – the 1,000-yr settlement, for example, is about 1 cm.

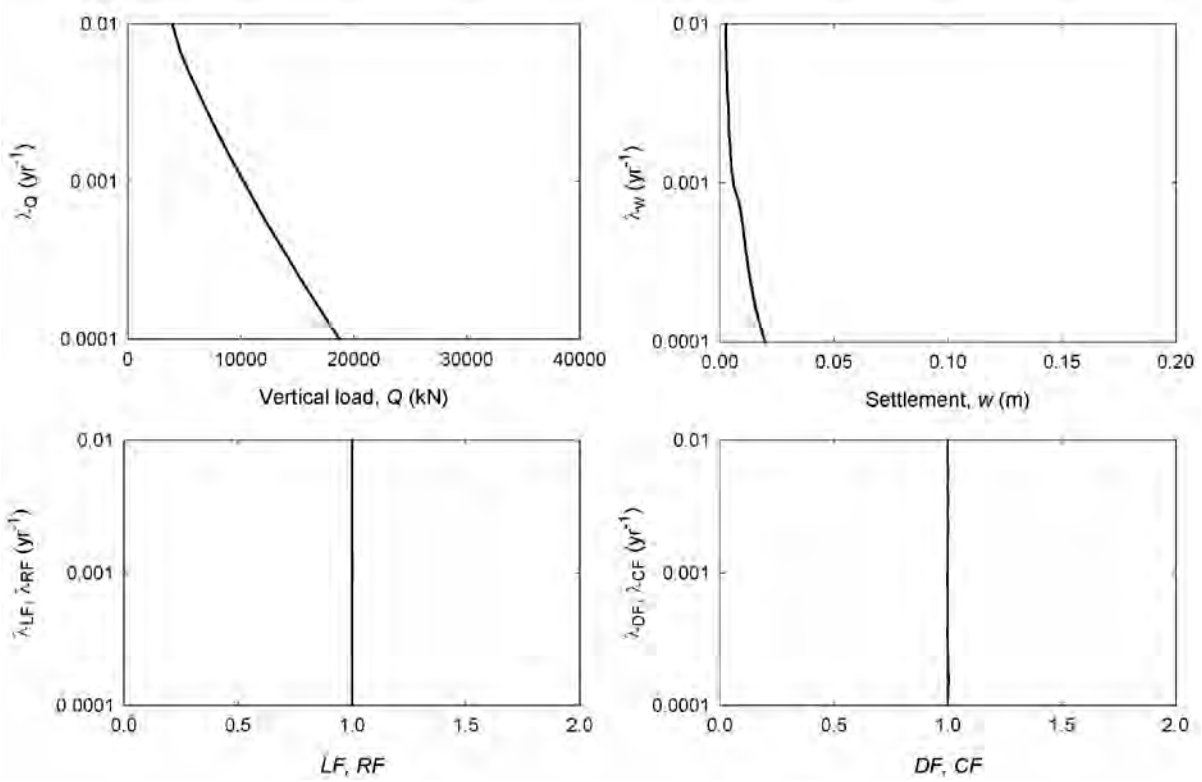

Fig 6.13. Results of single load component (i.e., $w = f(Q)$) analysis with no uncertainty. All three vertical load and settlement hazard curves are plotted, but are coincident.

The next two sets of analyses showed the effects of adding the other load components to the settlement calculation while still holding all uncertainty values at zero. Settlements are expected to increase with increasing lateral load and overturning moment amplitudes. Figure 6.14 shows the results of the analyses in which the effects of vertical and lateral loads were considered, and Figure 6.15 shows the results of analyses in which vertical loads, lateral loads, and overturning moments were all considered. For these sets of analyses, the settlements should be expected to increase as the different load components are added. Because uncertainty was set to zero, the load and settlement hazard curves should be coincident and the load, resistance, demand, and capacity factors should all be zero. The figures show that all of these expectations were generally realized. A small oscillation in the zero-uncertainty settlement hazard curve (upper right curve in Figure 6.14), which is of numerical origin, leads to a more prominent oscillation in the settlement demand factor (lower right curve). The zero-uncertainty case, in which computed probabilities change instantaneously from 0 to 1 when the threshold value of a variable is crossed, can be particularly sensitive to numerical discretization considerations; this issue disappears for the more realistic case of finite uncertainties. For a given return period, the settlements increase as more load components are considered. When all components of the *LM* vector are considered, the settlements are approximately twice those obtained for the single component analysis.

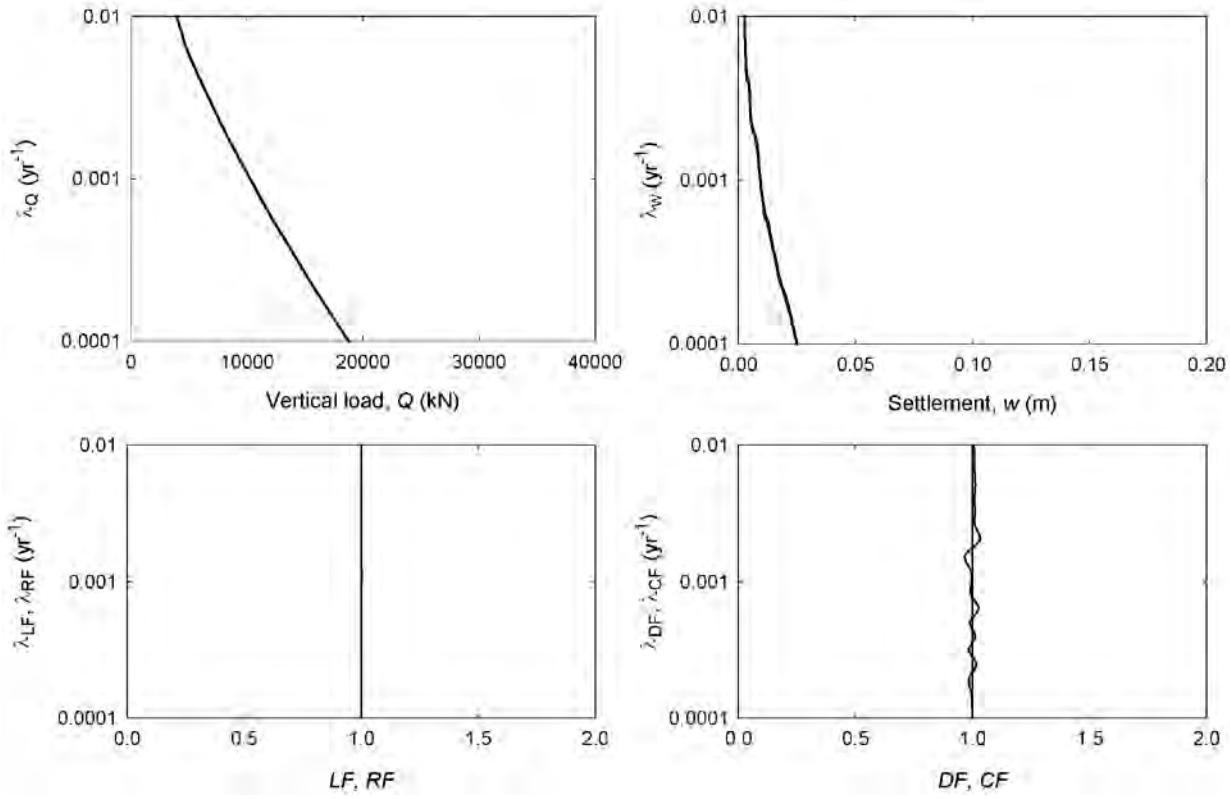

Figure 6.14. Results of dual load component (i.e., $w = f(Q,V_x)$) analysis with no uncertainty. All three vertical load and settlement hazard curves are plotted, but are coincident.

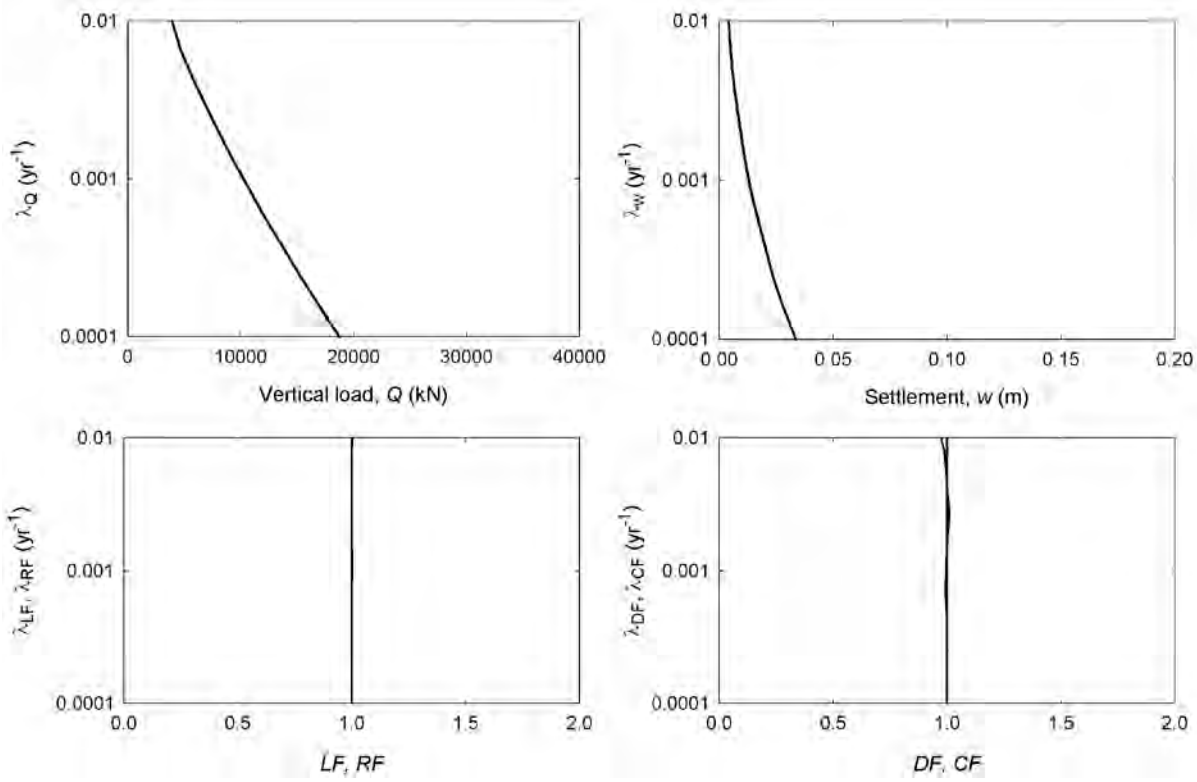

Fig 6.15. **Results of full load measure vector (i.e., $w = f(Q,V_x,V_y, M_x, M_y)$) analysis with no uncertainty. All three vertical load and settlement hazard curves are plotted, but are coincident.**

The next step involved the consideration of uncertainty in the *IM-LM* (S_a-Q) relationship. This relationship would normally be the product of a structural analysis that establishes the median relationship between ground motion intensity and the loads imposed upon a pile foundation. The dispersion of the structural loads is also required. This dispersion may be estimated by means of multiple structural analyses, or it may be estimated based on past experience. For this analysis, a dispersion $\beta_{LM} = \sigma_{\ln LM|IM} = 0.30$ was used. With the inclusion of uncertainty in vertical load, the Q_1 (vertical load including load uncertainty) should be greater than the Q_0 (vertical load with zero uncertainty) hazard curve, and the Q_2 (vertical load capacity) hazard curve should be coincident with the Q_1 curve due to the absence to load capacity uncertainty. These effects should be expected to migrate into the settlement hazard curves with analogous effects. Figure 6.16 presents the results of these analyses, in which the anticipated behaviors are all observed.

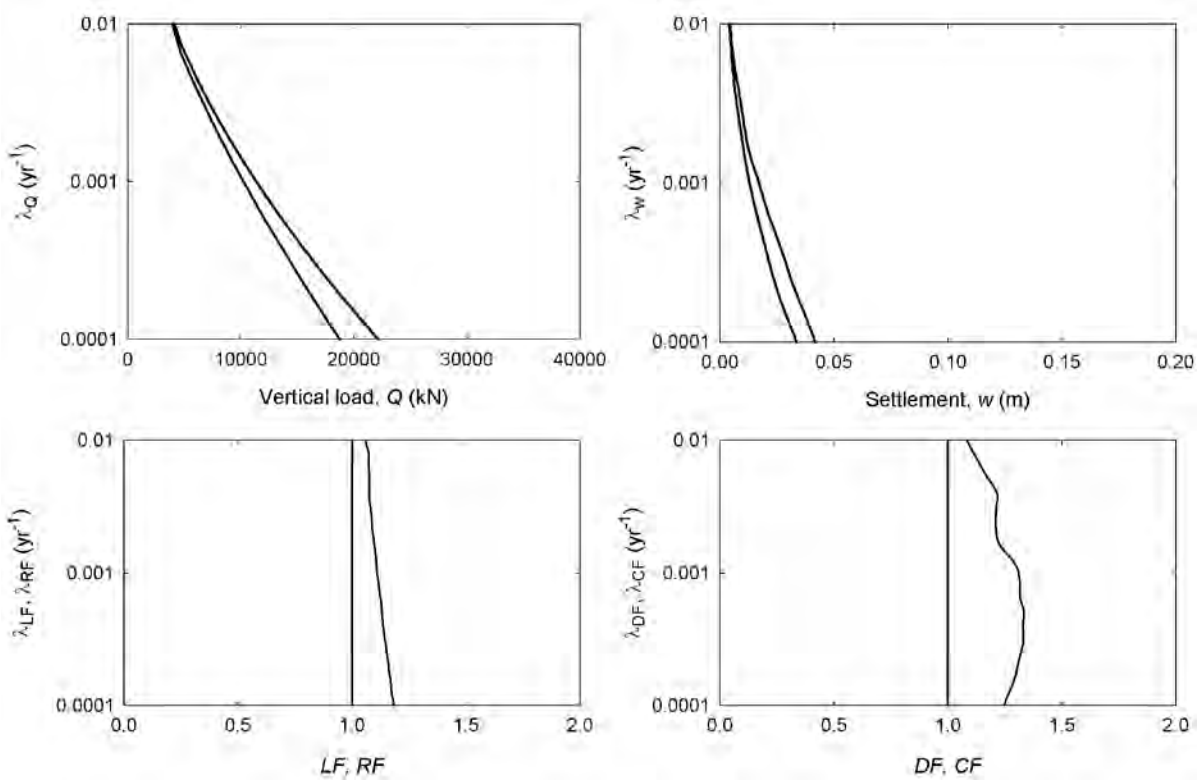

Figure 6.16. Results of analyses with inclusion of uncertainty in *IM-LM* relationship (β_L = 0.30). Left-most hazard curves in upper plots are zero-uncertainty curves (Q_0 and w_0); right-most curves in lower plots are coincident curves (Q_1 and Q_2, w_1 and w_2).

Figure 6.17 shows the results of adding uncertainty in the *LM-EDP* (Q-w) relationship to that in the *IM-LM* (S_a-Q) relationship. Uncertainty in settlement given loading was characterized by a dispersion, β_R = 0.50. The additional uncertainty, as expected, doesn't affect the load hazard curves or the load and resistance factors, but pushes the w_1 hazard curve farther to the right of the w_0 hazard curve. The w_2 hazard curve, due to the lack of uncertainty in displacement capacity, is coincident with the w_1 hazard curve. The additional uncertainty leads to a significantly higher demand factor.

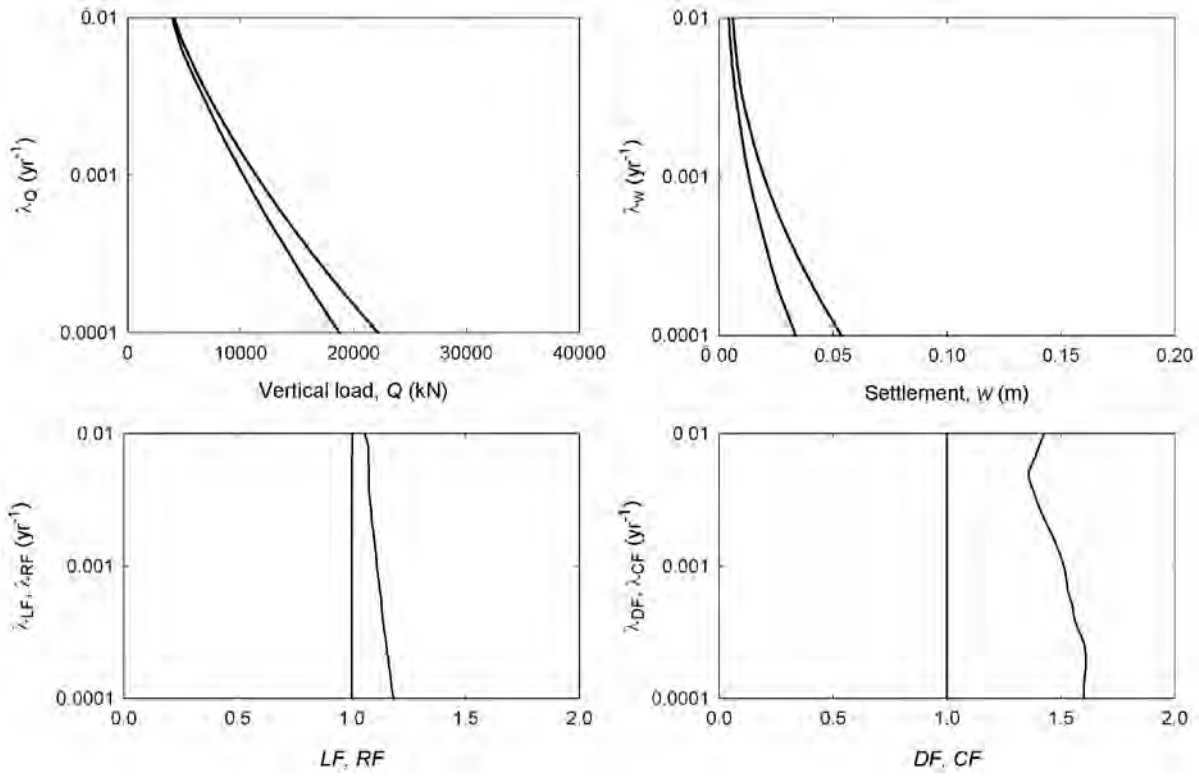

Figure 6.17. Results of analyses with inclusion of uncertainty in *LM-EDP* relationship (β_R = 0.50). Left-most hazard curves in upper plots are zero-uncertainty curves (Q_0 and w_0); right-most curves in lower plots are coincident curves (Q_1 and Q_2, w_1 and w_2).

The next steps were to add uncertainties in capacities, both force capacities and displacement capacities. To this point, all uncertainties in capacities have been zero, so all resistance factors and capacity factors have been equal to 1.0. Figure 6.18 shows the effects of uncertainty in vertical in force capacity, which was assumed to be lognormally distributed with dispersion, β_{CQ} = 0.3. The uncertainty in force capacity causes the vertical load capacity (Q_2) curve to move to the right of the Q_1 curve and the resistance factor to drop below 1.0. The displacement capacity is unaffected by the addition of load capacity uncertainty so the w_2 curve remains coincident with the w_1 curve and the capacity factor remains at 1.0.

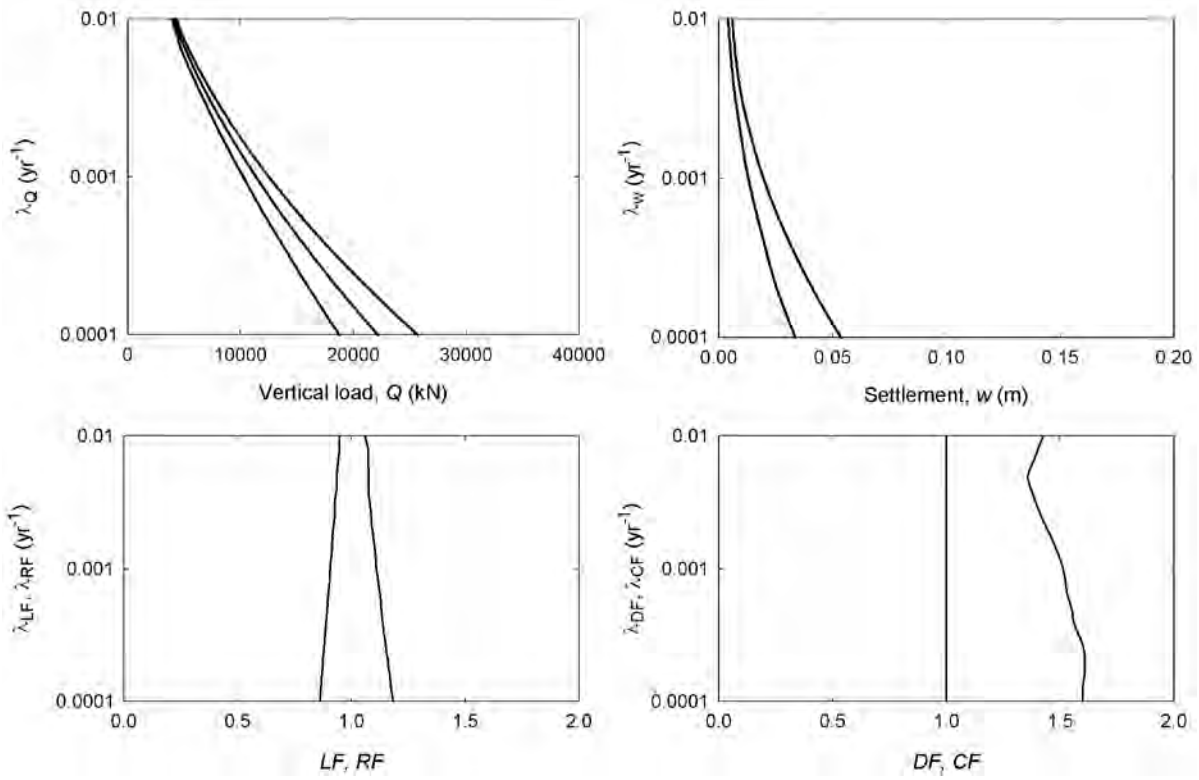

Figure 6.18. Result of analyses with uncertainty in force capacity included along with uncertainties in force and response.

The effects of uncertainty in response capacity are illustrated in Figure 6.19. Uncertainty in allowable displacement was assumed to be lognormally distributed with dispersion, $\beta_{Cw} = 0.6$. This uncertainty causes the settlement capacity curve (w_2) to move to the right of the w_1 curve and the capacity factor to drop below 1.0. The demand and capacity factors tend to oscillate to some degree due to minor fluctuations in the settlement hazard curves. The behavior of all hazard curves and design factor curves is as would be expected.

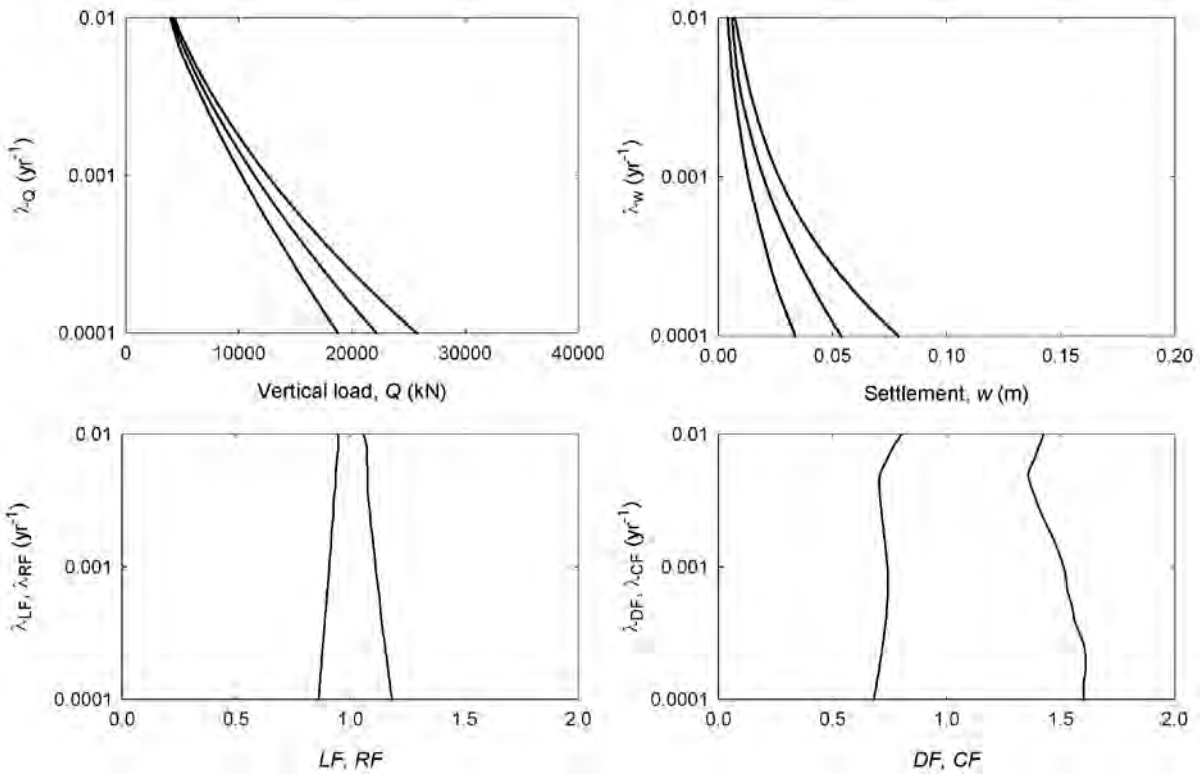

Figure 6.19. Result of analyses with uncertainty in force capacity and response capacity included with uncertainty in force and response.

Finally, uncertainties in static and reference loads were added to the other loads. Dispersions of 0.1 were assumed for these variables. The effects of those uncertainties, as shown in Figure 6.20, were negligible.

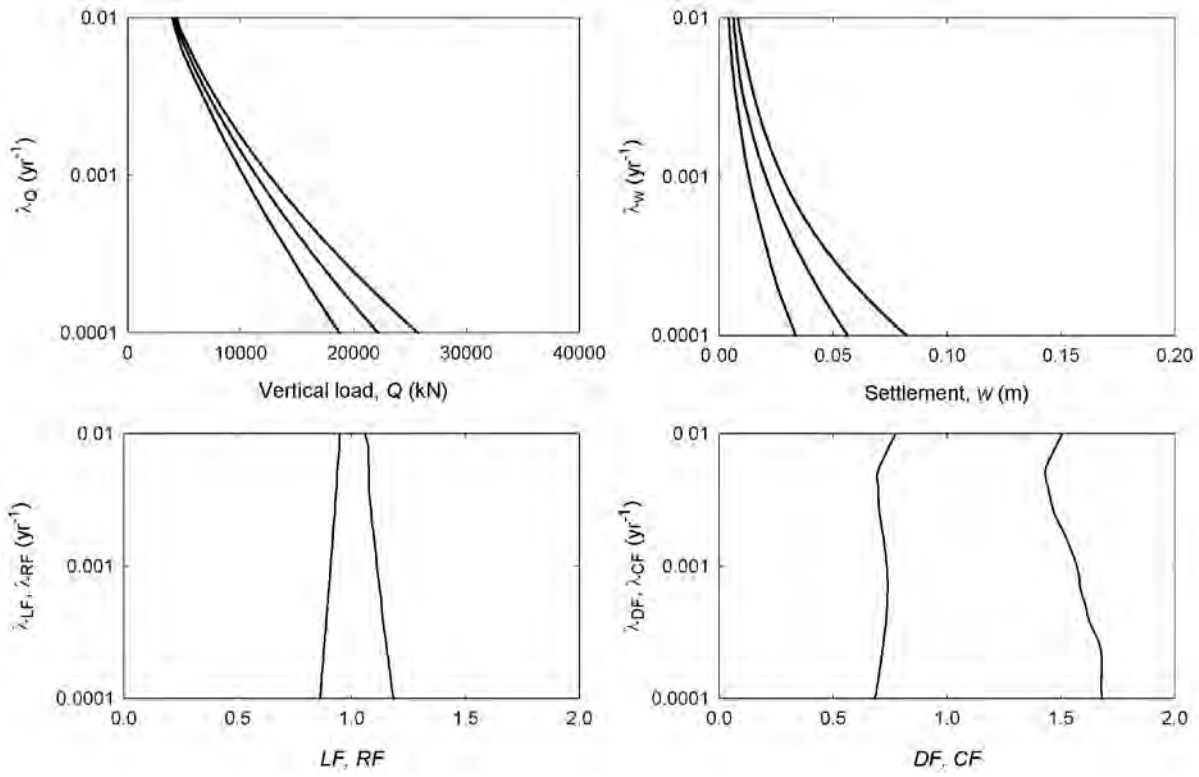

Figure 6.20. Result of analyses with uncertainty in static and reference loads, force, response, force capacity, and response capacity.

6.8 DISCUSSION

This chapter has presented a framework for the evaluation of design factors that are tied to a user-selected return period of limit state exceedance. This framework follows from one developed for structures by Jalayer and Cornell using an approach analogous to that which underlies the PEER framework for performance-based earthquake engineering. The framework had to be extended, however, to account for the intermediate load measure variable and the five-dimensional vector nature of both loading and response for a pile group.

Both closed-form and numerical solutions are derived. The closed-form solution requires a number of assumptions about variable distributions and about the forms of the median relationships between the variables, and is limited to the scalar problem. It is quite useful, however, for illustrating the factor that most strongly affect design factors, and for checking, albeit in a limited way, the accuracy of the numerical solution.

A computer program was written to compute the design factors for general conditions. The program requires the user to provide data on the structural loading, the geometry and properties of the foundation, the soil conditions, and the ground motion hazards. It then performs the required calculations for five components of loading and five components of response. Because these calculations involve integration in five dimensions, they are time-consuming. The program was executed using data that conformed to the assumptions of the

closed-form solution and was shown to match the results of the closed-form solution very well for various permutations of different relationships and uncertainty levels. The program was then executed in vector mode, i.e., with all components of loading and response computed simultaneously. The performance under these conditions was found to be reasonable, although numerical issues related to integration increment size led to a degree of fluctuation in design factor with return period for some cases.

7 Design Factors

7.1 INTRODUCTION

The framework described in Chapter 6 can be used to determine load, resistance, demand, and capacity factors for pile groups under different initial conditions in different seismic environments. As indicated previously, there are a virtually infinite number of bridge and pile group configurations with a virtually infinite number of different initial conditions, response relationships, and uncertainty levels. In order to illustrate the framework and the results it can produce, an extensive series of analyses were performed. The purpose of these analyses was to establish the general range of load and resistance factors, and of displacement-based demand and capacity factors, for a typical pile group, and to illustrate the sensitivities of those factors to a number of different quantities. The results of the analyses illustrate the effects of uncertainty on load and resistance factors and on demand and capacity factors, and help illustrate the prospects for load- and displacement-based approaches to improved seismic design of pile foundations.

7.2 DESIGN FACTORS

Seismic design can be accomplished in a number of different ways. Historically, design has been based on loads and resistances, and reliability-based design has commonly been implemented using a load and resistance factor approach. For essentially static loading conditions, time-invariant load and resistance factors can be developed for a given reliability index, or probability of failure. For seismic design, however, load and resistance factors must account for the variability in loading that can occur – high levels of loading can occur in strong earthquakes that occur relatively rarely, and lower levels of loading can occur in weaker earthquakes that occur more frequently. To develop a design that considers all potential levels of loading and their likelihoods of occurrence in a particular area, performance-based concepts can be used to combine the results of probabilistic seismic hazard analyses with probabilistic structural and foundation response analyses to predict a mean annual rate of failure, which is approximately equal to an annual probability of failure. Load and resistance factors consistent with an annual probability of failure can then be determined.

More recently, seismic design has moved toward a displacement basis since performance is more closely related to displacements than to forces. The process of predicting displacements from forces, however, involves additional uncertainty and that uncertainty, while not well understood by the geotechnical engineering profession at this time, is recognized as being substantial. A performance-based framework can be developed to express displacement demand and capacity factors that are consistent with an annual probability of exceeding some allowable

displacement. Since these demand and capacity factors reflect uncertainties in load and in displacement given load, they can be expected to be more extreme, i.e., displacement-based demand factors to be higher than load factors and displacement-based capacity factors to be lower than resistance factors.

7.3 PARAMETRIC ANALYSES

A series of parametric analyses were performed to illustrate the behavior of both load-based and displacement-based design factors. To make the amount of data manageable, the parametric analyses were conducted with respect to a "base case" system that was considered to be representative of the conditions that might exist for an actual bridge foundation. Deviations from the base case conditions were analyzed to explore the effects of various parameters on design factors. Other base cases could also be used with the program developed for this project.

7.3.1 Base Case Conditions

The analyses were performed relative to a set of base case conditions. The base case consisted of a particular structure supported by a particular pile foundation in a particular seismic environment. The characteristics of the base case model were described in detail in Section 5.2.1, but are reviewed briefly again below.

7.3.1.1 Structure and Pile Group

The base case structure was idealized as a concentrated mass at the top of a single distributed-mass column. The loading applied to the foundation was assumed to be related to the 5% damped spectral acceleration at a period of 0.5 sec, i.e., $S_a(0.5)$.

The base case pile group is a 5x5 group of 61-cm (24-inch) steel pipe piles spaced at 2.5 diameters center-to-center. The individual piles are 19.3 m (60 ft) long, and are connected by a 1.07 m (3.5 ft) thick pile cap with plan dimensions of 3.96 m by 3.96 m (13 ft by 13 ft). The top of the pile cap is flush with the ground surface.

7.3.1.2 Loading Conditions

The structural model of a single mass atop a single column is overly simplified for most actual bridges. In order to extract more information from each analysis, lateral loads and overturning moments were assumed to develop at different rates in the different orthogonal directions. The loading functions were selected more for their ability to illustrate different levels of response and their effects on load, resistance, capacity, and demand factors than for their applicability to a particular structure. The five individual components of loading were taken as indicated in Table 7.1. The relationships indicate different levels of loading for each of the components; four of the five are linear and one is nonlinear. Different loading relationships were selected for the different horizontal directions to avoid computing duplicate responses and in recognition that most bridges will respond differently in the longitudinal and transverse directions.

Table 7.1. Base case *IM-LM* relationships.

Component	Symbol (units)	Relationship
Vertical load	Q (kN)	$Q = 8487 S_a(0.5)$
Lateral load, *x*-direction	V_x (kN)	$V_x = 2122[S_a(0.5)]^{0.9}$
Lateral load, *y*-direction	V_y (kN)	$V_y = 4244 S_a(0.5)$
Moment, *x*-direction	M_x (kN-m)	$M_x = 3106 S_a(0.5)$
Moment, *y*-direction	M_y (kN-m)	$M_y = 6212 S_a(0.5)$

7.3.1.3 Uncertainty Levels

The base case model includes a number of sources of uncertainty. Because little statistical data is available to constrain most of the uncertainties, most of them had to be estimated. The values used in the base case analyses are listed in Table 7.2.

Table 7.2. Base case uncertainty levels.

Quantity	Distribution	Parameter
Static loads	Normal	$COV_{SL} = 0.10$
Reference loads	Normal	$COV_{RL} = 0.10$
Load measure	Lognormal	$\beta_L = \sigma_{\ln LM \mid IM} = 0.30$
Engineering demand parameter	Lognormal	(see Table 5.8)
Force capacity	Lognormal	$\beta_{C,LM} = 0.30$
Displacement capacity	Lognormal	$\beta_{C,EDP} = 0.60$

Note that uncertainty in the earthquake ground shaking intensity is accounted for in the probabilistic seismic hazard analysis used to determine the $S_a(0.5)$ hazard curve. The value of β_L, therefore, represents the uncertainty in loading given some value of $S_a(0.5)$. Similarly, the value of β_R represents the uncertainty in response given some level of loading.

7.3.2 Ground Motion Hazards

At each site, ground motion hazard data was expressed in terms of spectral acceleration for a 5% damped oscillator with a natural period of 0.5 sec. Values of S_a(0.5 sec) were obtained for each of 16 site locations spread across California and Washington. The spectral accelerations assumed V_{s30} = 360 m/sec from the USGS 2008 deaggregation website (https://geohazards.usgs.gov/deaggint/2008/). Table 7.1 shows the spectral acceleration values at six return periods for each of the sites.

Table 7.3 Spectral acceleration (*T* = 0.5 sec) values (g) for 16 cities in California and Washington (g).

State	City	Return Period (yrs)					
		72	224	475	975	2475	4975
California	Eureka	0.2730	0.6985	1.2556	1.9001	2.8567	3.6304
	Fresno	0.1389	0.2209	0.2884	0.3654	0.4856	0.5986
	Irvine	0.2700	0.4483	0.6049	0.7988	1.1450	1.5123
	Los Angeles	0.3485	0.6646	0.9598	1.3156	1.8677	2.3265
	Redding	0.1267	0.2258	0.3204	0.4469	0.6654	0.8671
	Sacramento	0.1636	0.2552	0.3286	0.4055	0.5211	0.6210
	San Diego	0.1598	0.2703	0.3952	0.6077	1.0878	1.5368
	San Francisco	0.3729	0.6774	0.9274	1.2019	1.5841	1.8875
Washington	Aberdeen	0.1534	0.3773	0.6379	0.9897	1.6008	2.1804
	Bellingham	0.1562	0.3125	0.4516	0.6159	0.8705	1.0904
	Olympia	0.2130	0.4357	0.6385	0.8792	1.2390	1.5503
	Richland	0.0482	0.1036	0.1573	0.2282	0.3560	0.4885
	Seattle	0.2181	0.4359	0.6307	0.8598	1.2120	1.5132
	Spokane	0.0363	0.0795	0.1211	0.1780	0.2800	0.3857
	Vancouver	0.1060	0.2685	0.4291	0.6210	0.9223	1.1762
	Yakima	0.0799	0.1571	0.2292	0.3169	0.4649	0.5982

Hazard curves for the 16 sites are shown graphically in Figure 7.1. The curves can be seen to cover a wide range of seismicity levels and to have wide ranges of sensitivity of spectral acceleration to return period. 975-yr spectral accelerations range from 0.41 g to 1.9 g for the California sites and from 0.18 g to 0.98 g for the Washington sites. Ratios of 4,975-yr to 72-yr spectral accelerations (a measure of hazard curve slope, or sensitivity of spectral acceleration to return period) range from 3.8 to 13.3 for the California sites and from 6.9 to 14.2 for the Washington sites. Low values of this ratio indicate sites where frequent motions are strong relative to more rarely occurring motions. The 16 sites include some of the most seismically active areas in the United States, areas dominated by crustal seismicity and areas dominated by subduction zones, and areas dominated by nearby faults and areas most strongly affected by distant faults. This selection of sites is considered sufficiently broad to allow general conclusions about load and resistance factor behavior to be drawn.

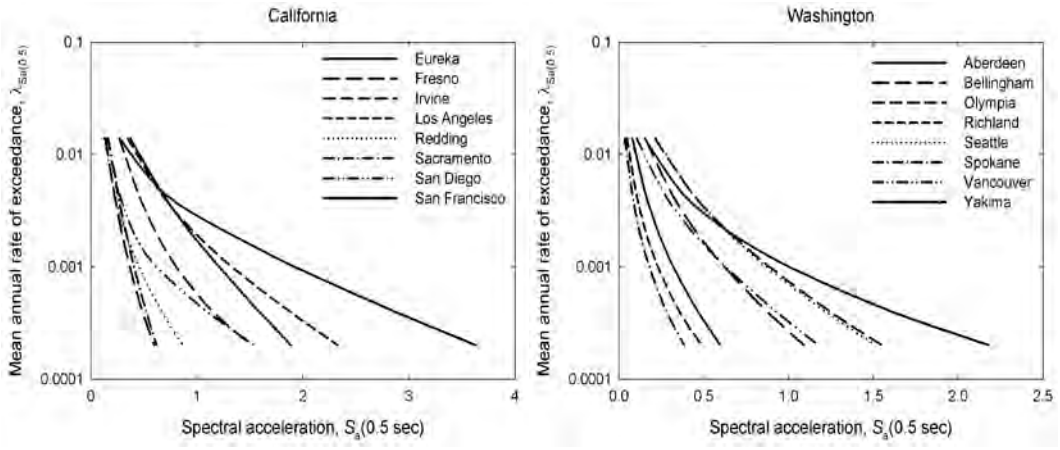

Figure 7.1 Spectral acceleration hazard curves for selected cities in California and Washington.

7.3.3 Base Case Response and Design Factors

The initial base case analyses were performed assuming that the base case site was located in San Francisco. With the high seismicity of the San Francisco Bay Area, the spectral accelerations at long return periods were quite high. The computed response for vertical load and vertical displacement are shown in terms of hazard curves in Figure 7.2. The hazard curves are shown for mean annual rates of exceedance (or annual probabilities) ranging from 0.0001 yr^{-1} to 0.01 yr^{-1}, which corresponds to a return period range of 100 to 10,000 yrs. The full hazard curves were computed for a broader range of return periods, but the range shown here focuses on levels commonly used for design of civil structures.

In the sections that follow, hazard curves are plotted in groups of three curves corresponding to a particular set of conditions. Within each set, the left-most curve represents the zero-uncertainty conditions, i.e., LM_0 (Section 6.4.1) or EDP_0 (Section 6.5.1). The middle curve includes uncertainty in the system the loading for LM_1, and in both loading and response for EDP_1. Finally, the right-most curve represents the limit state with uncertainty in loading, response, and capacity (LM_2 for load components and EDP_2 for response components). To avoid excessive clutter, the individual curves will not be labeled in the figures; their meanings are considered to be understood by the reader.

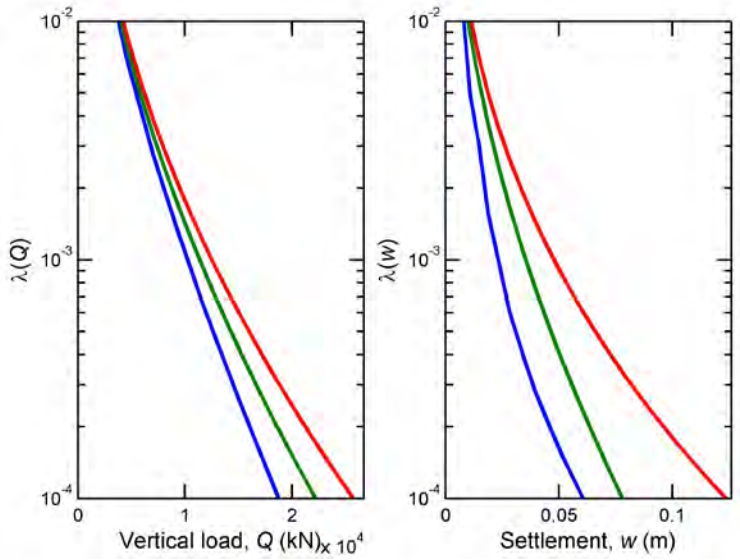

Figure 7.2 **Hazard curves for vertical load and settlement for base case system in sand profile located in San Francisco. Blue curves represent zero-uncertainty values, Q_0 and w_0. Green curves represent values considering load and response uncertainty, Q_1 and w_1. Red curves indicate values considering capacity uncertainty, Q_2 and w_2.**

Both sets of hazard curves appear to be well-behaved. As expected, low levels of force and settlement are exceeded relatively frequently and high levels more rarely. The zero uncertainty cases (blue curves) are the lowest for both load and settlement. The curves that include uncertainty in loads and displacements (green curves) are higher than the blue curves, illustrating the "amplifying" characteristics of uncertainty that were described in Chapter 3. Finally, the limit state (red) curves, which include the effects of uncertainty in force and displacement capacities, are the highest curves. It should be noted that, although the settlement curves are presented here with the vertical load curves, the settlements are also influenced by both lateral loads and both overturning moments.

The load and response hazard curves can be used to determine load and resistance factors, and capacity and demand factors, respectively, as described in Sections 6.4.1 and 6.5.1. Figure 7.3 presents load and resistance factors computed directly from the hazard curves of Figure 7.2. In Figure 7.3, load and demand factors are shown in blue and resistance and capacity factors are shown in green. In all subsequent plots, load and demand factors will have values greater than one and resistance and capacity factors will have values less than one. With that understanding, the individual curves will not be labeled in the figures. The load and resistance factors can be seen to vary smoothly with return period, and to deviate from values of 1.0 at increasing rate with increasing return period (i.e., decreasing mean annual rate of exceedance, λ). The rate of increase appears to be nearly constant on the semi-logarithmic plot, and the curve is quite smooth. The displacement capacity and demand curves also show a trend of increasing deviation from 1.0 with increasing return period, but the curves, particularly the demand curve, are not as smooth as the load and resistance factor curves.

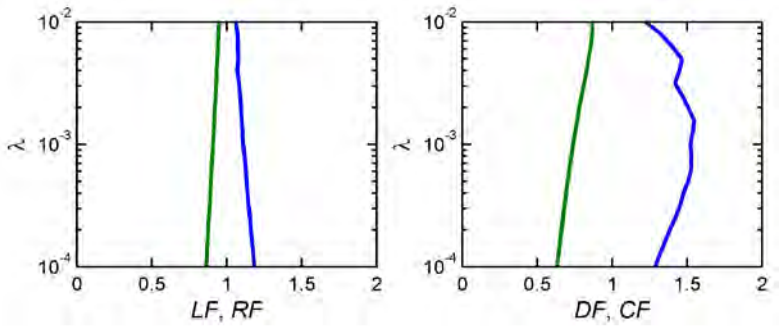

Figure 7.3 **Load and resistance factor curves, and demand and capacity factor curves for base case system in sand profile located in San Francisco. Blue (right-most) curves represent load and demand factors. Green (left-most) curves represent resistance and capacity factors.**

The source of this behavior, which is pervasive throughout the numerically-computed results that follow, lies primarily in the calculation of the zero-uncertainty settlement curve. The zero-uncertainty vertical load curve is a function only of spectral acceleration, a scalar quantity, so the median *IM-LM* relationship can be inverted numerically to compute the median load at a particular spectral acceleration directly; as a result, the zero-uncertainty load value is as smooth as the spectral acceleration hazard curve. The zero-uncertainty settlement curve, however, is a function of all five components of the *LM* vector and must therefore be computed by numerical integration over the cumulative distribution functions of all possible combinations of the five forces/moments. These cumulative distribution functions, however, are step functions for the zero-uncertainty case, which means that there is a sudden jump in the contribution of each increment to the zero-uncertainty settlement value; perfect resolution of the location of this jump, which would provide a perfectly smooth settlement hazard curve, would require infinitely small increments of each of the components of the *LM* vector. The numerical integration process necessarily uses finite increments, so its smoothness depends on the size of the increments over which the integration is performed. The time required to perform the integration, however, increases as a power function of the number of integration increments.

The competing goals of accuracy and speed require a compromise, the result of which is a zero-uncertainty settlement curve that is not perfectly smooth. Close examination of the zero-uncertainty settlement hazard curve (blue curve) in Figure 7.2 reveals that it has some fluctuations about what would be a perfectly smooth curve of the same general shape, particularly at lower settlement values where the three curves are relatively close together. Actually, the curve with consideration of uncertainty (green curve) also has some fluctuations but they are smaller than those of the zero-uncertainty curve. When the demand factor is calculated as the ratio of the settlement including uncertainty to the zero-uncertainty settlement, the fluctuations in the hazard curves lead to readily visible fluctuations in the computed demand factor, and also to more subtle fluctuations in the capacity curve. These fluctuation should be recognized as being of numerical origin, and not interpreted as reflecting real variations associated with small changes in return period.

Hazard curves for all *LM* and *EDP* components from the base case analysis are shown in Figures 7.4 and 7.5. The *EDP* hazard curve plots cover the ranges over which each *EDP* component was computed. The ranges are not known in advance of the analysis, and so some of

the curves, particularly for parameters with high uncertainties, plot only partially within the bounds of the graphs. Those curves are computed for broader *EDP* ranges than appear in the graphs, though, so the design factors computed over the plotted ranges are still applicable. In examining the moment and rotation hazard curves, it is important to recall the notation used in this investigation – the moments, M_x and M_y, act in the *x*- and *y*-directions while the rotations, θ_x and θ_y, act about the *x*- and *y*-axes. Thus, in the absence of other components, the moment, M_x, would produce the rotation, θ_y, and the moment, M_y, would produce the rotation, θ_x. This nomenclature explains why the θ_y values are smaller than the θ_x values when the M_y values are greater than the M_x values.

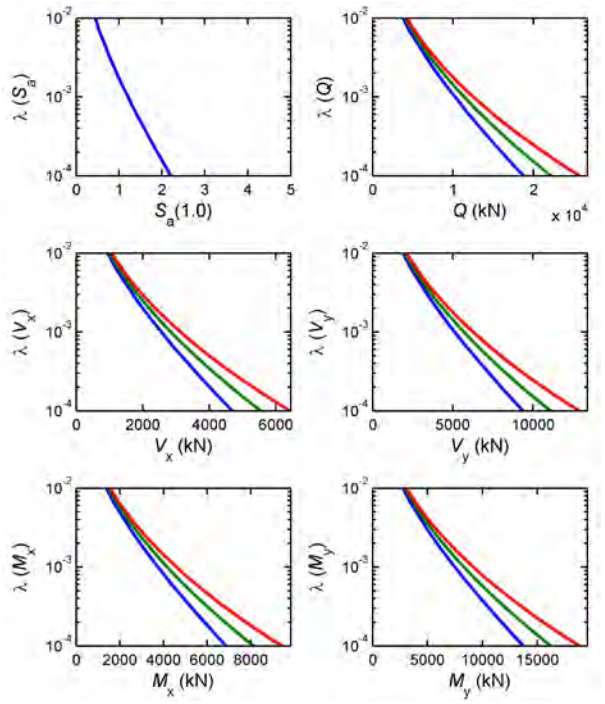

Figure 7.4. ***LM*** **hazard curves for base case analysis of San Francisco site.**

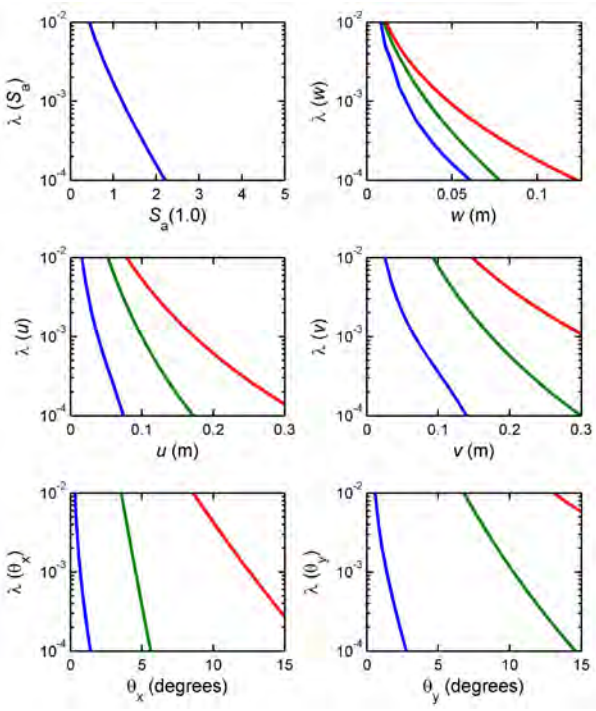

Figure 7.5. ***EDP*** **hazard curves for base case analysis of San Francisco site.**

The load and resistance factors computed from the *LM* hazard curves of Figure 7.4 are presented in Figure 7.6. The load and resistance factors can be seen to be very well behaved. Because the uncertainty levels of the various *LM* components were taken to be the same, the load and resistance factors have similar values, even though the *LM* hazard curves themselves do not. Load factors increase with increasing return period, and have values ranging from about 1.1 to 1.2. These values result directly from the spectral acceleration hazard curve, the assumption of linear S_a-Q behavior, and the vertical load dispersion value of $\beta_L = 0.3$.

Demand and capacity factors are shown in Figure 7.7. The demand factors can be seen to be considerably larger than the load factors shown in Figure 7.6. This behavior results from the additional uncertainty in response given loading. The values of the demand factors are different for the different components of response due both to differences in the uncertainties of the

different components (e.g., β_w = 0.434 and $\beta_{\theta y}$ = 0.740) and the different sensitivities of the response components to the different load components.

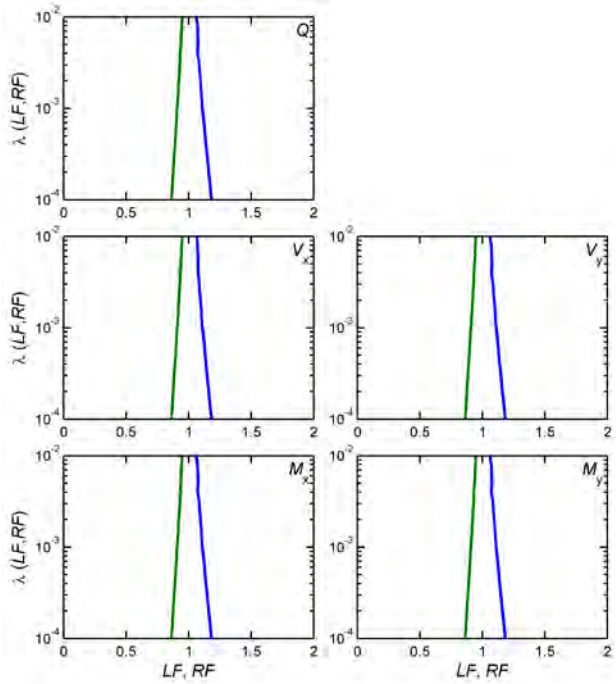

Figure 7.6. Load and resistance factors from base case analysis of San Francisco site.

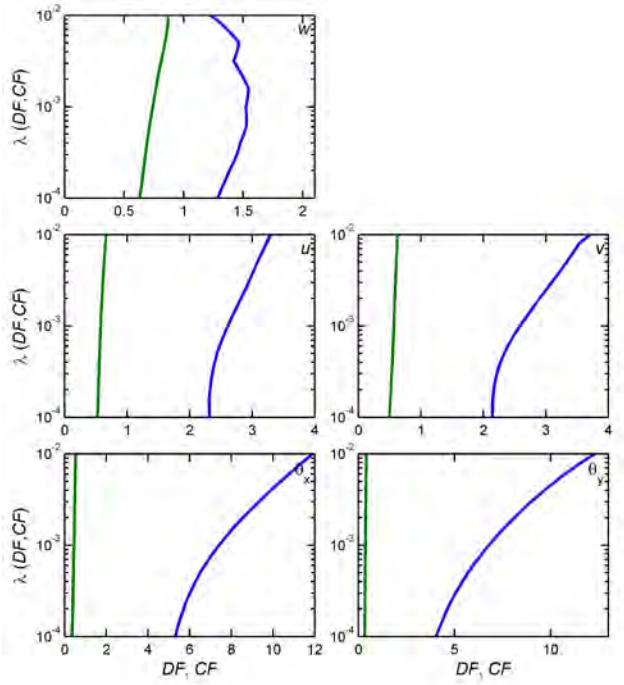

Figure 7.7. Demand and capacity factors from base case analysis of San Francisco site.

7.3.4 Effects of Local Seismicity

One of the primary benefits of the performance-based approach developed in this research is the manner in which it accounts for local seismicity, i.e., ground motion hazards. Whereas conventional design is based upon ground motions with a specific return period, the performance-based approach integrates loads and responses over all levels of ground shaking. The resulting load and response hazard curves account for small earthquakes and low levels of ground shaking that occur frequently, large earthquakes and high levels of ground shaking that occur only rarely, and all other levels of shaking in between. In this manner, they provide a more complete indication of the expected levels of load and response in areas of different seismicity.

Different areas of the country have very different levels and rates of seismic activity. Even within the states of California and Washington, Figure 7.1 shows a wide variety of seismic ground motion hazards. To investigate the effects of local seismicity on load, resistance, demand, and capacity factors, the base case system was assumed to be located at each of the 16 sites listed in Table 7.3. Two pairs of sites are used to illustrate the effects of local seismicity on loads, response, and design factors.

Eureka and Irvine are both located in California and have hazard curves of similar hazards (i.e., mean annual rates of exceedance, or return periods) at low levels of shaking, but very different hazard levels at strong shaking levels. The 72-yr spectral accelerations at these two locations are nearly equal (0.273g for Eureka and 0.270g for Irvine), but the 4,975-yr values differ by a factor of about 2.4 (3.63g for Eureka and 1.51g for Irvine). The Eureka hazard curve is much flatter than the Irvine curve, indicating that many more instances of strong shaking per instance of weak shaking are expected in Eureka than in Irvine.

The horizontal load (V_x) and lateral displacement (u) hazard curves computed for Eureka and Irvine are shown in Figures 7.8 and 7.9. The lateral load hazards at relatively short return periods (λ_{V_x} = 0.01 yr^{-1} or T_R = 100 yrs) are similar, as would be expected since the hazard curves are close to each other at short return periods. The lateral loads at long return periods (λ_{V_x} = 0.0001 yr^{-1} or T_R = 10,000 yrs), however, are much different – the lateral loads at Eureka are more than double those at Irvine. The spread between the *LM* hazard curves, which reflects the values of the load and resistance factors, are also different at Eureka and Irvine. The displacement hazard curves are also quite different. The displacement curves at Eureka at 100 hrs are somewhat higher than those at Irvine, but the Eureka displacement values at 10,000 yrs are about 1.7 times larger than those at Irvine. Although they indicate smaller displacements for the same return period, the Irvine displacement hazard curves can also be seen to be spaced more widely than the Eureka curves.

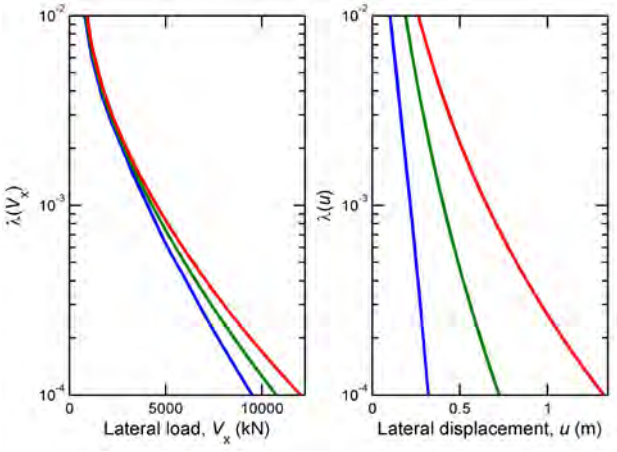

Figure 7.8 Hazard curves for horizontal load and lateral displacement for Eureka.

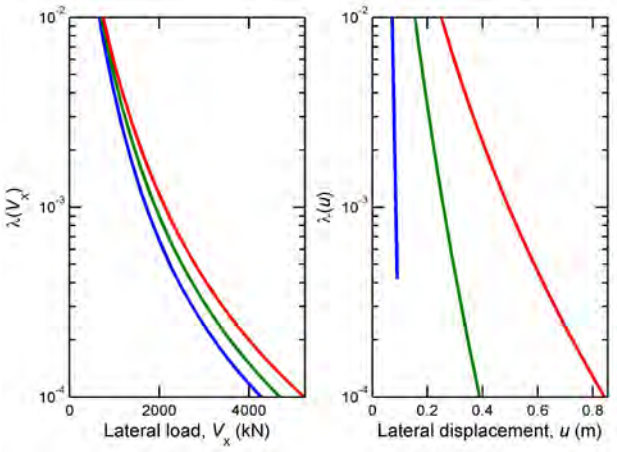

Figure 7.9 Hazard curves for horizontal load and lateral displacement for Irvine.

The design factors corresponding to the load and displacement hazard curves for Eureka and Irvine are shown in Figures 7.10 and 7.11. Although loads and displacements at Eureka are higher than those at Irvine at all return periods, the design factors are different for the two locations. The load and resistance factors are similar at return periods of 100 and 10,000 yrs, but the load factors are somewhat higher and the resistance factors somewhat lower for Irvine than for Eureka. More significant differences can be seen in the demand and capacity factors – the demand factors for Irvine are higher at all return periods, and particularly at longer return

periods, for Irvine than for Eureka. The capacity factors are slightly lower for Irvine than for Eureka.

It is useful to compare the design factors from these analyses with those obtained for the closed-form solution. Under the idealized conditions for which the closed-form solutions are applicable, the design factors are not affected by return period. As shown in Figures 6.12 and 6.13, for example, plots of load, resistance, demand, and capacity factors from the closed-form solution are all vertical. The numerically-computed design factors shown in Figures 7.10 and 7.11, however, do vary with return period – the load and demand factors increase with increasing return period and the resistance and capacity factors decrease with increasing return period. Since the load and displacement models used in the numerical analyses satisfy the assumptions of the closed-form solution, the observed return period dependence of the design factors results from the non-power law form of the actual spectral acceleration hazard curves.

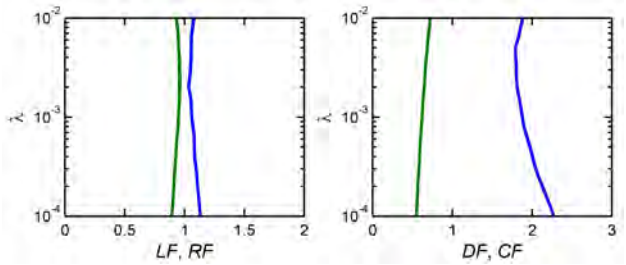

Figure 7.10 **Load and resistance factors and demand and capacity factors for lateral loads and displacements at Eureka.**

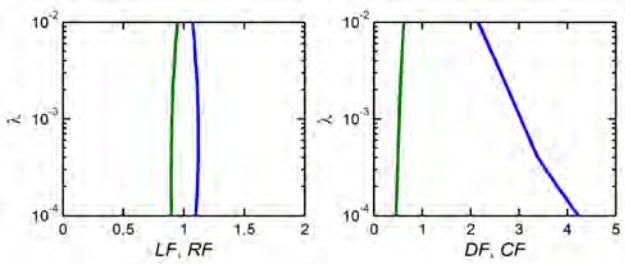

Figure 7.11 **Load and resistance factors and demand and capacity factors for lateral loads and displacements at Irvine.**

Additional insight can be gained by comparing two other sites. Seattle and Aberdeen have spectral acceleration hazard curves that cross at a return period near 475 yrs. The Aberdeen curve, however, is flatter than the Seattle curve, which indicates that it has lower hazards for weak levels of shaking and higher hazards for stronger shaking. The load and displacement hazard curves for Aberdeen and Seattle are shown in Figures 7.12 and 7.13. The lateral loads at the 100-yr return period are higher for Seattle than for Aberdeen, but the opposite is true at the 10,000-yr return period level. With respect to displacements, the displacement hazards at Aberdeen are higher than those at Seattle for the entire range of return periods.

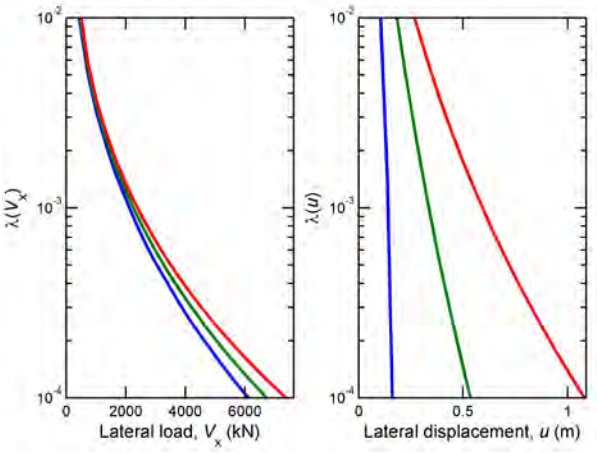

Figure 7.12 Hazard curves for horizontal load and lateral displacement for Aberdeen.

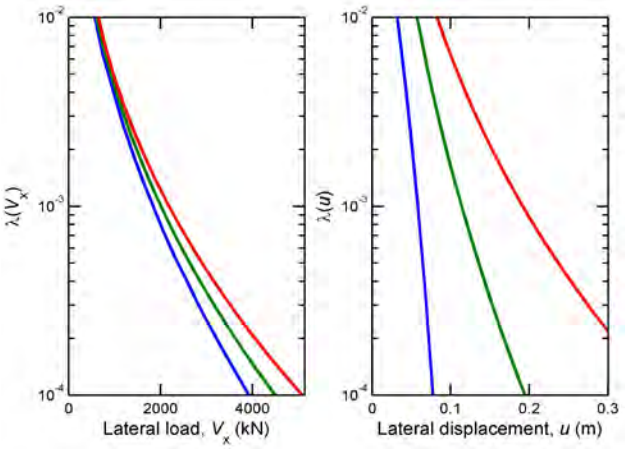

Figure 7.13 Hazard curves for horizontal load and lateral displacement for Seattle.

As shown in Figures 7.14 and 7.15, the load and resistance factors for Aberdeen deviate from 1.0 slightly less than the Seattle factors, and the capacity factors are similar. The demand factors for Aberdeen are close to those for Seattle at relatively short return periods, but are significantly higher for longer return periods.

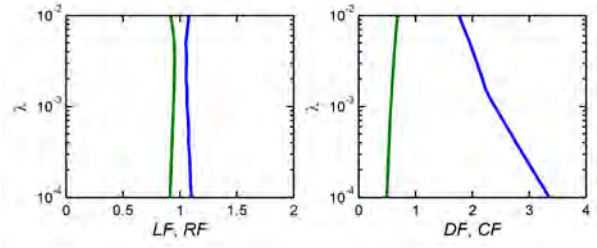

Figure 7.14 Load and resistance factors and demand and capacity factors for lateral loads and displacements at Aberdeen.

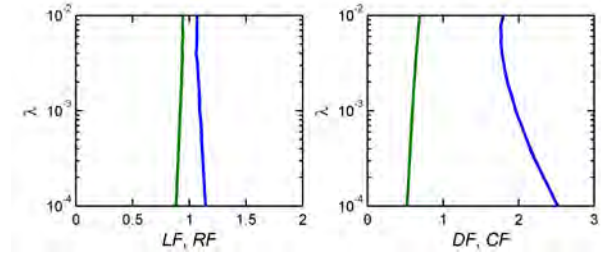

Figure 7.15 Load and resistance factors and demand and capacity factors for lateral loads and displacements at Seattle.

As indicated in Equation 3.27, a seismic hazard curve can usually be approximated over some range of ground motion hazards by a power law relationship

$$\lambda_{IM}(im) = k_0 (IM)^{-k} \tag{3.27}$$

in which k_0 controls the "height" and k the "slope" of the hazard curve. Given two points on a ground motion hazard curve – (IM_1, λ_{IM_1}) and (IM_2, λ_{IM_2}) – the values of k_0 and k that describe the hazard curve within (and slightly beyond) the range between IM_1 and IM_2 can be computed as

$$k = -\frac{\log(\lambda_{IM1} / \lambda_{IM2})}{\log(im_1 / im_2)} \tag{7.1a}$$

and

$$k_0 = \lambda_{IM1} \cdot (im_1)^{-\log(\lambda_{IM1}/\lambda_{IM2})/\log(im_1/im_2)} \tag{7.1b}$$

The 475- and 2,475-yr USGS spectral acceleration hazard values from Table 7.3, were used to compute the values of k_0 and k shown in Table 7.4.

Table 7.4 Coefficients for idealized power law approximation of spectral acceleration hazard curve.

Location		Coefficient, k_0	Coefficient, k
California	Eureka	4.0482	0.02830
	Fresno	5.8042	6.1E-06
	Irvine	4.5846	0.00075
	Los Angeles	4.7106	0.00766
	Redding	4.1469	7.46E-05
	Sacramento	6.5811	5.54E-06
	San Diego	2.8351	0.00051
	San Francisco	5.9783	0.00632
Washington	Aberdeen	3.4328	0.00203
	Bellingham	4.7710	0.00021
	Olympia	4.8118	0.00113
	Richland	3.7118	8.74E-06
	Seattle	4.8079	0.00102
	Spokane	3.6438	3.91E-06
	Vancouver	4.1732	0.00029
	Yakima	4.3072	1.49E-05

According to the closed-form solutions given in Equations 6.45, the demand and capacity factors should be influenced by the slope of the ground motion intensity hazard curve and the curvatures inherent in the load and response relationships. The variation of 10,000-yr demand factors with the slope coefficient, k, is shown for all five response variables in Figure 7.16. The demand factors can be seen to decrease with increasing value of k, i.e., with increasing spectral acceleration hazard curve slope. Thus, the expected trend of steeper ground motion hazard curves leading to higher demand factors is seen, albeit with some scatter, in the numerical results. This result shows the importance of utilizing the entire ground motion hazard curve in the determination of design factors.

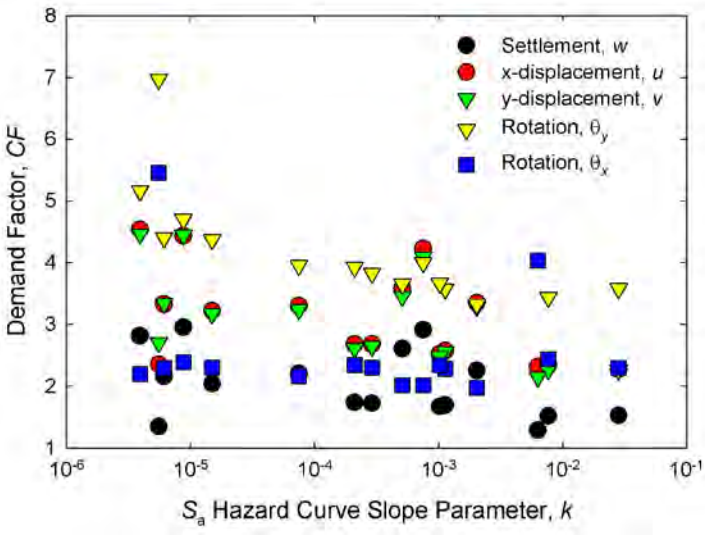

Figure 7.16. Illustration of reduction of demand factor with increasing ground motion hazard curve slope.

7.3.5 Effects of Pile Group Size

The size of a pile group will affect the loads it attracts and the manner in which it responds to those loads. A series of analyses were performed assuming that 3x3, 5x5, and 7x7 pile groups existed at the same site and wee subjected to the same loading. Given that the loading was the same for each pile group size, the load hazard curves should be expected to be the same. Figure 7.17 shows that the vertical load hazard curves are identical and that the load and resistance factors are also the same (Figure 7.18) for all three pile group sizes.

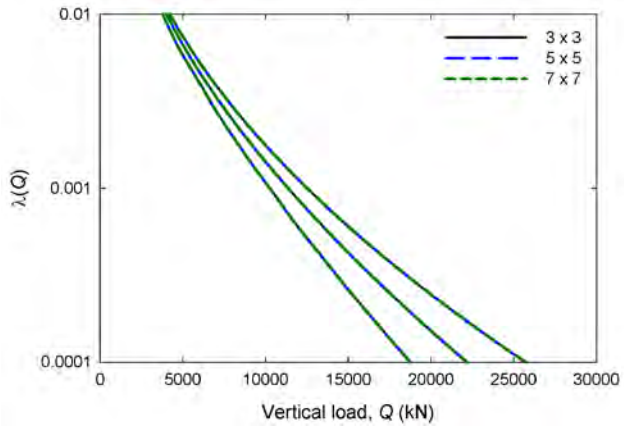

Figure 7.17 Effect of pile group size on vertical load hazard curves.

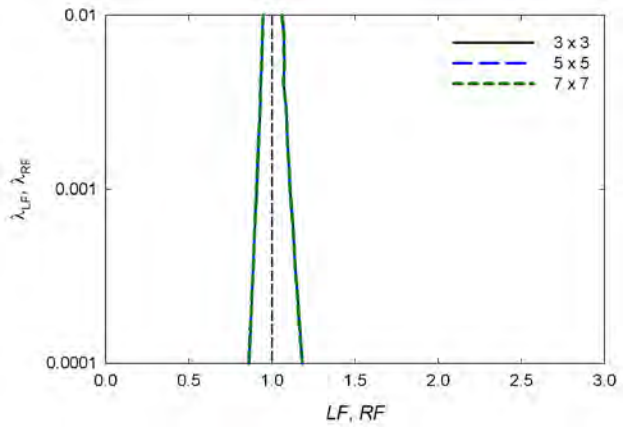

Figure 7.18 Vertical load and resistance factors for pile groups of different sizes.

The pile group responses, however, should be expected to be different with the 3x3 pile group tending to displace/rotate more than the 5x5 pile group, and the 5x5 pile group to displace/rotate more than the 7x7 pile group. This behavior shows up clearly in Figure 7.19 – the settlement hazard curves for the 3x3 pile group fall well to the right of those of the 5x5 pile group and, in turn, the 7x7 pile group. The corresponding demand and capacity factors (Figure 7.20), however, are much more tightly grouped. The zero-uncertainty settlement curve oscillations lead to oscillations in the demand factors, but the demand factors for all the foundation sizes are relatively consistent. The capacity factors are all quite consistent.

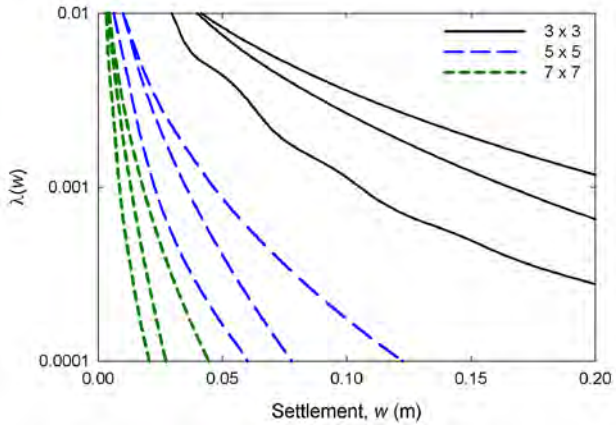

Figure 7.19 **Effect of pile group size on settlement hazard curves.**

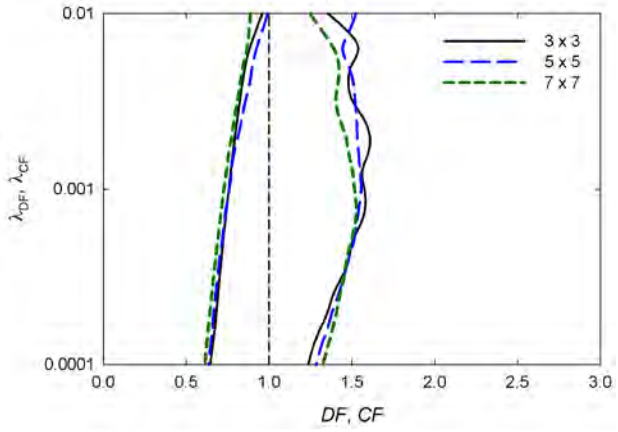

Figure 7.20 **Settlement displacement demand and capacity factors for pile groups of different sizes.**

The behavior observed for the other components of loading and response behaved in a similar manner. Figures 7.21 and 7.22 show that the horizontal load hazard curves and the load and resistance factors are all identical. Figure 7.23 shows that lateral displacements increase with decreasing pile group size, and that the curves are spread more widely than the settlement hazard curves shown in Figure 7.19. Accordingly, the settlement demand factors (Figure 7.24) are higher and capacity factors lower than for the settlement demand and capacity factors. The lateral displacement demand factors show a smoother shape and a more persistent trend of increasing demand factor with increasing foundation size.

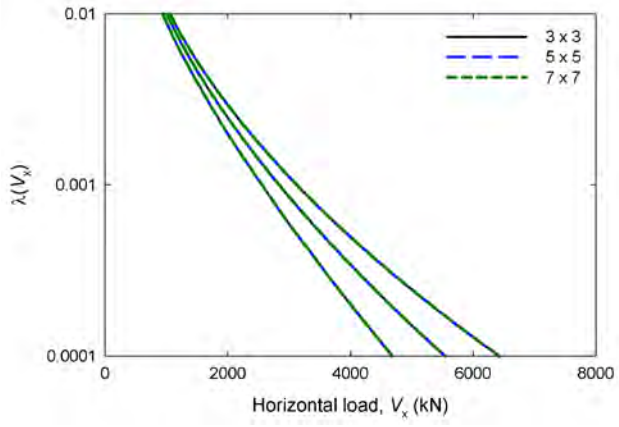

Figure 7.21 **Effect of pile group size on lateral load hazard curves.**

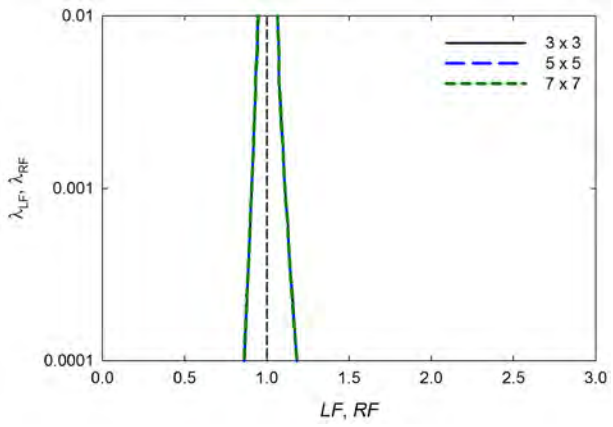

Figure 7.22 **Lateral load and resistance factors for pile groups of different sizes.**

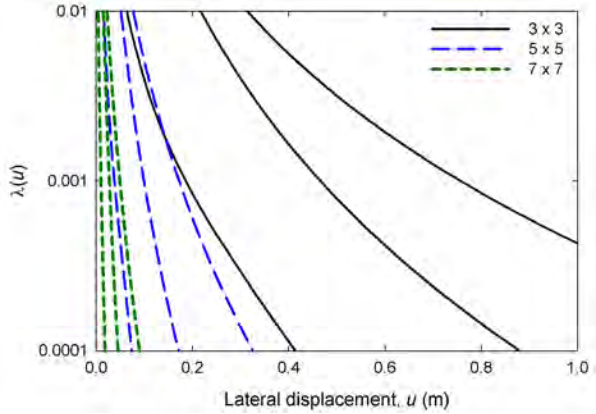

Figure 7.23 **Effect of pile group size on lateral displacement hazard curves.**

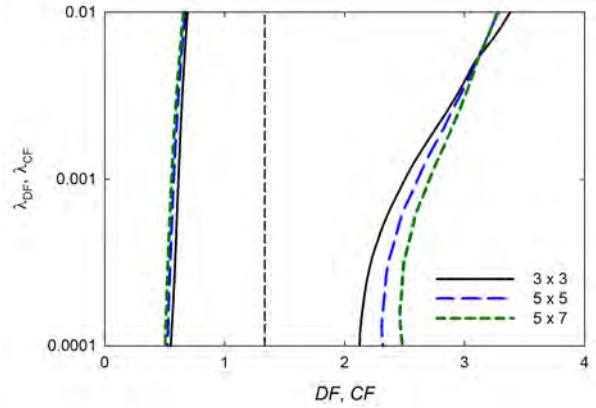

Figure 7.24 **Lateral displacement demand and capacity factors for pile groups of different sizes.**

7.3.6 Effects of Initial Static Loads

The displacement and/or rotation of a bridge foundation under seismic loading is also influenced by the level of static loading that exists before and during earthquake shaking. To investigate the effects of static loading on design factors, a series of analyses were performed with the base case foundation subjected to different levels of static loading. Five load cases with different levels of all five load components were defined as indicated in Table 7.5.

Table 7.5 **Static load cases.**

Static Loads	Case 1	Case 2	Case 3	Case 4	Case 5
Q_s	20	40	60	80	100
V_{xs}	5	10	15	20	25
V_{ys}	5	10	15	20	25
M_{xs}	10	20	30	40	50
M_{ys}	10	20	30	40	50

The lateral displacement hazard curves for all five load cases are shown in Figure 7.25. The three sets of hazard curves for each static load case each show a progression of increasing displacement with increasing initial static loads – in other words, each set of five curves indicate, from left to right, the results for Cases 1-5, respectively. Similar behavior was observed for the other components of displacement and for other site locations.

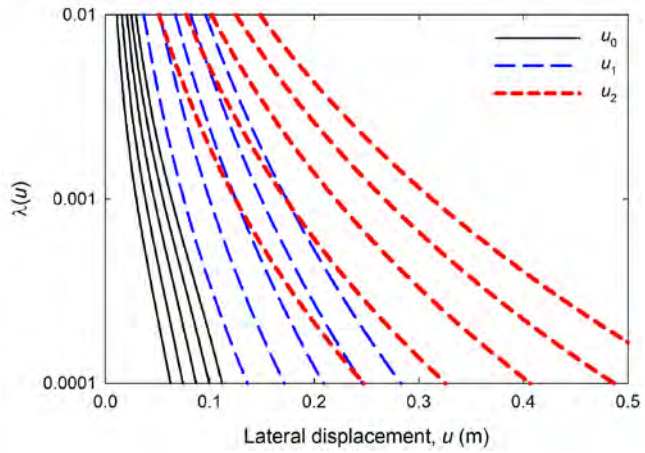

Figure 7.25 Effects of static loads on lateral displacement hazard curves. Each set of five curves represents, from left to right, static load cases 1-5 as defined in Table 7.5.

Variations in displacement hazard curves due to differences in static loads lead to variations in demand and capacity factors. The demand and capacity factors for the five static load cases are shown in Figure 7.26. The demand factors can be seen to decrease with increasing return period, but at a rate that decreases with increasing initial static load level. At short return periods, the demand factor is insensitive to static load level, but the degree of sensitivity increases with increasing return period. The capacity factors tend to decrease with increasing initial static load level, but at a relatively slow rate.

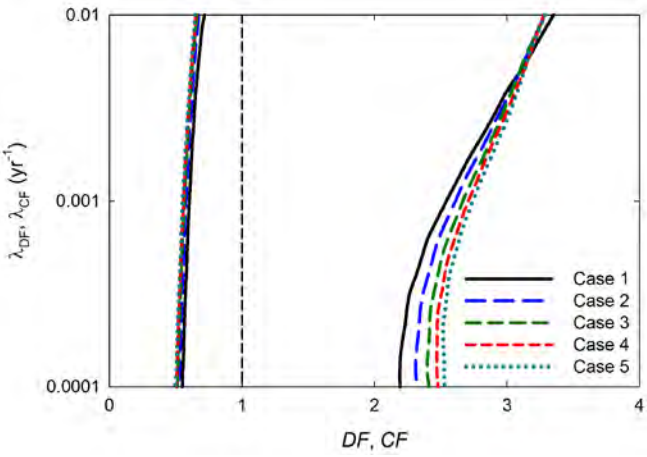

Figure 7.26 Demand and capacity factors for base case system subjected to static load cases defined in Table 7.5.

7.3.7 Effects of Structural Behavior

The characteristics of a bridge structure can strongly affect the loading imposed on a pile foundation, and consequently affect the displacement/rotation of that foundation. A typical bridge structure will exhibit essentially linear response under low levels of loading, such as the type of earthquake shaking that occurs at low return periods. Many bridge structures are designed to respond inelastically under strong shaking, however, and the resulting nonlinear response can impose limits on the amplitudes of loading imposed on their foundations.

In order to investigate the effects of structural behavior on pile foundation response and accompanying design factors, a series of analyses assuming different *IM-LM* response characteristics was performed. In these analyses, the structure was assumed to exhibit hyperbolic *IM-LM* response with the hyperbolic parameters adjusted to produce different degrees of nonlinearity. Considering the lateral load-displacement response, a hyperbolic *IM-LM* relationship can be defined as

$$V_x = \frac{KS_a}{1 + \frac{V_{x,\max} S_a}{K}} \tag{7.2}$$

where K and $V_{x,max}$ are constants. The variable, K, represents the initial slope of the *IM-LM* relationship, i.e., the ratio of V_x to S_a at low S_a values, and $V_{x,max}$ is the maximum value of V_x, which is reached at very large S_a values. Figure 7.27 shows the relationships between lateral load and spectral acceleration for four assumed *IM-LM* relationships with different values of maximum lateral load. All four relationships have the same initial slope, but exhibit different degrees of nonlinearity due to the different maximum lateral load values.

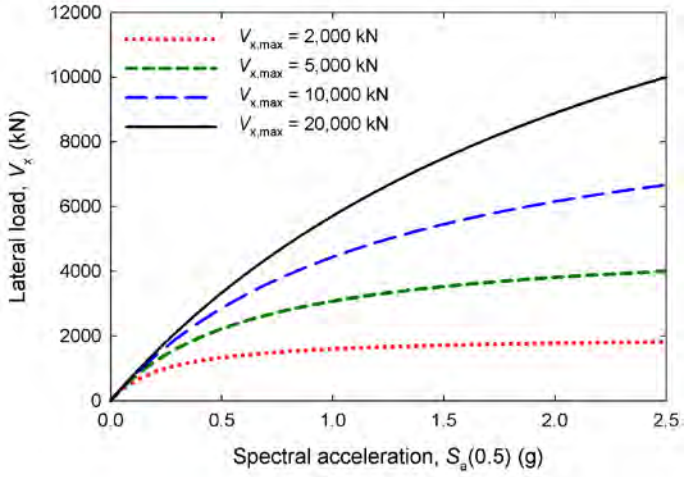

Figure 7.27 Variation of lateral load with spectral acceleration for different nonlinear structural models.

The effect of structural response on lateral load hazard curves is shown in Figure 7.28. As the degree of nonlinearity increases (i.e., as the lateral load for a given S_a value decreases), the lateral loads at a given return period decrease, which is to be expected given the relationships illustrated in Figure 7.27. The decreasing lateral load values are accompanied by steepening of

the lateral load hazard curves. The positions and shapes of the lateral load hazard curves interact with the uncertainties in lateral loads (which were identical for all four *IM-LM* relationships) to affect the load and resistance factors. Figure 7.29 shows that the load factors increase and resistance factors decrease with increasing degree of nonlinearity. This behavior is consistent with the steepening of the lateral load hazard curves. Thus, the load values decrease with increasing degree of nonlinearity, but the load factors increase and capacity factors decrease.

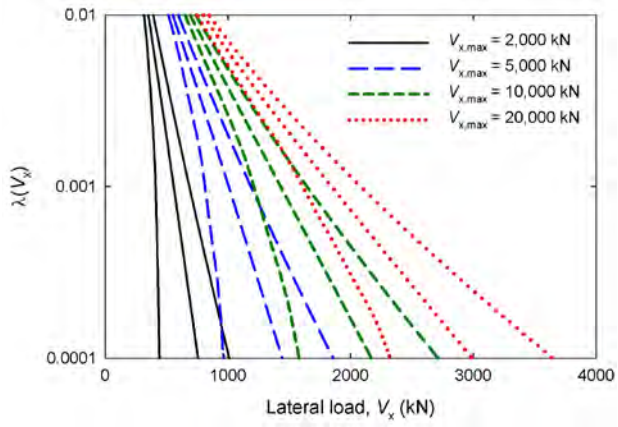

Figure 7.28 **Effects of structural response nonlinearity on lateral load hazard curves.**

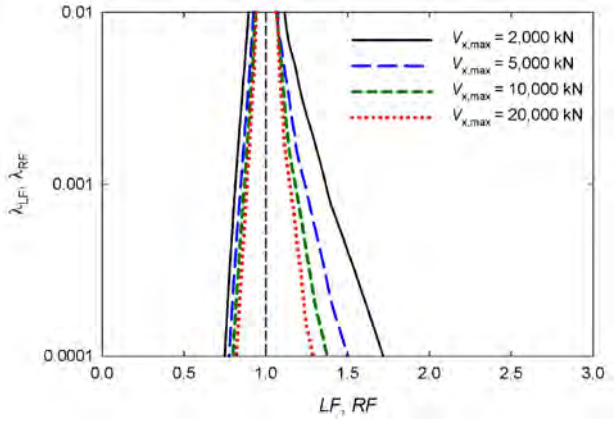

Figure 7.29 **Effects of structural response nonlinearity on load and resistance factors.**

The effects of structural response nonlinearity on the displacement hazard curves is shown in Figure 7.30. Because the structural response affects all three lateral load hazard curves, it also affects all three lateral displacement hazard curves. As the level of structural response nonlinearity increases, the lateral displacement hazards decrease and the curves become steeper. The resulting displacement demand factors, as shown in Figure 7.31, tend to increase with increasing structural response nonlinearity.

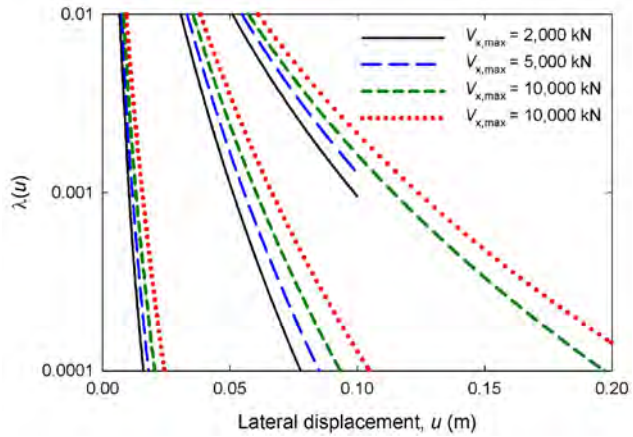

Figure 7.30 **Effects of structural response nonlinearity on lateral displacement hazard curves.**

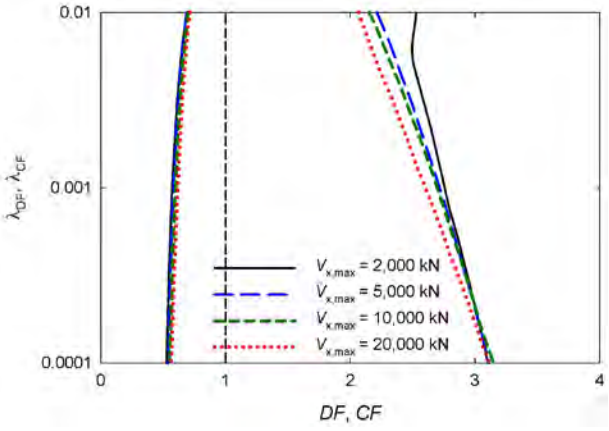

Figure 7.31 **Effects of structural response nonlinearity on demand and capacity factors.**

7.3.8 Effects of Load Measure Uncertainty

The dynamic loading applied to a pile foundation depends on the characteristics of the ground motion and of the bridge supported by the foundation. First-mode spectral acceleration is commonly used as an intensity measure, but record-to-record variability as well as uncertainties in the physical characteristics of the bridge and the models used to predict bridge response will lead to uncertainties in the predicted structural response. A series of analyses were performed with different levels of *LM* uncertainty; the effects of four different levels on lateral load hazard curves and resulting load and resistance factors are shown in Figures 7.32 and 7.33, respectively. The load measure uncertainty does not affect the zero-uncertainty lateral load (LM_0) value, but it does cause the other (LM_1 and LM_2) hazard curves to move to the right by amounts that depend on the uncertainly level. As would be expected, increasing *LM* uncertainty leads to higher load factors. The resistance factors, however, are unaffected by the uncertainty in load measure.

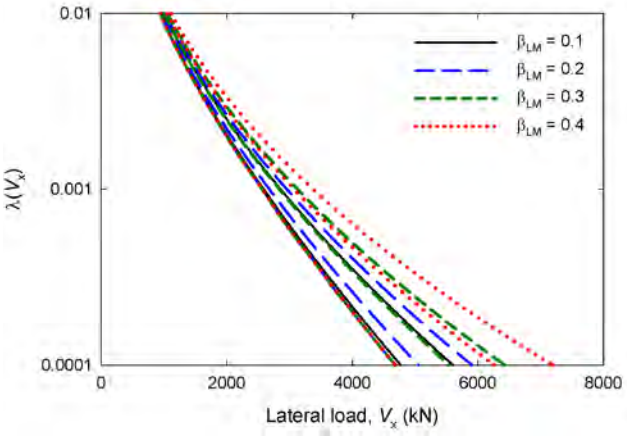

Figure 7.32 **Lateral load hazard curves for different levels of uncertainty in lateral load given spectral acceleration.**

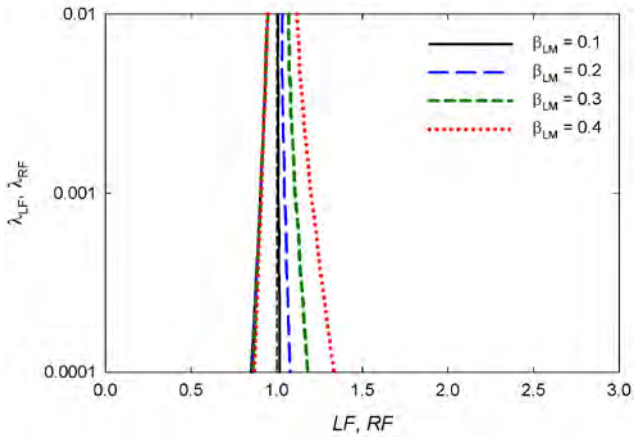

Figure 7.33 **Load and resistance factors for different levels of uncertainty in lateral load given spectral acceleration.**

The effects of load measure uncertainty propagate through the response analyses to influence the response levels and the demand factors. Figure 7.34 illustrates the effects of lateral load uncertainty on the lateral displacement hazard curves. The zero-uncertainty displacements are not affected by lateral load uncertainty, but increasing levels of load measure uncertainty push the other displacement hazard curves (i.e., the curves for EDP_1 and EDP_2, in this case u_1 and u_2) to the right. This effect manifests itself in increasing displacement demand factors, as shown in Figure 7.35. Although the displacement hazard curves that reflect capacity are also moved to the right due to load measure uncertainty, they are moved in a proportional manner that does not affect the capacity factor.

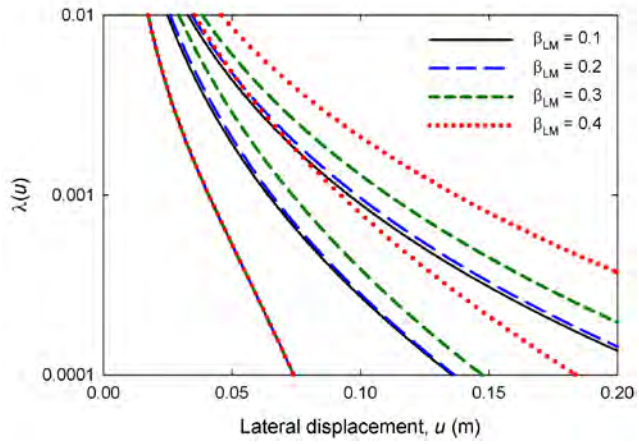

Figure 7.34 **Lateral displacement hazard curves for different levels of uncertainty in lateral load given spectral acceleration.**

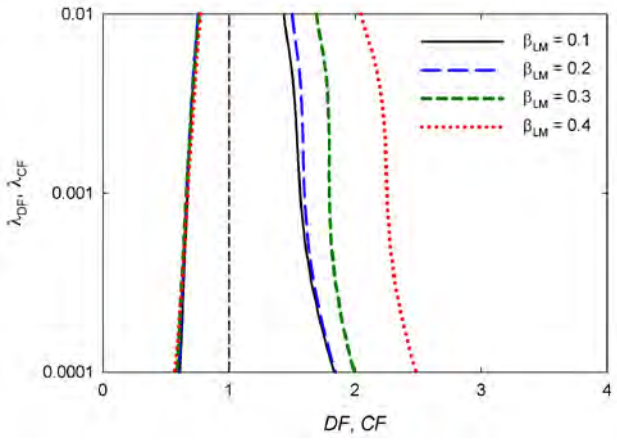

Figure 7.35 **Demand and capacity factors for different levels of uncertainty in lateral load given spectral acceleration.**

7.3.9 Effects of Engineering Demand Parameter Uncertainty

As indicated in Chapter 5 and quantified in Table 5.4, prediction of pile cap displacements given seismic loading is highly uncertain. As predictive models improve and as more data is generated, this uncertainty can be reduced, but the values indicated by the OpenSees analyses performed in this study remain relatively high. To investigate the effects of uncertainties in displacements on design factors, analyses were performed with several different assumed *EDP* uncertainty levels. The results of those analyses are illustrated with respect to lateral loads and lateral displacements. Figures 7.36 and 7.37 illustrate the effects of uncertainty in displacement on lateral load hazard curves and load and resistance factors. The figures show the expected result that uncertainty in the displacements given loading have no effect on the loading or the load-based design factors.

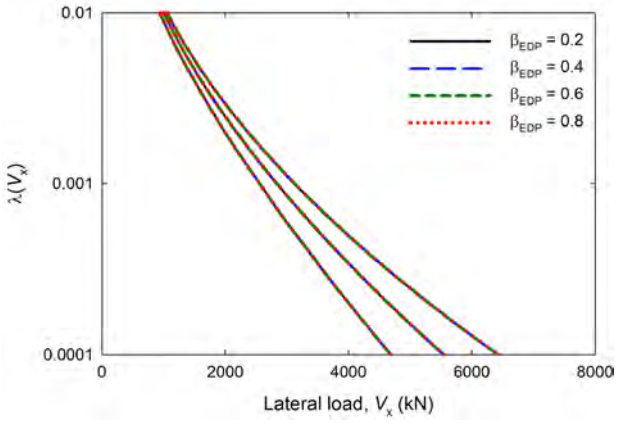

Figure 7.36 **Lateral load hazard curves for different levels of uncertainty in lateral displacement.**

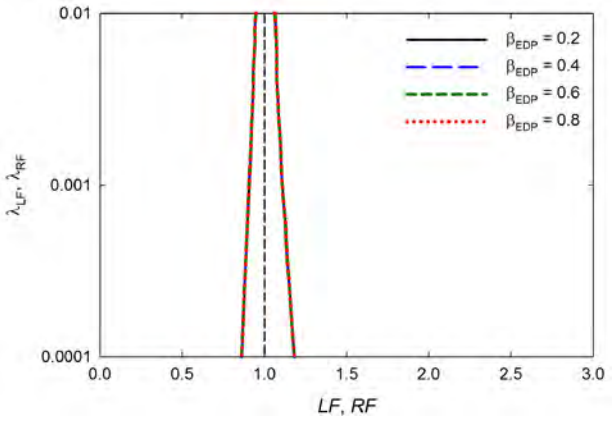

Figure 7.37 **Load and resistance factors for different levels of uncertainty in lateral displacement.**

The uncertainty in lateral displacement has a strong effect on the lateral displacement hazard curves. As shown in Figure 7.438, the lateral displacement hazard curves considering uncertainty and capacity move to the right with increasing uncertainty level; the zero-uncertainty displacement hazard curves are all identical. The variations on displacement hazard curves produce corresponding differences in design factors. Figure 7.39 shows that displacement demand factors increase significantly with increasing displacement uncertainty. The effects of uncertainty in displacement on capacity factors, however, are very small.

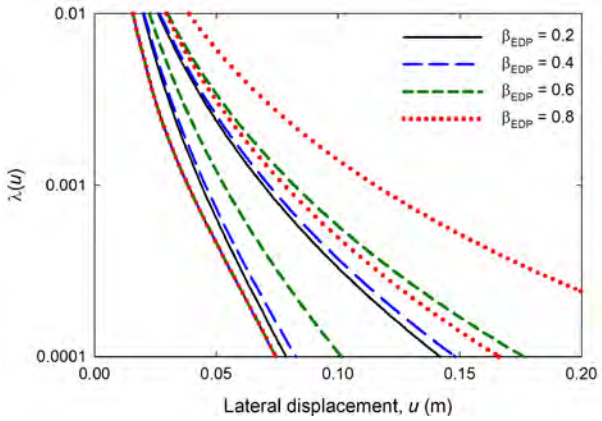

Figure 7.38 **Lateral displacement hazard curves for different levels of uncertainty in lateral displacement.**

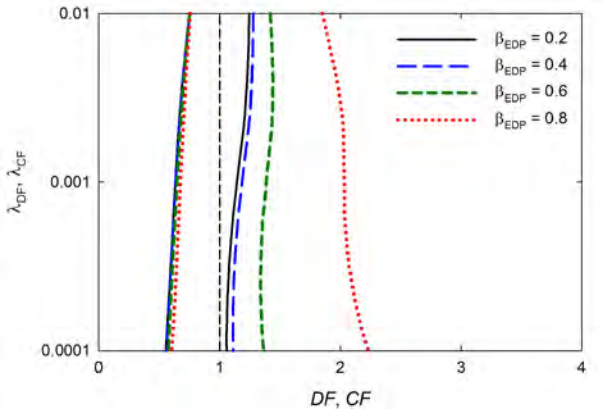

Figure 7.39 **Demand and capacity factors for different levels of uncertainty in lateral displacement.**

7.3.9.1 Effect of Soil Type

The calculations can be performed for any foundation model for which *LM-EDP* behavior has been characterized. Table 5.4 presented such relationships for pile foundations in a clay deposit. The pile group capacity for the clay site is considerably lower than for the sand deposit, which is to be expected given the fundamental differences in the resistances of such soils to foundation loading. The manner in which axial and lateral load resistance is mobilized in clays and sands are significantly different as well. Once the capacity of a foundation in clay is mobilized, displacements increase much more rapidly than in the case of sands in which resistance tends to continue to increase due to increases in effective confining pressure.

The vertical load-settlement response for the base case system in clay is shown in Figure 7.40. Compared with the foundation in sand, shown in Figure 7.2, the settlements are considerably larger for the foundation in clay, and they increase much more quickly with increasing return period. The zero-uncertainty (blue) settlement hazard curve can be seen to fluctuate mildly from a smooth shape due to the size of the integration increment. Because the range of settlements for the foundation in the clay profile was much larger than for the sand profile, the integration increment was also higher. A smoother curve could be obtained with a smaller integration increment, but the required calculations would take longer.

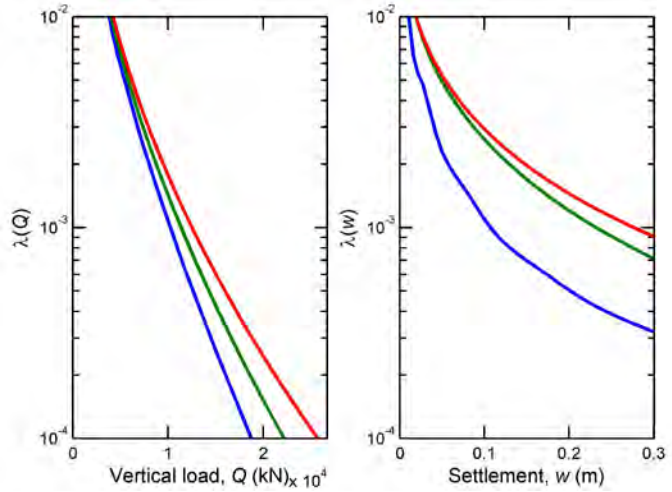

Figure 7.40 **Hazard curves for vertical load and settlement for base case system in clay profile located in San Francisco. Blue curves represent zero-uncertainty values, Q_0 and w_0. Green curves represent values considering load and response uncertainty, Q_1 and w_1. Red curves indicate values considering capacity uncertainty, Q_2 and w_2.**

Figure 7.41 presents load and resistance factors computed directly from the hazard curves of Figure 7.40. The load and resistance factors can be seen to vary smoothly with return period, and to deviate from values of 1.0 at increasing rate with increasing return period (i.e., decreasing mean annual rate of exceedance, λ). The rate of increase appears to be nearly constant on the semi-logarithmic plot, and the curve is quite smooth. The displacement demand factor curve also varies with return period, first increasing and then decreasing as was observed for the sand profile in Figure 7.3. The demand factors for the clay profile case are generally larger than those for the sand profile; the capacity factors are also somewhat larger.

The demand factor curve is not as smooth as the load factor curve due to the previously described fluctuations in the zero-uncertainty settlement curve. The capacity factor curve is generally smoother than the demand factor curve, but has a portion that drops suddenly at a return period somewhat above 1,000 yrs. The fluctuations in the settlement hazard curves lead to fluctuations in the demand and capacity factors.

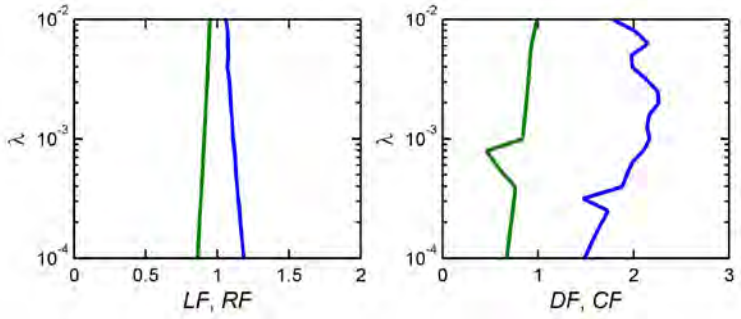

Figure 7.41 **Load and resistance factor curves, and demand and capacity factor curves for base case system in clay profile located in San Francisco. Blue curves represent load and demand factors. Green curves represent resistance and capacity factors.**

7.4 DISCUSSION

Relatively small-scale fluctuations in response hazard curves lead to larger fluctuations in demand and capacity factors. While the program seeks to minimize these fluctuations, the only way to remove them completely is to reduce the integration increments to very low values. The drawback of that approach is the exponential increase in the number of increments required to perform the design factor calculations. Since the program execution is already relatively time-consuming with the integration increments used to generate the figures in this chapter, increasing it further through the use of smaller integration increments is not appealing. A more practical solution is to numerically smooth the design factor curves in a manner than captures the main trends of behavior while reducing the small-scale fluctuations.

8 Summary, Conclusions, and Recommendations for Future Research

8.1 INTRODUCTION

Highway bridges, by virtue of their large size, long spans, or locations in areas of poor soil conditions, are frequently supported on pile foundations. These foundations may be subjected to vertical and horizontal loads, and to overturning moments. These forces and moments may, as in the cases of gravity loads and dead loads, be essentially constant in amplitude and direction with time, or they may vary with time. Variable loading may be of relatively low amplitude and high predictability, as in the case of traffic loads, or may be of much higher amplitude with high levels of unpredictability. Extreme loads, such as those that may be imposed by storms, vehicular impact, or earthquakes, occur infrequently, but can have very high impacts on foundation loading and bridge performance.

This report describes the results of a research investigation intended to develop and illustrate advanced procedures for design of pile foundations subjected to earthquake loading. The procedure makes use of a framework for performance-based earthquake engineering evaluation developed by the Pacific Earthquake Engineering Research (PEER) Center. For practical application to the pile foundation design problem, in which an infinite number of possible bridge types and configurations is combined with a virtually infinite number of different pile foundation types and geometries in a virtually infinite number of possible soil conditions, the PEER framework had to be modified and extended. The result is a framework and computational model for the evaluation of design factors, i.e., load and resistance factors for force-based design, and analogous demand and capacity factors for displacement-based design. These factors are developed in a manner that accounts more completely for local seismicity than currently available procedures, and therefore provides designs with a more complete and consistent consideration of earthquake loading.

8.2 SUMMARY

The use of pile foundations and the manner in which they mobilize resistance to applied loads was reviewed. Procedures for estimation of axial load capacity can be based on pile geometry and soil strength characteristics, driving resistance with simple pile driving formulae, driving resistance with wave equation analyses based on measurements during driving, and from pile load tests. These procedures require different forms of information and provide results with different levels of uncertainty. Each can be used to predict a pile capacity, i.e., a limiting force beyond which “failure” would be considered to have occurred. For piles in clay, exceedance of

the axial pile capacity leads to the relatively rapid onset of large deformations. Exceedance of pile capacity in sands, however, does not lead to such rapidly increasing deformations. Procedures such as that of Davisson (ref) have proven effective for consistent estimation of axial pile capacities. Piles subjected to lateral loading behave differently than in axial loading due to the fact that piles are so much more flexible when loaded in their transverse direction than when loaded axially. The lateral load response of pile foundations is evaluated using soil-structure interaction principles in which the stiffness of the soil affects the movement of the pile and the movement of the pile affects the stiffness of the soil. For laterally loaded pile problems, the notion of "failure" is often defined in terms of relative pile displacements, often expressed as a fraction of the diameter of the pile. Pile groups allow very heavy column loads to be shared by multiple piles all connected to a common pile cap. The behavior of the group may be affected by the orientation and spacing of the piles within the group. When piles are spaced closely, the zones of the soil stressed by individual piles may overlap in such a manner that the capacity of the group is not equal to the sum of the capacities of the individual piles. Such group effects can affect the behavior of the pile group, although the exact manner in which they do so is difficult to determine for the case of seismic loading in which the directions of the resultant forces are changing continuously in three dimensions.

The design of foundations requires criteria for acceptable performance of the foundation, and performance can be described in a number of different ways. Foundations have historically been designed to have the capacity to resist the maximum anticipated loading, with the assumption that a load greater than the capacity would cause failure of the foundation. In some cases, exceedance of capacity can lead to large and damaging deformations, but in other cases it may not. The notions of performance, which can be expressed in terms of loads and resistances, deformations and allowable deformations, or in terms of physical damage or losses are reviewed and compared. The notion of uncertainty and its effects on foundation performance are reviewed and procedures for its consideration in design, e.g., through reliability-based design are described. The implementation of reliability-based design through the use of load and resistance factors is introduced. Finally, the PEER framework for performance-based earthquake engineering evaluation is described and a modified version of it, suitable for the task of evaluating foundation performance, is developed.

The response of pile foundations to earthquake loading is complex. A pile group can be subjected to three orthogonal loads – one vertical, and two horizontal – and two overturning moments. Torsional loading and response of individual foundations is generally not significant. Therefore, a given loading state consists of five different load components even under static loading conditions. For some bridge and foundation configurations, the static lateral loads and overturning moments may be relatively low, but they may be higher for other configurations. Under seismic conditions, in which the bridge and its foundations are subjected to three-dimensional motions that can translate into significant dynamic forces and overturning moments in all directions, the loading can be extremely complex and severe. A two-step analysis process consistent with the modification of the PEER performance-based earthquake engineering framework was developed to allow consideration of multiple bridge and foundation configurations. In this framework, a structural analysis is performed with an approximate model of the foundation to identify the loading histories applied to the foundation under earthquake loading conditions. In the second stage, the loading from the first stage is applied to the foundation and the response computed. Both analyses were implemented in the OpenSees (OpenSource for Earthquake Engineering Simulation) finite element analysis program. The

foundation model used discrete *p-y*, *t-z*, and *Q-z* curves to represent interaction of the pile foundation with the surrounding soil and modeled the pile cap as being rigid. The use of the discrete interaction elements was validated by comparison of predicted response with responses measured in full-scale static pile load tests and dynamic (centrifuge) model tests. The discrete model was found to predict responses that were consistent with the observed responses. It should be noted, however, that very little data on the actual performance of full-scale pile groups under strong dynamic loading is available; as a result, the type of statistical analyses often used to calibrate LRFD procedures is not possible for the case of seismically-loaded pile foundations.

With the numerical model developed and validated, an extensive series of dynamic response analyses were performed. A structural model consistent with one used in the ATC49 study that developed guidelines for LRFD was developed and used to determine the loading imposed on different pile group foundations. The structure was assumed to have a fundamental period of 0.5 or 1.0 sec in accordance with the periods of bridges commonly used in highway applications. Pile groups of five different configurations were analyzed in both sand and clay profiles. The pile groups were subjected to 36 different combinations of initial static loads and then subjected to 50 different earthquake ground motions. The responses under all of these conditions were examined, and it was determined that they could be grouped after normalizing loads/moments and displacements/rotations by reference values. The reference values were taken as the values nominally associated with "failure" – for example, the vertical reference load was the failure load identified by the commonly used Davisson (ref) procedure, and the vertical reference displacement was the displacement corresponding to the Davisson failure load. When normalized displacements/rotations were plotted as functions of normalized loads/moments, the behavior from widely varying foundation configurations fell within relatively consistent bands. In order to maximize the breadth of the response characterization, the normalized load and displacement approach was used to characterize pile group response. By performing thousands and thousands of analyses for many different combinations of loads and configurations, a data set of pile foundation response to dynamic loading was developed. Multiple regression analyses were performed to identify functional relationships describing the variation of displacements and rotation with loads and moments. It should be noted that all five components of displacement and rotation are influenced by all five components of load and overturning moment. The uncertainties in the predicted displacements and rotations conditional upon the known loads and moments were also characterized.

The data generated by the OpenSees structural and foundation response analyses provided, upon characterization by the regression analyses, a simple probabilistic model for the response of pile foundations to earthquake loading. The model could, by eliminating consideration of all uncertainties in structural and foundation characteristics and in the loading and response models, predict the deterministic (or median) response of a foundation to seismic loading. It could also allow consideration of those uncertainties to compute distributions of dynamic loads and moments or displacements and rotations. In seismic design, however, probability distributions are not commonly used directly because the dimension of time must be considered – earthquake-induced loads can vary from the very weak loading associated with small earthquakes that occur relatively frequently to the very strong loading that occurs only rarely. Seismic loading and response are commonly described in terms of hazard curves that show the mean annual rate of exceedance (approximately equal to the mean annual probability) of some level of ground motion. In conventional seismic design, a design ground motion level is selected based on some specified mean annual rate of exceedance (or its reciprocal, the return

period). The PEER performance-based framework utilizes the entire hazard curve so that all levels of ground motion are considered. A modification of that framework was developed to allow computation of hazard curves with and without uncertainty in loads, responses, and capacities. This framework was then extended to allow computation of load and resistance factors for load-based performance evaluations, and of demand and capacity factors for displacement-based evaluations. These design factors are tied to return periods, so that one can select load (or demand) and resistance (or capacity) factors that will produce designs with specified return periods of limit state exceedance. With the aid of certain assumptions, closed-form expressions for the design factors were developed to provide basic insight into the factors that most strongly affect their values. For more general conditions, however, computation of the design factors for up to five components of load/response requires numerical integration in up to five dimensions, a problem that proves to be both difficult and time-consuming. A computer program was developed to carry out these integrations and to compute the design factors for virtually any set of conditions. The program was validated by checking its agreement with the closed-form solution when the assumptions of the closed-form solution were made, and by checking the general reasonableness of its solutions with various parametric permutations.

Finally, the program was used to explore the effects of different parameters and uncertainty levels on load and response hazard curves and on design factors. A base case structure/foundation system was assumed to be located in eight California and eight Washington cities, all distributed in areas ranging from very low to very high seismicity. For each case, load and displacement hazard curves were computed, as were load and resistance factors and demand and capacity factors. Examples of the computed hazard curves were presented; in some cases, all five hazard curves were presented and, in other cases, one or two components were presented as examples of the loads, responses, and design factors. Examples from locations with different levels of seismicity included San Francisco, Eureka, and Irvine in California, and Aberdeen and Seattle in Washington. Analyses were reported for pile groups of different size – 3x3, 5x5, and 7x7 groups all assumed to be located in San Francisco were analyzed and their hazard curves and design factors compared. The seismic response of pile groups is influenced by the initial, static loads applied to them. A set of five initial load cases was evaluated, with each having increasing static load amplitudes (or decreasing static factors of safety). Hazard curves and design factors were computed and compared for all five load cases. The nature of structural response can also influence foundation response. Analyses were performed considering structures that responded nonlinearly to ground motions with three levels of nonlinearity. The different degrees of structural nonlinearity were observed to significantly influence both load and demand factors with a smaller effect on resistance and capacity factors. The design factor framework considers the effects of uncertainties, so analyses were performed with different levels of uncertainty in loading given ground motion intensity, in response given loading and in load and displacement capacities. Finally, the effects of different soil type were computed and compared.

8.3 CONCLUSIONS

The research described in this report was directed toward development and implementation of a performance-based framework for the establishment of reliability-based design factors for pile foundations. The process of developing this framework in a form that could be applied to the multitude of possible bridge, foundation, site, and subsurface conditions that foundation

designers must consider led to an extension of the PEER PBEE framework. That extension was pursued from both theoretical and practical perspectives. Finally, the numerical implementation of the procedures developed in this research were applied to different pile foundation systems located in different seismic regions. All of these activities allowed a number of conclusions to be drawn.

1. The pile group response problem is complicated. Prediction of the complete response requires prediction of five components of response – three displacements and two rotations – each of which is affected by five components of both static and dynamic loading. The various components of loading can have different relative amplitudes and different degrees of correlation depending on the nature of the bridge, the site, and individual ground motions. The loads may be linearly or nonlinearly related to the ground motion and the response may be linearly or nonlinearly related to the loading.

2. The OpenSees finite element program is capable of representing the static and dynamic response of three-dimensional pile groups subjected to loading produced by three–dimensional ground motions in a practical manner. OpenSees has nonlinear, inelastic, discrete *p*-*y*, *t*-*z*, and *Q*-*z* elements that can represent the most important effects of the complex interaction between piles and soil under static and seismic loading in a relative efficient manner computationally. The OpenSees model used in this research has been shown capable of producing good predictions of pile response in full-scale static load tests and of seismic pile group response in centrifuge model tests.

3. Essentially no data is available for calibration of reliability-based design procedures using the type of statistical analyses commonly used for calibration of LRFD procedures. Data on the seismic response of full-scale pile foundations subjected to earthquake loading is virtually non-existent. While a framework for handling uncertainty in pile foundation seismic response can be developed, the appropriate values of that uncertainty are themselves uncertain.

4. A two-stage approach is useful for evaluating the potential responses of different pile foundations supporting different bridges at different sites. Because of the virtually infinite number of combinations of bridge, site, foundation, and soil conditions, the problem of predicting foundation response from ground motions was subdivided into two stages. The first stage involves predicting foundation loads from ground motions, and the second stage involves predicting foundation response from foundation loading. This modular approach can be handled in a performance-based design framework, and offers great flexibility in terms of evaluating the effects of different structural and geotechnical factors on foundation response and design.

5. Theoretical, closed-form solutions can be developed for individual, scalar cases and extended to the two-stage approach to compute load- and displacement-based design factors. These solutions require certain assumptions about the shapes of ground motion hazard curves and load/response models – the assumptions can be approximately consistent with general trends of actual behavior, but they do not accurately represent actual behavior. The closed-form solutions do, however, provide insight into the relative importance of factors that affect hazard curves and design factors, and can be used to

check numerical solutions when those solutions are applied to idealized problems that satisfy the required assumptions.

6. The closed-form solutions indicate that design factors are influenced by the slope of the ground motion hazard curve, the levels of curvature of the load and response models, and the uncertainties in the load and response models.

7. For realistic problems, in which hazard curves and load/response models may not have the forms required for the closed-form solution, and where individual response components are influenced by multiple load components, the load and response hazard curves and the load- and displacement-based design factors must be computed numerically. The calculations require numerical integration, which is relatively straightforward and fast for a single variable; the accuracy of the calculations increases with decreasing size of the integration increment but the time required for the calculations increases. For the pile problem, the numerical solution requires integration over all components of loading, with consideration of uncertainty, for all components of response. This means that the integration must be performed in five dimensions for each of five response components; the total number of calculations is proportional to the product of the number of integration increments in each direction. If each loading variable is divided into 100 increments, a total of $100^5 = 10$ billion probabilistic calculations would need to be performed – such a computational burden would be very time-consuming to satisfy.

8. The computational process could be sped up by using different numbers of integration increments for different variables. In the calculations described in this report, primary and secondary loading variables were defined – the vertical load was the primary variable for settlement (vertical displacement) and all other load components were secondary variables. The same approach was used for the other response components. Since they had the greatest effect on the various response components, the primary variables were discretized more finely than the secondary variables. With this approach, cutting the number of integration increments of the secondary variables in half led to a reduction in total calculations by a factor of $2^4 = 16$.

9. Examination of the pile group load-response data from the OpenSees analyses indicated that the responses of different pile groups subjected to different levels of loading could be combined to a great degree through the use of normalized load and response variables. The normalized loads were defined as the loads divided by reference loads, which were taken as the loads causing "failure" as commonly (and consistently) defined in foundation design. The normalized displacements were taken as the displacements divided by reference displacements, which were the displacements associated with the reference loads. Expressions for normalized displacements as functions of normalized loads developed through regression analyses on a large database of OpenSees simulations showed that differences between the median responses for different systems were small relative to the overall uncertainties in displacements.

10. Parametric analyses using a computer program developed to carry out the performance-based calculations were performed to investigate the influence of a number of factors on design factors. The results of these parametric analyses led to the following conclusions:

(a) Actual design factors vary with return period, in contrast to the constant nature of design factors from the closed-form solutions. The design factors can increase or decrease with return period depending on the nature of the spectral acceleration hazard curve and the load/response model behavior.

(b) Loading hazard curves, which are computed directly from the spectral acceleration hazard curve are well behaved with the relatively simple loading models used in this research. With more complex loading models, the loading hazard curves could exhibit more complex behavior.

(c) Design factors are affected by the entire ground motion hazard curve. The position of the hazard curve influences load and demand factors, but so does the slope of that curve. Steeper ground motion hazard curves lead to larger load and resistance factors.

(d) Displacement demand factors are larger than load factors and displacement capacity factors are smaller than resistance factors. In many cases, the differences are quite large. The differences result from the additional uncertainty involved in predicting displacements given loads, which can be appreciable. In general, earthquake-induced loads can be predicted more accurately than earthquake-induced displacements.

(e) The size of a pile group affects design factors to an degree that depends on the definition of reference loads and reference displacements. If the reference values are independent of group size, as in the case of vertical loads (per pile), load factors will be unaffected by pile group size. Because response components, such as settlement, are affected by multiple load components, however, they will be affected by group size.

(f) Static loads influence the likelihood of reaching limit states and have strong effects on hazard curves, but can also affect design factors. Demand factors are affected more than capacity factors, and the effect of static load increases within increasing return period.

(g) Structural behavior also influences foundation loading and response. Increasing nonlinearity of structural response, as may occur when columns yield, tend to reduce loading on the foundation, which in turn reduces median displacements. These reductions, however, steepen the load and response hazard curves, which tends to increase load and demand factors. Resistance and capacity factors are reduced, but at a much lower rate than the load and capacity factors are increased.

(h) Uncertainties in estimated loads (given ground motion intensity) and displacements (given loads) play a strong role in determining design factors. With all other things being equal, uncertainties act as "amplifiers" for load and demand factors and "attenuators" for resistance and capacity factors. Increasing uncertainty, for a given return period, will lead to higher load and demand factors and lower resistance and capacity factors.

These conclusions are based on observations made over the course of the research project. During the project, parametric analyses explored the influence of a number of quantities

and parameters on design factors, but there are many more possible permutations of parameters, relationships, and uncertainties that can be examined. Such efforts will undoubtedly lead to better understanding of design factors and additional conclusions about their behavior.

8.4 RECOMMENDATIONS FOR FUTURE RESEARCH

The research described in this report was carried out over an extended period of time, in fact, a more extended period of time than was originally anticipated. As the research progressed, complexities and interdependencies were discovered and addressed as appropriately as possible. As with many research projects, a look backward reveals things that could have been done differently, and things that could be done to extend or better support the goals of the work. Some of those items are briefly discussed in the following paragraphs.

The OpenSees analyses were effective and are considered to provide a good indication of pile group behavior for the conditions considered. Additional analyses could provide a more extensive database with which to develop load and resistance models. Most permutations of different conditions were performed with a suite of 50 ground motions. In retrospect, these analyses could have been performed with a smaller number of motions, which would have allowed more sets of conditions to be analyzed. Relatively late in the study, a number of additional analyses were performed with 10 motions to attempt to define median behavior. In such cases, where different numbers of data points are used for different sets of conditions, mixed effects regression could be used to better characterize the uncertainty in the models. Alternatively, with smaller numbers of motions, it would have been easier to simulate different conditions using the same number of motions.

Additional analyses with a wider variety of different structural characteristics, including significantly different loading amplitudes in different directions, would provide a more robust database upon which to build a response model. With the assumed free-standing, single-mass structure utilized in the analyses performed in the majority of the analyses reported here, correlations between loading components, e.g., lateral load and overturning moment, were probably greater than would be expected in most actual bridge structures.

Additional exploration or development of the OpenSees pile model to allow improved performance under larger pile displacements would be helpful. Cases in which loads and deformations became significantly larger than the reference load and displacements tended not to converge and to cause the program to crash. There is a concern that the behavior described by the regression equations (Table 5.4) indicates displacements and rotations that do not increase as quickly as they should at high normalized loads and overturning moments. Improved *p-y*, *t-z*, and *Q-z* elements could allow the development of larger pile cap displacements/rotations, which would allow more accurate description of response at larger, but perhaps still tolerable for long return periods, displacements and rotations.

Smooth functions could be fit to the computed hazard curves to allow computation of smoother design factors. Alternatively, smooth functions could be fit to the computed design factors to avoid fluctuations of design factors with return period that are of numerical origin.

Optimization of the numbers of integration increments for the different load components could lead to faster execution times. In the current version of the program, parameters are characterized as primary or secondary variables. By testing different combinations of integration

increments, it may be possible to increase execution speed by customizing the integration scheme for specific problems. The use of parallel processing would be particularly effective for the design factor calculations.

9 References

AASHTO, (1997). Standard Specifications for Highway Bridges: 16th Edition (1996 with 1997 interims). AASHTO, Washington, D.C.

AASHTO, (2010). Standard Specifications for Highway Bridges: 17th Edition, AASHTO, Washington, D.C.

Allen, T.M. (2005a). "Development of the WSDOT Pile Driving Formula and Its Calibration for Load and Resistance Factor Design (LRFD)", Prepared for Washington State Department of Transportation and in cooperation with U.S. Department of Transportation, Federal Highway Administration. March, 2005.

Allen, T.M. (2005b). "Development of geotechnical resistance factors and downdrag load factors for LRFD foundation strength limit state design," *Report FHWA-NHI-05-052*, National Highway Institute, Federal Highway Administration, 41 pp.

Allen, T. (2007). "Development of a new pile driving formula and its calibration for load and resistance factor design," Transportation Research Record, Volume 2004, Issue 1, pp. 20-27.

API, (1993). "Recommended practice for planning, designing and constructing fixed offshore platforms – load and resistance factor design," *API Recommended Practice 2A-LRFD* (RP 2A-LRFD), First Edition, Washington, D.C.

Applied Technology Council (1978). "Tentative provisions for the development of seismic regulations for buildings, *ATC 3-06*, Applied Technology Council, Palo Alto, California.

Applied Technology Council (2003)."Recommended LRFD guidelines for the seismic design of highway bridges," *MCEER/ATC-49*, Applied Technology Council, Redwood City, California.

Beatty, C.I. (1970). "Lateral test on pile groups," *Foundation Facts*, VI(1), 18-21.

Becker, D.E. (1996a). Eighteenth Canadian geotechnical colloquium: Limit states design for foundations. Part I. An overview of the foundation design process. *Canadian Geotechnical Journal*, 33, 956-983.

Becker, D.E. (1996b). Eighteenth Canadian geotechnical colloquium: Limit states design for foundations. Part II. Development for the National Building Code of Canada. *Canadian Geotechnical Journal*, 33, 984-1007.

Boulanger, R.W., Curras, C.J., Kutter, B.L. Wilson, D.W. and Abghari, A., (1999). Seismic soil-pile-structure interaction experiments and analysis," *Journal of Geotechnical and Geoenvironmental Engineering*, ASCE, 125(9), 750-759.

Brown, D.A. and Bollman, H.T. (1993). Pile-supported bridge foundations designed for impact loading. Appended document to *Proceedings of Design of Highway Bridges for Extreme Events, Crystal City, VA, p. 265-281*.

Brown, D.A., Morrison, C., and Reese, L.C., (1988). Lateral load behavior of pile group in sand. *Journal of Geotechnical Engineering*, ASCE, 114(11), 1261-1276.

Coduto, D.P. (2001). *Foundation design: Principles and practices.* Upper Saddle River, NJ: Prentice Hall, Second edition, 883 pp.

Cornell, C.A. and Krawinkler, H. (2000). "Progress and challenges in seismic performance assessment," *PEER News*, April, 1-3.

Davisson, M.T. (1973). High capacity piles.In Innovations in Foundation Construction, proceedings of a lecture series, Illinois Section ASCE, Chicago.

Deierlein, G.G., Krawinkler, H., and Cornell, C.A. (2003). "A framework for performance-based earthquake engineering," *Proceedings*, 2003 Pacific Conference on Earthquake Engineering.

Department of Energy (1994). "Natural phenomena hazards design and evaluation criteria for Department of Energy Facilities", *DOE-STD-1020-94*, U. S. Dept. of Energy, Washington, D. C.

Gates, M. (1957), "Empirical Formula For Predicting Pile Bearing Capacity," Civil Engineering, Vol 27, No.3, March: 65-66.

Gazetas, G. (1991). "Foundation vibrations," in *Foundation Engineering Handbook*, 2nd edition, H.-Y. Fang, editor, Van Nstrand Reinhold, pp. 553-593.

Haldar, A. and Mahadevan, S. (2000). *Probability, Reliability, and Statistical Methods in Engineering Design*, John Wiley & Sons, New York, 304 pp.

Hannigan, P.J., Goble, G.G., Thendean, G., Likins, G.E. and Raushe, F. (1997). *Design and construction of driven pile foundations*. Report No. FHWA-HI-97-013, Federal Highway Administration, Washington, D.C.

Jalayer, F. and Cornell, C.A. (2003). "A technical framework for probability-based demand and capacity factor design (DCFD) seismic formats," *Report PEER 2003/08*, Pacific Earthquake Engineering Research Center, Berkeley, California, 106 pp.

Jones, A.L., Kramer S.L., and Arduino, P. (2002). *Estimation of uncertainty in geotechnical properties for performance-based earthquake engineering*. PEER Report No.2002/16, Pacific Earthquake Engineering Research Center, University of California, Berkeley.

Luco, N. and Cornell, C. A. (1998). "Seismic drift demands for two SMRF structures with brittle connections", *Structural Engineering World Wide 1998*, Elsevier Science Ltd., Oxford, England, 1998, Paper T158-3.

Matlock, H., (1970). "Correlations for design of laterally loaded piles in soft clay," Proceedings of the II Annual Offshore Technology Conference, Houston, Texas, (OTC 1204), pp. 577-594.

Mokwa, R.L. (1999). Investigation of the resistance of pile caps to lateral loading. *PhD thesis*, Virginia Polytechnical Institute.

Mosher, R.L. (1984). Load transfer criteria for numerical analysis of axially loaded piles in sand. US Army Engineering Waterways Experimental Station, Automatic Data Processing Center, Vicksburg, Mississippi.

Nelder, J,A. and Mead, R. (1965). "A simplex method for function minimization". *Computer Journal*, 7: 308–313.

Novak et al. 1993. "DYNA4 – A computer program for foundation response to dynamic loads," *User's Manual*, Geotechnical Research Centre, University of Western Ontario.

Ovesen, N.K. (1964). "Anchor slabs, calculation methods and model tests," *Bulletin No. 16*. The Danish Geotechnical Institute, Copenhagen.

Phoon, K.K., and Kulhawy, F.H. (1999a). Characterization of geotechnical variability. *Canadian Geotechnical Journal*, 36, 612-624.

Phoon, K.K., and Kulhawy, F.H. (1999b). Evaluation of geotechnical property variability. *Canadian Geotechnical Journal*, 36, 625-639.

Randolph, M. F. , Leong, E. C. , and Houlsby, G. T. (1991). "*One-dimensional analysis of soil plugs in pipe pile* ." *Geotechnique* , **41** (**4**), **587–598** .

Reese, L.C. and O'Neill, M.W. (1987). *Drilled shafts: Construction procedures and design methods.* Report No. FHWA-HI-88-042, U.S. Department of Transportation, Federal Highway Administration, Office of Implementation, McLean, Virginia.

Reese, L.C. and Van Impe, W.F. (2001). *Single piles and pile groups under lateral loading.* A. A. Balkema, Rotterdam.

Reese, L.C., Allen, J.D. and Hargrove, J.Q. (1981). "Laterally loaded piles in layered soils," *Proceedings*, Tenth International Conference on Soil Mechanics and Foundation Engineering, Stockholm, 15-19 June, 2, 819-822.

Reese, L.C., Allen, J.D. and Hargrove, J.Q. (1981). Laterally loaded piles in layered soils. *Proceedings of the tenth international conference on soil mechanics and foundation engineering, Stockholm*, 15-19 June, 2, 819-822.

Reese, L.C., Cox, W.R. and Koop F.D. (1974). "Analysis of laterally loaded piles in sand," *Proceedings*, 6th Offshore Technology conference, Houston, Texas, (2(OTC2080)), 473-485.

Reese, L.C., Cox, W.R. and Koop, F.D. (1975). "Field testing and analysis of laterally loaded piles in stiff clay," *Proceedings*, 7th Offshore Technology Conference, Houston, Texas, (2(OTC2312)), 672-690.

Salgado, R. (2006). The Engineering of Foundations, McGraw-Hill, Columbus, Ohio, 896 pp.

SEAOC (1995). *Vision 2000: Performance-based seismic engineering of buildings*, Structural Engineers Association of California, Sacramento, California.

Shin, H-S.(2007). "Numerical modeling of a bridge system & its application for performance-based earthquake engineering," *PhD Thesis*, University of Washington, Seattle, Washington.

Stewart, J.P. , and Mylonakis, G.(2010). "Baseline Knowledge Report on Soil-Foundation-Structure Interaction of Building Structures". *Applied Technology Council.*

U.S. Army Corps of Engineers, (1997). Introduction to probability and reliability-based methods for geotechnical engineering. *Engineering Technical Letter 1110-2-547*, Department of the Army, Washington.

Vijayvergiya, V.N. (1977). "Load-movement characteristics of piles," *Proceedings*, Port 77 Conference, American Society of Civil Engineers, New York, NY.